รายงานวิจัยฉบับสมบูรณ์

การศึกษาบทบาทในเชิงหน้าที่ของของเอ็นไซม์ไพรูเวทคาร์บอกซิเลซและการควบคุมการแสดงออกในเซลล์มะเร็งเต้านมแพร่กระจาย

Functional investigation of pyruvate carboxylase and its transcriptional regulation in metastasis breast cancer

โดย ศาสตราจารย์ ดร ศราวุฒิ จิตรภักดี และคณะ

วันที่เสร็จโครงการ 30 เมษายน 2560

สัญญาเลขที่ BRG5780007

รายงานวิจัยฉบับสมบูรณ์

การศึกษาบทบาทในเชิงหน้าที่ของของเอ็นไซม์ไพรูเวทคาร์บอกซิเลซและการควบคุมการแสดงออกในเซลล์มะเร็งเต้านมแพร่กระจาย

Functional investigation of pyruvate carboxylase and its transcriptional regulation in metastasis breast cancer

คณะผู้วิจัย

1. ศาสตราจารย์ ดร ศราวุฒิ จิตรภักดี	ภาควิชาชีวเคมี คณะวิทยาศาสตร์ มหาวิทยาลัยมหิดล
2.รองศาสตราจารย์ พญ ชนิตรา ธุวจิต	คณะแพทยศาสตร์ศิริราชพยาบาล มหาวิทยาลัยมหิดล
3. ดร.พินน์นราห์ โรจนวิรัตน์	ภาควิชาชีวเคมี คณะวิทยาศาสตร์ มหาวิทยาลัยมหิดล
4. Professor Michael MacDonald	University of Wisconsin-Madison, USA
5. นางสาวพัชริยา พรรณศิลป์	ภาควิชาชีวเคมี คณะวิทยาศาสตร์ มหาวิทยาลัยมหิดล

สนับสนุนโดยสำนักงานกองทุนสนับสนุนการวิจัย
(ความเห็นในรายงานนี้เป็นของผู้วิจัย สกว. ไม่จำเป็นต้องเห็นด้วยเสมอ)

Abstract

We examined the expression of PC by immunohistochemistry of paraffin-embedded breast tissue sections of 57 breast cancer patients with different stages of cancer progression. PC was expressed in the cancerous areas of breast tissue at higher levels than in the non-cancerous areas. We also found statistical association between the levels of PC expression and tumor size and tumor stage ($P < 0.05$). The involvement of PC with these two parameters was further studied in four breast cancer cell lines with different metastatic potentials; i.e., MCF-7, SKBR3 (low metastasis), MDA-MB-435 (moderate metastasis) and MDA-MB-231 (high metastasis). The abundance of both PC mRNA and protein in MDA-MB-231 and MDA-MB-435 cells was 2-3-fold higher than that in MCF-7 and SKBR3 cells. siRNA-mediated knockdown of PC expression in MDA-MB-231 and MDA-MB-435 cells resulted in a 50% reduction of cell proliferation, migration and in vitro invasion ability, under both glutamine-dependent and glutamine-depleted conditions. MDA-MB-231 cells containing PC knockdown showed a marked reduction in viability and proliferation rates suggesting the perturbation of pathways that are involved in cancer invasiveness. Strong PC suppression lowered glucose incorporation into downstream metabolites of oxaloacetate, the product of the PC reaction, including malate, citrate and aspartate. Levels of pyruvate, lactate, the redox partner of pyruvate, and acetyl-CoA were also lower suggesting the impairment of mitochondrial pyruvate cycles. Serine, glycine and 5-carbon sugar levels and flux of glucose into fatty acids were decreased. ATP, ADP and NAD(H) levels were unchanged indicating that PC suppression did not significantly affect mitochondrial energy production. The data indicate that the major metabolic roles of PC in invasive breast cancer are primarily anaplerosis, pyruvate cycling and mitochondrial biosynthesis of precursors of cellular components required for breast cancer cell growth and replication.

We also combine the literature data on the miRNAs that potentially regulate 40 metabolic enzymes responsible for metabolic reprogramming in cancers, with additional miRs from computational prediction. By combining known and predicted interactions of oncogenic transcription factors (TFs) (c-MYC, HIF1α and p53), sterol regulatory element binding protein 1 (SREBP1), 40 metabolic enzymes, and regulatory miRs we have established one of the first reference maps for miRs and oncogenic TFs that regulate metabolic reprogramming in cancers. The combined network shows that glycolytic enzymes are linked to miRs via p53, c-MYC, HIF1α, whereas the genes in serine, glycine and one carbon metabolism are regulated via the c-MYC, as well as other regulatory organization that cannot be observed by investigating individual miRs, TFs, and target genes.

บทคัดย่อ

จากการศึกษาการแสดงออกของเอ็นไซม์ pyruvate carboxylase (PC) ในเนื้อเยื่อมะเร็งเต้านมของผู้ป่วย 57 รายที่ถูกวินิจฉัยว่าเป็นมะเร็งเต้านมในระยะที่ 1-4 โดยวิธี Immunohistochemistry พบว่าเอนไซม์ PC มีการแสดงออกสูงในเนื้อเยื่อมะเร็งเต้านมเมื่อเปรียบเทียบกับเนื้อเยื่อปกติของผู้ป่วยรายเดียวกัน ผลการวิเคราะห์ทางสถิติพบว่า ระดับการแสดงออกของเอนไซม์นี้ มีความสัมพันธ์กับระยะของมะเร็งเต้านม และขนาดของก้อนเนื้อมะเร็ง ซึ่งความเกี่ยวข้องของเอ็นไซม์ PC กับระยะและขนาดของมะเร็งเต้านมได้นำมาศึกษาต่อในเซลล์มะเร็งเต้านมแบบเพาะเลี้ยงที่มีระดับความสามารถในการแพร่กระจายต่างกัน เช่น เซลล์ MCF-7, SKBR3 (มีความสามารถในการแพร่กระจายต่ำ), MDA-MB-435 (มีความสามารถในการแพร่กระจายปานกลาง) และ MDA-MB-231 (มีความสามารถในการแพร่กระจายสูง) พบว่าในเซลล์มะเร็งที่มีความสามารถในการแพร่กระจายสูง เช่น MDA-MB-231 และ MDA-MB-435 จะมีการแสดงออกของเอนไซม์ PC ทั้งในระดับ mRNA และโปรตีนสูงกว่าเซลล์มะเร็งเต้านมที่มีความสามารถในการแพร่กระจายต่ำ เช่น MCF-7 and SKBR3 ประมาณ 2-3 เท่า การยับยั้งการแสดงออกของเอ็นไซม์ PC ด้วยsiRNA ในเซลล์ MDA-MB-231 และ MDA-MB-435 พบว่ามีผลทำให้การเจริญเติบโต การเคลื่อนที่ และการแพร่กระจายของเซลล์มะเร็งในหลอดทดลองลดลงถึง 50% ทั้งในสภาวะที่มีและไม่มีกลูตามีน และเพื่อยืนยันผลการทดลองข้างต้น จึงทำการสร้างเซลล์ MCF-7 ให้มีการสร้างเอ็นไซม์ PC เพิ่มขึ้น พบว่าทำให้อัตราการเจริญเติบโต, การเคลื่อนที่ และความสามารถในการแพร่กระจายของเซลล์มะเร็งในหลอดทดลองเพิ่มขึ้น 2 เท่า คณะผู้วิจัยได้ทำการสร้างเซลล์ที่ถูกยับยั้งเอนไซม์ PC อย่างถาวรโดยใช้เซลล์ MDA-MB-231 ซึ่งเป็นเซลล์มะเร็งเต้านมที่มีความสามารถในการแพร่กระจายสูง และทำการวัดระดับ metaboliteโดย LC-MS และใช้คาร์บอนไอโซโทปติดตามที่น้ำตาลกลูโคสและกลูตามีน ในเซลล์ MDA-MB-231 ที่ถูกยับยั้งเอนไซม์ PC พบว่ามีการลดลงของ TCA cycle intermediate เช่น citrate และ malate ซึ่งการลดลงดังกล่าวมีผลทำให้การดึงสาร TCA cycle intermediate ไปสังเคราะห์สารต่างๆเช่น serine, glycine, aspartate และ กรดไขมัน ทำได้น้อยลง ซึ่งสารเหล่านี้เป็นองค์ประกอบของโปรตีน, ไขมัน และนิวคลีโอไทด์ ซึ่งจำเป็นต่อการเจริญเติบโตของเซลล์ นอกจากนี้ระดับของ pyruvate, acetyl Co-A และ lactate ซึ่งเป็น redox partner ของ pyruvate ก็ลดลงเช่นกัน การลดลงของ citrate และ malate ชี้ให้เห็นถึงความบกพร่องของ pyruvate cycle ระหว่างไมโทคอนเดรียและ cytosol ดังนั้นเซลล์ที่ถูกยับยั้ง PC จึงมีอัตราการเจริญเติบโตที่ช้าลง จากผลการทดลองทั้งหมดนี้แสดงให้เห็นถึงบทบาททางเมตาบอลิซึมของเอ็นไซม์ PC ในการส่งเสริมการเจริญเติบโตและการดำรงอยู่ของเซลล์มะเร็งเต้านมที่มีความสามารถในการแพร่กระจายสูง

นอกจากนี้คณะผู้วิจัยยังได้ศึกษาขอบข่ายการควบคุมเอ็นไซม์ในขบวนการเมตาบอลิซึมในเซลล์มะเร็งต่าง ๆ โดยวิธี computational biology พบว่าการแสดงออกของเอ็นไซม์ควบคุมเมตาบอลิซึมถูกควบคุมในแบบเครือข่ายผ่าน oncogenic transcription factor ได้แก่ HIF1a, p53 และ c-myc และ SREBP1 ในระดับ transcription และ miRNA.

Keywords: Pyruvate carboxylase, cancer, metastasis, metabolism, \ anapleorsis, aerobic glycolysis, mass spectroscopy, transcription, miRNA

Executive summary

Significane

Breast cancer is one of the most common malignancies in women, with an estimated one million cases diagnosed every year, and remains one of the cancer types that causes an extremely high mortality rate worldwide (McPherson, et al., 2000; Jemal et al., 2010). This incidence is also increasing in Thailand. Based on the data reported by the National Cancer Institute, Thailand, approximately 45% of all cancer cases are diagnosed as breast cancer (Jordan et al., 2009). The high incidence of breast cancer is also associated with the women who live in a westernized lifestyle. Long term survival is more likely if the cancer remains localized to the breast tissue. Despite advances in the prevention, diagnosis and development of new therapies for cancer, a substantial proportion of women who succumb to breast cancer are diagnosed with metastasis either at an initial period or during the course of treatment. Although surgical removal of the primary tumor is always a preferred treatment, relapse of the cancer at local or distant sites may occur due to the micrometastases undetectable during the first diagnosis (Saphner et al., 1996). Furthermore, metastatic breast cancer is incurable as much of the cancer develops resistance to the current chemotherapy (Hortobagyi, 2000). Like other types of cancer, breast cancer results from genetics and alterations of environmental factors, which in turn cause an aberrant proliferation of cells. Genetic factors definitely predispose women to breast cancer. For example, mutations of the BRCA1 and BRCA2 genes, which encode proteins involved in the DNA-repair system, are well known to put women into high disease susceptibility (Mili et al., 1994; Wooster et al., 1995). Amplification or over-expression of several oncogenes, for example ERBB2 or HER-2, a member of the epidermal growth factor receptor (EGFR) family, transforms normal cells into malignant cells (Harari and Yarden, 2000). It is clear that when combined with genetic factors, deregulation of metabolism of normal cells as the result of overwhelming activation of growth factor signaling, contributes to the development of cancer (Zardavas et al., 2013). As a result of their rapid proliferation rate, most tumors have to adapt their metabolism in order to accommodate both energy and structural components needed for the rapidly dividing cells (Cairns et al., 2011).

Similar to other cancers, regardless of tissue oxygen levels, breast cancer oxidizes glucose excessively via glycolysis known as the Warburg effect. Mitochondrial energy production by oxidative phosphorylation is essentially normal or occasionally slightly repressed in cancer cells [Lee et al., 2012]. This and other recent indirect evidence suggests that mitochondrial

metabolism could be important in other ways, such as for supplying the substrates for biosynthesis of fatty acids, amino acids and nucleic acids as the structural and functional components of the rapidly dividing cells [Lee et al., 2012 Vander Heiden et al., 2009]. In this regard, “anaplerosis”, which is the net mitochondrial biosynthesis of certain citric acid cycle intermediates [Owen et al., 2002], could be extremely important for cancer cell proliferation and invasiveness. However, there is a paucity of data on the role of individual metabolic pathways that support cancer cell growth and survival, especially in breast cancer. Pyruvate carboxylation and glutaminolysis are the two major anaplerotic reactions that replenish citric acid cycle intermediates when they are depleted by their export from the mitochondria for biosynthetic reactions that take place mostly in the extramitochondrial compartment of the cell. A major anaplerotic reaction involves the carboxylation of pyruvate to oxaloacetate catalyzed by pyruvate carboxylase (PC) followed by oxaloacetate's conversion to malate, citrate and aspartate and their export from mitochondria to the cytosol where they become precursors for the synthesis of carbohydrates, lipids and amino acids [Jitrapakdee et al., 2008]. Glutaminolysis involves the conversion of glutamine to glutamate by glutaminase followed by oxidative deamination of glutamate to α-ketoglutarate catalyzed by glutamate dehydrogenase. α-Ketoglutarate is then converted to other citric acid cycle intermediates that can be exported from the mitochondria to the cytosol [Moreadith et al., 1984]. Different cancers use these anaplerotic reactions to various degrees [Cheng et al., 2011; Fan et al., 2009; Sellers et al., 2015].

Objectives

1. To investigate the association between the degree of overexpression of PC and various breast cancer stages in breast tissue samples

2. To investigate the necessities of PC in supporting growth, proliferation and invasion of metastasized breast cancer cell lines.

3. To identify the shuttle that is associated with overexpression of PC in metastasized cancer cell lines.

4. To identify the transcription factors which are responsible for transcriptional activation of the PC gene promoter in metastasized breast cancer cell lines.

PART I Investigation of association between the degree of overexpression of PC and clinical parameters (objective 1).

A previous study has reported the overexpression of PC in solid lung tumor tissue [Fan et al., 2009]. To examine whether this was the case for breast cancer, we performed immunohistochemistry (IHC) staining using an anti-PC antibody on breast tissue sections collected from 57 patients who had stages I-IV of breast cancer using anti-PC antibody. Fifty-seven paraffin-embedded breast cancer tissue sections were collected under the protocols approved by Siriraj Institute Revision Board, Faculty of Medicine Siriraj Hospital, Mahidol University (COA no. Si 230/2014), and all clinical investigation were conducted according to the principles expressed in the Declaration of Helsinki. The written informed consent was obtained from each participant who enrolled in the study. Those breast tissues were diagnosed invasive ductal carcinoma. Firstly, the antigen was retrieved by incubation with 10 mM citrate buffer pH 6 at 95°C for 1 h. The sections were blocked with 2% (w/v) BSA for 20 min before incubating with 1:1,000 dilution of anti-chicken PC antibody [Rohde et al., 1991] at room temperature overnight. Excess primary antibody was removed by washing with 1x PBS for 10 min before incubating with specific anti-rabbit EnVision+system-HRP labelled polymer (DAKO) at room temperature for 30 min. The secondary antibody was washed with 1x PBS for 10 min before 0.05% (w/v) 3,3'-diaminobenzidine (DAB) solution was applied to the sections and incubated at room temperate for 5 min. The sections were counter-stained with Mayer's hematoxylin, dipped in 1% (w/v) lithium carbonate and washed with tap water for 5 min. Finally, the sections were mounted with Permount and examined under the microscope. PC expression was semi-quantitatively scored on the basis of percentage of PC-positive cells and the immunostaining intensity. Grading for the percentage of PC-positive cancer cells were as follows: 1 for 1–25%; 2 for 26–50%; 3 for 51–75% and 4 for 76–100%. The intensities of PC staining in cancer tissues were as follows: 0, unstained; 1, slightly; 2, intermediate and 3, strongest staining. The interpretation of PC expression was performed by the scores of the percent positive cells (1–4) multiplied by the scores of staining intensity (0–3) to reach the total final immunohistochemistry (IHC) score of 0–12. The results were then categorized as follows; low expression, IHC score ≤ 6; and high expression, IHC score > 6. All samples were anonymous and independently scored by two investigators of whom one is a pathologist.

RESULT

In contrast to the non-cancerous area of the tissue sections, (Fig 1A), PC was highly expressed in the cancerous areas of the breast tissues (Fig 1B). The expression levels of PC

expression also varied in different stages of cancer (Fig 1C–1F). Expression of PC in stromal fibroblasts and infiltrating immune cells was rarely observed.

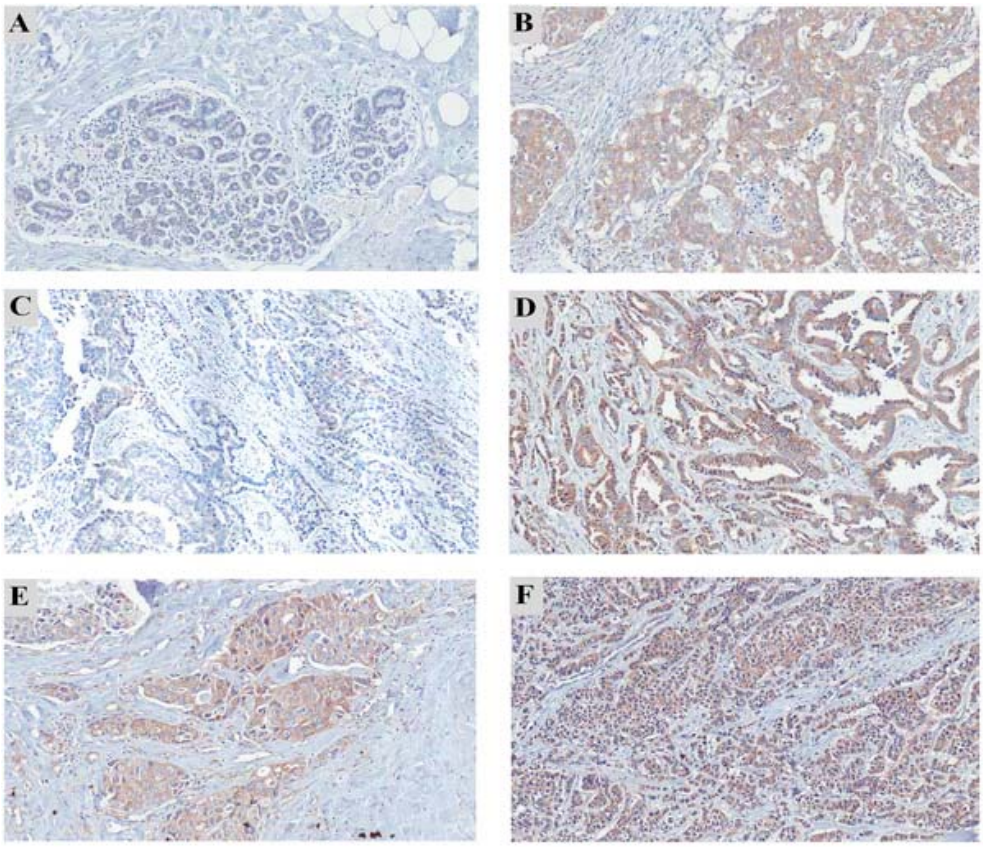

Fig 1. Immunohistochemistry staining of PC in paraffin-embedded breast tissue sections of patients with various stages of breast cancer. (A) Normal adjacent area of breast tissue showing weak staining of PC compared to strong staining in the cancerous area (B) of the same tissue. The representative samples showing different expression levels of PC in different stages of breast cancer: (C) stage 1, (D) stage 2, (E) stage 3 and (F) stage 4. Original magnification, 100x.

PC expression was detected in breast tissues of most cancer patients (96% of the total studied cases) except two cases which were stage I. Overall, 72% of breast cancer tissues showed a low expression level of PC whereas 28% had a high expression level of PC (Table 1). Based on grouping the patients into early stage without distant metastasis (stages I-III) and late stage with distant metastasis (stage IV), 67% (4 in 6 cases) of breast cancer with distant metastasis showed a high expression level of PC. In contrast, only 24% (12 in 51 cases) of patients without metastasis had a high level of PC expression. Univariate analysis showed a significant correlation between PC expression level and stage IV ($P = 0.046$). Interestingly,

PC expression showed a significant correlation with the tumor size (Table 1) (P = 0.033) i.e., PC was poorly expressed in most tumor cases with small volume (<4 cm3) (86%, 25/29). The other clinicopathological parameters including histological type, invasion, estrogen receptor (ER), progesterone receptor (PR) and HER2 expression did not show statistical associations with PC expression.

Table 1. Univariate analysis of expression level of PC in breast tissues and clinicopathological parameters.

Variable (Total cases)		PC expression (IHC score)		P-value
	No of case	Low (≤ 6)	High (> 6)	
Tumor volume (cm^3) (52)				
≤ 4	28	24	4	0.033*
> 4	24	14	10	
Tumor staging (57)				
I	18	15	3	0.225
II	22	17	5	0.555
III	11	7	4	0.482
IV	6	2	4	0.046*
Histological type (56)				
Well-differentiated	7	6	1	0.661
Moderately-differentiated	30	20	10	0.365
Poorly-differentiated	19	15	4	0.543
Invasion (57)				
Absence	24	18	6	0.769
Presence	33	23	10	
ER (57)				
High (4)	38	29	9	0.356
Low (0–3+)	19	12	7	
PR (57)				
High (4)	17	14	3	0.342
Low (0–3+)	40	27	13	
HER2 (57)				
Negative	37	27	10	1.00
Positive	20	14	6	

doi:10.1371/journal.pone.0129848.t001

Immunohistochemistry staining of PC expression in breast cancer tissue samples with different degrees of ER/PR/HER2 expression collected from 57 patients show that the level of PC expression IS NOT correlated with expression of these three receptors as shown below [P = 0.356 for ER; P = 0.342 for PR; P = 1.00 for HER2] in clinical samples as shown in Table below.

Receptor expression	PC expression levels		
	no	low	high
$ER^-, PR^-, HER2^-$	0	4	1
$ER^+, PR^+, HER2^+$	0	10	2
$ER^+, PR^+, HER2^-$	2	16	7
$ER^-, PR^-, HER2^+$	0	5	2
$ER^+, PR^-, HER2^-$	0	5	2
$ER^+, PR^-, HER2^+$	0	1	0

Also shown below is the variation of PC expression in breast tissues of four patients which are triple negative for ER/PR/HER2 expression.

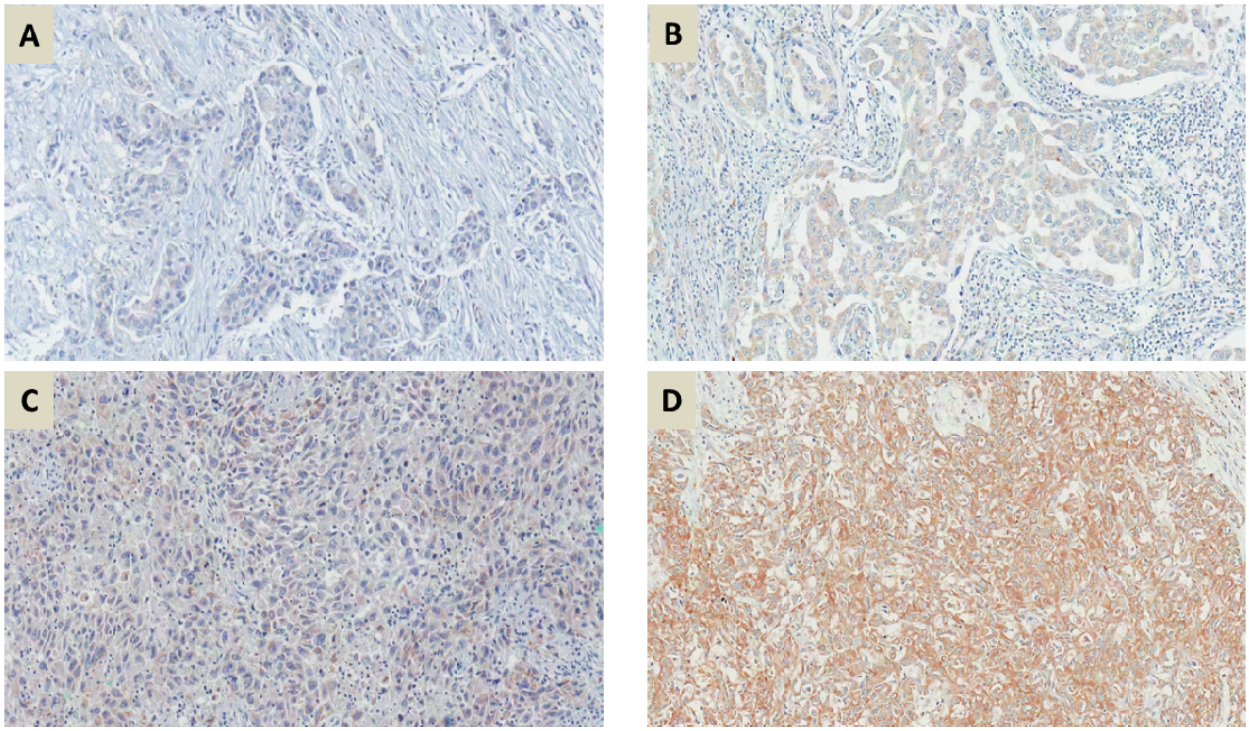

Figure 2. Representatives of immunohistochemistry staining of PC in paraffin embedded breast tissues of four patients, which are ER/PR/HER2 negative.

PART II 2. Investigation the necessities of PC in supporting growth, proliferation and invasion of metastasized breast cancer cell lines (objective 2).

Because the degree of PC expression showed statistical association with tumor size and stage, we hypothesized that PC was required to support tumor growth and invasion of

breast cancer cells. We examined the above hypothesis by investigating the expression levels of PC in breast cancer cell lines with different degrees of motility, namely, MCF-7, SKBR3, MDA-MB-435 and MDA-MB-231.

Cell culture

Human breast cancer cell lines, MCF-7 (ATCC:HTB22) [Soule et al., 1973] and MDA-MB-231(ATCC: HTB26) [21], MDA-MB-435 (ATCC:HTB129) and SKBR3 (ATCC: HTB-30) were grown in Dulbecco's modified Eagle's medium (DMEM) (Gibco) supplemented with 10% (v/v) fetal bovine serum (FBS). The cells were maintained at 37°C with 5% CO2. The glutamine-independent MDA-MB-231 cell line was established by progressive depletion of glutamine in the culture medium from 4 mM to 0 mM. In brief, cells were grown in DMEM supplemented with 2 mM glutamine for 2 weeks, 1 mM for 2 weeks, 0.5 mM for 2 weeks and no glutamine, respectively. After 1 month of growing this cell line in the absence of glutamine, it was used for subsequent experiments.

siRNA transfection of and overexpression of PC

6 x 105cells of MDA-MB-231 cells or 3.5 x 105cells of MDA-MB-435 were plated in 35-mm dish containing 2 ml of DMEM supplemented with 10% (v/v) FBS and maintained at 37°C with 5% CO2 for 24 h. 50 pmole (25 nM) or 100 pmole (50 nM) of siRNA targeted to human PC (Cat.no. 4390824, Ambion) were transfected to MDA-MB-231 or MDA-MB-435, respectively using Lipofectamine 2000 transfection reagent (Invitrogen) in the Optimem-reduced serum medium (Invitrogen). Same amounts of scrambled control siRNA were also transfected to both cell lines. The transfected cells were maintained in 2 ml complete medium for 2 days. The cells were subsequently harvested for RT-PCR and Western blot analyses.

MCF-7 cells overexpressing PC were generated by transfection of plasmid encoding human PC (pEF-PC) [Jitrapakdee et al., 1999]. In brief, 2 x 105 cells of MCF-7 were plated in 2 ml complete DMEM medium in 35 mm-dish 24 h before transfecting with 4 μg of pEF-PC plasmid. Upon 48 h post-transfection, the stable MCF-7 cells overexpressing PC cells were selected with 0.5 μg/mL puromycin for one week. The stable lines were expanded for another week before proliferation, migration and invasion assays were performed.

Reverse transcription polymerase chain Reaction (RT-PCR)

Total RNA was extracted from cells using TRIzolReagent (Gibco) following the manufacturer's instructions. Initially the random hexamers-primed RNA was carried out in a

10 µl-reaction mixture containing 2 µg of total RNA and 200 ng of random hexamers (Promega) at 70°C for 5 min, before being chilled at 4°C. Reverse transcription was initiated by adding 10 µl of mixture containing 1xImProm-II reaction buffer, 3 mM MgCl2, 0.5 mM dNTP mix and 160 units of ImProm-II reverse transcriptase (Promega), to the primed-RNA mixture and the reaction was incubated at 25°C for 5 min, 42°C for 60 min and 70°C for 15 min, respectively. The cDNA was stored at -20°C until used.

Quantitative real-time PCR

Quantitative real time PCR was performed in a 12 µl-reaction mixture containing 6 µl of 2xKAPA probe Fast qPCRmaster mix Universal (KAPA Biosystems), 2 µl of cDNA, 1 µM of forward and reverse primers and 0.5 µM of fluorogenic probe as described previously [Thonpho et al., 2010]. The thermal profiles consisted of initial incubation at 50°C for 2 min and 95°C for 10 min followed by 40 cycles of denaturation at 95°C for 15 sec and annealing/extension at 60°C for 1 min in Mx3000P Q- PCR system (Agilent Technologies). To identify the PC mRNA isoforms expressed in breast cancer cell lines, quantitative real time PCR was performed in a 20 µl-reaction mixture containing 10 µl of 2x KAPA SYBR FAST qPCR Master mix universal (KAPA Biosystems), 200 nM each of specific forward primer for detecting each isoform of PC mRNA and reverse primers [Thonpho et al., 2013], and 2 µl of cDNA. The thermal profiles consisted of initial incubation at 95°C for 10 min followed by 40 cycles of denaturation at 95°C for 30 sec, annealing at 60°C for 30 sec and extension at 72°C for 30 sec in Mx 3000P Q- PCR systems (Agilent Technologies). Expression of PC mRNA was normalized with that of 18s ribosomal RNA gene, and was shown as the relative gene expression. Fold change was calculated using the comparative CT method (ΔΔCT method) [Livak et al., 2001].

Western blot analysis

MCF-7, MDA-MB-231 and MDA-MB435 cells grown in T75 cm2 flask were trypsinized with 0.05% (v/v) trypsin-EDTA. The detached cells were centrifuged at 3,000 xg for 5 min, cell pellet was re-suspended in 150 µl of RIPA buffer (50 mM Tris-HCl pH 7.4, 150 mM NaCl, 1 mM EDTA, 0.25% sodium deoxycholate, 1% (v/v) NP-40 and 1x protease inhibitor cocktail (Roche). 70 µg of protein lysate were subjected to discontinuous SDS-PAGE [26] under reducing conditions. The proteins were transferred to a polyvinylidenedifluoride (PVDF) membrane by Semi-Dry Transfer Cell (BIO-RAD) for 1.5 h. The membrane was incubated in 15 ml of blocking solution [5% (w/v) skim milk in 1% (v/v) Tween 20 in PBS-

T] at 4°C overnight. For detecting PC protein, the blot was incubated with1:5,000 dilution of rabbit anti-chicken PC polyclonal antibody [Rohde et al., 1991] for 2 h. The blot was briefly washed in PBS-T before incubating with 1:5,000 dilution of goat anti-rabbit IgG conjugated with horseradish peroxidase (HRP) (DAKO) for 1 h. For detection of β-actin, mouse anti-actin monoclonal antibody (sc-8432) (Santa Cruz) and sheep anti-mouse IgG conjugated with HRP (GE healthcare) were used for primary and secondary antibodies, respectively. The immunoreactive bands were detected using an enhanced chemiluminescence substrate (Perkin Elmer). The images were captured using Chemiluminescence Imaging System (Syngene).

Proliferation assay

Cell proliferation was determined by counting the viable cells for 7 days. At 48 h post-transfection, the 1 x 10^5 cells of MDA-MB-231, MDA-MB-435 or MCF-7 overexpressing PC were plated into 35 mm dishes and grown in the absence or presence of 4 mM glutamine for 1, 2, 3, 4, 5, 6 and 7 days, at 37°C in CO2 incubator. At each time point, the cells were trypsinized, stained with 0.4% trypan blue and counted under a microscope. The results are presented as means + standard deviations of two independent experiments.

Wound healing assay

1.5 x 10^5 cells of MDA-MB-231, MDA-MB-435 and MCF-7 overexpressing PC were replated in 24-well plate in DMEM containing no serum overnight before the artificial wound was generated by scratching the monolayer with a pipette tip. The wound's closure (width) of the PC knockdown at 0 and 48 h was measured and shown as the mean + standard deviation of that of the scrambled control which was arbitrarily set as 100%.

In vitro invasion assay

In vitro invasion assays were performed by plating 1.2 x 10^5 of MDA-MD-231, MDA, MDA-MB-435 or MCF-7 cells in 200 µl of serum-free medium containing 4 mM or 0 mM glutamine into the upper chamber of Transwell (6.5-mm diameter polyvinylpyrrolidone-free polycarbonate filter of 8-µm pore size) (Corning, NY, USA) which was pre-coated with 20 µg Matrigel (BD Biosciences) while the lower chamber contained medium supplemented with 10% (v/v) FBS for 4 h (for MDA-MB-231) or with 20% FBS for 24 h (for MCF7 and MDA-MB-435) at 37°C. The non-invaded cells in the upper compartment were removed and the chamber was washed twice with 1x PBS. The cells that had invaded through the matrix were fixed with 4% (v/v) paraformaldehyde in 1x PBS for 20 min and stained with 0.5%

crystal violet in 25% (v/v) methanol overnight, followed by two washes with tap water. Finally, the invaded cells were counted under a microscope and the percentage of invasion was compared with that of the scrambled control cell which was arbitrarily set as 100%.

As shown in Fig 3A, the motilities of MDA-MB-435 and MDA-MB-231 are 10-fold and 75-fold higher than those of MCF-7 and SKBR3 cells, respectively. Consistent with the motility phenotype, MCF-7 and SKBR3 cell lines possess low expression level of PC mRNA while MDA-MD-231 and MDA-MB-435 cell lines express PC mRNA 4-fold and 2-fold higher than MCF-7 (Fig 3B). The two alternative PC mRNA isoforms, namely variant 1 and variant 2 which differ in their 5'-untranslated regions, are differentially transcribed from two alternative promoters, the distal and the proximal promoters, respectively [24]. To examine which of these two PC mRNA isoforms was up-regulated in MDA-MB-231 and MDA-MB-435 cells, quantitative real-time PCR using primers specific for variants 1 and 2 was performed. As shown in Fig 3C, expression of variant 1 was up-regulated in all cell lines however both MDA-MB-231 and MDA-MB-431 possessed expression of variant 1 more than MCF-7 and SKBR3. Western blot analysis of PC protein of these four cell lines was also consistent with their motility phenotype and PC mRNA expression i.e. the abundance of PC in MDA-MB-231 and MDA-MB-435 are 4.5-fold higher than in MCF-7 and SKBR3 (Fig 3D and 3E).

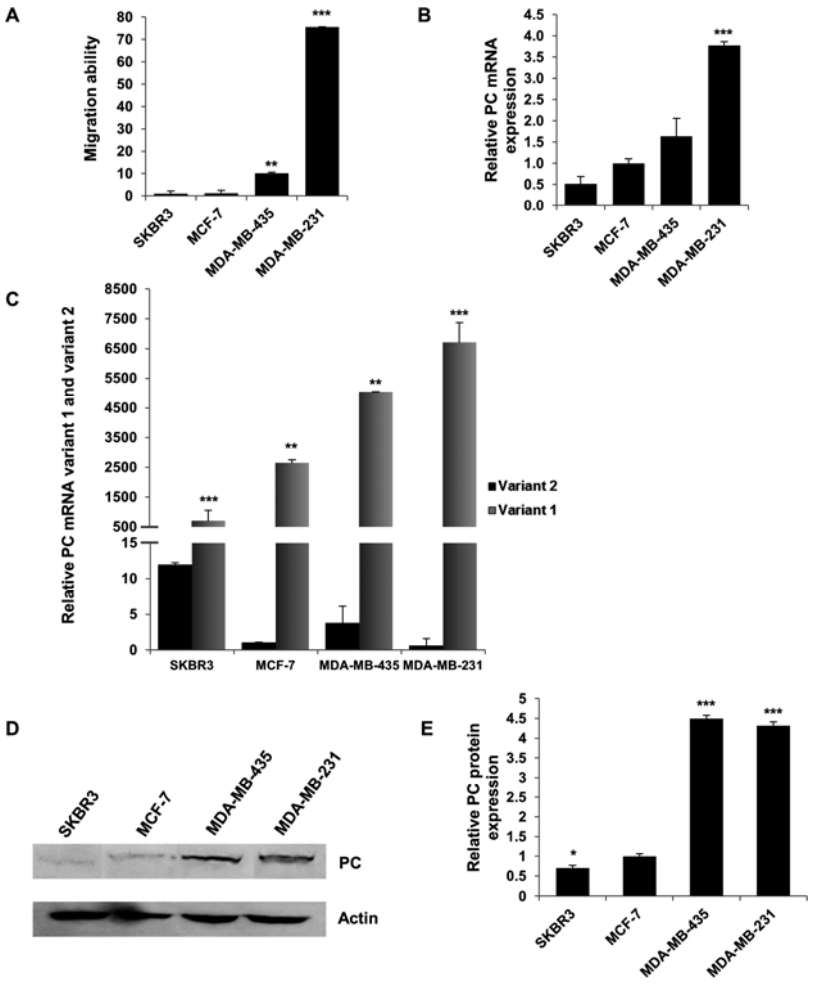

Fig 3. Migration ability of various breast cancer cell lines and the expression levels of PC in these cell lines. A, Migration ability of SKBR3, MCF-7, MDA-MB-435 and MDA-MB-231. B, Q-PCR analysis of PC mRNA expression in the above cell lines. The expression of PC was normalized with the expression of 18s rRNA gene and shown as the relative gene expression. The relative PC expression in MCF-7 was arbitrarily set as 1. C, Real time PCR analysis of PC mRNA variant 1 and 2 expression in the above cell lines. The expression of PC was normalized with the expression of 18s rRNA gene and shown as the relative gene expression. The expression of the relative PC mRNA variants in MCF-7 was arbitrarily set as 1. D, Western blot analysis of PC protein in the above cell lines. The blot was also probed with anti-actin antibody to serve as loading control. E, The immunoreactive band intensity of PC in D was quantitated and normalized with that of the β-actin and shown as the relative PC expression. The statistical analysis was conducted using student's t-test where *P < 0.05, **P < 0.01, ***P < 0.001.

Suppression of PC expression lowers growth, migration and invasion ability of highly metastasized breast cancer cell lines

We next examined whether overexpression of PC in the MDA-MB-231 cell line was necessary to support its growth and invasion ability. We suppressed expression of PC in this cell line by siRNA and assessed the phenotypes of the knockdown cells. As shown in Fig 4A and 4B, suppression of PC expression in MDA-MB-231 resulted in 90% and 80% decreases in PC mRNA and PC protein levels, respectively.

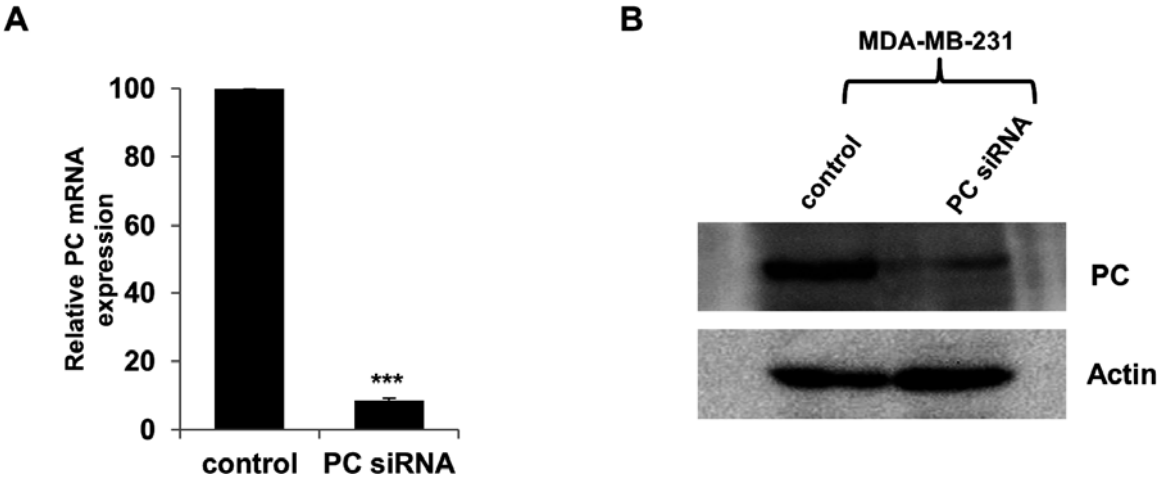

Fig 4. siRNA-mediated suppression of PC expression in MDA-MB-231 cell line.

Real time PCR analysis of PC mRNA expression in MDA-MB-231 cells transfected with scrambled control (Control) or PC siRNA. The PC mRNA level was determined by Q-PCR at 48 h post-transfection (A). Western blot analysis of PC protein in the PC knockdown MDA-MB-231 and the scrambled control (B). The statistical analysis was conducted using student's t-test ***$P \leq 0.001$.

PC knockdown MDA-MB-231 cell line did not affect proliferation in the first day but showed a 50% reduction in growth by day 2 (Fig 5A). Similar degrees of reduction were observed until day 7. Real-time PCR analysis also confirmed that the retarded proliferation rate of this cell line was accompanied by suppression of PC mRNA throughout day 7 (Fig 5B). Because suppression of PC expression did not completely inhibit the cell proliferation rate, the ability of the PC knockdown MDA-MB-231 cells to grow in the complete growth medium may have resulted from the compensation of anaplerosis via glutaminolysis. To examine whether this latter pathway contributes to the survival of the PC knockdown cells, the glutamine-independent PC deficient MDA-MB-231 cell line was generated. In the

absence of glutamine supplementation in the medium, any anaplerotic reaction would rely exclusively on a PC-catalyzed reaction. We generated the glutamine-independent MDA-MB-231 cell line (Gln-) by gradually depleting glutamine from the culture medium before transfecting this cell line with PCsiRNA so that the phenotype of this cell line became glutamine-independent and PC deficient (Gln^-/PC^--MDA-MB-231). The Gln^-/PC^--MDA-MB-231cells grown in the glutamine-free medium showed a growth rate similar to the control cell line in the first two days but showed approximately 30–40% reduction of cell proliferation from day 3 until day 7 (Fig 5C). Real time PCR analysis also confirmed that the retarded proliferation rate of this cell line was accompanied by suppression of PC mRNA throughout day 7 (Fig 5D).

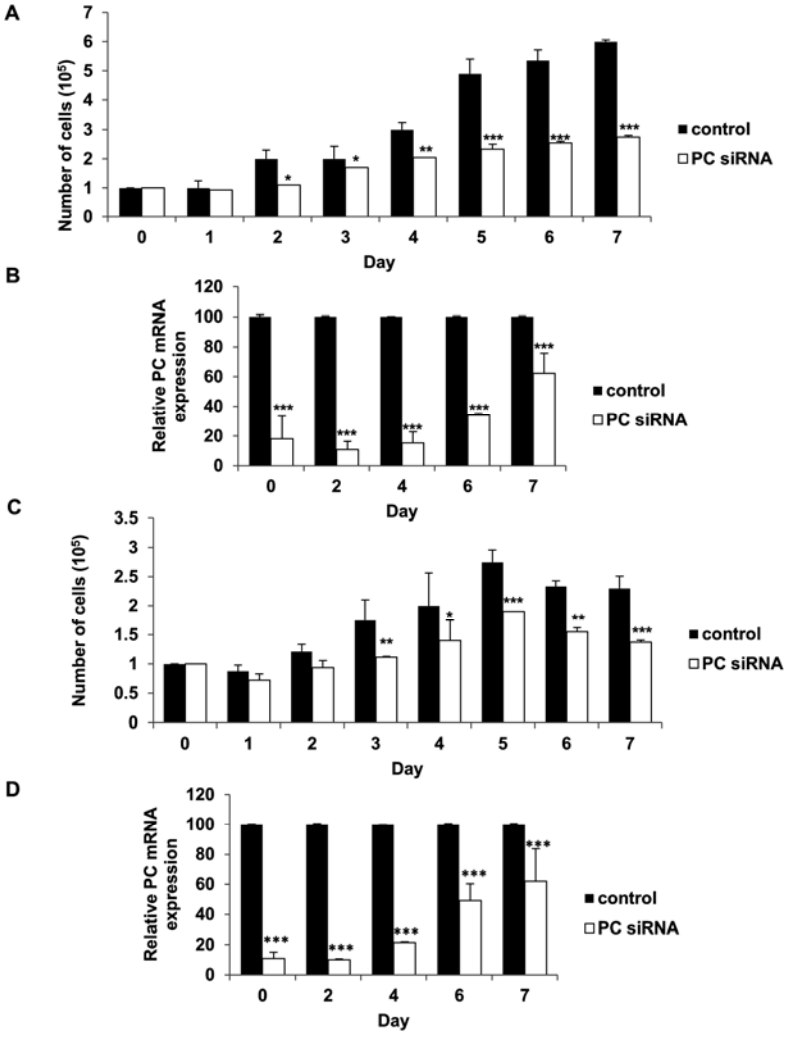

Fig 5. Suppression of PC expression in MDA-MB-231 retarded proliferation both in glutamine-nourished and glutamine-depleted conditions. MDA-MB-231 cells were transiently transfected with PC or scrambled control siRNAs. At 48 h post transfection cells were trypsinized, re-plated and grown in the presence of 0 mM or 4 mM glutamine for 7

days. The proliferation rate of the PC knocked down (PC siRNA) and the control MDA-MB-231 cell lines (Control) grown in the medium containing 4 mM (A) or 0 mM (C) glutamine. The relative expression of PC mRNA in the knocked down MDA-MB-231 cells grown in the presence of 4 mM (B) or 0 mM (D) glutamine throughout the assay. The results are means obtained from two independent experiments, each in triplicate. The statistical analysis was conducted using ANOVA test where *$P < 0.05$, **$P < 0.01$, ***$P < 0.001$.

As the levels of PC expression were significantly correlated with the stages of cancer progression, we hypothesized that PC was involved in the aggressive phenotypes of breast cancer cells, particularly migration and invasion. We investigated whether PC was required to support migration and invasion ability of MDA-MB-231 cells. We first examined the ability of the PC knockdown MDA-MB-231 cells to migrate across a wound. As shown in Fig 6A and 6B, the PC knockdown cells exhibited a 40% reduction of migration across the wound compared to the scrambled control. A similar degree of reduction was observed from the glutamine-independent PC knockdown cell line (Fig 6C and 6D).

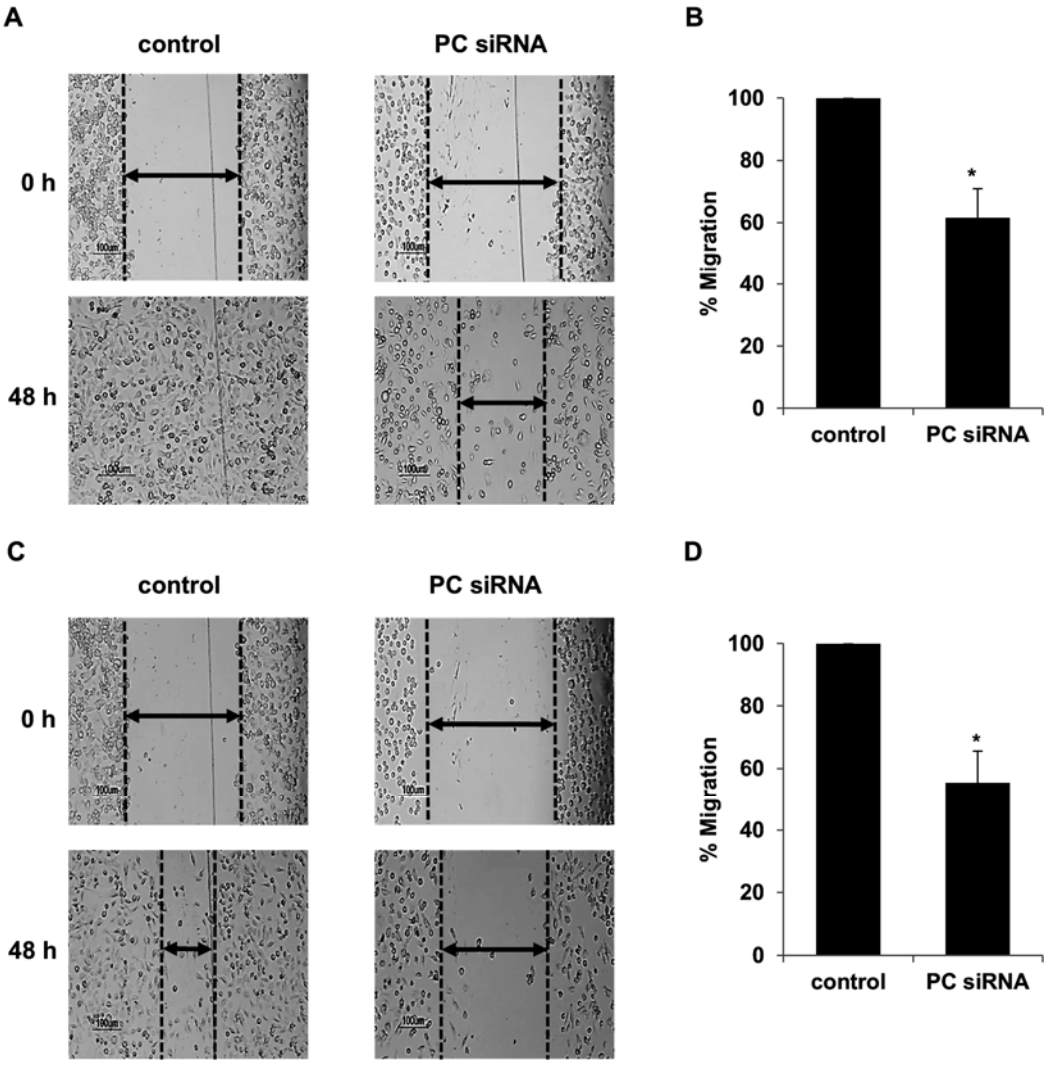

Fig 6. Suppression of PC expression in MDA-MB-231 cells reduced migration. Representative images of wound-healing assays. MDA-MB-231 cells were transiently transfected with PC or scrambled control siRNAs. At 48 h post transfection, wound-healing assays were performed as described in the materials and methods. (A, C) Representative images of the PC knockdown (PC siRNA) or scrambled control cells (Control) migrated across the wound areas in the presence of 4 mM (A) or absence of glutamine (C). The wound's closure (width) of the PC knockdown was measured and shown as the means + standard deviation of that of the scrambled control which was arbitrarily set as 100% (B, D). The results were obtained from two independent experiments, each in triplicate. The statistical analysis was conducted using student's t-test where *$P < 0.05$.

We next examined the ability of the knockdown cells to invade through an extracellular matrix by performing an in vitro invasion assay using transwell coated with

Matrigel. As shown in Fig 7A and 7B, the PC knockdown cells showed a 40% reduction of their invasion ability. However, the reduced invasion ability was more pronounced (60%) in the glutamine-independent knockdown MDA-MB-231 cells (Fig 7C and 7D).

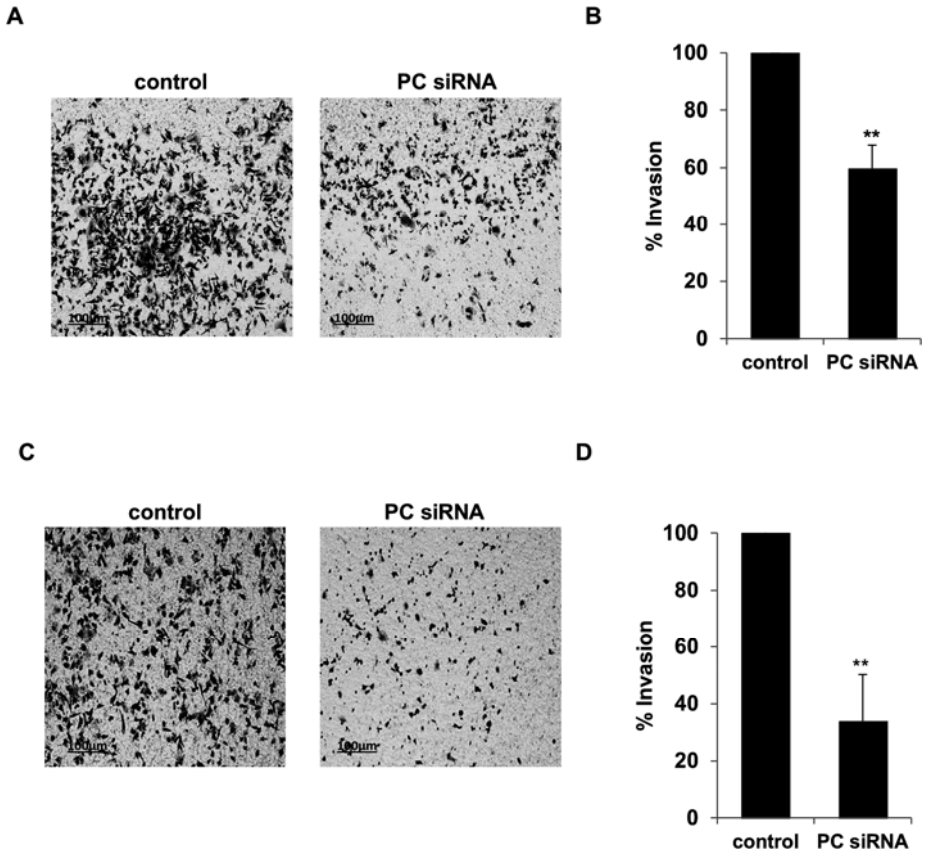

Fig 7. Suppression of PC expression in MDA-MB-231 lowers invasion ability. MDA-MB-231 cells were transiently transfected with PC or scrambled control siRNAs. At 48 h post transfection, an in vitro invasion assay was performed for 4 h in the presence of 4 mM (A) or 0 mM (C) glutamine. The number of PC siRNA-transfected cells that invaded the transwell coated with Matrigel was counted in 5 different fields and shown as means + standard deviation in comparison with that of the scrambled control which was arbitrarily set as 100% (B, D). The results were obtained from three independent experiments, each done in duplicate. The statistical analysis was conducted using student's t-test where ** $P < 0.01$.

We also performed similar experiments in MDA-MB-435 cells which also bear a high level of PC protein although its migration ability is less than MDA-MB-231. Suppression of PC mRNA expression by 80% (Fig 8A) resulted in 70% down-regulation of PC protein (Fig 8B and 8C). The PC knockdown MDA-MD-435 cells showed retarded growth rates at day 4

onwards (Fig 8D). Suppression of PC was also associated with 40% reduction of cell migration (Fig 8E) and 50% reduction of invasion ability (Fig 8F). Similar results were obtained when the knockdown cells were grown in the absence of glutamine (data not shown).

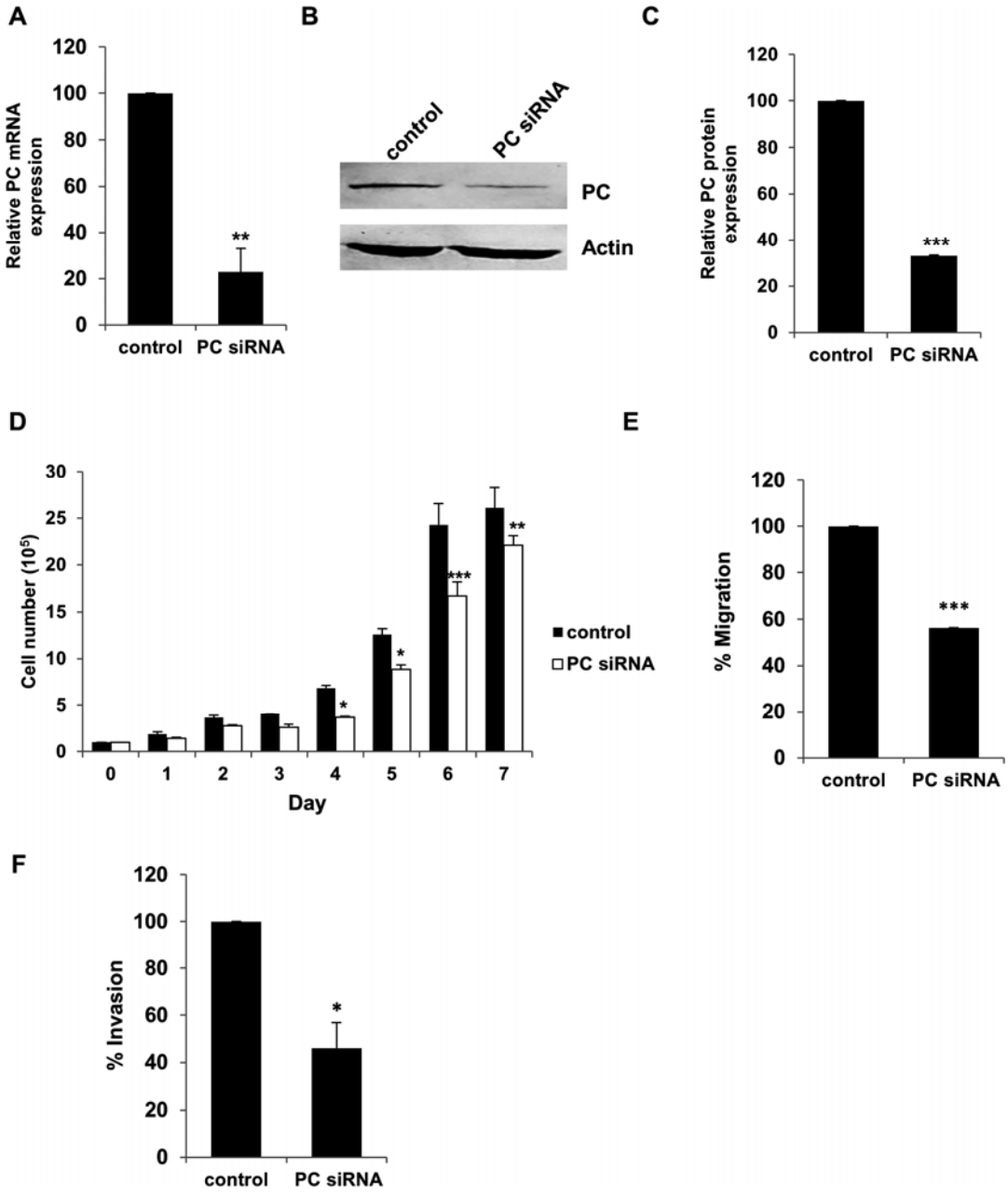

Fig 8. Suppression of PC expression in MDA-MB-435 cells reduces their proliferation, migration and invasion. PC mRNA expression in the knockdown MDA-MB-435 was quantitated by Q-PCR (A). Western blot analysis of MDA-MB-435 cells transfected with PC siRNA (PC siRNA) or scrambled control (Control) (B). The band intensity of PC in B was

quantitated and normalized with β-actin band and expressed as relative PC expression (C). Proliferation assay (D), migration assay (E) and invasion assay (F) of the PC knockdown MDA-MB-435 cells. The statistical analyses in B, C, E and F were conducted using student's t-test while in D was conducted using ANOVA test. *P < 0.05, **P < 0.01, ***P < 0.001.

Overexpression of PC in MCF-7 cells increases their proliferation and in vitro invasion

To confirm whether overexpression of PC in breast cancer cells with low metastatic ability would increase their proliferation rate and invasion ability, we generated stable MCF-7 cell overexpressing PC. As shown in Fig 9A, the proliferation rate of MCF-7 cells at day 3 onward of MCF-7 with overexpressed PC was 2-fold higher than the MCF-7 cell line transfected with an empty vector. Similar results were observed when the MCF-7 cell line with overexpressed PC was grown in glutamine-depleted medium (Fig 9B). It is noted that the level of endogenous PC was slightly increased in the MCF-7 cell line harboring empty vector when these cells were grown in the absence of glutamine, suggesting a compensatory increase of PC expression in response to the deprivation of glutamine. MCF-7 cells with overexpressed PC also showed 2-fold and 2.5-fold increases in the migration and invasion ability, respectively. Similar results were obtained when the cells were assayed under glutamine-depleted medium (Fig 9C and 9D).

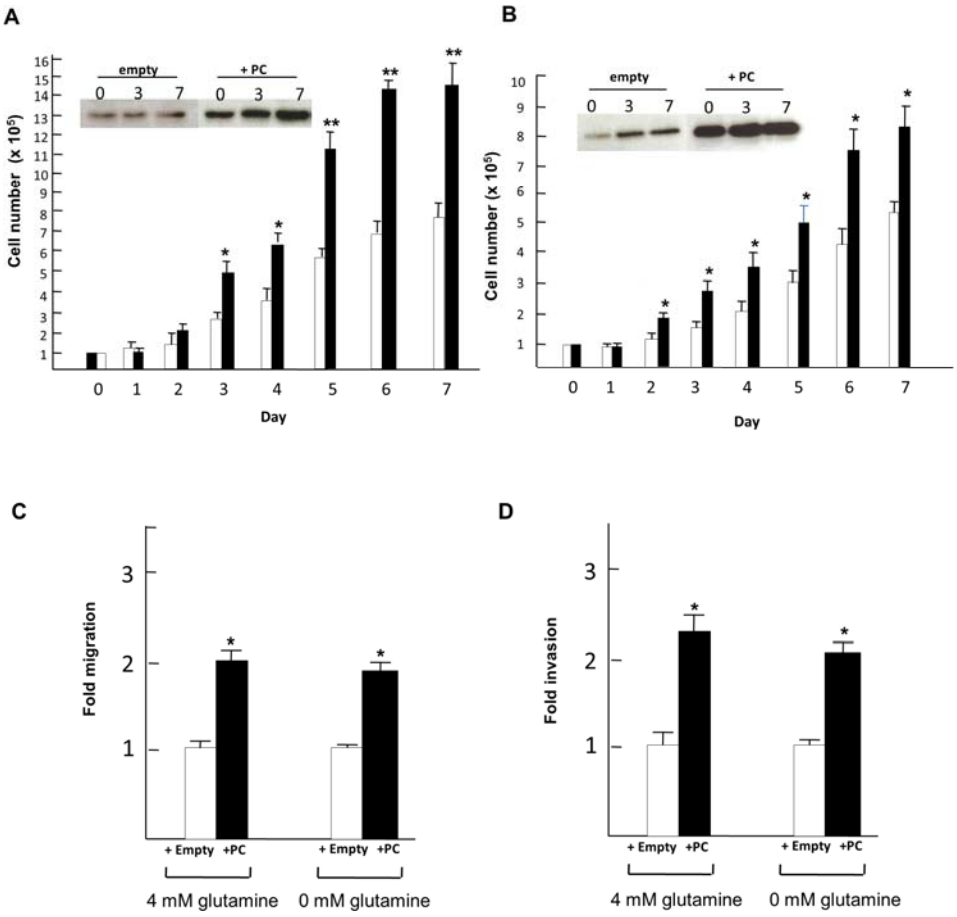

Fig 9. Overexpression of PC in MCF-7 cells increases their proliferation, migration and invasion. Proliferation rate of MCF-7 cells overexpressing PC grown in the medium containing 4 mM (A) or 0 mM glutamine (B). Insets in A and B are the Western blot analysis of MCF-7 cells transfected with empty vector (+empty, white bars) or with overexpressed PC (+PC, black bars) at days 0, 3 and 7. MCF-7 cells overexpressing PC grown in the presence or absence of glutamine were also subjected to migration (C) and invasion (D) assays. The statistical analysis was conducted using student's t-test where * $P < 0.05$, ** $P < 0.01$.

Discussion

Here we show that PC is also highly expressed in breast cancer tissue but not in the normal breast tissue. The statistical association between the levels of PC expression and the tumor size and stage prompted us to investigate the role of this enzyme in supporting growth and invasion. That expression of PC was highly abundant in two aggressive breast cancer cell lines, i.e. MDA-MB-231 and MDA-MB-435 but low in less aggressive cell lines, i.e. MCF-7 and SKBR3 hints at the involvement of this enzyme in the aggressive phenotype of these two metastatic cell lines. Suppression of PC expression in both MDA-MB-231 and MDA-MB-

435 cells retarded cell proliferation rate, suggesting that these cell lines modestly depend on anaplerosis via the PC reaction. The necessity for PC in supporting growth of MDA-MB-231 cells appears to be different from the SF-XL glioblastoma cell line which utilizes glutaminolysis rather than pyruvate carboxylation as the primary anaplerotic reaction [DeBerardinis et al., 2007] because suppression of PC expression does not affect its growth under glutamine-dependent conditions [Sellers et al., 2015]. However, under glutamine-depleted growth conditions, the PC-knockdown SF-XL glioblastoma cell line shows marked reduction (>80%) of proliferation [Sellers et al., 2015], indicating that the glioblastoma cell line uses pyruvate carboxylation as an alternative route to support its growth during glutamine-depleted conditions. However this is not the case for MDA-MB-231 and MDA-MB-435 cells because suppression of PC expression still allows them to grow, albeit at the 50% reduced proliferation rate observed under glutamine-dependent growth conditions. A similar but not identical phenotype of the PC-knockdown MDA-MB-231 and MDA-MB-435 cells was observed under glutamine-independent growth conditions. An involvement of PC in the growth phenotype of MDA-MB-231 cells is also consistent with the association between the levels of PC expression and sizes of breast tumor in clinical samples. Low expression levels of PC in breast tumors with a smaller size of tumor (< 4 cm3) may limit their growth compared with the larger size of tumors which contain higher levels of PC expression ($P < 0.05$) [Table 1]. The above observations were also confirmed by overexpression of PC in MCF-7, which is a low metastatic cell line. MCF-7 cells overexpressing PC show enhanced growth rate, motility and invasion. The enhanced growth phenotype of MCF-7 with overexpressed PC was consistent with previous reports which show that ectopic expression of PC in many mammalian cell lines enhances cell growth and biomass production [33,34,35].

Although several studies have pointed to the importance of PC in providing oxaloacetate which is the first TCA cycle intermediate, that in turn is converted to other precursor molecules such as citrate required for lipid and nucleic acid synthesis for rapid tumor growth, not much is known as to whether PC is required to support migration and invasion ability of some tumors [Fan et al., 2009; Cheng et al., 2011; Sellers et al., 2015]. Our present study is the first report to show a strong association between the levels of PC expression in breast tissues of patients and stages of cancer progression ($P < 0.05$), which suggests PC is involved in metastasis. This was also studied in MDA-MB-231 and MDA-MB-435 cells. Suppression of expression of PC markedly reduced both migration and invasion ability through an extracellular matrix under both glutamine-nourished and glutamine-depleted conditions, suggesting that PC is required to support these aggressive

phenotypes of MDA-MB-231 cells. The negative staining of PC expression by immunohistochemistry in the normal area of breast tissue is consistent with the low level of expression of PC in the MCF-7 cell line. The transcriptional mechanism underlying overexpression of PC in MDA-MB-231 over MCF-7 is due to the selective activation of the distal rather than the proximal promoter of the human PC gene (Fig 2C). The specific transcription of the distal rather than the proximal promoter of the human PC gene may be attributed to the presence of different putative transcription factor binding sites of both promoters [Thonpho et al., 2013] during the transition of a low to a high metastatic phenotype. Interestingly, Lee et al. (2012) have shown that the MCF-7 cells stimulated with Wnt 1 or Wnt3a ligands, or ectopically expressed with Snail, a target transcription factor of Wnt signaling, show a marked increase in PC expression. Because the Wnt signaling pathway also induces Snail-dependent epithelial-mesenchymal transition (EMT), which is responsible for invasion and metastasis in many tumors [Thiery et al., 2006; Yook et al., 2006], the authors suggest that anaplerosis via up-regulation of PC expression is one of several metabolic responses of breast tumor during EMT [Lee et al., 2012]. Although this study underscores that the Wnt signaling pathway is important for transcriptional induction of the PC gene, the authors cannot detect direct binding of Snail, an effector transcription factor in response to Wnt signaling to the distal promoter of human PC gene [Lee et al., 2012]. The lack of statistical association between expression of PC and ER as well as PR and HER2 in cancer breast tissues indicates that PC is not regulated by these hormones or growth factor. This is also consistent with the phenotypes of MCF-7 and MDA-MB-231 cells which are ER+ and ER-, respectively [Holliday and Speirs, 2011].

In summary we have shown that PC is expressed in breast cancer at a higher level than in the normal breast tissue, and exhibits a statistical association with tumor size and the progression of metastasis. Using the highly metastatic breast cancer cell lines, MDA-MB-231 and MDA-MB-435 as models, we showed that suppression of PC expression markedly reduces the proliferation, migration and in vitro invasion ability of cells, highlighting the possible roles of PC in supporting these processes during oncogenesis and progression of breast cancer.

PART III Identification of biochemical and metabolically changes in the PC knockdown cells

To identify which biochemical pathways and metabolites are altered by PC knockdown and contribute to the slow proliferation and decreased motility phenotypes in

MDA-MB-231 cells, stable PC knockdown MDA-MB-231 breast cancer cell line were generated and the levels of metabolites in the cells were analyzed by mass spectroscopy. This will enable us to locate which metabolic pathways that are perturbed.

Designation of Pcx shRNA constructs and generation of Pcx-knockdown MDA-MB-231 cell lines.

Six different shRNAs targeted to human pyruvate carboxylase (hPcx) coding sequence (ACCESSION BC011617.2) were designed using "siRNA Wizard v 3.1" (http://www.invivogen.com/sirnawizard/design.php). The oligonucleotides corresponding to the shRNA sequences with BamHI or HindIII restriction sites overhang at their 5′-ends were synthesized by Eurofins (Fisher Scientific, USA), and their sequences are shown in Table 1. Double stranded oligonucleotide cassettes with BamHI and HindIII sites at 5′- and 3′-ends were generated upon annealing each pair of oligonucleotides, and subsequently ligated at the BamHI and HindIII sites of the modified pSilencer 2.1-U6 puro TOL2 vector (Ambion, USA). The constructs carrying six different Pcx shRNA cassettes in the pSilencer 2.1-U6 puromycin vector were sequenced to confirm the correct oligo nucleotide sequence. Similarly, a scrambled shRNA control from Ambion (Life Technologies) (5′-ACTACCGTTGTTATAGGTG-3′) was cloned into the same vector to serve as a control.

Table 2

Oligonucleotides used to generate shRNA constructs for suppressing human pyruvate carboxylase (PC) expression.

Sequence name	Sequence (5′ 3′)	Length (bp)
PC 179 (forward)	GATCCTCGGAGTATAAGCCCATCAAGAATGTGCTTTTCTTGATGGGCTTATACTCCTTTTTGGAAA	66
PC 179 (reverse)	AGCTTTTCCAAAAAGGAGTATAAGCCCATCAAGAAAAGCACATTCTTGATGGGCTTATACTCCGAG	66
PC 847 (forward)	GATCCTCGGAACATCCTGCACCTGTATGTGCTTTACAGGTGCAGGATGTTCCTTTTTGGAAA	62
PC 847 (reverse)	AGCTTTTCCAAAAAGGAACATCCTGCACCTGTATGTGCTTTACAGGTGCAGGATGTTCCGAG	62
PC 2054 (forward)	GATCCTCCGTGGTCTTCAAGTTCTGTTGTGCTTACAGAACTTGAAGACCACGTTTTTGGAAA	62
PC 2054 (reverse)	AGCTTTTCCAAAAACGTGGTCTTCAAGTTCTGTTGTGCTTACAGAACTTGAAGACCACGGAG	62
PC 2096 (forward)	GATCCTCGGATGTCTTCCGTGTGTTTGATGTGCTTTCAAACACACGGAAGACATCCTTTTTGGAAA	66
PC 2096 (reverse)	AGCTTTTCCAAAAAGGATGTCTTCCGTGTGTTTGATGTGCTTTCAAACACACGGAAGACATCCGAG	66
PC 2653 (forward)	GATCCTCGCAACTCGGACGTGTATGATGTGCTTTCATACACGTCCGAGTTGCTTTTTGGAAA	62
PC 2653 (reverse)	AGCTTTTCCAAAAAGCAACTCGGACGTGTATGAAAGCACATCATACACGTCCGAGTTGCGAG	62
PC 3436 (forward)	GATCCTCGGAAGGTGATAGACATCAAAGTGTGCTTCTTTGATGTCTATCACCTTCCTTTTTGGAAA	66
PC 3436 (reverse)	AGCTTTTCCAAAAAGGAAGGTGATAGACATCAAAGTGTGCTTCTTTGATGTCTATCACCTTCCGAG	66

Generation of MDA-MB-231 PC knockdown cell lines.

Approximately 1 × 10^6 MDA-MB-231 cells were plated in a 35-mm culture dish (6-well plate) containing DMEM supplemented with 100 units/ml penicillin and 100 µg/ml streptomycin, and grown at 37 °C with 5% CO2 overnight. The cells were then transfected with 2.0 µg of shRNA expression constructs along with 1.0 µg of pCMV-Tol2 vector using Lipofectamine2000 (Life Technologies, USA). After 24 h, the cells were selected in the

complete medium containing 0.5 μg/ml puromycin (Invitrogen, USA) that was maintained throughout the selection. The MDA-MB-231 cell line stably transfected with a scrambled shRNA construct was similarly generated. Multiple puromycin resistant colonies were formed after 15 days of selection. Thus each "cell line" is actually a population of PC knockdown cells rather than a single clone. The selected cells were expanded and maintained in selection media at all times before subsequent biochemical analyses.

Quantitative real time reverse transcriptase polymerase chain reaction (QRT-PCR)

Total RNA was extracted from cells using RNeasy mini kit (Qiagen) following the manufacturer's instructions. The 10 μl RT reaction contained 2 μg of total RNA and oligo(dT) primers (Ambion) at 85 °C for 3 min and chilled at 4 °C. Reverse transcription was initiated by adding 10 μl of mixture containing 2 μl 10x RT buffer, 0.5 mM dNTP mix, 2 units of RNase inhibitor and reverse transcriptase (Ambion), to the primed-RNA mixture and the reaction was incubated at 43 °C for 60 min, 92 °C for 10 min and held at 4 °C, respectively. The cDNA was stored at − 20 °C until used. Quantitative real time PCR was performed using SYBR Premium Ex Taq (Takara) using MyiQ™ single-color real time PCR detection system (BioRad). The standard curve of PC cDNA was obtained from amplification plots of PC prepared from various dilutions of MDA-MB-231 cDNAs. The expression of PC mRNA was normalized to the glutamate dehydrogenase (GLUD) mRNA level and is shown as the relative gene expression. Fold change was calculated using the Δ Q method. The thermal profiles consisted of initial denaturation at 95 °C for 3 min followed by 40 cycles of denaturation at 95 °C for 10 s and annealing at 60 °C for 20 s and extension at 72 °C for 30 s.

Cell viability assay

The numbers of viable cells were determined with the CellTiter 96® AQueous One Solution Cell Proliferation Assay (MTS) kit (Promega). Four thousand cells of various stable PC knockdown MDA-MB-231 cell lines were plated into 96 well plates and grown in DMEM supplement with 10% (v/v) FBS, 100 units/ml penicillin and 100 μg/ml streptomycin, at 37 °C in a CO2 incubator overnight. Twenty microliters of CellTiter one solution reagent was added to the cells and incubated at 37 °C in CO2 incubator for 1 h. The amount of soluble formazan was measured immediately using a 96-well plate reader (Molecular Devices) at 490 nm. The absorbance is directly proportional to the number of viable cells in culture.

Cell proliferation

2×10^4 cells of the PC-knockdown MDA-MB-231 or the scrambled shRNA control cell line were plated into 35 mm2 dishes and cultured in complete DMEM supplemented with 1.0 μg/ml puromycin at 37 °C with 5% CO_2. Cells were trypsinized and counted by staining with 0.4% (w/v) trypan blue (Gibco) at days 4, 5, 6 and 7.

PC enzyme activity

The cells were trypsinized off tissue culture plates with 0.05% trypsin and 0.5 mM EDTA. The cell pellet was washed twice with PBS and suspended in KMSH solution containing a protease inhibitor mixture (Pierce). PC enzyme activity was measured as previously described [Hanson et al., 2008]. Ten microliters of the homogenate was incubated in a final volume of 50 μl of enzyme reaction mixture of 100 mM KCl, 10 mM MgCl2, 2 mM Na-ATP, 0.1% Triton X-100, 1 mM DTT, 1.6 mM acetyl CoA, 20 mM NaHCO3, 0.2 μCi [^{14}C]NaHCO3, and 100 mM Tris-Cl buffer, pH 7.85 with or without 8 mM pyruvate at 37 °C for 30 min. The reaction was stopped by adding 50 μl 10% (v/v) trichloroacetic acid and after 10 min, 80 μl of the mixture was removed and added to a 20 ml scintillation vial that was left open for 2 h to allow evaporation of the unincorporated CO_2. Then, 0.5 ml of water and 5 ml of Scintisafe scintillation mixture (catalog number SX21-5, Fisher Scientific) were added to the vial and the carbon fixed was measured by liquid scintillation spectrometry. Background radioactivity present in the absence of pyruvate was subtracted from the radioactivity in the presence of pyruvate to give the enzyme rate attributable to PC enzyme activity.

Measurement of pyruvate, malate and citrate from PC knockdown cells by alkali enhanced fluorescence

The cells were maintained in DMEM cell culture medium (contains 25 mM glucose and 4 mM glutamine) 10% (v/v) FBS 100 units/ml penicillin and 100 μg/ml streptomycin with 0.5 μg/ml puromycin on 150 mm. culture plates. The media was changed to RPMI 1640 cell culture medium (contains 2 mM glutamine) modified to contain 5 mM glucose the day before the experiment. On the day of the experiment the cells were washed twice with PBS and once with Krebs Ringer solution. Five milliliters of Krebs Ringer bicarbonate solution, pH 7.3, containing no glucose was added to the plates of cells, and the cells were incubated at 37 °C. After 10 min Krebs Ringer bicarbonate solution containing 10 mM glucose was added and the cells were incubated at 37 °C. After 35 min all liquid was quickly removed from the cells and the plates were put on ice. Then 0.75 ml of 6% PCA was added and the cells were scraped off the plates and transferred into the microtube. The mixture was homogenized and

centrifuged to precipitate the protein and the supernatant fraction was neutralized with 30% KOH. The resulting precipitated potassium perchlorate was removed by centrifugation and the metabolite concentrations in the neutralized extract were measured by alkali enhanced fluorescence, as previously described [Hansan et al., 2008].

Metabolites analysis by LC-MS and GC-MS

The cells were maintained in DMEM supplemented with 10% (v/v) FBS, 100 units/ml penicillin, 100 µg/ml streptomycin, and 0.5 µg/ml puromycin. Cells were plated at a density of 14 × 103 cells/cm2 in 6 cm culture dishes at 37 °C and 5% CO2 in a humidified atmosphere to 70% confluence over 5 days prior to experimentation. On the day of an experiment metabolism was stopped in four plates of each cell line and cells were harvested and saved for LC-MS analysis (time zero control). The medium was changed to DMEM without FBS modified to contain 10 mM 13C6-glucose plus 2 mM glutamine or 2 mM 13C5-glutamine plus 10 mM glucose. Four plates of each cell line were used for each condition. After incubation for 1 h, metabolism of cells was stopped and cells were harvested and analyzed with LC-MS as previously described [Lorenz et al., 2011; Lorenz et al., 2013].

Enzyme activities

Homogenates were prepared and activities of all enzymes except citrate synthase were measured as previously described [MacDonald et al., 2011]. The activity of citrate synthase was measured as described in reference [Srere et al., 1969].

RESULT

The PC enzyme activity of the MDA-MB-231 cell line, which is a highly invasive breast cancer cell line, was 10-fold higher than the PC enzyme activity of the less invasive breast cancer cell line MCF-7 (Table 3).

Table 3

Pyruvate carboxylase (PC) enzyme activity is much higher in the invasive breast cancer cell line MDA-MB-231 than in the less invasive breast cancer cell line MCF-7. Results are means ± SE nmol CO_2 fixed/min/mg cell protein of 4 replicate measurements.

Cell line	PC enzyme activity (nmol CO_2 fixed/min)
MDA-MB-231	13.2 ± 0.6
MCF-7	1.2 ± 0.2

Six shRNA constructs (PC179, PC847, PC2054, PC2096, PC2653 and PC3436) targeted to human PC mRNA were transfected to MDA-MB-231 cells. The stable cell lines were named according to the first nucleotide of the PC mRNA sequence targeted. Fig. 10A and 10 B show that the degree of knockdown of PC mRNA correlated fairly well with the degree of knockdown of PC enzyme activity and PC protein in the various PC targeted cell lines. As we have previously observed, knockdown of PC enzyme activity and PC protein, although correlated well with the degree of mRNA knockdown was in general slightly less than the knockdown of PC mRNA [Hansan et al., 2008]. Cell line PC 2096 4B possessed a PC mRNA level of approximately 10% compared to the scrambled shRNA control cell line, while cell lines PC 179 1A, PC 847 2C, PC 2054 3D, PC 3436 6A and PC 3436 6C contained PC mRNA levels of 20–40% that of the scrambled shRNA control cell line. Only modest reductions (50–70%) of PC mRNA level were observed in cell lines PC 179 1B, PC 2054 3A and PC 2096 4C, while the level of PC mRNA was not decreased in cell lines PC 2653 5A and PC 2653 5B. PC enzyme activity of these cell lines was proportional to the levels of PC mRNA, with PC enzyme activity being lowest (5%) in the PC 2096 4B cell line (Fig. 10B). Cell lines PC 2096 4B, PC 179 1A, PC 847 2C, PC 2054 3D, PC 3436 6C and PC 2653 5B showed the highest, modest and lowest PC knockdown levels, respectively.

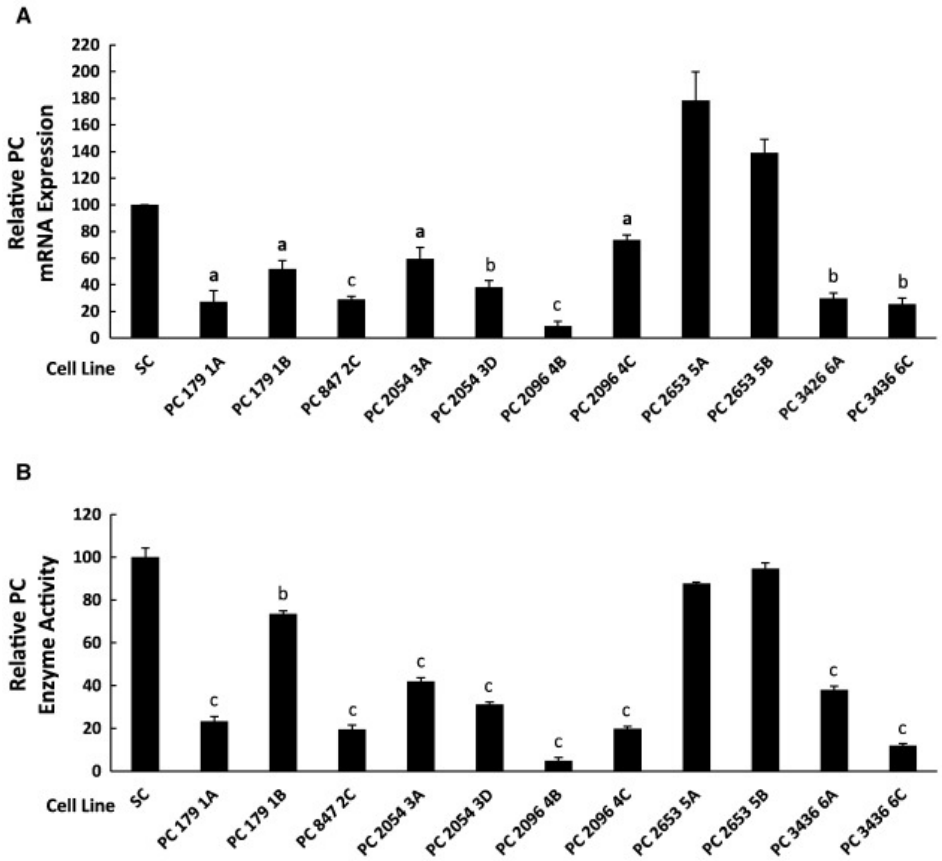

Figure 10. Decreased pyruvate carboxylase mRNA levels induced by gene silencing correlate with decreased PC enzyme activity in multiple cell lines derived from the breast cancer cell line MDA-MB 231. A, Relative pyruvate carboxylase (PC) mRNA expression in various PC knockdown cell lines (179 1A, 179 1B, 847 2C, 2054 3A, 2054 3D, 2096 4B, 2096 4C, 2653 5A, 2653 5B, 3426 6A, 3436 6C and scramble control (SC)). B, PC enzyme activity of PC knockdown cell lines relative to that of the scramble control which was arbitrarily set as 100%. ap < 0.05; bp < 0.01; cp < 0.001 vs scramble control.

Cell lines with lower PC mRNA and enzyme activity showed lower cell viability (Fig. 11A and 11 B). We selected two cell lines, PC 847 2C and PC 2096 4B, for further analysis of cell growth. Both knockdown cell lines showed decreased cell numbers at day 4, that became more obvious at days 5–7, with the PC 847 2C cell line showing a 35% lower cell count vs. the scrambled shRNA control cell line at day 7 and the PC 2096 B cell line showing a 65% lower cell count vs. the control cell line at day 7 (Fig. 11C).

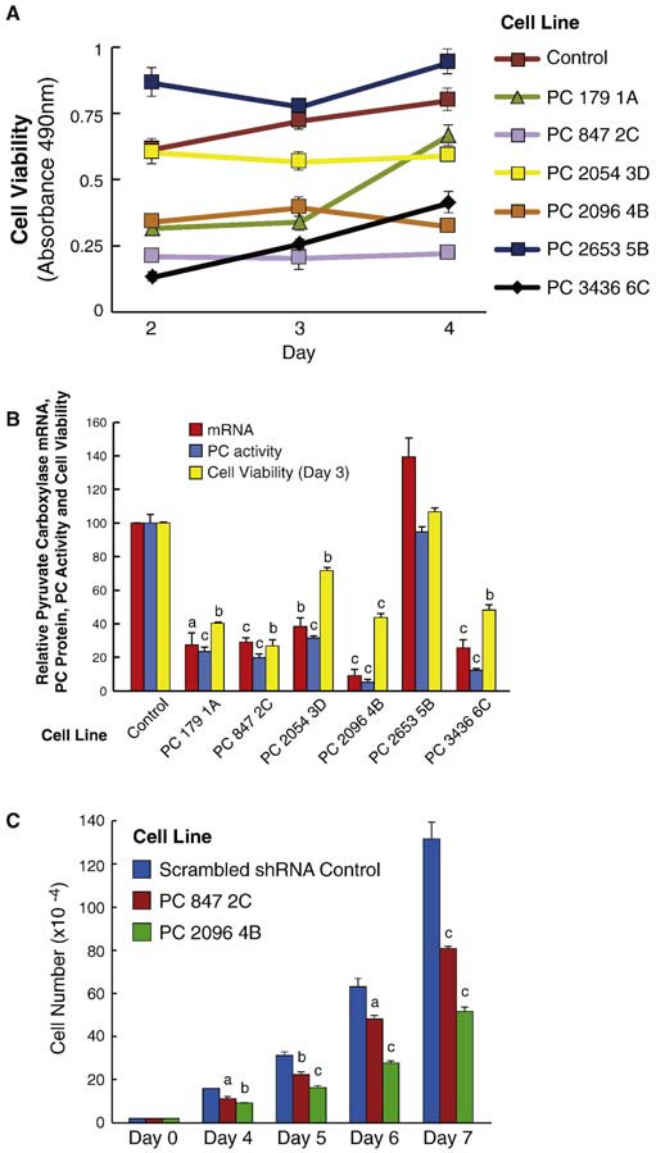

Fig. 11. Knockdown of pyruvate carboxylase (PC) mRNA and PC enzyme activity correlate with decreased breast cancer cell viability and growth. A, Viability of cells was measured with the MTS assay at days 2, 3 and 4. $p > 0.001$ vs the RNA scramble control of the four cell lines with the lowest viability. $p < 0.05$ for PC 2054 3D vs the control. B, PC mRNA, PC enzyme activity and viability of various knockdown cells at day 3. $a_p < 0.05$; $b_p < 0.01$, $c_p > 0.001$ vs RNA scramble control. C. Decreased cell counts in the PC 2096 4B and PC 847 2C cell lines with knockdown of PC. $a_p < 0.05$; $b_p < 0.01$, $c_p > 0.001$ vs RNA scramble control.

Because most cancers use glucose and glutamine as the two main carbon sources for both energy production and biosynthesis [Vander Heiden et al., 2009], we used uniformly labeled

^{13}C6-glucose or ^{13}C5-glutamine and LC-MS or GC-MS to track the fluxes of these two substrates into the synthesis of various metabolites. This allowed us to distinguish which of the fluxes of the carbon sources might be more impaired in the PC knockdown cell lines PC 847 2C and PC 2096 4B compared to the shRNA scramble control MDA-MB-231 cell line. Prior to the experiment these three cell lines were maintained in DMEM cell culture medium for four or more days. DMEM is the standard cell culture medium used for maintaining the MDA-MB-231 cell line and it contains 25 mM glucose and 4 mM glutamine. For the LC-MS/MS analysis experiment, the cell lines were maintained for 1 h in DMEM medium modified to contain either 10 mM U-^{13}C6 glucose plus 2 mM unlabeled glutamine or 2 mM U-^{13}C5 glutamine plus 10 mM unlabeled glucose. For the experiment to look for a crossover point in the levels of the metabolites around the PC reaction, the cells were incubated in the presence of 5 mM glucose in RPMI 1640 cell culture medium because the high concentration of glucose in the DMEM medium would produce high levels of metabolites possibly obscuring a crossover point in the levels of the metabolites.

As expected, because PC is a mitochondrial enzyme its suppression did not affect the levels of glycolytic intermediates as glucose-6-phosphate, fructose-6-phosphate and fructose bisphosphate were not altered in each of these PC knockdown cell lines (Fig. 12A and 12 B). Also as expected, glucose-6-phosphate and fructose-6-phosphate were labeled from U-13C6 glucose but not from U-^{13}C5 glutamine (Fig. 12C and D).

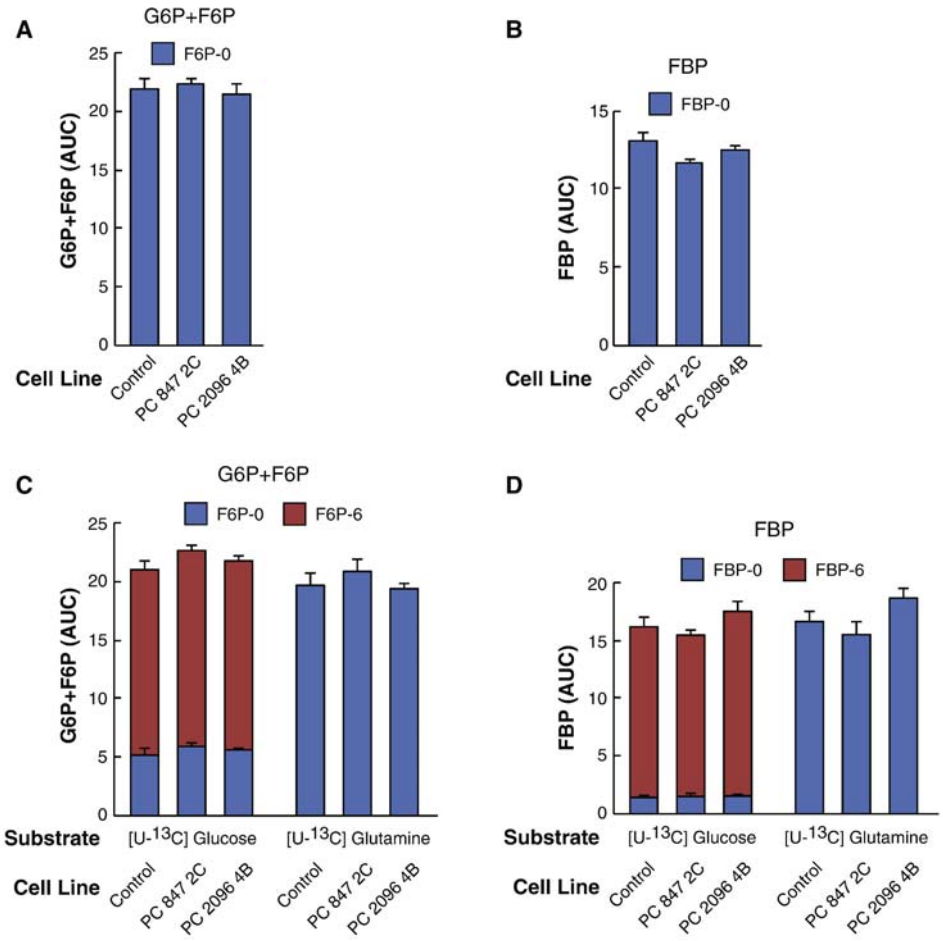

Fig. 12. **Knockdown of pyruvate carboxylase (PC) expression does not alter the levels of glycolytic intermediates glucose-6-phosphate plus fructose-6-phosphate or fructose-biphosphate from U-13C6-glucose or U-13C5-glutamine in MDA-MB-231-derived cell lines.** PC 847 2C and PC 2096 4B or a scramble shRNA control cell line were maintained in DMEM cell culture medium (contains 25 mM glucose and 4 mM glutamine) and 10% FBS for four or more days. Cells were then maintained in DMEM medium containing either 10 mM [U-13C6] glucose or 2 mM [U-13C5]glutamine for 1 h before metabolism was stopped and cells were analyzed by LC-MS/MS as described under Experimental Procedures. A, The levels of glucose-6-phosphate (G6P) plus fructose-6-phosphate (F6P) before the uniformly labeled glucose or glutamine was added (zero time point). B, The level of fructose-1,6-bisphosphate (FBP) before the uniformly labeled glucose or glutamine was added (zero time point). C and D, Upon adding the labeled glucose or glutamine to the culture media, the metabolites were extracted and analyzed by LC-MS/MS spectroscopy. Fractions of different isotopomers of U-13C glucose-6-phosphate plus U-13C fructose-6-phosphate or fructose-biphosphate are shown within the bars. AUC indicates “area under the curve”.

The immediate product of the PC reaction is oxaloacetate which is then directly converted to malate and citrate (Fig. 13). Oxaloacetate is very unstable and its concentration in most tissues is so low (about 5 μM) that it is impractical to accurately measure its concentration. Therefore, the levels of 13C incorporation into the immediate metabolites of oxaloacetate, which are citrate and malate, were measured. In the mass spectrometry experiments using either LC-MS/MS or GCMS, metabolite levels were measured in the cell lines immediately before (zero time control) and then 60 min after 10 mM [U^{-1}3C]glucose or 2 mM [U-13C]glutamine were added to the cells. Strong suppression of PC expression (cell line PC 2096 4B) markedly decreased the levels of both citrate and malate and decreased the incorporation of carbon from glucose and glutamine into citrate and malate (Fig. 14). Citrate was mainly + 2 labeled with 13C6-glucose, suggesting that pyruvate dehydrogenase supplied acetyl-CoA that was incorporated into citrate in the citrate synthase reaction. In contrast, malate was about equally + 2 labeled and + 3 labeled from 13C6-glucose. This indicates that the + 3 labeled malate came from oxaloacetate formed in the PC reaction and the + 2 labeled malate came from the citric acid cycle after the pyruvate dehydrogenase reaction produced + 2 labeled acetyl-CoA that was incorporated into citrate that then became + 2 labeled malate after flux through the citrate-pyruvate cycle or through the citric acid cycle. 13C5 labeled glutamine produced mostly + 4 labeled citrate and malate that entered mitochondrial metabolism through α-ketoglutarate derived from glutamate in the glutamate dehydrogenase reaction. The decreased 13C incorporation into malate and citrate from glucose and glutamine in the PC 2096 4B cell line can be explained by PC knockdown inhibiting pyruvate flux through the citrate-pyruvate and the malate-pyruvate cycles.

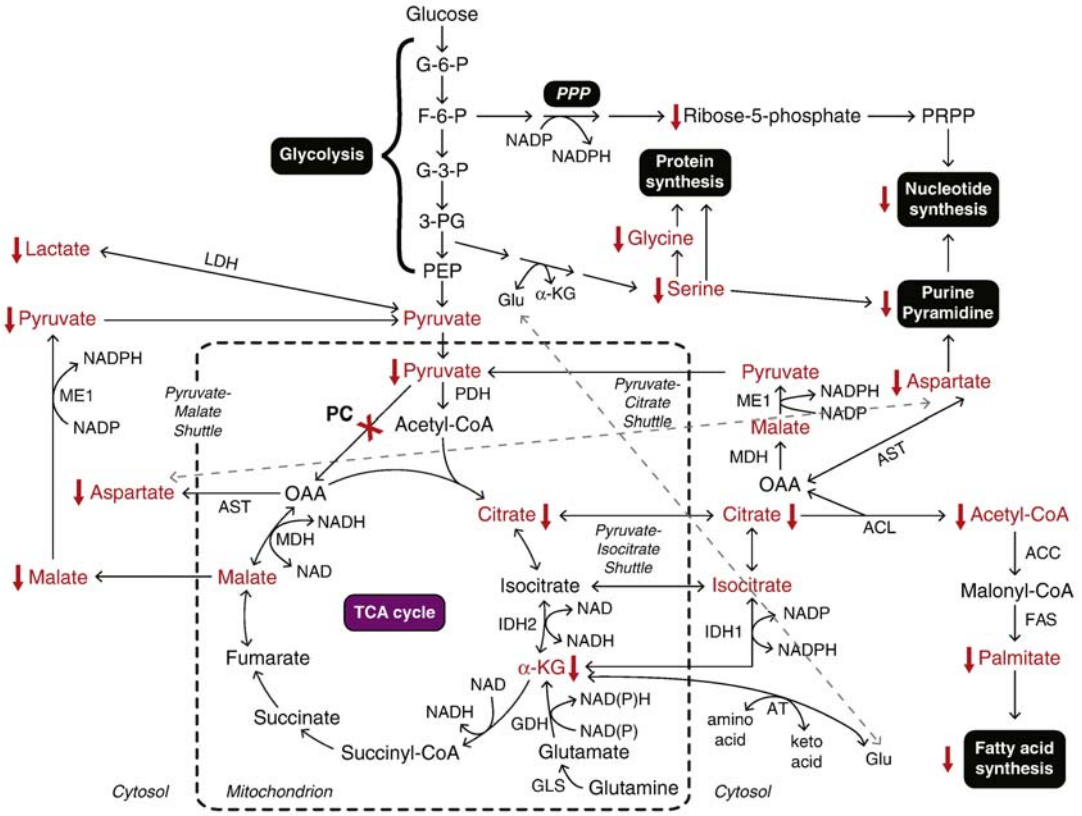

Fig. 13. Schematic summary of metabolic pathways disturbance caused by suppression of pyruvate carboxylase in MDA-MB-231-derived cell lines. The abbreviations used are: ACC, acetyl-CoA carboxylase; α-KG, α-ketoglutarate; AT, aminotransferase; ACL, ATP-citrate lyase; AST, aspartate aminotransferase; F-6-P, fructose-6-phosphate; FAS, fatty acid synthase; G-3-P, glyceraldehyde-3-phosphate; G-6-P, glucose-6-phosphate; GDH, glutamate dehydrogenase; GLS, glutaminase; Glu, glutamate; IDH1, isocitrate dehydrogenase 1; IDH2, isocitrate dehydrogenase 2; LDH, lactate dehydrogenase; MDH, malate dehydrogenase; ME, cytosolic malic enzyme; 3-PG, 3-bisphosphoglycerate; PC, pyruvate carboxylase; PDH, pyruvate dehydrogenase; PEP, phosphoenolpyruvate; PPP, pentose phosphate pathway; PRPP, phosphoribosylpyrophosphate. Metabolites that are altered in the knockdown cell lines are shown in red.

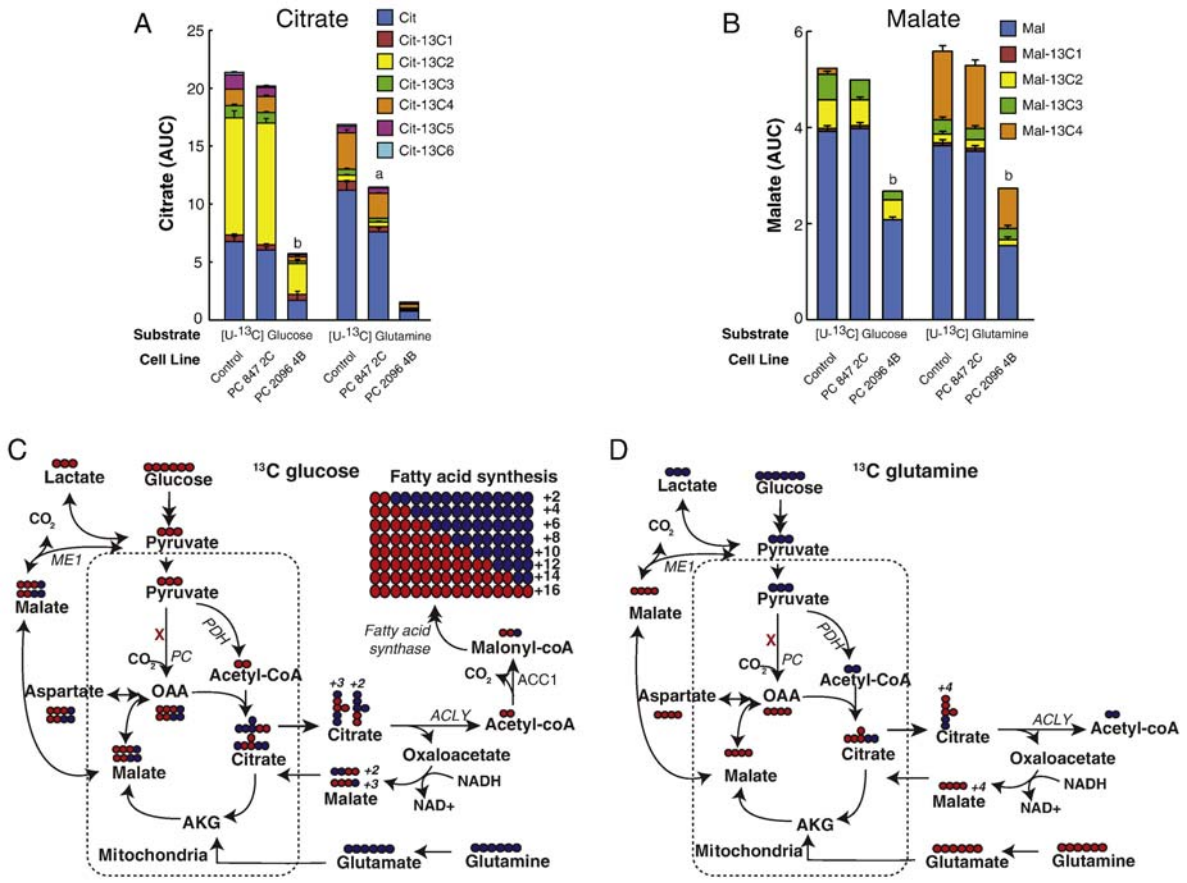

Fig. 14. Decreased labeled citrate and malate from U-^{13}C6-glucose or U-^{13}C5-glutamine in pyruvate carboxylase (PC) knockdown cell lines derived from the MDA-MB-231 breast cancer cell line. PC 847 2C and PC 2096 4B cell lines or the scramble control cell line were maintained in the presence of U-^{13}C6 glucose or U-^{13}C5 glutamine for 1 h in the same experiment described in Fig. 3. Fractions of different isotopomers of 13C citrate (A) and 13C malate (B) in the PC knockdown cell lines and scramble control cell line are shown within the same bars. ap < 0.01, bp < 0.001 vs scramble control. Metabolic pathways showing incorporation and distribution of labeled carbon from 13C6-glucose (C) or 13C5-glutamine (D) to various downstream metabolites. Labeled glucose and glutamine are indicated in red while unlabeled glucose and glutamine are indicated in blue. Abbreviations: ACC1, acetyl-CoA carboxylase1; α-KG, α-ketoglutarate; ACLY, ATP-citrate lyase; PC, pyruvate carboxylase; PDH, pyruvate dehydrogenase.

To confirm the mass spectrometry measurements the levels of malate and citrate were measured by alkali-enhanced fluorescence in cell lines maintained in RPMI 1640 tissue culture medium (usually contains 11.1 mM glucose and 2 mM glutamine) modified to contain

a physiologically normal concentration of glucose (5 mM) (and still 2 mM glutamine) for one day followed by a brief starvation period in the presence of no fuel and then a 35 min incubation period in Krebs Ringer bicarbonate buffer solution containing 10 mM glucose. Similarly to the mass spectrometry measurements of malate and citrate in the cell lines maintained in DMEM cell culture medium the cell lines with knocked down PC maintained in the modified RPMI 1640 medium followed by the Krebs Ringer solution, the PC knockdown cell lines PC 847 2C, PC 2096 4B and PC 179 1A, showed decreased levels of malate and citrate compared to the control cell line containing a scrambled shRNA (Fig. 15).

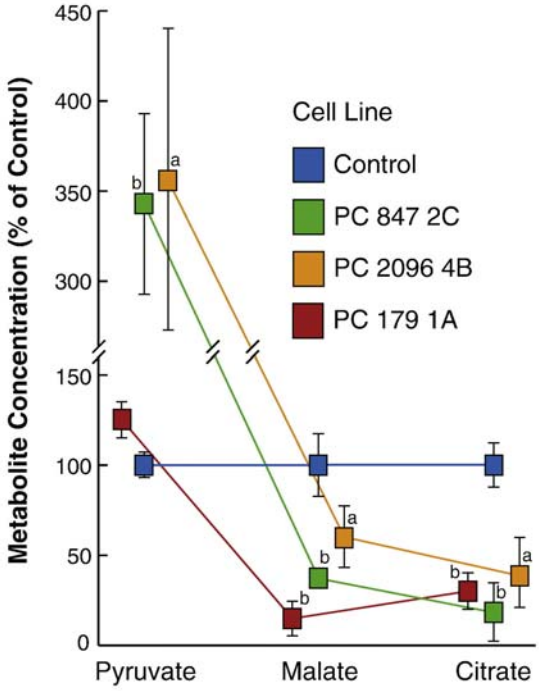

Fig. 15. **An increase in pyruvate and decreases in malate and citrate in pyruvate carboxylase (PC) knockdown MDA-MB-231 cells show a cross over point at the PC consistent with inhibition of the PC reactio**n. PC 847 2C, PC 2096 4B and PC179 1A cell lines and the scramble shRNA control cell line were maintained in RPMI 1640 medium containing 5 mM glucose for 22 h and then in Krebs Ringer bicarbonate solution containing 10 mM glucose for 35 min before the concentrations of metabolites were measured as described under Experimental Procedures. The concentrations of each metabolite in the three PC knockdown cell lines are shown relative to those of the scramble shRNA control cell line were measured by alkali enhanced fluorescence. $a_p < 0.05$, $b_p < 0.01$ vs scramble control.

The mass spectrometry measurements showed that pyruvate was mostly labeled from glucose rather than from glutamine (Fig. 14A). Suppression of PC caused a marked reduction in the level of glucose-derived pyruvate in the mass spectrometry experiments in which the cells were cultured in DMEM for four or more days prior to the experiment (see Fig. 14A). Since pyruvate is the substrate for the PC reaction, it might be expected that suppression of PC expression would result in the accumulation of pyruvate, which is the substrate of PC, as we previously observed in pancreatic beta cells with knocked down PC [Hasan et al., 2008]. The lower levels of pyruvate seen in the PC knockdown cell lines were likely due to decreased malate and citrate cycling to pyruvate because the levels of these two metabolites were markedly decreased by PC knockdown (Fig. 14). As shown in Fig. 13, malate can exit mitochondria and be converted back to pyruvate by malic enzyme in the cytosol. Pyruvate can then re-enter mitochondria and be reconverted to oxaloacetate by PC (the pyruvate-malate shuttle) (MacDonald et al., 1995; MacDonald et al., 2005). Alternatively in the pyruvate-citrate shuttle, citrate can exit mitochondria and be converted to oxaloacetate and acetyl-CoA by ATP-citrate lyase [MacDonald et al., 2005; Farfari et al., 2000]. Oxaloacetate can then be converted to malate by cytosolic malate dehydrogenase. Malic enzyme can then convert malate to pyruvate the same as in the pyruvate-malate cycle. The malate-pyruvate and citrate-pyruvate cycles are very active in pancreatic beta cells where PC protein and enzyme activity are high and support these cycles (MacDonald et al., 1995; MacDonald et al., 2005). The low pyruvate also explains the low level of lactate (Fig. 16B), which is the redox partner of pyruvate, in these cells. Because glycolysis was not inhibited (Fig. 12), the decreased 13C6-glucose incorporation into pyruvate and lactate in the two PC knockdown cell lines (Fig. 16A and 16B) can only be explained by a decreased activity of pyruvate cycling due to decreased PC enzyme activity.

The concentration of glucose in the cell culture medium can have a strong influence on the concentration of pyruvate in the cells. As mentioned above, for LC-MS or GC-MS analysis the cells were maintained for four or more days in DMEM cell culture medium right up to the time of the experiment when the cells were maintained in DMEM medium modified to contain 10 mM glucose and 2 mM glutamine for 60 min. DMEM contains a high concentration of glucose (25 mM glucose) and glutamine (4 mM) which are much higher concentrations of these fuels than in the RPMI 1640 cell culture medium that was modified to contain 5 mM glucose (and contains 2 mM glutamine) that the cells were maintained in for 24 h before the cells were incubated in Krebs Ringer bicarbonate solution for the experiments in which malate, citrate and pyruvate were measured by alkali enhanced fluorescence.

Because the concentration of glucose was so high in the DMEM medium, it was expected that this could cause a higher level of pyruvate in both the control and PC knockdown cell lines making it difficult to see a crossover point with an expected even higher level of pyruvate in the PC knockdown cell lines. Therefore the incubation conditions of the experiment shown in Fig. 15 were made identical to those of a previous experiment with pancreatic beta cells in which the cell lines were incubated in the presence of the physiological concentration of glucose and glucose-starved for a short time period enabling us to observe an increase in pyruvate after glucose (10 mM) was added to the cells for 30 min [Hasan et al., 2008]. Similarly to experiments in which pure beta cells with knocked down PC were maintained at a physiological concentration of glucose prior to a 35 min incubation with 10 mM glucose, an increase in pyruvate was observed along with the decreases in malate and citrate in all three PC knockdown cell lines shown in Fig. 15. This crossover point with high pyruvate and low malate and low citrate [Hasan et al., 2008] is consistent with a block at the PC reaction [MacDonald et al., 1995; MacDonald et al., 2005]. The levels of malate and citrate were much lower in cell line PC 179 1A than in the other two PC knockdown cell lines shown in Fig. 6, and the level of pyruvate was increased less than in the other two cell lines in this cell line (only 24% higher than in the control cell line, as compared to 350% higher in the other two PC knockdown cell lines (Fig. 15). Cell line PC 179 1A also showed a 50% lower level of malic enzyme that, in addition to the extremely low levels of the substrates malate and citrate could contribute to decreased pyruvate cycling.

The decreased levels of acetyl-CoA (Fig. 16C) and the decreased labeling of acetyl-CoA from glucose (Fig. 16D) in the PC 2096 4B cell line are also likely due to the decreased citrate levels. Most of the + 2 labeled acetyl-CoA would be expected to come from the pyruvate dehydrogenase reaction. However, there was slightly decreased + 2 labeling of acetyl-CoA from glucose and from glutamine in the PC 2096 4B cell line (Fig. 16D) and this can only be explained by the decreased PC enzyme activity inhibiting flux of citrate through the citrate-pyruvate cycle. The lower concentrations of total cellular acetyl-CoA (Fig. 16C) and lower 13C incorporation into acetyl-CoA (Fig. 16D) in the PC knockdown cells are consistent with a lower cytosolic level of acetyl-CoA resulting from decreased formation of mitochondrial citrate and its export to the cytosol via the pathway that uses ATP citrate lyase shown in Fig. 13.

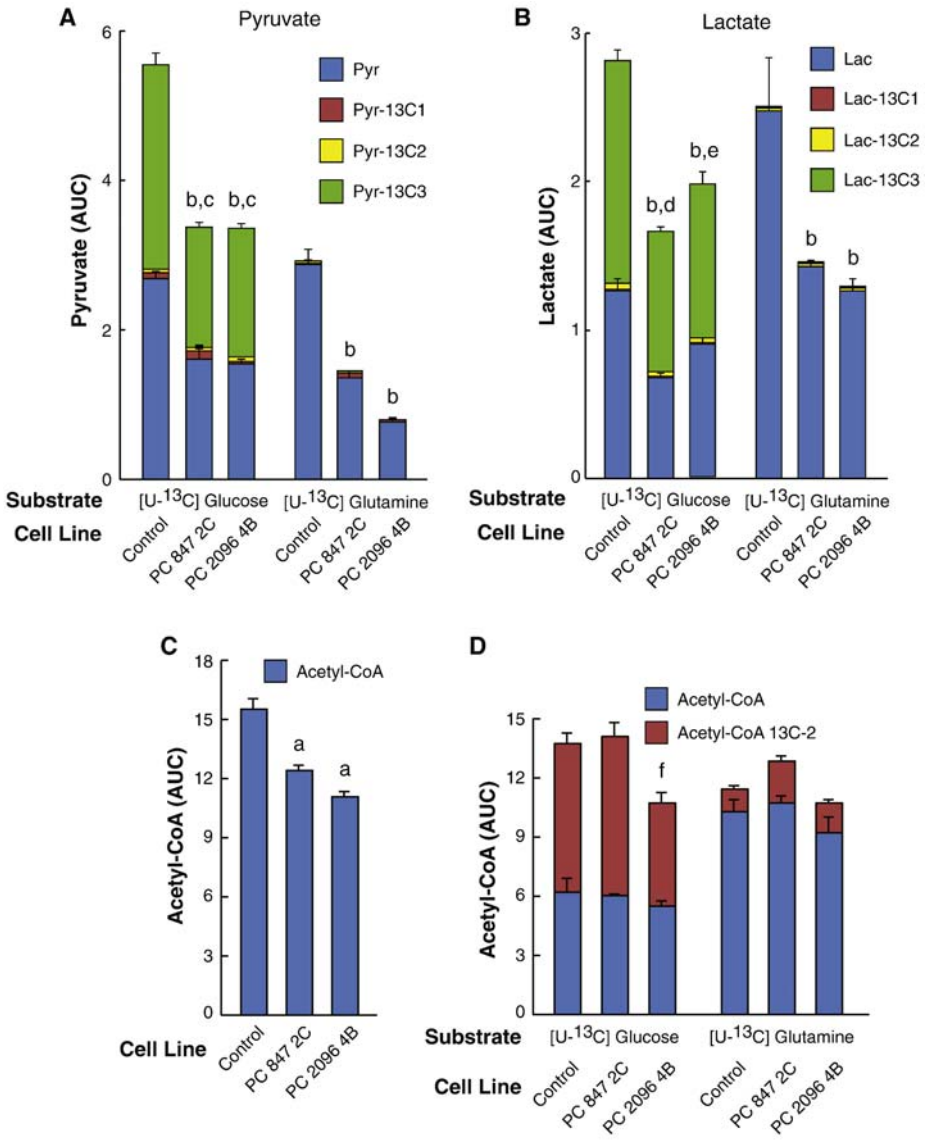

Fig. 16. Decreased labeled pyruvate, lactate and acetyl-CoA from U-13C6-glucose or U-13C5-glutamine in pyruvate carboxylase (PC) knockdown cell lines derived from the MDA-MB 231 breast cancer cell line. PC 847 2C and PC 2096 4B cell lines or scramble control cell line were maintained in the presence of U-13C6 glucose or U-13C5 glutamine for 1 h in the same experiment described in Fig. 3. Fractions of different isotopomers of 13C-pyruvate (A), 13C–lactate (B) or 13C-acetyl-CoA (D) in the PC knockdown cell lines and the scramble control cell line are shown within the same bars. C, The levels of acetyl-CoA in cells before labeled glucose or glutamine was added to the culture media. ap < 0.01; bp < 0.001 total metabolite vs scramble control same substrate; cp < 0.01 Pyr-13C3 vs scramble control; dp < 0.001 or ep < 0.01 Lac-13C3 vs scramble control; fp < 0.05 acetyl-CoA-13C2 vs scramble control.

Aspartate was labeled from both glucose and glutamine, albeit slightly more from glutamine, indicating that both nutrients contribute to aspartate synthesis (Fig. 17). Aspartate is produced directly from oxaloacetate catalyzed by aspartate aminotransferase. Suppression of PC expression should lower oxaloacetate, resulting in a lowered level of aspartate. As expected, the decrease of + 2 and + 3 aspartate from glucose and + 4 labeled aspartate from glutamine in the PC 2096 4B cell line are consistent with a depleted oxaloacetate level caused by PC suppression in the case of labeling from glucose and decreased activity of the citrate-pyruvate cycle in the case of labeling from glutamine (Fig. 17). Both PC 847 2C and PC 2096 4B knockdown cell lines showed decreased levels of serine and glycine (Fig. 17). The negligible or absent incorporation of 13C from glucose and glutamine into both amino acids is due to the short incubation time of the cells in the presence of the labeled glucose or glutamine and indicates that the levels of these two amino acids was low before two cells were incubated in the presence of the labeled fuels.

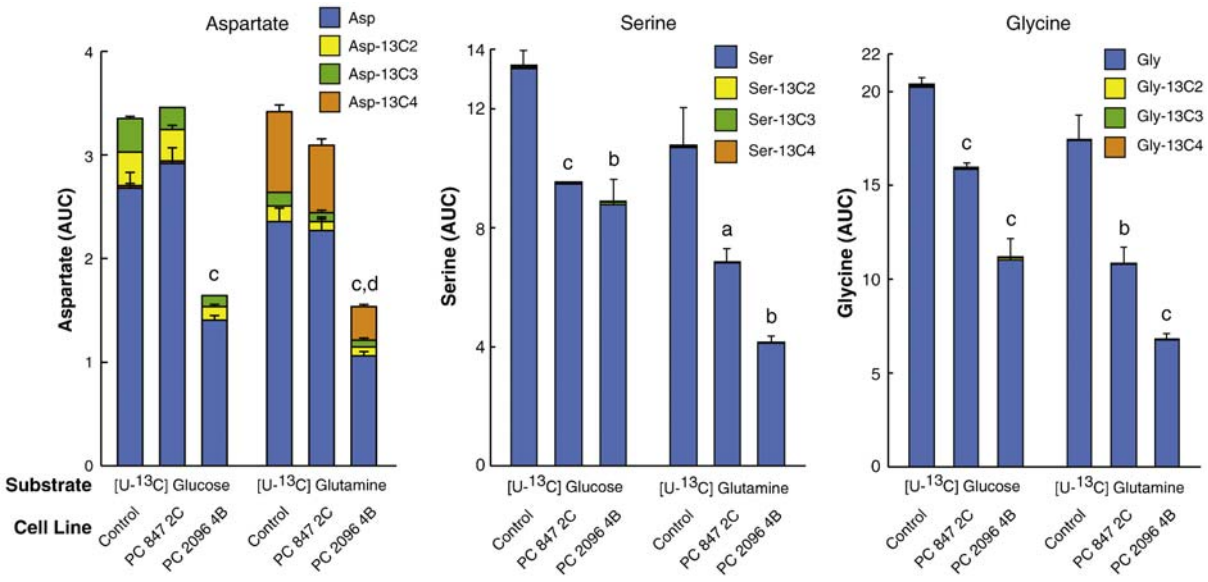

Fig. 17. Decreased labeled aspartate, glycine and serine from U-13C6-glucose or U-13C5-glutamine in pyruvate carboxylase (PC) knockdown cell lines derived from MDA-MB 231 breast cancer cell line. PC 847 2C and PC 2096 4B cell lines or the shRNA scramble control cell line were maintained in the presence of U-13C6-glucose or U-13C5-glutamine for 1 h in the same experiment described in Fig. 3. Fractions of different isotopomers of 13C aspartate, 13C-glycine and 13C-serine between the PC knockdown cell lines and scramble control cell lines are shown within the same bars. ap < 0.05, bp < 0.01 and cp < 0.001 total metabolite level vs scramble control. dp < 0.001 vs Asp-13C4.

Fatty acids act as a sink for carbon flowing from mitochondrial citrate and then through cytosolic acetyl-CoA and malonyl-CoA (Fig. 13). Thus, the 13C incorporation from glucose into palmitate is an indication of the rate of flux of glucose through biosynthetic pathways. Cell lines were incubated in the presence of the 13C-labeled glucose for 18 h. Fig. 18 shows that suppression of PC decreased the incorporation of glucose carbon into palmitate. This is consistent with PC suppression inhibiting the mitochondrial synthesis of citrate and consequently the export of citrate to the cytosol thus lowering the supply of cytosolic acetyl-CoA and malonyl-CoA needed for fatty acid synthesis as depicted in Fig. 13.

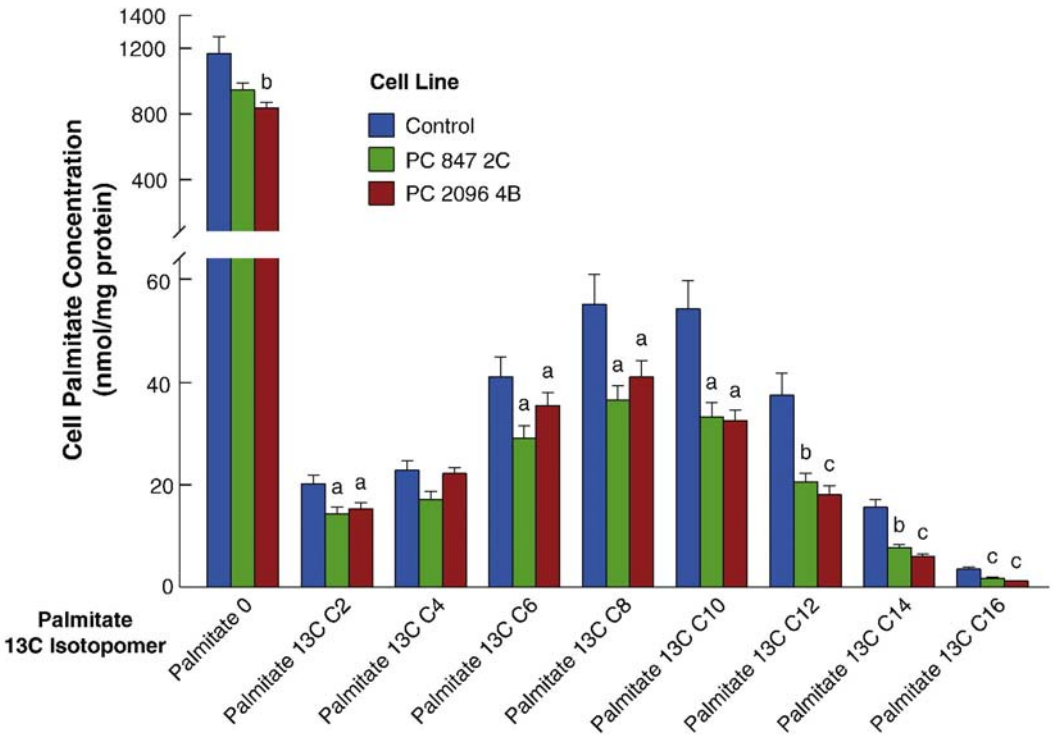

Fig. 18. Decreased U-13C6-glucose incorporation into palmitate in pyruvate carboxylase (PC) knockdown cell lines derived from the MDA-MB-231 breast cancer cell line. PC 847 2C and PC 2096 4B cell lines or the shRNA scramble control cell line were maintained in DMEM for 24 h or longer without labeled glucose of glutamine (the same as the zero time control shown in Fig. 3A and B). Cells were then maintained for 18 h in DMEM modified to contain 10 mM [U-13C6]glucose and 13C incorporation into palmitate was measured by LC-MS/MS. ap < 0.05, bp < 0.01 and cp < 0.001 vs scramble control.

Table 4 and the heat map in Fig. 19 show several selected metabolites that were altered in the strong knockdown cell line PC 2096 4B or both PC knockdown cell lines. In addition to the metabolites discussed above moderate or strong suppression of PC resulted in the decreased levels of α-ketoglutarate, ADP-glucose, GDP-fucose and GDP-mannose while decreases in the levels of ribose-5-phosphate, CTP, hypoxanthine, UDP and GDP were observed only in the strong PC suppression cell line PC 2096 4B (Fig. 19 and Table 4).

Table 4

Selected metabolites that are altered in pyruvate carboxylase (PC) knockdown MDA-MB-231 cell lines.

Metabolite	KD cell line PC 847 2C		KD cell line PC 2096 4B	
	Fold change	P-value	Fold change	P-value
Ribose-5-phosphate	0.98	NS	0.84	$P < 0.05$
α-ketoglutarate	0.70	$P < 0.05$	0.72	$P < 0.05$
ADP-glucose	0.85	$P < 0.05$	0.80	$P < 0.01$
CTP	0.9	NS	0.70	$P < 0.01$
Hypoxanthine	1.01	NS	0.84	$P < 0.05$
UDP	0.78	NS	0.70	$P < 0.05$
GDP	0.85	NS	0.76	$P < 0.05$
GDP-fucose	0.84	$P < 0.05$	0.76	$P < 0.005$
GDP-mannose	0.84	$P < 0.05$	0.45	$P < 0.005$

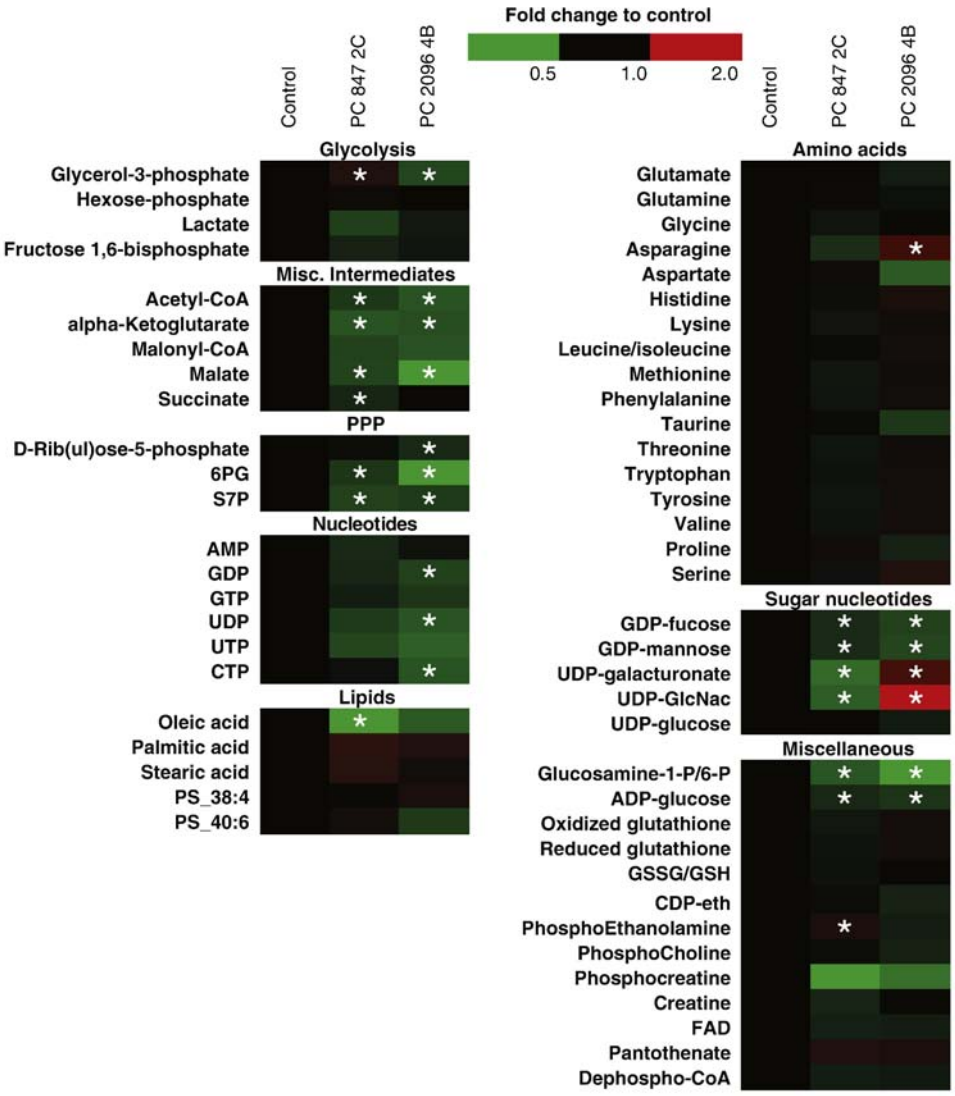

Fig. 19. Heat map showing global lowering of metabolites in pyruvate carboxylase (PC) knockdown MDA-MB 231 breast cancer cell lines. Metabolites were measured by LC-MS in the same experiments shown in Fig. 3 at the zero time point, i.e. before a 13C labeled substrate was added. Metabolite levels are coded by m/z. The asterisk indicates different from the scramble control cell line with $p < 0.05$.

Suppression of PC caused no or a very slight and insignificant reduction of unlabeled and labeled ATP and ADP from glucose (Fig. 20, left panel) such that the ATP/ADP ratio was unaltered by PC knockdown. This indicates that the energy charge of the cell was not impaired by PC knockdown. The slightly decreased levels of ADP and ATP in the PC 2096 4B cell line may be linked to the lowered levels of ribose-5-phosphate (see Table 4 and Fig. 19), which supplies the ribose moiety of these nucleotides and/or decreased aspartate (Fig.

17) which contributes to nitrogen-donation in purine ring synthesis. The levels of NADH and NAD+ including NADH/NAD+ ratios were not different between the knockdown cells and the scramble control (Fig. 20) also indicating that the energy charge of the cell was not affected by PC not down.

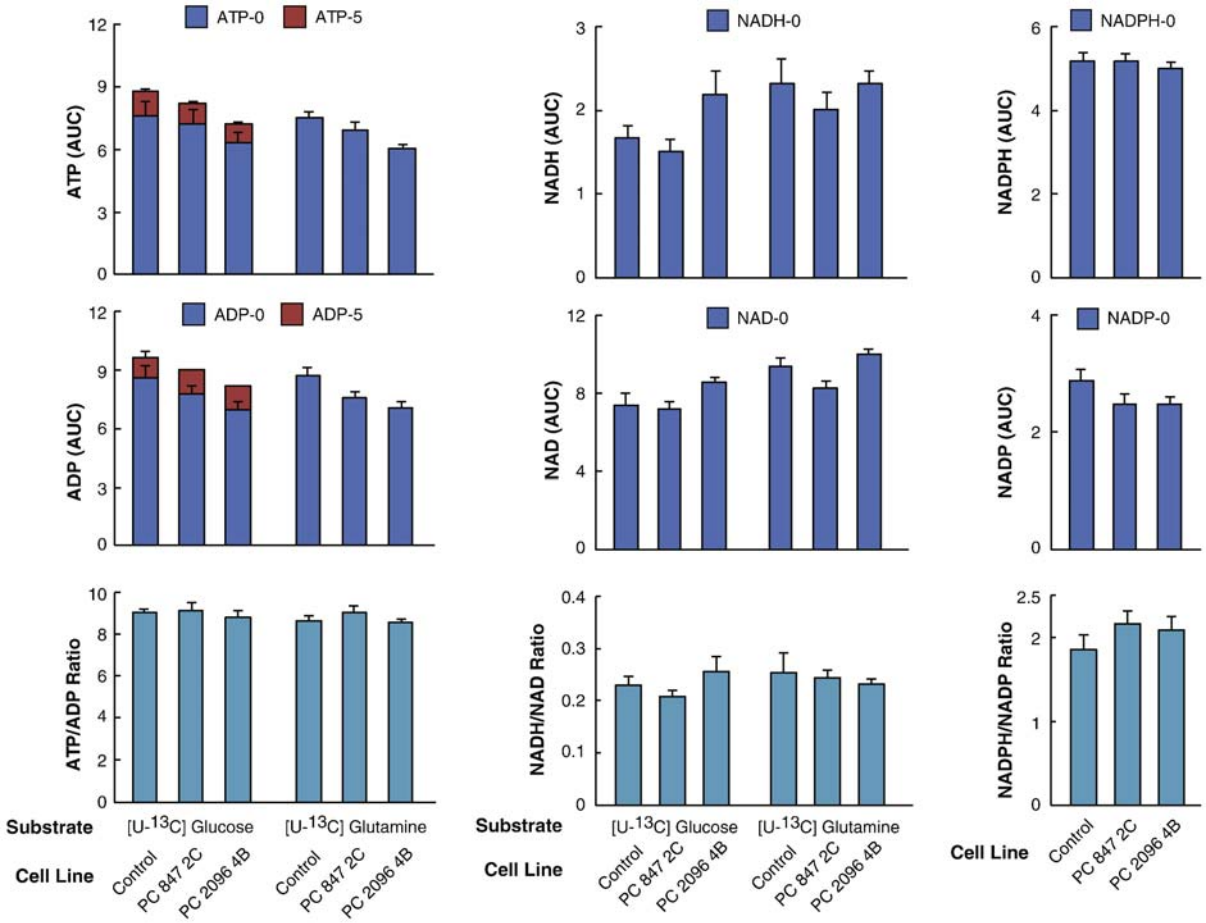

Fig 20. Normal ATP and ADP concentrations, ATP/ADP ratio, NAD(P)H and NAD(P) concentrations and NAD(P)H/NAD(P) ratios in pyruvate carboxylase (PC) knockdown cell lines derived from the MDA-MB-231 breast cancer cell line supplied with U-13C6-glucose or U-13C5-glutamine. PC 847 2C and PC 2096 4B cell lines or the shRNA scramble control cell line were maintained in the presence of U-13C6 glucose or U-13C5 glutamine for 1 h in the same experiment described in Fig. 3. Fractions of different isotopomers of 13C-ATP and 13C-ADP and levels of the pyridine nucleotides NAD(P), NAD(P)H (which showed no incorporation of 13C) between the PC knockdown cell lines and scramble control group are shown within the same bars. ap < 0.01 vs total metabolite same substrate control.

We measured the activities of several mitochondrial and cytosolic enzymes that catalyze reactions of anaplerosis/cataplerosis including pyruvate cycling or might influence the levels of the metabolites measured in our study. As shown in Fig. 13, these included cytosolic malic enzyme, NADP-isocitrate dehydrogenase, ATP-citrate lyase, glutamate dehydrogenase, aspartate aminotransferase and citrate synthase. The activity of only one enzyme in the PC knockdown cells was significantly different from that of the scrambled shRNA control cell line. This was malic enzyme and in two of the three cell lines with very low PC malic enzyme activity was about 50% lower than that of the control cell line (Fig. 21). Malic enzyme activity was not lower in the PC cell line with moderate knockdown of PC, PC 847 2C (Fig. 21). The shRNA nucleotide sequences used to target the PC mRNA were not similar to any of the nucleotide sequence of cytosolic malic enzyme mRNA. Therefore, the lower malic enzyme activities were probably a response to the effects of lower PC enzyme activity. The 50% lower activity of malic enzyme in the cell lines with severe knockdown of PC might contribute to the lower pyruvate levels seen in these cell lines (Fig. 16) due to lower pyruvate cycling from malate and citrate. The enzyme activities were measured in the cell lines after they had been frozen for several months and then re-plated. Unfortunately the cell line PC 2096 4B with one of the lowest levels of PC and that was used for mass spectrometry studies would not grow after having been stored frozen so that the enzyme activities could not be measured in this cell line.

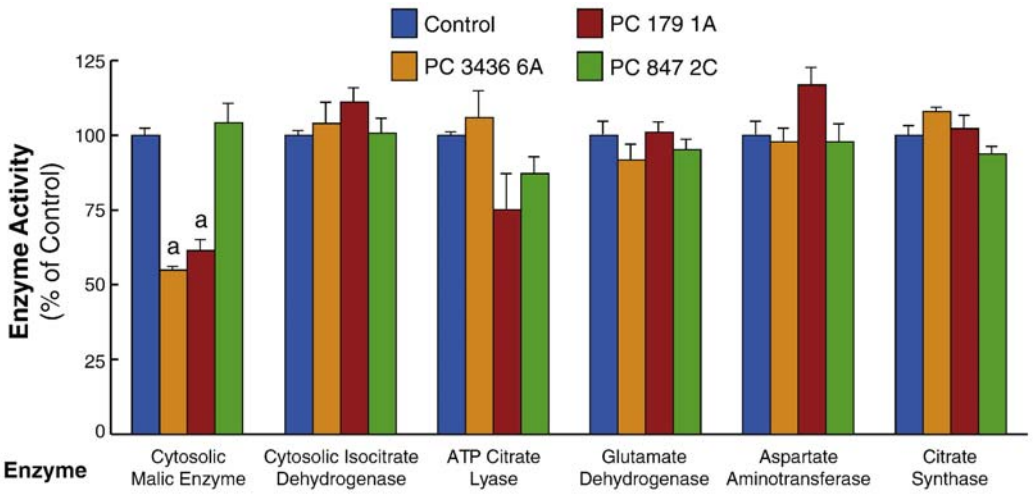

Fig. 21. Malic enzyme is the only enzyme out of several anaplerotic/cataplerotic pyruvate cycling enzymes that is decreased in breast cancer cell lines with severely knocked down

pyruvate carboxylase (PC). Cell lines PC 3436 6A and PC 179 1A possess severely lower levels of pyruvate carboxylase enzyme activity and cell line and PC 847 2C possesses moderately decreased PC activity compared to the scrambled shRNA control cell line. These cell lines show low cell proliferation rates compared to the control cell line. The lower level malic enzyme in two cell lines with severely knocked down PC is consistent with lower pyruvate cycling and lower malate, citrate and pyruvate levels in these cell lines (means ± SE, ap < 0.01 vs scramble control). Only malic enzyme showed decreased activity vs the control cell lines.

To examine whether knocking down of PC expression affect EMT program, attributing to lowered cell migration and invasion abilities, we performed Western blot of EMT markers i.e., E-cadherin namely E-cadherin and vimentin, which are epithelial and mesenchymal marker, respectively rather than measuring the expression of Snail/Slug markers because these two proteins are well-known targets of Snail/Slug. As shown in Figure 22 below, in the absence or presence of aspartate, the expression of E-cadherin in parental MDA-MB-231, moderate knockdown and strong knockdown cells cannot be detected in these three cell lines but is highly detectable in MCF-7 which still retains epithelial character. This result is consistent with previous report, demonstrating that E-cadeherin expression was not detectable in MDA-MB-231 cells. The expression of vimentin which represents mesenchymal polarity was not altered in the two PC knockdown cells. This result suggests that the reduced migration/invasion ability of PC knockdown MDA-MB-231 cells previously observed in our PLoS One publication was not attributed to the loss of EMT marker expression. The reduced mobility/invasive phenotype could secondary to the perturbed cellular metabolism especially those involved in cellular replication, which in turn affects ability of cells to migrate and invade.

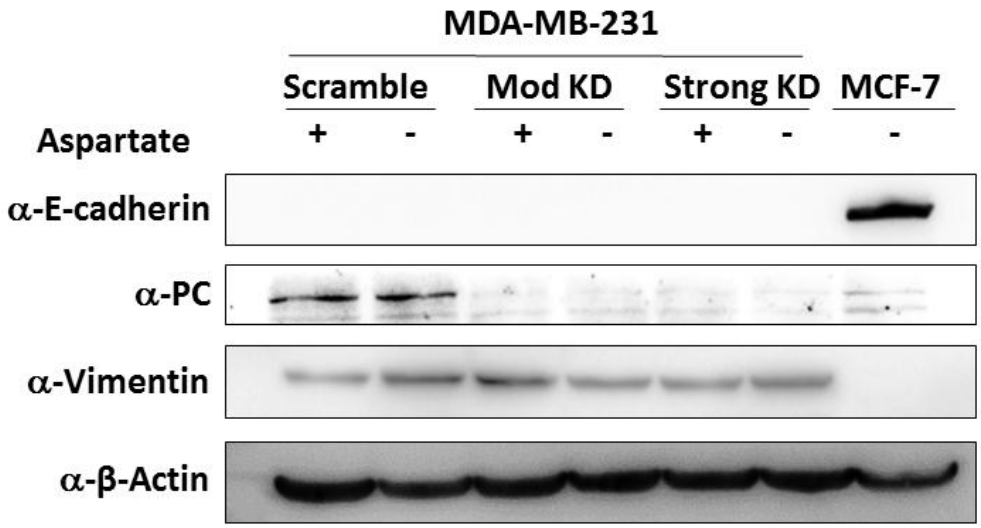

Figure 22. Western blot analyses of epithelial-mesenchymal transition (EMT) marker expression in 20 □g of lysates prepared from scrambled control MDA-MB-231 parental cells, moderate knockdown PC and strong knockdown PC cell lines grown in the absence or presence of 2.5 mM aspartate at day 5. The lysate of MCF-7 cells were also used as the positive control for E-cadherin expression. Also shown are the expression of PC and □-actin.

Discussion

The role of PC in cancer cell proliferation

Pyruvate carboxylation is an important anaplerotic reaction that replenishes citric acid cycle intermediates when they intermediates are removed from mitochondria by their export to the cytosol (cataplerosis). Anaplerosis and cataplerosis are necessary for gluconeogenesis in liver and kidney, lipogenesis in liver and adipose tissue, glutamate synthesis in astrocytes and glucose-induced insulin secretion in pancreatic beta cells [Jitrapakdee et al., 2008; Hasan et al., 2008; Farfari et al., 2000; Jitrapakdee et al., 2005 ; Jitrapakdee et al., 2010]. We and others have shown that PC mRNA and PC protein are up-regulated in many cancers [Cheng et al., 2011; Fan et al., 2009; Sellers et al., 2015; Phannasil et al., 2015]. In the current study we generated multiple stable PC knockdown MDA-MB-231-derived cell lines by shRNA with various levels of PC knockdown and investigated the biochemical changes associated with the defects in growth and motility phenotypic defects of the PC knockdown cells. The various degrees of decreases in PC mRNA and PC enzyme activity were correlated with the decreased cell proliferation rates among the cell lines. This is a confirmation of the relationship between PC enzyme levels and proliferation rates in breast cancer cells. This

retarded proliferation phenotype of the PC knockdown MDA-MB-231 cell lines was also similar to that of the transient knockdown of PC in the MDA-MB-231 cell line that we reported prevously [Phannasil et al., 2015]. A dose-dependent suppression effect on metabolism and inhibition of insulin secretion were also observed in the rat insulinoma cell line INS-1 832/13 with different degrees of PC suppression [Hasan et al., 2008]. A similar disturbance of common metabolites was observed in both moderate and strong PC suppression MDA-MB-231-derived cells as shown in Table 3 and Fig. 5 ; Fig. 6.

Knockdown of PC inhibits anaplerosis

The central metabolic pathway affected by the suppression of PC appears to lie within the anaplerosis. The product of the PC reaction is oxaloacetate, which immediately condenses with acetyl-CoA to produce citrate or is converted to malate in the mitochondrial malate dehydrogenase reaction. Suppression of PC resulted in the depletions of malate and citrate levels as expected (Fig. 14 ; Fig. 15). Suppression of PC decreased the levels of total citrate and malate and ^{13}C incorporation into their isotopomers from $^{13}C_6$-labeled glucose and $^{13}C_5$-labeled glutamine (Fig. 15). This indicates that PC knockdown inhibits anaplerosis from both pyruvate carboxylation and glutaminolysis.

PC knockdown lowers pyruvate cycling

In contrast to suppression of PC expression in pancreatic beta cells, in which the knockdown cells showed a metabolic crossover point with increased levels of pyruvate and low levels of malate and citrate [Hasan et al., 2008], suppression of PC in MDA-MB-231 cell lines showed lowered levels of pyruvate and lactate when cells were maintained in the presence of a high concentration of glucose (25 mM) (in DMEM cell culture medium) prior to the experiment (Fig. 14). Similar to experiments with pancreatic beta cells [Hasan et al., 2008], when the PC knockdown cells were maintained in a cell culture medium containing a lower and physiologic concentration of glucose (5 mM) before glucose was added as in the experiments with beta cells, pyruvate was increased and malate and citrate were decreased indicating a crossover point and a block at the PC reaction (Fig. 15). The changes in the levels of pyruvate, lactate, malate and citrate raise the possibility of certain pathway(s) in which these three metabolites are connected. In pancreatic beta cells, there is a cycling of pyruvate into mitochondria known as the pyruvate-malate shuttle [MacDonald, 1995; MacDonald et al., 2005] as well as in the pyruvate-citrate cycle [Farfari et al., 2000; MacDonald et al., 2005]. In the pyruvate-malate shuttle PC converts pyruvate to oxaloacetate followed by the conversion

of oxaloacetate to malate by mitochondrial malate dehydrogenase, enabling malate to exit mitochondria. In the cytosol malate is in turn converted back to pyruvate by cytosolic malic enzyme, allowing pyruvate to re-enter mitochondria for carboxylation again by PC (Fig. 13). In the citrate-pyruvate shuttle citrate is exported from the mitochondria and cleaved to oxaloacetate in the ATP citrate lyase reaction. The oxaloacetate is then reduced to malate catalyzed by cytosolic malate dehydrogenase. The resulting malate then participates in the pyruvate-malate shuttle as shown in Fig. 13. These cycles provide cytosolic NADPH, a coupling factor, required for glucose-induced insulin secretion in pancreatic beta cells [MacDonald, 1995; Jitrapakdee et al., 2010] and lipid synthesis in many different tissues. In addition, the acetyl-CoA derived from the ATP citrate lyase reaction can be converted to malonyl-CoA and utilized for lipid synthesis in the cytosol. The higher levels of PC mRNA and PC protein [Phannasil et al., 2015] and PC enzyme activity (Table 3) in the highly metastatic MDA-MB-231 cell line than in the low metastatic MCF-7 cell line suggest that similar to pyruvate cycling operative in pancreatic beta cells, pyruvate cycling is important for cell invasiveness or metastasis in breast cancer. In the PC knockdown MDA-MB-231 cells, the depleted levels of malate and citrate caused by the chronic suppression of PC may slow down the overall pyruvate cycling rate, resulting in the low level of pyruvate (Fig. 16).

Interestingly, the level of cytosolic malic enzyme was 50% lower in two of the three cell lines with severe knockdown of PC studied. The shRNA nucleotide sequence used to target the PC mRNA was not similar to any of the nucleotide sequence of the malic enzyme mRNA indicating the lower level of the malic enzyme was not due to an off target effect of PC targeting. Therefore, the lower malic enzyme level was probably a down-regulatory response of the cell to a lower level of the substrate malate for reasons that are not exactly clear. In any case, the 50% lower level of malic enzyme is probably enough lower to contribute to decreased conversion of malate to pyruvate and thus a decrease in pyruvate cycling.

Generalized effects of PC knockdown on metabolite precursors needed for cell structure and energy production

Since citrate and malate are the two major citric acid cycle intermediates that are capable of exiting mitochondria for the biosynthesis of lipids, nucleic acids and certain amino acids, the reduction in the cellular levels of nucleotides (Table 4 and Fig. 19), aspartate, glycine, serine (Fig. 19) and lower glucose carbon incorporation into palmitate (Fig.18.) are consistent with the anaplerotic/cataplerotic role of PC in growth of breast cancer cells.

Transamination of oxaloacetate with glutamate catalyzed by aspartate aminotransferase would produce aspartate. Therefore, it is likely that the lowered level of oxaloacetate caused by suppression of PC may be responsible for the low level of aspartate (Fig. 17). A lowered level of aspartate was also reported in the PC knockdown non-small cell lung cancer (NSCLC), which showed a marked decrease in the cellular aspartate level [Sellers et al., 2015]. In renal adenocarcinoma and paraganglioma cancers harboring loss of function mutations of succinate dehydrogenase, PC was found essential to support cancer proliferation [Cardaci et al., 2015; Lussey-Lepoutre et al., 2015]. Suppression of PC slows down proliferation of these cancers, concomitant with reduced cellular levels of aspartate. Supplementation of the knockdown cancer cells with aspartate rescued this slow growth phenotype. As aspartate is the structural component of several biomolecules including the backbone of purine and pyrimidine rings in nucleic acids, the decreased levels of nucleotides (Fig. 19 and Table 4) and aspartate observed in the PC knockdown MDA-MB-231 cells can potentially slow the synthesis of these nucleotides, contributing to the low rates of cell proliferation. As the ribose-5-phosphate is also the backbone of nucleotides, the lowered level of total ribose-5-phosphate in the knockdown cells as shown in Table 3 and may also contribute to the decreased levels of some nucleotides and their derivatives i.e. hypoxanthine, ADP-glucose, UDP, GDP, GDP-mannose and GDP-fucose. Similar to our study, the PC knockdown non-small cell lung cancer (NSCLC) also showed reduction of glucose- and glutamine- derived CTP and UTP levels [Sellers et al., 2015].

The marked reduction of serine and glycine levels in the PC knockdown cells may underlie the retarded growth phenotype of the knockdown cells because serine contributes to various biosynthetic pathways including protein synthesis, phospholipids and nucleotides which are in high demand during tumorigenesis [Possemato et al., 2011].

The perturbation of serine biosynthesis may occur during the conversion of 3-phosphoglycerate to serine. The conversion of 3-phosphoglycerate to serine is mediated through three sequential reactions (see Fig. 13). The first reaction is the conversion of 3-phosphoglycerate to 3-phosphohydroxypyruvate by phosphoglycerate dehydrogenase followed by further conversion to 3-phosphoserine by phosphoserine aminotransferase before the final conversion to serine by protein serine phosphatase. Then phosphoserine aminotransferase catalyzes the transfer of the amino group from glutamate to 3-

phosphohydroxypyruvate. Because glutamate is produced from α-ketoglutarate via a transamination reaction, the lowered level of α-ketoglutarate in the PC-knockdown MDA-MB-231 cells (Fig.19) may in turn lower the rate of glutamate formation which consequently affects the transamination reaction catalyzed by phosphoserine aminotransferase. Interestingly, up-regulation of serine and glycine biosynthesis caused by amplification of phosphoglycerate dehydrogenase gene copy number was also reported to contribute to oncogenesis in melanoma and breast cancer [Possemato et al., 2011; Locasale, 2013)]. Suppression of phosphoglycerate dehydrogenase expression in several breast cancer cell lines including MDA-MB-231 cells, lowered serine biosynthesis concomitant with a decreased cell proliferation rate, indicating the crucial role of serine in supporting breast cancer growth. Suppression of phosphoglycerate dehydrogenase expression in invasive breast cancer cells also reduces the level of α-ketoglutarate which is produced from the transamination of glutamate [Locasale et al., 2011]. These findings mirror the PC knockdown MDA-MB-231 cells that showed lowered levels of α-ketoglutarate and serine in the current study.

Lowered levels of total cellular acetyl-CoA in the PC knockdown cell lines can most likely be attributed to decreased export of citrate from mitochondria causing decreased citrate available for conversation to oxaloacetate and acetyl-CoA catalyzed by ATP citrate lyase in the cytosol. The latter route for acetyl-CoA regeneration also forms part of alternate route of pyruvate cycling: the well-known pyruvate/citrate cycle [Owen et al., 2002; Farfari et al., 2000; MacDonald et al., 2005] (Fig. 13).

In addition to the lowered levels of certain mitochondrial metabolites, pyruvate cycling and nucleotide synthesis, we also found that suppression of PC causes a reduction of glucose incorporation into palmitate (Fig. 18), suggesting that inhibition of anaplerosis caused by PC knockdown results in lower fatty acid synthesis which restricts membrane biogenesis of the newly dividing cells.

Suppression of PC only slightly and insignificantly lowered the concentrations of ATP and ADP without affecting the ATP/ADP ratio and NAD(P)(H) concentrations (Fig. 20) indicating suppression of PC did not seriously affect the cell energy charge. The decreases in other nucleotides and nucleotide derivatives (Table 4 and Fig. 11) can be attributed to decreased nucleotide biosynthesis via the reduced level of ribose-5-phosphate which is a backbone nucleotide derivatives and decreased aspartate which is a precursor for purine and pyrimidine synthesis.

Since we studied the MDA-MB-231 cell line which is triple negative for estrogen receptor (ER), progesterone receptor (PR) and epidermal growth factor receptor 2 (HER2) in

our study, one might argue whether overexpression of PC is a specific characteristic of breast cancer cell lines. Using various other breast cancer cell lines expressing these three receptors differently, we found no correlation between the expression of these receptors and PC expression. For example, the two most invasive breast cancer cell lines, MDA-MB-231 and MDA-MB-435, which are $ER^{-/}PR^{-}/HER2^{-}$ and $ER^{-}/PR2^{-}/HER2^{+}$, respectively, express PC much higher than MCF-7 and SKBR3 cell lines, which are $ER^{+}/PR^{+}/HER2^{-}$ and $ER^{-}/PR^{-}/HER2^{+}$, respectively (Phannasil et al., 2015). Furthermore, unlike MDA-MB-231, MCF-10A, a non-invasive cell line that is also negative for those three receptors was found to possess an extremely low level of PC enzyme activity (data not shown). Most importantly, our clinicopathological investigation of breast cancer patients has also shown that the level of PC expression was not correlated with the status of these receptors in breast cancer tissues of patients but rather shows a positive correlation with tumor size and stages (10). Thus the level of expression of PC appears to be independent of the status of ER, PR and HER2 receptor expression.

Conclusion

Fig. 13 summarizes the disturbance of various metabolic pathways resulting in the growth retarded phenotype of PC knockdown MDA-MB-231 cells. In conclusion, suppression of PC expression in MDA-MB-231 breast cancer cells results in the lowered levels of citrate, malate and α-ketoglutarate. The depleted levels of these metabolites perturb mitochondrial cataplerosis for the synthesis of serine, glycine, aspartate and fatty acids which are used as the building blocks for synthesis of proteins, lipids and nucleotides. The lowered levels of citrate and malate also impair pyruvate cycling between mitochondria and cytosol. This global perturbation of biosynthesis contributes to the retarded growth phenotype of the PC knockdown MDA-MB-231 cells. The findings that suppression of PC inhibits cell proliferation in glioblastoma [Cheng et al., 2011], NSCLC [Sellers et al., 2015], renal carcinoma, paraganglioma [Cardaci et al., 2015; Lussey-Lepoutre et al., 2015) and, in our study, breast cancer, highlights the crucial role of PC in cancer cell growth and suggests PC may be an attractive drug target of cancer treatment.

PART IV *Identification of transcription factors that regulate overexpression of PC in MDA-MB-231 cells*

As reported previously, the differential expression of PC in MDA-MB-231 and MCF-7 cells is resulted from activation distal promoter (hP2) of human PC gene. This differential

expression likely attributes to binding of the transcription factors that are highly abundant or activated in MDA-MB-231 cell lines to the crucial *cis*-acting elements in hP2 promoter. The nucleotide sequence of hP2 promoter is shown in Figure 23. JASPAR transcription factor database was first used to predict the putative transcription factor site as shown in Figure 23.

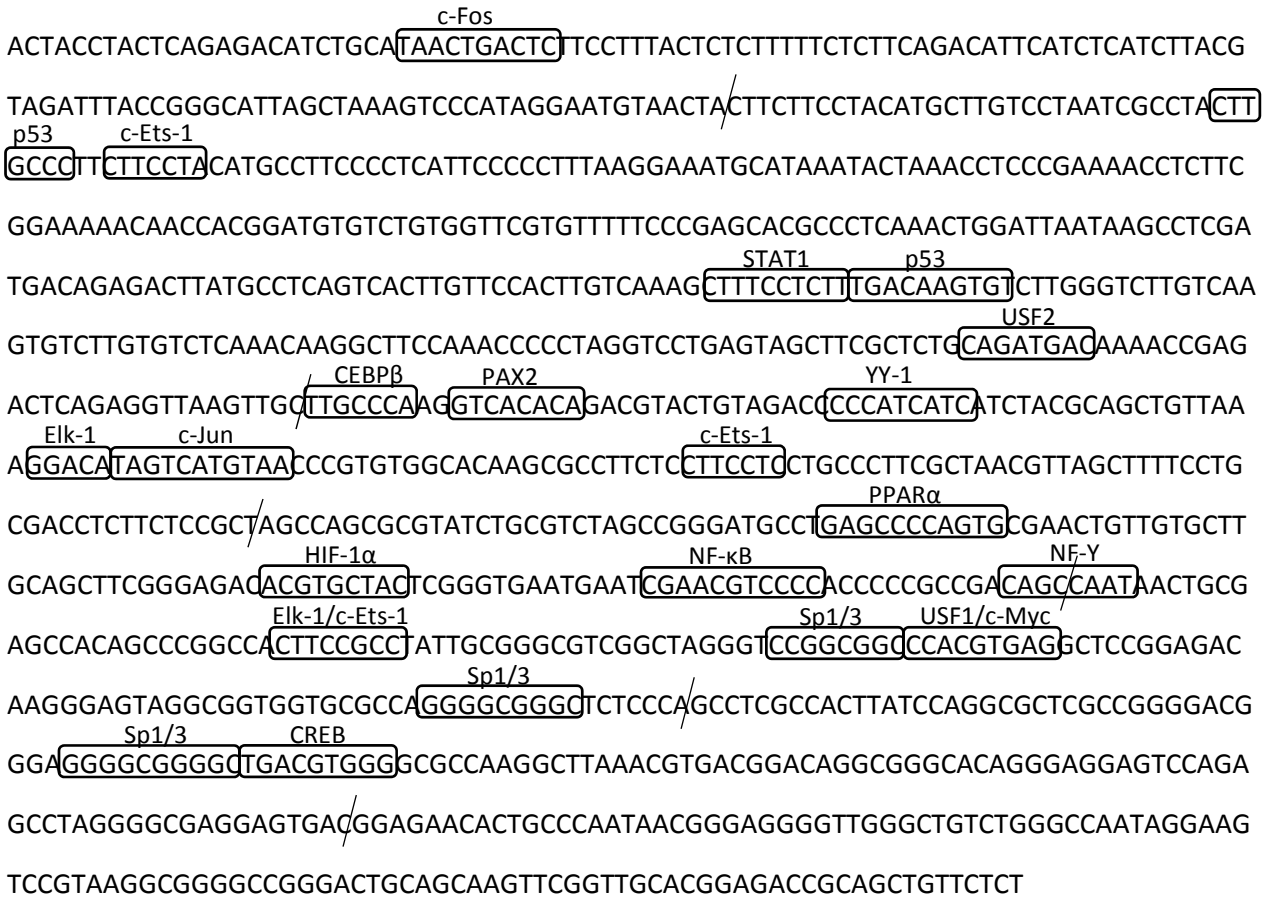

Figure 23 Nucleotide sequence of hP2 promoter with various putative transcription factor binding sites identified by JASPAR program.

To identify regulatory region(s) of the PC gene promoter and the transcription factors that control PC expression in MDA-MB-231, a series of chimeric reporter constructs containing various lengths of P2 promoter of human PC gene ligated to the luciferase reporter gene were produced, as shown in Figure 24. These constructs were then transfected into MDA-MB-231 and MCF-7 breast cancer cell lines, representing highly invasive and non-invasive breast cancer cell lines, respectively. The idea is to identify specific DNA sequence that controls expression of PC in MDA-MB-231 cells. The deleted DNA sequence upon transfecting into MDA-MB-231 cells shows marked reduction of luciferase would reflect its

crucial role in positive regulation while that shows increased expression of luciferase would reflect its crucial role as a repressor element.

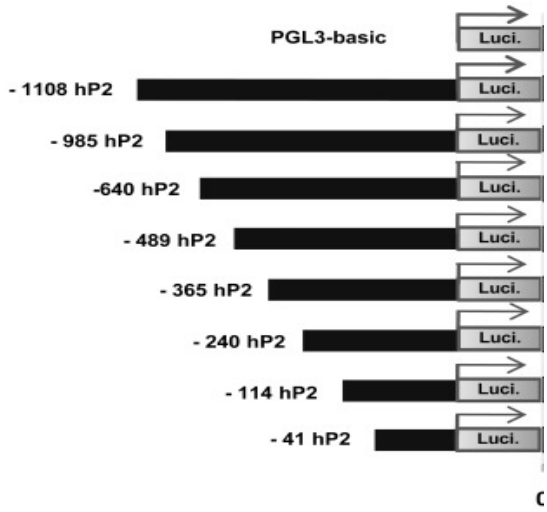

Figure 24 Generation of chimeric reporter constructs containing 5'-truncated human PC promoter.

As shown in Figure 25, in MDA-MB-231 cells, deletions of promoter elements locating between regions -985 to -640 showed marked increased of promoter activity, indicating there is a repressor element locating within this region while deletions of nucleotides -640 to -489 showed increased promoter activity. Deletion of nucleotides between -365 to -240 and -114 dramatically decreased promoter activity indicating the presence of a strong activator sequence(s) between these two regions.

In MCF-7 however; there is only two control region; one acts as a strong repressor locating between nucleotides -489 to -365 and one strong activator sequence, locating between nucleotides -665 to -114, similar to MDA-MB-231 cells. By comparing the expression of the various reporter genes in MDA-MB-231 cells, this can be concluded that (i) common activator sequence(s) that directs transcript of PC in both cell lines is determined by DNA sequence locating between nucleotides -365 to -114. (ii) common repressor sequence(s) that inhibits transcription of PC in both cell lines is located between nucleotides -1108 to -

985. (iii) One repressor and one activator elements locating between nucleotides -985 and -640 and -640 and -489, respectively work as MDA-MB-231-specific.

MDA-MB-231

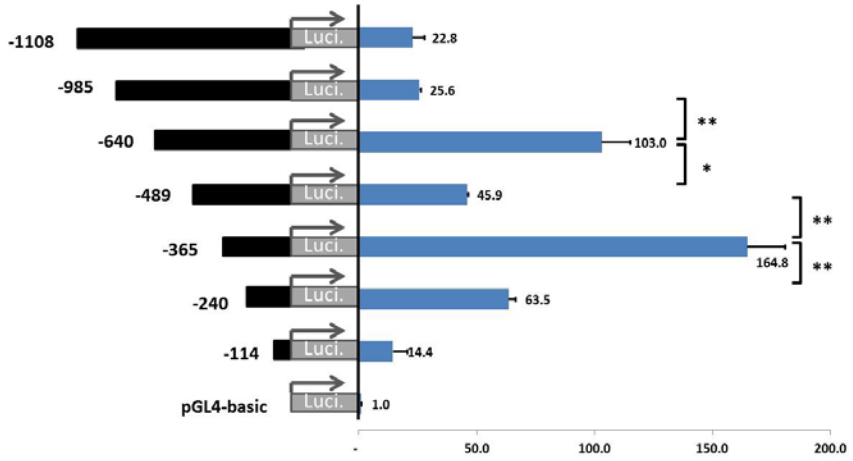

MCF-7

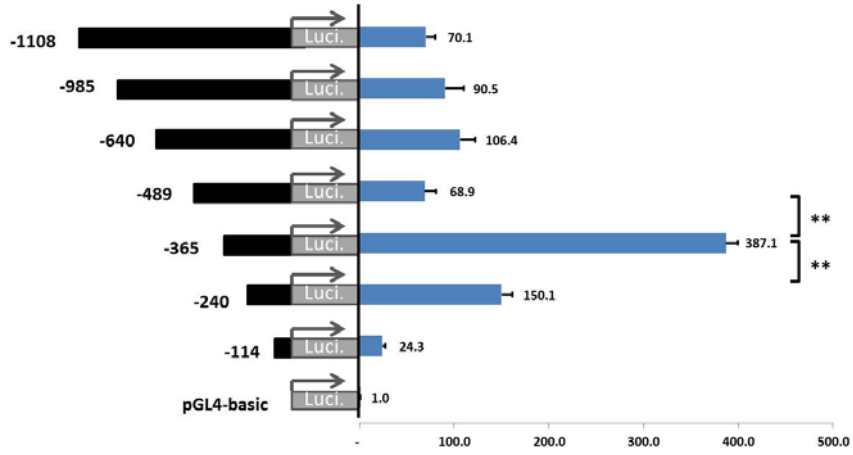

Figure 25. Expression of luciferase reporter gene driven by various lengths of human PC promoters in MDA-MB-231 and MCF-7 cells.

To sub-localize the common positive regulatory region within these regions both in MDA-MB-231 and MCF-7 cells, 25-bp internal deletions (M1, M2, M3, M4 and M5) were carried out across -365 and -240 in the promoter of human PC gene, and the resulting mutants were transfected into both cell lines. As shown in Figure 26, the activator sequences were localized within three distinct positions, -340 to -315, -315 to -290 and -265 to -240, respectively because deletions of these sequences dramatically decreased the promoter activity in both cell lines.

MDA-MB-231

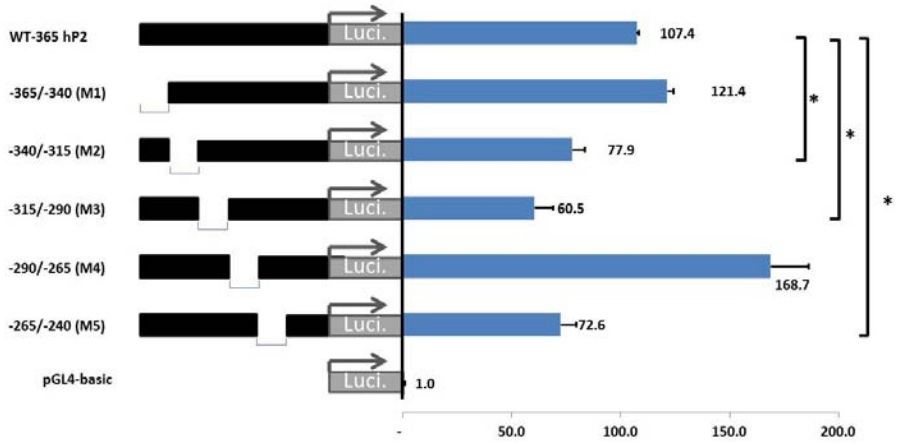

MCF-7

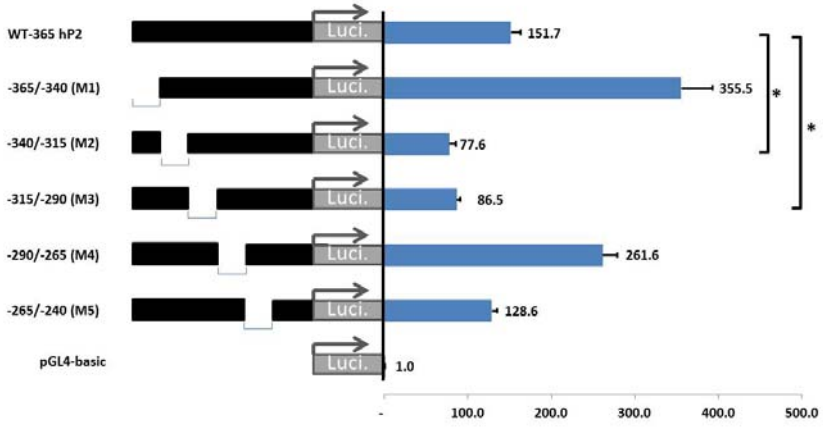

Figure 26 Localization of activator sequence locating between nucleotides -365 and -240 in human PC promoter.

The regulatory sequence locating between nucleotides -640 and -489 that confers MDA-MB-231-specific activity was similarly identified by generating 25-bp internal deletion mutants (M1, M2, M3, M4, M5 and M6, respectively) across this area and the mutants were transfected into MDA-MB-231 and MCF-7 cells. As shown in Figure 27, in MDA-MB-231 cells, the activator sequence was clearly located within four sub-regions; -640 to -615, -615 to -590, -590 to -565 and -541 to -515. Interestingly, in MCF-7, the first three positions (-640 to -615, -615 to -590, -590 to -565) were suppressed by regions -590 to -565 and -541 to -515 (Fig 27).

MDA-MB-231

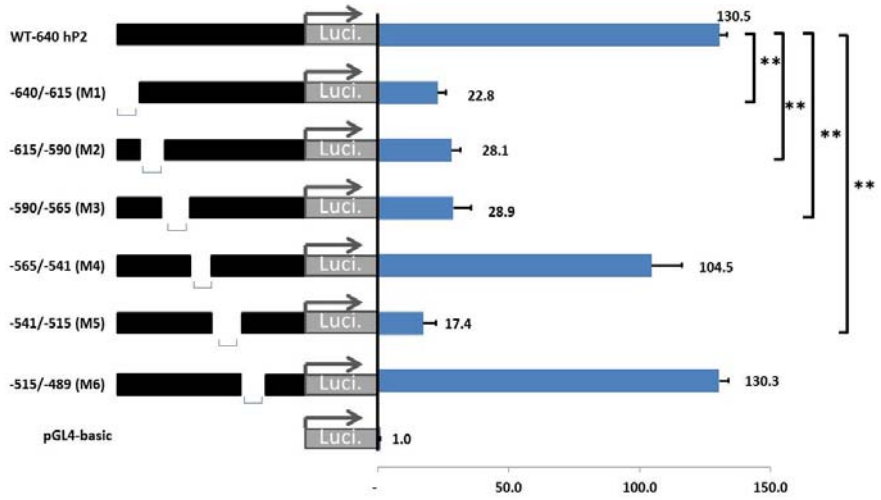

MCF-7

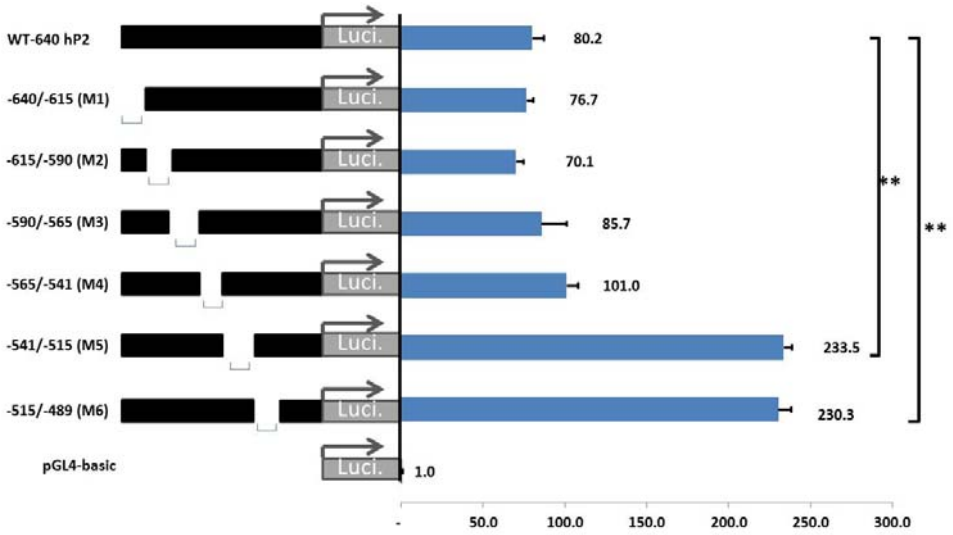

Figure 27 Localization of activator sequence locating between nucleotides -640 and -489 in human PC promoter.

Identification of nuclear protein binding to -640 to -489 of hP2 promoter.

As deletion of nucleotides between -640 to -515 markedly abolished the reporter activity in MDA-MB-231 cells, this suggests that these regions are the binding sites of certain transcription factors. To address this, the electrophoretic mobility shift assay (EMSA) was performed. Biotinylated double stranded oliognucleotide nucleotides corresponding to the deleted nucleotides in M1, M2, M3 and M5 mutants were incubated with MDA-MB-231

nuclear extract and ran on 4% native PAGE followed by blotting and chemiluminescence detection. As shown in Figure 28, there was one predominant DNA-protein complex was similarly observed in M1, M2, M3 and M5 (Figure 28). Mass spectroscopy analysis of these bands failed to identifiy any known transcription factors in databases.

The M1-M5 sequences are shown below:

M1 5’-TTGCCCAAGGTCACACAGACGTACT-3’

M2 5’-GTAGACCCCCATCATCATCTACGCA-3’

M3 5’-GCTGTTAAAGGACATAGTCATGTAA-3’

M5 5’- CTTCCTCCTGCCCTTCGCTAACGTTA-3’

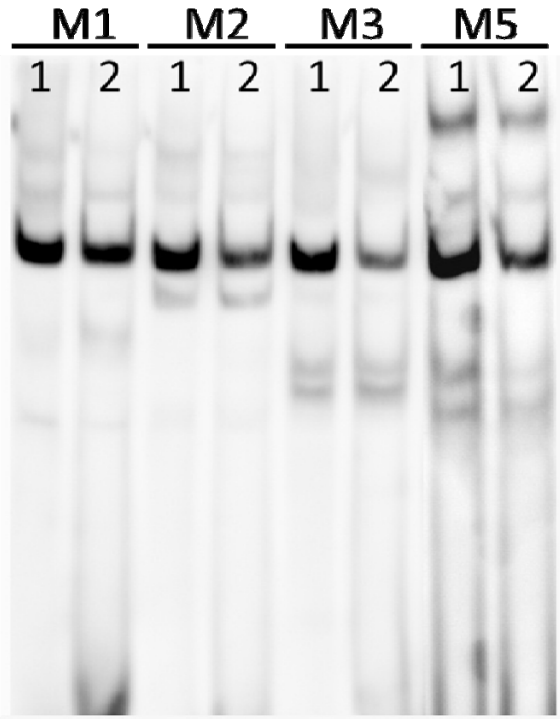

Figure 28 Electrophoretic mobility shift assay of double stranded oligonucleotides corresponding to the sequences located within the deleted regions of M1, M2, M3, M4 and M5 with MDA-MB-231 nuclear extract under low salt (1) and high salt (2) conditions.

Interaction of transcription factors, miRNAs and metabolic enzymes involved in metabolic reprogramming

To examine whether epigenetic regulation by miRNAs attribute to metabolic reworing in cancers , we analyzed interaction between oncogenic transcription factors, miRNAs and metabolic enzymes that involved metabolic reprogramming including aerobic glycolysis,

pentose phosphate pathway, de novo fatty acid synthesis, and serine and glycine metabolism. Although oncoproteins, c-MYC, HIF1α and p53 are the major drivers of this metabolic reprogramming, post-transcriptional regulation by microRNAs (miR) also plays an important role in finely adjusting the requirement of the key metabolic enzymes underlying this metabolic reprogramming. We also combine the literature data on the miRNAs that potentially regulate 40 metabolic enzymes responsible for metabolic reprogramming in cancers, with additional miRs from computational prediction. Our analyses show that: (1) a metabolic enzyme is frequently regulated by multiple miRs, (2) confidence scores from prediction algorithms might be useful to help narrow down functional miR-mRNA interaction, which might be worth further experimental validation. By combining known and predicted interactions of oncogenic transcription factors (TFs) (c-MYC, HIF1α and p53), sterol regulatory element binding protein 1 (SREBP1), 40 metabolic enzymes, and regulatory miRs we have established one of the first reference maps for miRs and oncogenic TFs that regulate metabolic reprogramming in cancers. The combined network shows that glycolytic enzymes are linked to miRs via p53, c-MYC, HIF1α, whereas the genes in serine, glycine and one carbon metabolism are regulated via the c-MYC, as well as other regulatory organization that cannot be observed by investigating individual miRs, TFs, and target genes.

Coordinate regulation of metabolic reprogramming in cancers by oncogenic transcription factors

Three major TFs, namely c-MYC, hypoxia inducible factor 1α (HIF1α) and p53 are responsible for simultaneous up-regulation of the above key metabolic enzymes [Li et al., 2015]. Aberrant expression of c-MYC is observed in more than 50% of cancers and it is one of the most amplified oncogenes. The c-MYC regulates various biological processes including proliferation, apoptosis and metabolic reprogramming [Dang et al., 2013]. Elevated c-MYC levels in turn bind to its target gene promoters, which contain a canonical E-box (CANNTG) element, resulting in increased mRNA transcripts. In normal situations, c-MYC expression is tightly regulated i.e., its expression is high during cell division but rapidly declines during cell cycle arrest [Kruiswijk et al., 2015]. In situations of metabolic alterations, c-MYC targets expression of genes encoding GLUT1, HK2, PDK1 and GLS1 [Li et al., 2015;Dang et al., 2013; Zeller et al., 2003].

The hypoxia-inducible factor (HIF1α), another key oncogenic TF, is functionally coordinated with c-MYC in controlling metabolic reprogramming in cancers [Dang et al., 2008]. HIF1α

exists into two forms: the non-hydroxylated and the hydroxylated forms. In the presence of oxygen, HIF1α undergoes hydroxylation by prolyl hydroxylase, making it prone to proteolysis. However, when oxygen concentration is low, HIF1α escapes hydroxylation, allowing it to enter to the nucleus where it is hetero-dimerized with HIF1β and binds to the hypoxia-responsive element (HRE) in the promoters of genes whose products are involved in angiogenesis and metabolism [Kroemer et al., 2008]. HIF1α's metabolic targets appear to overlap with those of c-MYC, including GLUT1, GLUT3, HK1, HK2, aldolase A, phosphoglycerate kinase (PGK), lactate dehydrogenase (LDH), monocarboxylic acid transporter 4 (MCT4), PDK1 and PKM2 [Li et al., 2015; Semenza et al., 2010].

Unlike c-MYC and HIF1α, p53 functions as a tumor suppressor protein. Expression of p53 is highly regulated as its expression is essentially low in unstressed cells whereas it becomes highly expressed under stress conditions such as oxidative damage, nutrient limitations and DNA damage [Kruiswijk et al., 2015]. De-regulation of p53 expression caused by mutations is associated with more than half of all cancers [Liu et al., 2015]. As a transcription factor, p53 binds to the promoter of other tumor suppressor genes such as those involved in cell cycle arrest, DNA repair, apoptosis and metabolism. In addition, p53 can regulate turnover of many proteins independently of transcription [Kruiswijk et al., 2015]. In regard to its regulatory roles on metabolism, p53 inhibits expression of GLUT1, GLUT3, GLUT4, phosphoglycerate mutase 1 (PGM 1), and thus blocking excessive entry of glucose through glycolytic flux [Kruiswijk et al., 2015; Schwartzenberg-Bar-Yoseph et al., 2004]. p53 inhibits expression of MCT1 and PDK2 while activates expression of PDH1α subunit of PDH complex thereby coupling glycolysis with oxidative phosphorylation [Berkers et al., 2013]. The p53 also down-regulates biosynthesis by decreasing the activity and abundance of glucose-6-phosphate dehydrogenase (G6PD) [Jiang et al., 2011] and decreasing expression of malic enzymes ME1 and ME2 [Kruiswijk et al., 2015; Berkers et al., 2013]. As these three enzymes provide NADPH for biosynthesis, reducing their expression or activities would favor oxidative rather than biosynthetic pathways. In addition to controlling pathways that provide NADPH, p53 can also regulate de novo fatty acid synthesis via down-regulating the expression of the sterol regulatory protein 1c (SREBP1c), which is a key transcriptional factor controlling expression of ACL and FAS genes [Berkers et al., 2013]. Therefore, loss-of-function mutations of p53 in cancers literally shift their metabolic phenotype from an oxidative fate to aerobic glycolysis and anabolism. The p53 protein also targets degradation of PEPCK and G6Pase in non-small cell lung cancer [Zhang et al., 2014; Goldstein et al., 2013].

Expanding the repertoire of miRNA target of the alterative expressed metabolic genes in cancer using computational prediction

It has now become clear that many cellular genes including those encoding metabolic enzymes are regulated by miRNAs [Rottiers et al., 2012]. Several studies have identified regulatory miRNAs of the key enzymes responsible for metabolic reprogramming while some miRNAs regulate the expression of oncogenic TFs (e.g. c-MYC, HIF1α and p53), which in turn regulate expression of those metabolic enzymes. Despite an increasing number of studies on regulation of metabolic genes through miRNAs in cancers, it is clear that the list of studies on miRNA-regulated metabolic enzymes in cancers is nowhere close to the completion. Furthermore, it is still not known whether some key metabolic enzymes e.g. HK1, Aldolase, MCT4, SHMT2, ACC1, can be regulated by certain miRNAs. Thus, here we sought to explore the repertoire of miRNAs that target expression of key enzymes involved in metabolic reprogramming in cancers by combining known interactions from literature (Table 1) and computational prediction (Table S1, Table S2). One of the most important challenges of computational prediction of miRNA is the specificity of the prediction algorithms, which are known to give a large number of false positives. To this end, we examined whether the prediction miRNAs are consistent with the functional validation shown in Table 1, and the predicted miRNA-mRNA interactions that would potentially be worth following up experimentally.

A list of 40 metabolic enzymes that are involved in metabolic reprogramming in cancers.

Enzyme	Full name	Gene	miRNA	References
Aerobic glycolysis, Warburg effect				
GLUT1	Glucose transporter 1	NM_006516	miR-1291 [123]	[124–126]
GLUT2	Glucose transporter 2	NM_000340	N/A	[124]
GLUT3	Glucose transporter 3	NM_006931	miR-195-5p [127], miR-106-5p [90,128]	[124,129,125,126]
GLUT4	Glucose transporter 4	NM_001042	N/A	[124,130,125]
HK1	Hexokinase1	NM_000188	N/A	[3]
HK2	Hexokinase2	NM_000189	miR-143 [131] [132]	[133,3]
Aldolase A	Aldolase A	NM_000034	N/A	[134]
PGAM1	Phosphoglycerate mutase 1	NM_002629	N/A	[135]
PKM2	Pyruvate kinase 2	NM_002654	miR-122, miR-133a, miR-133b,miR-326 [136–138]	[139,140]
LDHA	Lactate dehydrogenase A	NM_005566	miR-21 [141]	[142,143]
MCT1	Monocarboxylate transporter 1	NM_003051	miR-124 [144]	[145]
MCT4	Monocarboxylate transporter 4	NM_004696	N/A	[145,146]
Pentose phosphate pathway				
G6PD	Glucose-6-phosphate dehydrogenase	NM_000402	miR-206, miR-1 [120]	[20]
TKTL1	Transketolase-like1	NM_012253	miR-206, miR-1 [120]	[19]
Gluconeogenesis				
PCK1	Phosphoenolpyruvate carboxykinase 1	NM_002591	N/A	[39]
PCK2	Phosphoenolpyruvate carboxykinase 2	NM_004563	N/A	[38,37]
Tricarboxylic acid (TCA) cycle				
PDK1	Pyruvate dehydrogenase kinase 1	NM_002610	N/A	[147]
PDH	Pyruvate dehydrogenase	NM_003477	miR-26a [148]	[149]
IDH1	Isocitrate dehydrogenase 1	NM_005896	N/A	[28]
IDH2	Isocitrate dehydrogenase 2	NM_002168	miR-183 [150]	[28]
SDH-B	Succinate dehydrogenase complex iron sulfur subunit B	NM_003000	N/A	[27]
SDH-C	Succinate dehydrogenase complex subunit C	NM_003001	N/A	[27]
SDH-D	Succinate dehydrogenase complex subunit D	NM_003002	miR-210 [151]	[27]
FH	Fumarate hydratase	NM_000143	N/A	[27]
ME1	Malic enzyme 1	NM_002395	N/A	[152]
Glutaminolysis				
GLS1	Glutaminase 1	NM_014905	miR-23a, miR-23b [118]	[32]
GLS2	Glutaminase 2	NM_013267	miR-23a, miR-23b [118]	[153,154]
Serine, Glycine and one carbon metabolism				
SHMT2	Serine hydroxymethyltransferase 2	NM_005412	miR-193b [90,155]	[156]
SHMT1	Serine hydroxymethyltransferase 1	NM_004169	miR-198 [157]	[156]
MTHFD2	Methylenetetrahydrofolate dehydrogenase	NM_006636	miR-9 [158]	[156]
MTHFD1L	Methylenetetrahydrofolate dehydrogenase 1-like	NM_015440	miR-9 [158]	[156]
PHGDH	Phosphoglycerate dehydeogenase	NM_006623	N/A	[41]
PSAT1	Phosphoserine aminotransferase 1	NM_021154	miR-340 [159]	[160,161]
PSPH	Phosphoserine phosphatase	NM_004577	N/A	[161]
GNMT	Glycine-N-methyltransferase	NM_018960	N/A	[162]
de novo fatty acid synthesis				
CIC	Citrate carrier	NM_005984	N/A	[163]
ACLY	ATP citrate lyase Y	NM_001096	N/A	[152,164]
ACC1	Acetyl-CoA carboxylase 1	NM_198836	N/A	[152,165]
FASN	Fatty acid synthase	NM_004104	miR-320 [166]	[58,56,57]
SCD	Stearoyl-CoA desaturase	NM_005063	N/A	[152]

Abbreviation: not available (N/A).

The most frequently used algorithms and webtools currently available for miRNA prediction include miRanda–mirSVR [Betel et al., 2008] ; [Betel et al., 2010], DIANA-microT-CDS [Paraskevopoulou et al., 2013], TargetScan [Garcia et al., 2011; Agarwal et al., 2015] Pictar [Krek et al., 2005], miRDB [Wong et al., 2015], and RNA22 [Miranda et al., 2005], which use common features such as seed match and sequence conservation across the species [Peterson et al., 2014]. In brief, the seed match is a perfect pairing between miRNA and the 3′-UTR of mRNA targets, which usually starts at the 5′ end of miRNA at the positions 2 to 8. There are four main classes of canonical seed matches including (1) 6-mer (6 perfect nucleotide matches between miRNA at positions 2 to 7 and mRNA target), (2) 7mer-A1 (perfect match of miRNA at positions 2 to 7 with an A opposite position 1 of mRNA target), (3) 8-mer (perfect seed paring of miRNA at positions 2 to 8 with an A opposite position 1 of

mRNA target) [Lewis et al., 2005] and (4) 7mer-8mer (perfect match of miRNA at positions 2 to 8 and mRNA target) [Brennecke et al., 2005; Lewis et al., 2003]. However, these different seed matches do not reflect the degrees of gene expression suppression by miRNAs [Grimson et al., 2007].

With an aim to explore other potential miRNAs that may regulate key metabolic enzymes listed in Table 1, we choose two widely-used miRNA prediction tools that utilize different features to predict miRNA of the target mRNAs of interest, TargetScan7.0 and miRanda–mirSVR. The former predicts the miRNAs targeting a given gene based on the seed match and sequence conservation across the species, whilst the latter uses free energy binding between miRNA and mRNA targets, and the site accessibility for miRNA target prophecy [Peterson et al., 2014]. The context ++ scores and mirSVR scores were used as the parameters to indicate the confidence of predictions from the TargetScan7.0 and miRanda–mirSVR, respectively. The context ++ score is the sum of contribution from 14 features [Agarwal et al., 2015], such as site-type, 3′ pairing, the local AU content [Grimson et al., 2007], target site abundance, seed-pairing stability [Garcia et al., 2011]. The mirSVR scores, on the other hand, can also rank the empirical probability of down-regulation using supervised machine learning of mRNA expression changes as a result of specific microRNA transfection [Betel et al., 2010]. In short, the more negative context ++ scores and mirSVR scores from the predictions reflect the higher "likelihood" that the mRNA is targeted by miRNA, and thus down-regulated gene expression.

As shown in Fig. 29A, TargetScan7.0 predicted that 40 metabolic enzymes shown in Table 1 are regulated by 299 miRNAs (blue circle). Sixteen out of 40 metabolic enzymes were predicted to be regulated by 113 miRNAs. However, only 8 out of these 113 miRNAs have been reported to functionally regulate expression of these enzymes, leaving the other 105 miRNAs (yellow) whose functional verification is yet to be elucidated. We also noted that there are 14 miRNAs (red) that have been experimentally verified to regulate this set of metabolic genes but elude prediction by TargetScan7.0, suggesting a considerable degree of false negatives. TargetScan7.0 also predicted 186 additional miRNAs that are likely to regulate another 24 metabolic enzymes, whose regulatory miRNAs have not been studied.

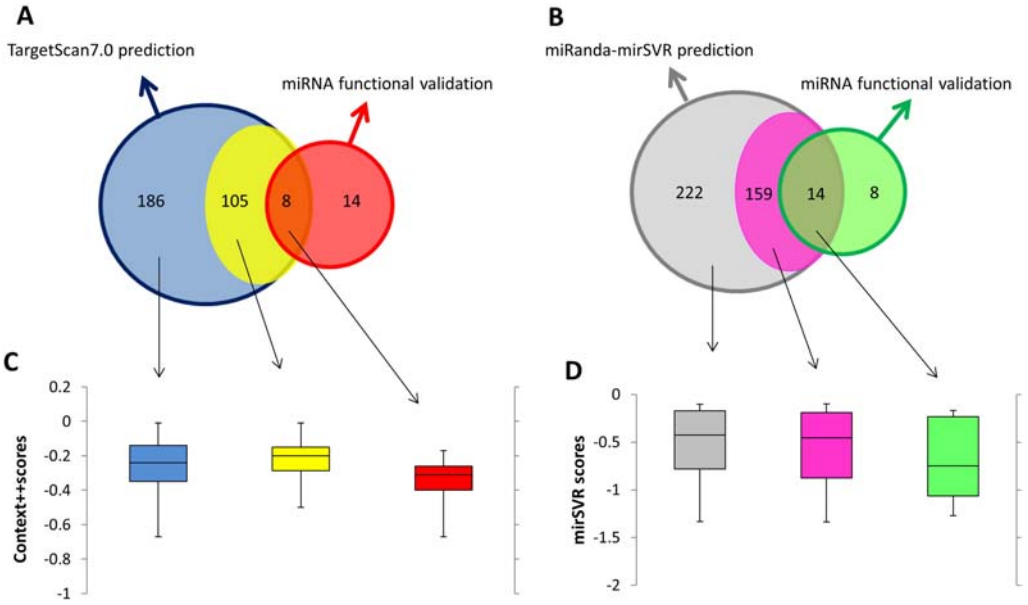

Figure 29. Venn diagrams and boxplots representing the association between miRNA prediction scores and their functional validation. The Venn diagrams of TargetScan7.0 (Fig. 29A) and miRanda–mirSVR (Fig. 29B) show the numbers of validated and predicted miRNAs that regulate metabolic enzymes in cancers. Boxplots illustrate the association of between context ++ scores (Fig. 29C) or miRanda–mirSVR scores (Fig 29D), and three miRNA groups: (1) experimentally validated miRNAs with prediction (2) miRNAs predicted to target metabolic enzymes with other verified miRNAs (3) the predicted miRNAs of altered metabolic enzymes whose functions have not been validated for any miRNA before.

In a similar trend but not identical, miRanda–mirSVR predicted that there are 395 miRNAs that can potentially regulate these metabolic enzymes (Fig. 29B). One hundred and seventy three miRNAs were predicted to regulate 16 metabolic enzymes while the other 222 miRNAs (gray) were predicted to target another 24 metabolic enzymes which are currently unknown to be regulated by any miRNAs. Within those 16 metabolic enzymes regulated by 173 miRNAs, only 14 miRNAs were independently reported to regulate expression of these metabolic enzymes while the functional verifications of the other 159 miRNAs (pink) are yet to be elucidated. Similar to the TargetScan7.0 prediction but with fewer numbers of false negatives, eight additional miRNAs have been reported to functionally regulate expression of these 16 metabolic enzymes but were not detected by the miRanda–mirSVR prediction.

Due to the issues of sensitivity and specificity of miRNA prediction algorithms mentioned earlier, we generated boxplots of the context ++ scores (Fig. 29C) and mirSRV

scores (Fig. 29D), in three miRNA groups: (1) experimentally verified miRNAs with prediction, (2) miRNAs predicted for target genes with other verified miRNAs, but their own functions are yet to be validated, and (3) the predicted miRNAs of metabolic enzymes whose functions have not be validated for any miRNA before (as outlined in the Venn diagrams). We did indeed observe a modest trend that the validated miRNAs have lower context ++ scores, than predicted miRNAs without validation; however, the number of miRNAs in each group is likely to be too small to give a statistical significant result. Similarly, the same can be said about the scores assigned to mirSVR prediction, indicating that confidence scores from the prediction might be useful as an extra indicator to extract the predicted miRNA that are likely to be "real" functional miRNAs, and would be worth further experimental validation.

MicroRNAs and oncogenic transcriptional regulatory networks

To observe the overall interplay of oncogenic TFs, metabolic enzymes, and regulatory miRNAs, we combined the experimentally validated (Table 1), the experimentally validated miRNA-target data from miRTarBase [Chou et al., 2016] and predicted interactions (from the two algorithms as shown in Fig. 29) into a regulatory network of TFs-metabolic enzymes and miRNA-TFs using Cytoscape [Shannon et al., 2003], as shown in Fig. 30 ; Fig. 31 Fig. 30 focuses on the known miRNAs that regulate expression of metabolic enzymes via controlling the expression of oncogenic TFs, whereas we expand the network to cover both validated and predicted miRNA-mRNA interactions in Fig. 30. The predicted interactions shown here are the overlaps of the two algorithms used: TargetScan7.0 and miRanda–mirSVR, shown as gray dashed edges, whereas the functional verified miRNA-gene targets from the Table 1 and miRTarBase database [Chou et al., 2016] are shown in black solid lines. The edges' colors (blue, red, green and purple) represent the miRNAs that regulate expression of metabolic enzymes through the expression of oncogenic TFs (HIF1α, c-MYC, p53, SREBP1, respectively), as in Fig. 30. The colors of node genes in Fig. 31 are classified by metabolic pathways: pale blue color for anaerobic glycolytic genes; white for enzymes involved in serine, glycine and one carbon metabolism; orange for GLS; blue-green nodes for enzymes in the TCA cycle; pink nodes for enzymes in the de novo fatty acid synthesis; gray nodes for gluconeogenic enzyme, and purple nodes for enzymes in the pentose phosphate pathway.

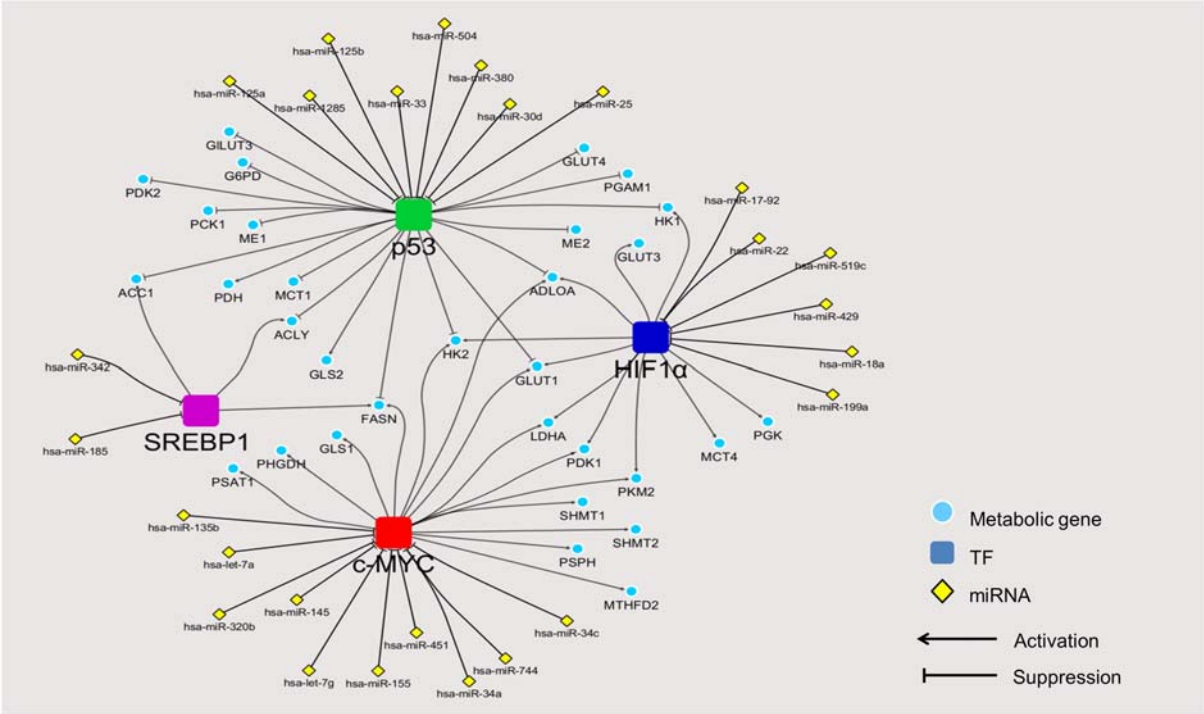

Fig. 30. Regulatory network of experimentally verified miRNAs and oncogenic transcription factors controlling metabolic reprogramming in cancers. The figure shows the integration of experimentally validated regulatory network of TFs-cancer metabolic genes and miRNAs-TFs.

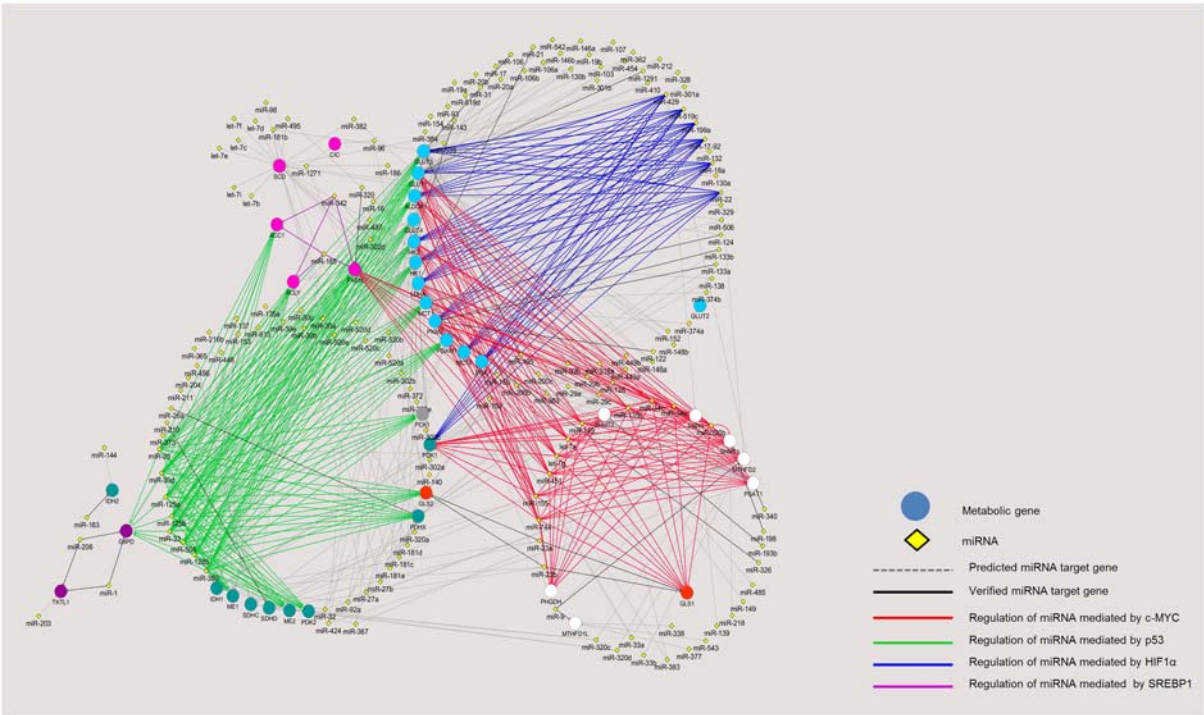

Fig. 31. Regulatory network of miRNAs and oncogenic transcription factors controlling metabolic reprogramming in cancers. The figure shows direct and indirect miRNAs-

metabolic genes interaction. The miRNAs that have already verified their regulatory function show in solid edges whereas the dash edges represent the overlap miRNAs from predictions only. In addition, direct interaction of experimentally verified miRNAs and gene targets are showed in black edges whilst the color edges (blue, green, red and purple) illustrate the interaction of miRNAs and cancer metabolic genes via oncogenic transcription factors. Blue edges represent the regulation of miRNA mediated HIF1α, green edges represent the regulation of miRNA mediated p53, red edges represent the regulation of miRNA mediated c-MYC and the purple edges represent the regulation of miRNA mediated SREBP1. The pale blue circle nodes show the anaerobic glycolytic genes, white circle nodes show genes in serine, glycine and one carbon metabolism, orange circle nodes show genes in glutaminolysis, pink circle nodes show genes in de novo fatty acid synthesis, purple circle nodes show genes in PPP pathways, gray circle node is PCK1 and the blue-green nodes show genes in TCA cycle.

Overall, our miRNAs and oncogenic transcriptional regulatory network depicts individual "modules" of post-transcriptional regulation by miRNA via major drivers of metabolic reprogramming in cancers, acting as hubs that link multiple incoming miRNAs (yellow nodes, Fig. 3) that can bind and suppress transcription of these oncogenes, to their downstream metabolic gene targets (blue nodes). For instance, the expression of c-MYC (red node in Fig. 3, and interaction between miRNA and targeting metabolic genes via c-MYC are in red lines in Fig. 4) is regulated by let-7a in Burkitt Lymphoma [Sampson et al., 2007], miR-145 in non-small cell lung cancer [Chen et al., 2010], let-7g and miR-744 in hepatocellular carcinoma cells [Lan et al., 2011; Lin et al., 2014] , miR-34 in prostate cancer cells [Yamamura et al., 2012], miR-135b in osteosarcoma cells [Liu et al., 2014], miR-155 in gastric carcinoma cells [Sun et al., 2014], miR-320b in colorectal cancer [Wang et al., 2015a] and miR-451 in head and neck squamous cell carcinoma [Wang et al., 2015b]. Suppression of these miRNAs contributes to overexpression of key metabolic enzymes in these tumors. Similarly, HIF1α (dark blue node) expression is regulated by several miRNAs including miR-17-92 in lung cancer cells [Taguchi et al., 2008], miR-519c and miR-18a in breast and lung cancer cells [Cha et al., 2010; Krutilina et al., 2014], miR-22 in colon cancer cells [Yamakuchi et al., 2011], miR-199a in non-small cell lung cancers [Ding et al., 2013] and miR-429 in human endothelial cells [Bartoszewska et al., 2015]. Ectopic expression of these miRNAs reduces the expression of vascular endothelial growth factor (VEGF), a crucial transcriptional target of HIF1α, thereby decreasing angiogenesis, a process of blood vessel formation required for tumor growth and metastasis [Deng et al., 2013]. Likewise, p53 (green

node), a tumor suppressor is also post-transcriptionally regulated by several miRNAs such as miR-25 and miR-30d in myeloma cells [Kumar et al., 2011], miR-125a in breast and hepatoblastoma cells [Zhang et al., 2009], miR-125b in neuroblastoma and lung fibroblalst cells [Le et al., 2009], miR-504 in breast and colon cancer cells [Hu et al., 2010], miR-1285 in neuroblastoma, hepatoblastoma and breast cancer cells [Tian et al., 2010], miR-33 in hematopoietic stem cells [Herrera-Merchan et al., 2010] and miR-380 in neuroblastoma cells [Swarbrick et al., 2010]. Tight regulation of these miRNAs results in substantial expression of p53 which then leads to cell cycle arrest, thus maintaining cells in the non-proliferative state [Hermeking et al., 2012]. In contrast, an aberrant overexpression of these p53-target miRNAs results in the down-regulation of p53, causing malignancy. Because this group of miRNAs exerts its effect on the oncogenic transformation, they are generally now classified as the "oncomiR" miRNAs [Esquela-Kerscher et al., 2006].

In addition to these three oncogenes, the sterol regulatory element binding protein (SREBP1, purple node) is also involved in metabolic reprogramming. SREBP1 is a TF that regulates expression of liver type-pyruvate kinase (PKL) and lipogenic enzymes, ACL, ACC and FAS, thus allowing de novo fatty acid synthesis from glucose in liver. Cancers also use SREBP1 to up-regulate expression of these lipogenic enzymes to support fatty acid synthesis. Similar to c-MYC, HIF1α and p53, expression of SREBP1 by itself is also regulated by miRNAs. miR-185 and miR-342 play important role in regulation of SREBP1 expression by direct binding to the 3′UTR of its mRNA [Li et al., 2013]. Of particular interest, most lipogenic enzymes are co-regulated by more than one TF. For example ACL and ACC1 are regulated by both SREBP1 and p53, while FASN is regulated by SREBP1, p53 and c-MYC. Expression of HK1 is co-regulated by HIF1a and p53 while that of LDHA and PKM2 are co-regulated by HIF1α and c-MYC. GLU1, HK2 and ALDOA are the only three enzymes that are regulated by p53, HIF1α and c-MYC. Interestingly, the expression of certain miRNAs that regulate these metabolic enzymes can also be regulated by an oncogenic TFs. Gao *et al*. (2009) showed that c-MYC indirectly regulates GLS expression in B lymphoma and prostate cancer by suppressing the expression of miR-23a/b that directly regulates the expression of GLS. Kim and coworkers also demonstrated that p53 blocks the expression of HK1, HK2, glucose-6-phosphate isomerase (GPI) and PDK1 by inducing miR-34a expression which in turn, down-regulates the expression of the above four enzymes [Kim et al., 2013].

Looking at the expanded miRNA–mRNA interaction networks (Fig. 4), we observe a global overview of how metabolic genes involving cancer progression are regulated by miRNA through their direct interaction (black lines for validated interactions and gray lines

for those predicted by TargetScan7.0 and miRanda–mirSVR), or through oncogenic TFs (colored edges). We have seen notable miRNAs such as miR-23a/b that directly control glutaminolysis, whereas the miR-1 and miR-206 are responsible for regulation of the PPP pathway genes, G6PD and TKTL1 [Gao et al., 2009; Sing et al., 2013]. The overall network also highlights the "hub" miRNA. miR-429, a tumor suppressor that down-regulates almost all genes in anaerobic glycolytic pathway (e.g. GLUTs) via the oncogenic TF HIF1α. The anaerobic glycolytic genes themselves are also targeted by several other miRNAs such as miR-22, miR-199a, miR-17-92 via HIF1α (blue edges), miR-30d, miR-25, miR-125a/b, miR-1285 via p53 (green edges), and miR-451, miR-155, let-7a, let-7g via c-MYC (red edges). The network also demonstrates other relationships between metabolic pathways and miRNA regulation via TFs. For instance, three out of five genes in de novo fatty acid synthesis pathway (ACC1, ACLY, and FASN) share regulation by miRNAs via p53 and SREBP1. The genes in the serine, glycine and one carbon metabolism pathways (white nodes) heavily rely on the regulation of miRNAs via c-MYC. Post-transcriptional regulatory networks have demonstrated intricate regulation of metabolic genes by different miRNAs [Rottiers et al., 2012; Feng et al., 2015; Vienberg et al., 2016]. Here, we aim to provide a detailed regulatory network of metabolic genes under direct control of miRNAs, or oncogenic TFs regulated by miRNAs. The high resolution network with complete labels can be found in Supplementary material (Fig. S1 and Table S3). Such overall organization of metabolic gene expression regulation cannot be observed by studying miRNAs, TFs, and target genes individually. Saying that, we note that the current version of network relies on the accuracy of the two prediction algorithms used in this study. The known interactions taken from literature might also be biased toward well-characterized oncogenes such as p53 or c-MYC.

In conclusion, our review not only provides the current status of understanding metabolic reprogramming in cancers but also establishes the regulatory network of miRNA-oncogenic TF-cancer metabolic genes that would provide benefits for research guidance in this emerging field the future.

SUMMARY AND IMPLICATIONS

In this research work, we have shown that metabolic rewiring via pyruvate carboxylation is vital for breast cancer growth. The expression level of PC is correlated with the degree of invasive of cancers, independent of ER/PR/HER2 expression. Biochemical studies show that the activity of this enzyme is essential to supports biosynthesis of various structural molecules such as amino acids, lipids and nucleotides. Depletion of PC expression by gene knockdown markedly lowered growth of breast cancer cell line MDA-MB-231 accompanied by reduced rate of mitochondrial anaplerosis. This in turn affects biosynthestic pathways in MDA-MB-231 cells. Overexpression of PC in highly invasive breast cancer cell line, MDA-MB-231 is attributed to selective activation of the proximal promoter (P1) of PC gene as judged by overexpression of P1-driven transcript. ***Inhibition of PC activity or expression provides a novel target for anti-cancer therapy***. From clinical point of view, PC expression is correlated with cancer growth and advanced stage of breast cancer progression. Therefore the use of PC as diagnostic marker may not be suitable as the enzyme expression would be detectable after cancer has progressed to stage III and IV which may be too late for effective chemo-or radiotherapy. Analysis of the expression of various metabolic genes that are altered in various cancers show that the regulation of these metabolic enzymes are mediated by interplay between key oncogenic transcription factors and miRNAs.

References

Agarwal V., Bell G.W., Nam J.W., Bartel D.P. Predicting effective microRNA target sites in mammalian mRNAs. Elife. 2015;4.

Bartoszewska S., Kochan K., Piotrowski A., Kamysz W., Ochocka R.J. The hypoxia-inducible miR-429 regulates hypoxia-inducible factor-1alpha expression in human endothelial cells through a negative feedback loop. FASEB J. 2015;29:1467–1479.

Berkers C.R., Maddocks O.D., Cheung E.C., Mor I., Vousden K.H. Metabolic regulation by p53 family members. Cell Metab. 2013;18:617–633.

Betel D., Wilson M., Gabow A., Marks D.S., Sander C. The microRNA.org resource: targets and expression. Nucleic Acids Res. 2008;36:D149–D153.

Betel D., Koppal A., Agius P., Sander C., Leslie C. Comprehensive modeling of microRNA targets predicts functional non-conserved and non-canonical sites. Genome Biol. 2010;11:R90.

Brennecke J., Stark A., Russell R.B., Cohen S.M. Principles of microRNA-target recognition. PLoS Biol.2005;3

Cairns RA, Harris JS, Mak TW, (2011) Regulation of cancer cell metabolism. Nat. Reviews Cancer 11, 85-95.

S. Cardaci, L. Zheng, G. MacKay, N.J. Van Den Broek, E.D. MacKenzie, C. Nixon, D. Stevenson, S Tumanov, V. Bulusu, J.J. Kamphorst, A. Vazquez, S. Fleming, F. Schiavi, G. Kalna, K. Blyth, D. Strathdee, E. Gottlieb. Pyruvate carboxylation enables growth of SDH-deficient cells by supporting aspartate biosynthesis. Nat. Cell Biol., 17 (2015), pp. 1317–1326

Cha S.T., Chen P.S., Johansson G., Chu C.Y., Wang M.Y. MicroRNA-519c suppresses hypoxia-Inducible factor-1alpha expression and tumor angiogenesis. Cancer Res. 2010;70:2675–2685.

Chen Z., Zeng H., Guo Y., Liu P., Pan H. miRNA-145 inhibits non-small cell lung cancer cell proliferation by targeting c-Myc. J Exp Clin Cancer Res. 2010;29:151.

T. Cheng, J. Sudderth, C. Yang, A.R. Mullen, E.S. Jin, J.M. Matés, R.J. DeBerardinis. Pyruvate carboxylase is required for glutamine-independent growth of tumor cells. Proc. Natl. Acad. Sci. U. S. A., 108 (2011), pp. 8674–8679.

Chou C.H., Chang N.W., Shrestha S., Hsu S.D., Lin Y.L. miRTarBase 2016: updates to the experimentally validated miRNA-target interactions database. Nucleic Acids Res. 2016;44:D239–D247

Dang C.V., Kim J.W., Gao P., Yustein J. The interplay between MYC and HIF in cancer. Nat Rev Cancer. 2008;8:51–56

Dang C.V. MYC, metabolism, cell growth, and tumorigenesis. Cold Spring Harb Perspect Med. 2013;3

DeBerardinis RJ, Mancuso A, Daikhin E, Nissim I, Yudkoff M, Wehrli S, et al. (2007) Beyond aerobic glycolysis: transformed cells can engage in glutamine metabolism that exceeds the requirement for protein and nucleotide synthesis. Proc Nat Acad Sci USA 104: 19345–50.

Ding G., Huang G., Liu H.D., Liang H.X., Ni Y.F. MiR-199a suppresses the hypoxia-induced Proliferation of non-small cell lung cancer cells through targeting HIF1alpha. Mol Cell Biochem. 2013;384:173–180.

Deng G., Sui G. Noncoding RNA in oncogenesis: a new era of identifying key players. Int J Mol Sci. 2013;14:18319–18349.

Esquela-Kerscher A., Slack F.J. Oncomirs — microRNAs with a role in cancer. Nat Rev Cancer. 2006;6:259–269

T.W. Fan, A.N. Lane, R.M. Higashi, M.A. Farag, H. Gao, M. Bousamra II, D.M. Miller. Altered regulation of metabolic pathways in human lung cancer discerned by (13) C stable isotope-resolved metabolomics (SIRM). Mol. Cancer, 8 (2009), p. 41

S. Farfari, V. Schulz, B. Corkey, M. Prentki. Glucose-regulated anaplerosis and cataplerosis in pancreatic beta-cells: possible implication of a pyruvate/citrate shuttle in insulin secretion. Diabetes, 49 (2000), pp. 718–726.

Feng L., Xu Y., Zhang Y., Sun Z., Han J. Subpathway-GMir: identifying miRNA-mediated metabolic subpathways by integrating condition-specific genes, microRNAs, and pathway topologies. Oncotarget. 2015;6:39151–39164.

Gao P., Tchernyshyov I., Chang T.C., Lee Y.S., Kita K. c-Myc suppression of miR-23a/b enhances mitochondrial glutaminase expression and glutamine metabolism. Nature. 2009;458:762–765.
Garcia D.M., Baek D., Shin C., Bell G.W., Grimson A. Weak seed-pairing stability and high target-site abundance decrease the proficiency of lsy-6 and other microRNAs. Nat Struct Mol Biol. 2011;18:1139–1146. [PubMed]
Goldstein I., Yizhak K., Madar S., Goldfinger N., Ruppin E. p53 promotes the expression of gluconeogenesis-related genes and enhances hepatic glucose production. Cancer Metab. 2013;1:9.
Grimson A., Farh K.K., Johnston W.K., Garrett-Engele P., Lim L.P. MicroRNA targeting specificity in mammals: determinants beyond seed pairing. Mol Cell. 2007;27:91–105.
Harari D, Yarden Y, (2000) Molecular mechanisms underlying ErbB2/HER2 action in breast cancer. Oncogenes 19, 6102-6114.
M. Hasan, M.J. Longacre, S.W. Stoker, T. Boonsaen, S. Jitrapakdee, M.A. Kendrick, M.J. MacDonald Impaired anaplerosis and insulin secretion in insulinoma cells caused by small interfering RNA-mediated suppression of pyruvate carboxylaseJ. Biol. Chem., 283 (2008), pp. 28048–28059
Hermeking H. MicroRNAs in the p53 network: micromanagement of tumour suppression. Nat Rev Cancer. 2012;12:613–626.
Herrera-Merchan A., Cerrato C., Luengo G., Dominguez O., Piris M.A. miR-33-mediated down-regulation of p53 controls hematopoietic stem cell self-renewal. Cell Cycle. 2010;9:3277–3285.
Holliday DL, Speirs V (2011) Choosing the right cell line for breast cancer research. Breast Cancer Res 13:215.
Hortobagyi GN, (2000) Devlopments in chemotherapy of breast cancer. Cancer 88, 3073-3079.
Hu W., Chan C.S., Wu R., Zhang C., Sun Y. Negative regulation of tumor suppressor p53 by microRNA miR-504. Mol Cell. 2010;38:689–699.
Jemal A, Siegel R, Xu J, Ward E, (2010) CA cancer. J. Clin. 60, 277-300.
Jiang P., Du W., Wang X., Mancuso A., Gao X. p53 regulates biosynthesis through direct inactivation of glucose-6-phosphate dehydrogenase. Nat Cell Biol. 2011;13:310–316
Jitrapakdee S, Walker ME, Wallace JC (1999) Functional expression, purification, and characterization of recombinant human pyruvate carboxylase. Biochem Biophys Res Communs 266:
S. Jitrapakdee, M. Slawik, G. Medina-Gomez, M. Campbell, J.C. Wallace, J.K. Sethi, S. O'Rahilly, A.J. Vidal-Puig. The peroxisome proliferator-activated receptor-γ regulates murine pyruvate carboxylase gene expression in vivo and in vitro. J. Biol. Chem., 280 (2005), pp. 27466–27476.
S. Jitrapakdee, M. St. Maurice, I. Rayment, W.W. Cleland, J.C. Wallace, P.V. Attwood. Structure, mechanism and regulation of pyruvate carboxylase. Biochem. J., 413 (2008), pp. 369–387.
S. Jitrapakdee, A. Wutthisathapornchai, J.C. Wallace, M.J. MacDonald. Regulation of insulin secretion: role of mitochondrial signaling. Diabetologia, 53 (2010), pp. 1019–1032.
Kim H.R., Roe J.S., Lee J.E., Cho E.J., Youn H.D. p53 regulates glucose metabolism by miR-34a. Biochem Biophys Res Commun. 2013;437:225–231.
Krek A., Grun D., Poy M.N., Wolf R., Rosenberg L. Combinatorial microRNA target predictions. Nat Genet. 2005;37:495–500.
Kroemer G., Pouyssegur J. Tumor cell metabolism: cancer's Achilles' heel. Cancer Cell. 2008;13:472–482.
Kruiswijk F., Labuschagne C.F., Vousden K.H. p53 in survival, death and metabolic health: a lifeguard with a licence to kill. Nat Rev Mol Cell Biol. 2015;16:393–405.
Krutilina R., Sun W., Sethuraman A., Brown M., Seagroves T.N. MicroRNA-18a inhibits hypoxia-inducible factor 1alpha activity and lung metastasis in basal breast cancers. Breast Cancer Res. 2014;16:R78
Kumar M., Lu Z., Takwi A.A., Chen W., Callander N.S. Negative regulation of the tumor suppressor p53 gene by microRNAs. Oncogene. 2011;30:843–853.
Lan F.F., Wang H., Chen Y.C., Chan C.Y., Ng S.S. Hsa-let-7g inhibits proliferation of hepatocellular carcinoma cells by downregulation of c-Myc and upregulation of p16(INK4A) Int J Cancer.

2011;128:319–331.
Le M.T., Teh C., Shyh-Chang N., Xie H., Zhou B. MicroRNA-125b is a novel negative regulator of p53. Genes Dev. 2009;23:862–876.
S.Y. Lee, H.M. Jeon, M.K. Ju, C.H. Kim, G. Yoon, S.I. Han, H.G. Park, H.S. Kang Wnt/Snail signaling regulates cytochrome C oxidase and glucose metabolism. Cancer Res., 72 (2012), pp. 3607–3617
Lee SY, Jeon HM, Ju MK, Kim CH, Yoon G, Han SI, et al. (2012) Wnt/Snail signaling regulates cytochrome C oxidase and glucose metabolism. Cancer Res 72:3607–3617.
Lewis B.P., Shih I.H., Jones-Rhoades M.W., Bartel D.P., Burge C.B. Prediction of mammalian microRNA targets. Cell. 2003;115:787–798.
Lewis B.P., Burge C.B., Bartel D.P. Conserved seed pairing, often flanked by adenosines, indicates that thousands of human genes are microRNA targets. Cell. 2005;120:15–20. [PubMed]
Li X., Chen Y.T., Josson S., Mukhopadhyay N.K., Kim J. MicroRNA-185 and 342 inhibit tumorigenicity and induce apoptosis through blockade of the SREBP metabolic pathway in prostate cancer cells. PLoS One. 2013;8
Li Z., Zhang H. Reprogramming of glucose, fatty acid and amino acid metabolism for cancer progression. Cell Mol Life Sci. 2015;73:377–392
Lin F., Ding R., Zheng S., Xing D., Hong W. Decrease expression of microRNA-744 promotes cell proliferation by targeting c-Myc in human hepatocellular carcinoma. Cancer Cell Int. 2014;14:58
Livak KJ, Schmittgen TD (2001) Analysis of relative gene expression data using real-time quantitative PCR and the 2(-Delta Delta C(T)) Method. Methods 25: 402–408.
Liu Z., Zhang G., Li J., Liu J., Lv P. The tumor-suppressive microRNA-135b targets c-Myc in osteoscarcoma. PLoS One. 2014;9
Liu J., Zhang C., Hu W., Feng Z. Tumor suppressor p53 and its mutants in cancer metabolism. Cancer Lett. 2015;356:197–203.
J.W. Locasale, A.R. Grassian, T. Melman, C.A. Lyssiotis, K.R. Mattaini, A.J. Bass, G. Heffron, C.M. Metallo, T. Muranen, H. Sharfi, A.T. Sasaki, D. Anastasiou, E. Mullarky, N.I. Vokes, M. Sasaki, R. Beroukhim, G. Stephanopoulos, A.H. Ligon, M. Meyerson, A.L. Richardson, L. Chin, G. Wagner, J.M. Asara, J.S. Brugge, L.C. Cantley, M.G. Vander Heiden. Phosphoglycerate dehydrogenase diverts glycolytic flux and contributes to oncogenesis. Nat. Genet., 43 (2011), pp. 869–874.
W. Locasale Serine, glycine and one-carbon units: cancer metabolism in full circle. Nat. Rev. Cancer, 13 (2013), pp. 572–583
M.A. Lorenz, C.F. Burant, R.T. Kennedy. Reducing time and increasing sensitivity in sample preparation for adherent mammalian cell metabolomics. Anal. Chem., 83 (2011), pp. 3406–3414
M.A. Lorenz, M.A. El Azzouny, R.T. Kennedy, C.F. Burant. Metabolome response to glucose in the β-cell line INS-1 832/13. J. Biol. Chem., 288 (2013), pp. 10923–10935
C. Lussey-Lepoutre, K.E. Hollinshead, C. Ludwig, M. Menara, A. Morin, L.J. Castro-Vega, S.J. Parker, M. Janin, C. Martinelli, C. Ottolenghi, C. Metallo, A.P. Gimenez-Roqueplo, J. Favier, D.A. Tennant. Loss of succinate dehydrogenase activity results in dependency on pyruvate carboxylation for cellular anabolism. Nat. Commun., 6 (2015), p. 8784
M.J. MacDonald. Feasibility of a mitochondrial pyruvate malate shuttle in pancreatic islets. Further implications of cytosolic NADPH in insulin secretion. J. Biol. Chem., 270 (1995), pp. 20051–20058
M.J. MacDonald, L.A. Fahien, L.J. Brown, N.M. Hasan, J.D. Buss, M.A. Kendrick. Perspective: emerging evidence for signaling roles of mitochondrial anaplerotic products in insulin s ecretion Am. J. Physiol. Endocrinol. Metab., 288 (2005), pp. E1–E15.
M.J. MacDonald, M.J. Longacre, S.W. Stoker, M.A. Kendrick, A. Thonpho, L.J. Brown, N.M. Hasan, S. Jitrapakdee, T. Fukao, M.S. Hanson, L.A. Fernandez, J. Odorico. Differences between human and rodent pancreatic islets: low pyruvate carboxylase, ATP citrate lyase and pyruvate carboxylation; high glucose-stimulated acetoacetate in human pancreatic islets. J. Biol. Chem., 286 (2011), pp. 18383–18396
McPherson K, Steel CM, Dixon JM, (2000) ABC of breast diseases: Breast cancer epidemiology, risk

factors and genetics. Br Med. J. 321, 624-628.
Mili Y, Swensen J, Shattuck-Eidens D, Futreat PA, Harshman K, Tavtigian S, et al. (1994) A strong candidate for the breast and ovarian cancer susceptibility gene BRCA1. Science 266, 66-71.
Miranda K.C., Huynh T., Tay Y., Ang Y.S., Tam W.L. A pattern-based method for the identification of MicroRNA binding sites and their corresponding heteroduplexes. Cell. 2006;126:1203–1217.
R.A. Moreadith, A.L. Lehninger. The pathways of glutamate and glutamine oxidation by tumor cell mitochondria. Role of mitochondrial NAD(P)+-dependent malic enzyme. J. Biol. Chem., 259 (1984), pp. 6215–6221
O.E. Owen, S.C. Kalhan, R.W. Hanson. The key role of anaplerosis and cataplerosis for citric acid cycle functionJ. Biol. Chem., 277 (2002), pp. 30409–30412.
Paraskevopoulou M.D., Georgakilas G., Kostoulas N., Vlachos I.S., Vergoulis T. DIANA-microT web server v5.0: service integration into miRNA functional analysis workflows. Nucleic Acids Res. 2013;41:W169–W173.
Peterson S.M., Thompson J.A., Ufkin M.L., Sathyanarayana P., Liaw L. Common features of microRNA target prediction tools. Front Genet. 2014;5:23.
P. Phannasil, C. Thuwajit, M. Warnnissorn, J.C. Wallace, M.J. MacDonald, S. Jitrapakdee. Pyruvate carboxylase is up-regulated in breast cancer and essential to support growth and invasion of MDA-MB-231 cells. PLoS One, 10 (2015), Article e0129848.
R. Possemato, K.M. Marks, Y.D. Shaul, M.E. Pacold, D. Kim, K. Birsoy, S. Sethumadhavan, H.K. Woo, H.G. Jang, A.K. Jha, W.W. Chen, F.G. Barrett, N. Stransky, Z.Y. Tsun, G.S. Cowley, J. Barretina, N.Y. Kalaany, P.P. Hsu, K. Ottina, A.M. Chan, B. Yuan, L.A. Garraway, D.E. Root, M. Mino-Kenudson, E.F. Brachtel, E.M. Driggers, D.M. Sabatini. Functional genomics reveal that the serine synthesis pathway is essential in breast cancer. Nature, 476 (2011), pp. 346–350.
Rohde M, Lim F, Wallace JC (1991) Electron-Microscopic Localization of Pyruvate-Carboxylase in Rat-Liver and Saccharomyces cerevisiae by Immunogold Procedures. Arch Biochem Biophys 290: 197–201.
Rottiers V., Naar A.M. MicroRNAs in metabolism and metabolic disorders. Nat Rev Mol Cell Biol. 2012;13:239–250.
Sampson V.B., Rong N.H., Han J., Yang Q., Aris V. MicroRNA let-7a down-regulates MYC and reverts MYC-induced growth in Burkitt lymphoma cells. Cancer Res. 2007;67:9762–9770.
Schwartzenberg-Bar-Yoseph F., Armoni M., Karnieli E. The tumor suppressor p53 down-regulates glucose transporters GLUT1 and GLUT4 gene expression. Cancer Res. 2004;64:2627–2633.
Saphner T, Tormey DC, Gray R, (1996) Annual hazard rates of recurrence for breast cancer after primary therapy. J. Clin. Oncol. 14, 2738-2746.
K. Sellers, M.P. Fox, M. Bousamra II, S.P. Slone, R.M. Higashi, D.M. Miller, A.N. Lane. Pyruvate carboxylase is critical for non-small-cell lung cancer proliferation. J. Clin. Invest., 125 (2015), pp. 687–698.
Semenza G.L. HIF-1: upstream and downstream of cancer metabolism. Curr Opin Genet Dev. 2010;20:51–56.
Shannon P., Markiel A., Ozier O., Baliga N.S., Wang J.T. Cytoscape: a software environment for integrated models of biomolecular interaction networks. Genome Res. 2003;13:2498–2504.
Soule HD, Vazguez J, Long A, Albert S, Brennan M (1973) A human cell line from a pleural effusion derived from a breast carcinoma. J Natl Cancer Inst 51: 1409–1416.
P.A. Srere ,in: J.M. Lowenstein (Ed.), Citrate Synthase in Methods in Enzymology, Citric Acid Cycle, vol. XIII, , Academic Press, Inc., New York, NY (1969)
Sun S., Sun P., Wang C., Sun T. Downregulation of microRNA-155 accelerates cell growth and invasion by targeting c-Myc in human gastric carcinoma cells. Oncol Rep. 2014;32:951–956.
Swarbrick A., Woods S.L., Shaw A., Balakrishnan A., Phua Y. miR-380-5p represses p53 to control cellular survival and is associated with poor outcome in MYCN-amplified neuroblastoma. Nat Med. 2010;16:1134–1140
Taguchi A., Yanagisawa K., Tanaka M., Cao K., Matsuyama Y. Identification of hypoxia-inducible

factor-1 alpha as a novel target for miR-17-92 microRNA cluster. Cancer Res. 2008;68:5540–5545.
Thiery JP, Sleeman JP (2006) Complex networks orchestrate epithelial-mesenchymal transitions. Nat Rev Mol Cell Biol 7: 131–42.
Thonpho A, Sereeruk C, Rojvirat P, Jitrapakdee S (2010) Identification of the cyclic AMP responsive element (CRE) that mediates transcriptional regulation of the pyruvate carboxylase gene in HepG2 cells. Biochem Biophys Res Communs 393: 714–9
Thonpho A, Rojvirat P, Jitrapakdee S, MacDonald MJ (2013) Characterization of the distal promoter of the human pyruvate carboxylase gene in pancreatic beta cells. PloS one 8: e55139.
Tian S., Huang S., Wu S., Guo W., Li J. MicroRNA-1285 inhibits the expression of p53 by directly targeting its 3′ untranslated region. Biochem Biophys Res Commun. 2010;396:435–439.
M.G. Vander Heiden, L.C. Cantley, C.B. Thompson. Understanding the Warburg effect: the metabolic requirements of cell proliferation. Science, 324 (2009), pp. 1029–1033
Vienberg S., Geiger J., Madsen S., Dalgaard L.T. MicroRNAs in metabolism. Acta Physiol (Oxf) 2016
Wang H., Cao F., Li X., Miao H., E J miR-320b suppresses cell proliferation by targeting c-Myc in human colorectal cancer cells. BMC Cancer. 2015a;15:748
Wong N., Wang X. miRDB: an online resource for microRNA target prediction and functional annotations. Nucleic Acids Res. 2015;43:D146–D152.
Wooster R, et al. (1995) Identification of the breast cancer susceptibility gene BRCA2. Nature 378, 789-792.
Yamakuchi M., Yagi S., Ito T., Lowenstein C.J. MicroRNA-22 regulates hypoxia signaling in colon cancer cells. PLoS One. 2011;6
Yamamura S., Saini S., Majid S., Hirata H., Ueno K. MicroRNA-34a modulates c-Myc transcriptional complexes to suppress malignancy in human prostate cancer cells. PLoS One. 2012
Yook JI, Li XY, Ota I, Hu C, Kim HS, Cha SY, et al. (2006) A Wnt-Axin2-GSK3beta cascade regulates Snail1 activity in breast cancer cells. Nat Cell Biol 8: 1398–1406.
Zardavas D, Baselga J, Piccart M, (2013) Emerging targeted agents in metastatic breast cancer. Nature Rev. Clin. Oncol. 10, 191-210.
Zeller K.I., Jegga A.G., Aronow B.J., O'Donnell K.A., Dang C.V. An integrated database of genes responsive to the Myc oncogenic transcription factor: identification of direct genomic targets. Genome Biol. 2003;4:R69.
Zhang P., Tu B., Wang H., Cao Z., Tang M. Tumor suppressor p53 cooperates with SIRT6 to regulate gluconeogenesis by promoting FoxO1 nuclear exclusion. Proc Natl Acad Sci U S A. 2014;111:10684–10689.
Zhang Y., Gao J.S., Tang X., Tucker L.D., Quesenberry P. MicroRNA 125a and its regulation of the p53 tumor suppressor gene. FEBS Lett. 2009;583:3725–3730.

Output

Publications

1. Phannasil P, Ansari IH, El Azzouny M, Longacre MJ, Rattanapornsompong K, Burant CF, MacDonald MJ, ***Jitrapakdee S**. (2017) Mass spectrometry analysis shows the biosynthetic pathways supported by pyruvate carboxylase in highly invasive breast cancer cells. Biochim Biophys Acta-Molecular Basis of Diseases. 1863(2):537-551. (Q1, Impact factor = 5.158)
2. Pinweha P, Rattanapornsompong K, Charoensawan V, ***Jitrapakdee S**. (2016) MicroRNAs and oncogenic transcriptional regulatory networks controlling metabolic reprogramming in cancers. Comput Struct Biotechnol J. 4;14:223-33. (Q2, cite score = 2.01)
3. Choosangtong K, Sirithanakorn C, Adina-Zada A, Wallace JC, ***Jitrapakdee S**, Attwood PV (2015) Residues in the acetyl CoA binding site of pyruvate carboxylase involved in allosteric regulation. FEBS Lett. 589(16):2073-9. (Q1, impact factor = 3.519).
4. Phannasil P, Thuwajit C, Warnnissorn M, Wallace JC, MacDonald MJ, ***Jitrapakdee S**. (2015) Pyruvate Carboxylase Is Up-Regulated in Breast Cancer and Essential to Support Growth and Invasion of MDA-MB-231 Cells. PLoS One. 10(6):e0129848. (Q1, impact factor = 3.73)

   ***Corresponding author**

Award

รางวัลศิษย์เก่าดีเด่นบัณฑิตวิทยาลัยมหาวิทยาลัยมหิดล สาขาการวิจัยปี 2558

Students' theses

1. Rattanapornsompong (2016) Biochemical characterization of pyruvate carboxylase knockdown MDA-MB-231 cell line under nutrient deprivation condtions. M.Sc. thesis, Faculty of Graduate Studies, Mahidol University.
2. Phannasil. (2015) Roles of pyruvate carboxylase in breast cancer. PhD.thesis, Faculty of Graduate Studies, Mahidol University.
3. Choosangtong. (2015) Investigating the expression of of mutated pyruvate carboxylase in acetyl-CoA binding site. M.Sc.thesis, Faculty of Graduate Studies, Mahidol University.

ภาคผนวก

PLOS ONE

RESEARCH ARTICLE

Pyruvate Carboxylase Is Up-Regulated in Breast Cancer and Essential to Support Growth and Invasion of MDA-MB-231 Cells

Phatchariya Phannasil[1], Chanitra Thuwajit[2], Malee Warnnissorn[3], John C. Wallace[4], Michael J. MacDonald[5], Sarawut Jitrapakdee[1]*

1 Department of Biochemistry, Faculty of Science, Mahidol University, Bangkok, Thailand, **2** Department of Immunology, Faculty of Medicine, Siriraj Hospital, Mahidol University, Bangkok, Thailand, **3** Department of Pathology, Faculty of Medicine, Siriraj Hospital, Mahidol University, Bangkok, Thailand, **4** School of Molecular and Biomedical Sciences, University of Adelaide, Adelaide, SA5005, Australia, **5** Childrens Diabetes Center, University of Wisconsin School of Medicine and Public Health, Madison, WI, United States of America

* sarawut.jit@mahidol.ac.th

Citation: Phannasil P, Thuwajit C, Warnnissorn M, Wallace JC, MacDonald MJ, Jitrapakdee S (2015) Pyruvate Carboxylase Is Up-Regulated in Breast Cancer and Essential to Support Growth and Invasion of MDA-MB-231 Cells. PLoS ONE 10(6): e0129848. doi:10.1371/journal.pone.0129848

Academic Editor: Pankaj K Singh, University of Nebraska Medical Center, UNITED STATES

Received: October 7, 2014

Accepted: May 13, 2015

Published: June 12, 2015

Data Availability Statement: All relevant data are within the paper.

Funding: This work was supported by grant BRG5780007 from the Thailand Research Fund and Mahidol University to SJ. PP was supported by the RGJ-PhD scholarship (PHD/0142/2552) from the Thailand Research Fund. The funders had no role in study design, data collection and analysis, decision to publish and preparation of the manuscript.

Competing Interests: The authors have declared that no competing interests exist.

Abstract

Pyruvate carboxylase (PC) is an anaplerotic enzyme that catalyzes the carboxylation of pyruvate to oxaloacetate, which is crucial for replenishing tricarboxylic acid cycle intermediates when they are used for biosynthetic purposes. We examined the expression of PC by immunohistochemistry of paraffin-embedded breast tissue sections of 57 breast cancer patients with different stages of cancer progression. PC was expressed in the cancerous areas of breast tissue at higher levels than in the non-cancerous areas. We also found statistical association between the levels of PC expression and tumor size and tumor stage ($P < 0.05$). The involvement of PC with these two parameters was further studied in four breast cancer cell lines with different metastatic potentials; i.e., MCF-7, SKBR3 (low metastasis), MDA-MB-435 (moderate metastasis) and MDA-MB-231 (high metastasis). The abundance of both PC mRNA and protein in MDA-MB-231 and MDA-MB-435 cells was 2-3-fold higher than that in MCF-7 and SKBR3 cells. siRNA-mediated knockdown of PC expression in MDA-MB-231 and MDA-MB-435 cells resulted in a 50% reduction of cell proliferation, migration and *in vitro* invasion ability, under both glutamine-dependent and glutamine-depleted conditions. Overexpression of PC in MCF-7 cells resulted in a 2-fold increase in their proliferation rate, migration and invasion abilities. Taken together the above results suggest that anaplerosis via PC is important for breast cancer cells to support their growth and motility.

Introduction

As a result of over-stimulation by growth factor signaling, most tumors adapt their metabolism in order to accommodate both energy and structural component needs during rapid proliferation [1]. Unlike differentiated cells, regardless of the presence of oxygen, most tumors

metabolize glucose via anaerobic glycolysis known as the 'Warburg effect' [2,3,4]. As the result of this metabolic shift, tumors consume large amounts of glucose, causing the accumulation of lactate. The enhanced glucose utilization via anaerobic glycolysis partly results from the over-expression of *c*-myc and hypoxia inducible factor-1α (HIF1α), which in turn stimulates expression of hexokinase II, lactate dehydrogenase (LDH), and the pyruvate kinase M2 isoform (PK-M2) that enhance glycolysis, and pyruvate dehydrogenase kinase (PDK) that can inhibit the oxidative decarboxylation of pyruvate by phosphorylation of pyruvate dehydrogenase. This phenomenon results in channeling of pyruvate into anaerobic glycolysis and limits its entry into mitochondria for oxidative phosphorylation and also shifts mitochondrial metabolism towards biosynthetic purposes [5,6,7,8]. Anaplerosis via pyruvate carboxylation and glutamate synthesis from glutamine (glutaminolysis) are the two major biochemical reactions which replenish TCA cycle intermediates withdrawn for biosynthetic pathways [9]. Furthermore, up-regulation of expression by c-*myc* of glutaminase, an enzyme which converts glutamine to glutamate is also observed in many tumors [10,11,12,13]. This high demand for glutamine is a hallmark of most tumors and was proposed as a target of cancer treatment. While growing evidence have now indicated that glutaminolysis is crucial for many cancers, limited information is available regarding the importance of pyruvate carboxylation via pyruvate carboxylase (PC) in cancers.

Fan *et al.* [14] have shown that over-expression of PC mRNA and protein was detected in solid cancerous lung tissue. ^{13}C Isotopomer-based metabolomic analysis reveals that pyruvate carboxylation flux is increased in the cancerous lung tissue compared to the paired non-cancerous lung tissues, suggesting that anaplerosis via pyruvate carboxylation is essential to fulfill the high anabolic demand of lung tumor during the establishment of primary tumorigenesis. By infusing ^{13}C-labeled glucose or ^{15}N-labeled glutamine in the patients with early-stage non-small cell lung cancer before tissue resection, the same group of investigator showed that the labeled glucose enters mitochondrial metabolism via pyruvate carboxylation while this not the case for ^{15}N-glutamine, indicating that anapleorosis via PC is the preferred route in non-small cell lung cancer [15]. Furthermore suppression of PC expression in non-small cell lung cancer cell lines resulted in the retardation of cell growth primarily due to the disruption of biosynthesis of lipid and nucleotide and imbalance of glutathione metabolism [15].

PC is also involved in brain tumor progression. Interestingly, many low grade glioblastomas possess a defect in the cytosolic isocitrate dehydrogenase (IDH1) which functions in converting isocitrate to α-ketoglutarate concomitant with the production of NADPH. The α-ketoglutarate once formed in the cytoplasm by IDH1 can re-enter mitochondria and be used for various biosynthetic pathways [16]. Mutation of IDH1 is predicted to impair mitochondrial metabolism in many cancers [17]. Izquierdo-Garcia *et al* [18] have recently engineered astrocytes to metabolically mimic low grade glioblastomas by expressing mutated IDH1 and found that these astrocytes bearing an IDH1 mutation bypass the IDH1 defect by up-regulating pyruvate carboxylation. In supporting this finding, Cheng *et al.* [19] have demonstrated that PC is highly abundant in some glioblastoma cell lines, and is required to support its growth under glutamine-independent conditions. The above evidence highlights the roles of PC in supporting the growth of lung and brain tumors.

Although PC has been shown to be highly abundant in these two types of tumor and appears to support growth of glioblastoma under glutamine-independent growth, it remains unclear whether PC is highly expressed in other types of cancer and is also required to support other aggressive phenotypes. Here we show that PC is overexpressed in breast cancer tissues, and that the level of expression is correlated with tumor size and stage. We also demonstrate that suppression of PC expression in a highly metastasized cell line, MDA-MB-231 markedly

reduces its proliferation, migration and *in vitro* invasion ability, indicating the importance of PC to support growth and invasion of breast cancer.

Materials and Methods

Cell culture

Human breast cancer cell lines, MCF-7 (ATCC:HTB22) [20] and MDA-MB-231(ATCC: HTB26) [21], MDA-MB-435 (ATCC:HTB129) and SKBR3 (ATCC: HTB-30) were grown in Dulbecco's modified Eagle's medium (DMEM) (Gibco) supplemented with 10% (v/v) fetal bovine serum (FBS). The cells were maintained at 37°C with 5% CO_2. The glutamine-independent MDA-MB-231 cell line was established by progressive depletion of glutamine in the culture medium from 4 mM to 0 mM. In brief, cells were grown in DMEM supplemented with 2 mM glutamine for 2 weeks, 1 mM for 2 weeks, 0.5 mM for 2 weeks and no glutamine, respectively. After 1 month of growing this cell line in the absence of glutamine, it was used for subsequent experiments.

siRNA transfection of and overexpression of PC

6 x 10^5cells of MDA-MB-231 cells or 3.5 x 10^5cells of MDA-MB-435 were plated in 35-mm dish containing 2 ml of DMEM supplemented with 10% (v/v) FBS and maintained at 37°C with 5% CO_2 for 24 h. 50 pmole (25 nM) or 100 pmole (50 nM) of siRNA targeted to human PC (Cat.no. 4390824, Ambion) were transfected to MDA-MB-231 or MDA-MB-435, respectively using Lipofectamine 2000 transfection reagent (Invitrogen) in the Optimem-reduced serum medium (Invitrogen). Same amounts of scrambled control siRNA were also transfected to both cell lines. The transfected cells were maintained in 2 ml complete medium for 2 days. The cells were subsequently harvested for RT-PCR and Western blot analyses.

MCF-7 cells overexpressing PC were generated by transfection of plasmid encoding human PC (pEF-PC) [22]. In brief, 2 x 10^5 cells of MCF-7 were plated in 2 ml complete DMEM medium in 35 mm-dish 24 h before transfecting with 4 μg of pEF-PC plasmid. Upon 48 h post-transfection, the stable MCF-7 cells overexpressing PC cells were selected with 0.5 μg/mL puromycin for one week. The stable lines were expanded for another week before proliferation, migration and invasion assays were performed.

Reverse transcription polymerase chain Reaction (RT-PCR)

Total RNA was extracted from cells using TRIzolReagent (Gibco) following the manufacturer's instructions. Initially the random hexamers-primed RNA was carried out in a 10 μl-reaction mixture containing 2 μg of total RNA and 200 ng of random hexamers (Promega) at 70°C for 5 min, before being chilled at 4°C. Reverse transcription was initiated by adding 10 μl of mixture containing 1xImProm-II reaction buffer, 3 mM $MgCl_2$, 0.5 mM dNTP mix and 160 units of ImProm-II reverse transcriptase (Promega), to the primed-RNA mixture and the reaction was incubated at 25°C for 5 min, 42°C for 60 min and 70°C for 15 min, respectively. The cDNA was stored at -20°C until used.

Quantitative real-time PCR

Quantitative real time PCR was performed in a 12 μl-reaction mixture containing 6 μl of 2xKAPA probe Fast qPCRmaster mix Universal (KAPA Biosystems), 2 μl of cDNA, 1 μM of forward and reverse primers and 0.5 μM of fluorogenic probe as described previously [23]. The thermal profiles consisted of initial incubation at 50°C for 2 min and 95°C for 10 min followed by 40 cycles of denaturation at 95°C for 15 sec and annealing/extension at 60°C for 1 min in

Mx3000P Q- PCR system (Agilent Technologies). To identify the PC mRNA isoforms expressed in breast cancer cell lines, quantitative real time PCR was performed in a 20 μl-reaction mixture containing 10 μl of 2x KAPA SYBR FAST qPCR Master mix universal (KAPA Biosystems), 200 nM each of specific forward primer for detecting each isoform of PC mRNA and reverse primers [24], and 2 μl of cDNA. The thermal profiles consisted of initial incubation at 95°C for 10 min followed by 40 cycles of denaturation at 95°C for 30 sec, annealing at 60°C for 30 sec and extension at 72°C for 30 sec in Mx 3000P Q- PCR systems (Agilent Technologies). Expression of PC mRNA was normalized with that of 18s ribosomal RNA gene, and was shown as the relative gene expression. Fold change was calculated using the comparative C_T method ($\Delta\Delta C_T$ method) [25].

Western blot analysis

MCF-7, MDA-MB-231 and MDA-MB435 cells grown in T75 cm^2 flask were trypsinized with 0.05% (v/v) trypsin-EDTA. The detached cells were centrifuged at 3,000 xg for 5 min, cell pellet was re-suspended in 150 μl of RIPA buffer (50 mM Tris-HCl pH 7.4, 150 mM NaCl, 1 mM EDTA, 0.25% sodium deoxycholate, 1% (v/v) NP-40 and 1x protease inhibitor cocktail (Roche). 70 μg of protein lysate were subjected to discontinuous SDS-PAGE [26] under reducing conditions. The proteins were transferred to a polyvinylidenedifluoride (PVDF) membrane by Semi-Dry Transfer Cell (BIO-RAD) for 1.5 h. The membrane was incubated in 15 ml of blocking solution [5% (w/v) skim milk in 1% (v/v) Tween 20 in PBS-T] at 4°C overnight. For detecting PC protein, the blot was incubated with1:5,000 dilution of rabbit anti-chicken PC polyclonal antibody [27] for 2 h. The blot was briefly washed in PBS-T before incubating with 1:5,000 dilution of goat anti-rabbit IgG conjugated with horseradish peroxidase (HRP) (DAKO) for 1 h. For detection of β-actin, mouse anti-actin monoclonal antibody (sc-8432) (Santa Cruz) and sheep anti-mouse IgG conjugated with HRP (GE healthcare) were used for primary and secondary antibodies, respectively. The immunoreactive bands were detected using an enhanced chemiluminescence substrate (Perkin Elmer). The images were captured using Chemiluminescence Imaging System (Syngene).

Proliferation assay

Cell proliferation was determined by counting the viable cells for 7 days. At 48 h post-transfection, the 1 x 10^5 cells of MDA-MB-231, MDA-MB-435 or MCF-7 overexpressing PC were plated into 35 mm dishes and grown in the absence or presence of 4 mM glutamine for 1, 2, 3, 4, 5, 6 and 7 days, at 37°C in CO_2 incubator. At each time point, the cells were trypsinized, stained with 0.4% trypan blue and counted under a microscope. The results are presented as means $\pm$ standard deviations of two independent experiments.

Wound healing assay

1.5 x 10^5 cells of MDA-MB-231, MDA-MB-435 and MCF-7 overexpressing PC were replated in 24-well plate in DMEM containing no serum overnight before the artificial wound was generated by scratching the monolayer with a pipette tip. The wound's closure (width) of the PC knockdown at 0 and 48 h was measured and shown as the mean $\pm$ standard deviation of that of the scrambled control which was arbitrarily set as 100%.

In vitro invasion assay

In vitro invasion assays were performed by plating 1.2 x 10^5 of MDA-MD-231, MDA, MDA-MB-435 or MCF-7 cells in 200 μl of serum-free medium containing 4 mM or 0 mM

glutamine into the upper chamber of Transwell (6.5-mm diameter polyvinylpyrrolidone-free polycarbonate filter of 8-μm pore size) (Corning, NY, USA) which was pre-coated with 20 μg Matrigel (BD Biosciences) while the lower chamber contained medium supplemented with 10% (v/v) FBS for 4 h (for MDA-MB-231) or with 20% FBS for 24 h (for MCF7 and MDA-MB-435) at 37°C. The non-invaded cells in the upper compartment were removed and the chamber was washed twice with 1x PBS. The cells that had invaded through the matrix were fixed with 4% (v/v) paraformaldehyde in 1x PBS for 20 min and stained with 0.5% crystal violet in 25% (v/v) methanol overnight, followed by two washes with tap water. Finally, the invaded cells were counted under a microscope and the percentage of invasion was compared with that of the scrambled control cell which was arbitrarily set as 100%.

Immunohistochemistry (IHC)

Fifty-seven paraffin-embedded breast cancer tissue sections were collected under the protocols approved by Siriraj Institute Revision Board, Faculty of Medicine Siriraj Hospital, Mahidol University (COA no. Si 230/2014), and all clinical investigation were conducted according to the principles expressed in the Declaration of Helsinki. The written informed consent was obtained from each participant who enrolled in the study. Those breast tissues were diagnosed invasive ductal carcinoma. Firstly, the antigen was retrieved by incubation with 10 mM citrate buffer pH 6 at 95°C for 1 h. The sections were blocked with 2% (w/v) BSA for 20 min before incubating with 1:1,000 dilution of anti-chicken PC antibody [27] at room temperature overnight. Excess primary antibody was removed by washing with 1x PBS for 10 min before incubating with specific anti-rabbit EnVision+system-HRP labelled polymer (DAKO) at room temperature for 30 min. The secondary antibody was washed with 1x PBS for 10 min before 0.05% (w/v) 3,3'-diaminobenzidine (DAB) solution was applied to the sections and incubated at room temperate for 5 min. The sections were counter-stained with Mayer's hematoxylin, dipped in 1% (w/v) lithium carbonate and washed with tap water for 5 min. Finally, the sections were mounted with Permount and examined under the microscope. PC expression was semi-quantitatively scored on the basis of percentage of PC-positive cells and the immunostaining intensity. Grading for the percentage of PC-positive cancer cells were as follows: 1 for 1–25%; 2 for 26–50%; 3 for 51–75% and 4 for 76–100%. The intensities of PC staining in cancer tissues were as follows: 0, unstained; 1, slightly; 2, intermediate and 3, strongest staining. The interpretation of PC expression was performed by the scores of the percent positive cells (1–4) multiplied by the scores of staining intensity (0–3) to reach the total final immunohistochemistry (IHC) score of 0–12. The results were then categorized as follows; low expression, IHC score ≤ 6; and high expression, IHC score > 6. All samples were anonymous and independently scored by two investigators of whom one is a pathologist.

Statistical analysis

All values were expressed as mean ± standard deviations. The statistical analysis was performed using Student's t-test, two way anova and univariate analysis where * $P < 0.05$, ** $P < 0.01$ and *** P value < 0.001.

Results

PC was overexpressed in breast cancer tissues and correlated with tumor size and late stage of tumor progression

A previous study has reported the overexpression of PC in solid lung tumor tissue [14]. To examine whether this was the case for breast cancer, we performed immunohistochemistry

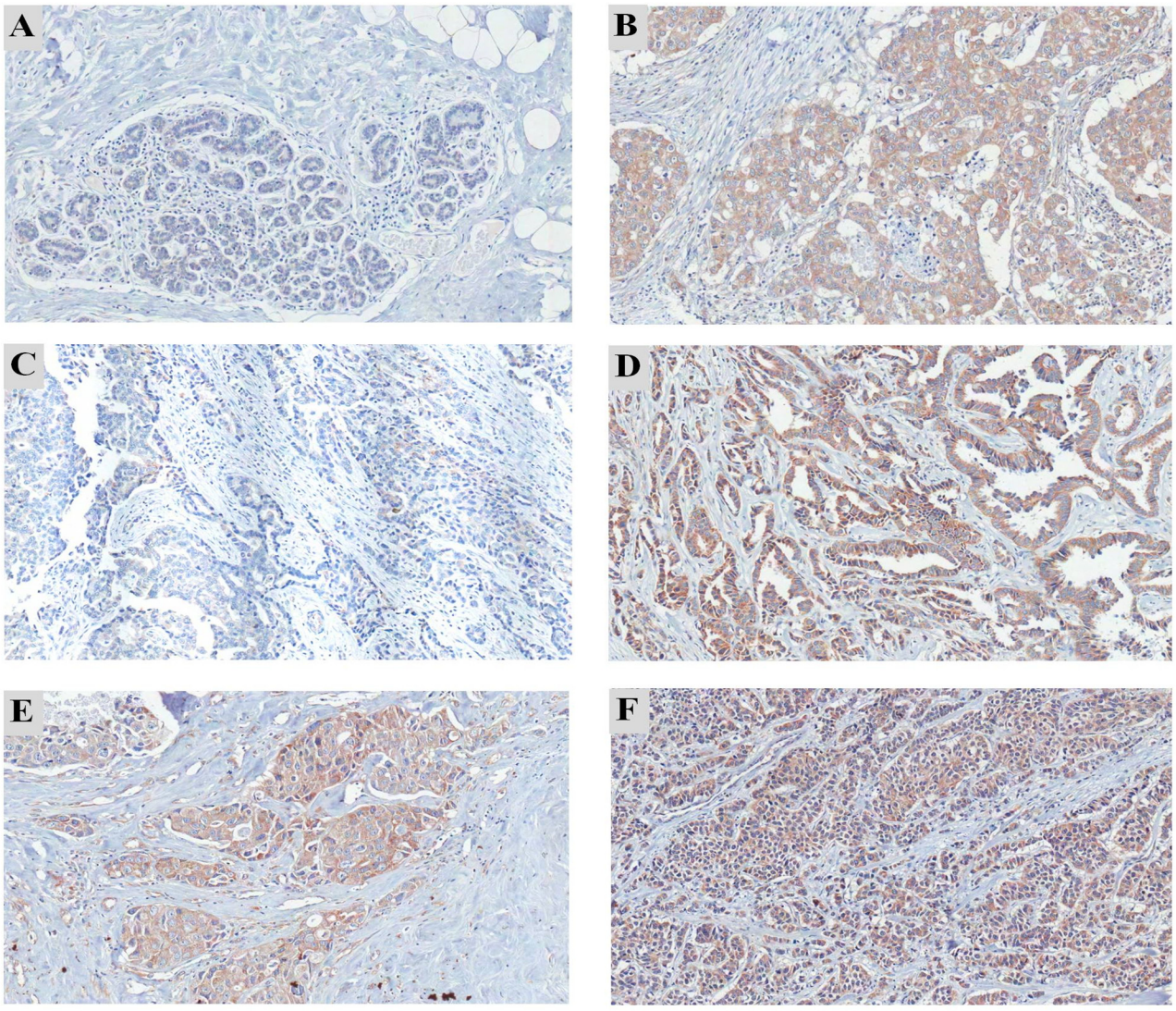

Fig 1. Immunohistochemistry staining of PC in paraffin-embedded breast tissue sections of patients with various stages of breast cancer. (A) Normal adjacent area of breast tissue showing weak staining of PC compared to strong staining in the cancerous area (B) of the same tissue. The representative samples showing different expression levels of PC in different stages of breast cancer: (C) stage 1, (D) stage 2, (E) stage 3 and (F) stage 4. Original magnification, 100x.

doi:10.1371/journal.pone.0129848.g001

(IHC) staining using an anti-PC antibody on breast tissue sections collected from 57 patients who had stages I-IV of breast cancer using anti-PC antibody. In contrast to the non-cancerous area of the tissue sections, (Fig 1A), PC was highly expressed in the cancerous areas of the breast tissues (Fig 1B). The expression levels of PC expression also varied in different stages of cancer (Fig 1C–1F). Expression of PC in stromal fibroblasts and infiltrating immune cells was rarely observed.

PC expression was detected in breast tissues of most cancer patients (96% of the total studied cases) except two cases which were stage I. Overall, 72% of breast cancer tissues showed a low expression level of PC whereas 28% had a high expression level of PC (Table 1). Based on grouping the patients into early stage without distant metastasis (stages I-III) and late stage with distant metastasis (stage IV), 67% (4 in 6 cases) of breast cancer with distant metastasis showed a high expression level of PC. In contrast, only 24% (12 in 51 cases) of patients without

Table 1. Univariate analysis of expression level of PC in breast tissues and clinicopathological parameters.

Variable (Total cases)		PC expression (IHC score)		P-value
	No of case	Low (≤ 6)	High (> 6)	
Tumor volume (cm^3) (52)				
≤ 4	28	24	4	0.033*
> 4	24	14	10	
Tumor staging (57)				
I	18	15	3	0.225
II	22	17	5	0.555
III	11	7	4	0.482
IV	6	2	4	0.046*
Histological type (56)				
Well-differentiated	7	6	1	0.661
Moderately-differentiated	30	20	10	0.365
Poorly-differentiated	19	15	4	0.543
Invasion (57)				
Absence	24	18	6	0.769
Presence	33	23	10	
ER (57)				
High (4)	38	29	9	0.356
Low (0–3+)	19	12	7	
PR (57)				
High (4)	17	14	3	0.342
Low (0–3+)	40	27	13	
HER2 (57)				
Negative	37	27	10	1.00
Positive	20	14	6	

doi:10.1371/journal.pone.0129848.t001

metastasis had a high level of PC expression. Univariate analysis showed a significant correlation between PC expression level and stage IV (P = 0.046). Interestingly, PC expression showed a significant correlation with the tumor size (Table 1) (P = 0.033) i.e., PC was poorly expressed in most tumor cases with small volume (<4 cm^3) (86%, 25/29). The other clinicopathological parameters including histological type, invasion, estrogen receptor (ER), progesterone receptor (PR) and HER2 expression did not show statistical associations with PC expression.

PC is highly abundant in metastasized breast cell lines, MDA-MB-231 and MDA-MB-435

Because the degree of PC expression showed statistical association with tumor size and stage, we hypothesized that PC was required to support tumor growth and invasion of breast cancer cells. We examined the above hypothesis by investigating the expression levels of PC in breast cancer cell lines with different degrees of motility, namely, MCF-7, SKBR3, MDA-MB-435 and MDA-MB-231. As shown in Fig 2A, the motilities of MDA-MB-435 and MDA-MB-231 are 10-fold and 75-fold higher than those of MCF-7 and SKBR3 cells, respectively. Consistent with the motility phenotype, MCF-7 and SKBR3 cell lines possess low expression level of PC mRNA while MDA-MD-231 and MDA-MB-435 cell lines express PC mRNA 4-fold and 2-fold higher than MCF-7 (Fig 2B). The two alternative PC mRNA isoforms, namely variant 1 and variant 2 which differ in their 5'-untranslated regions, are differentially transcribed from two alternative

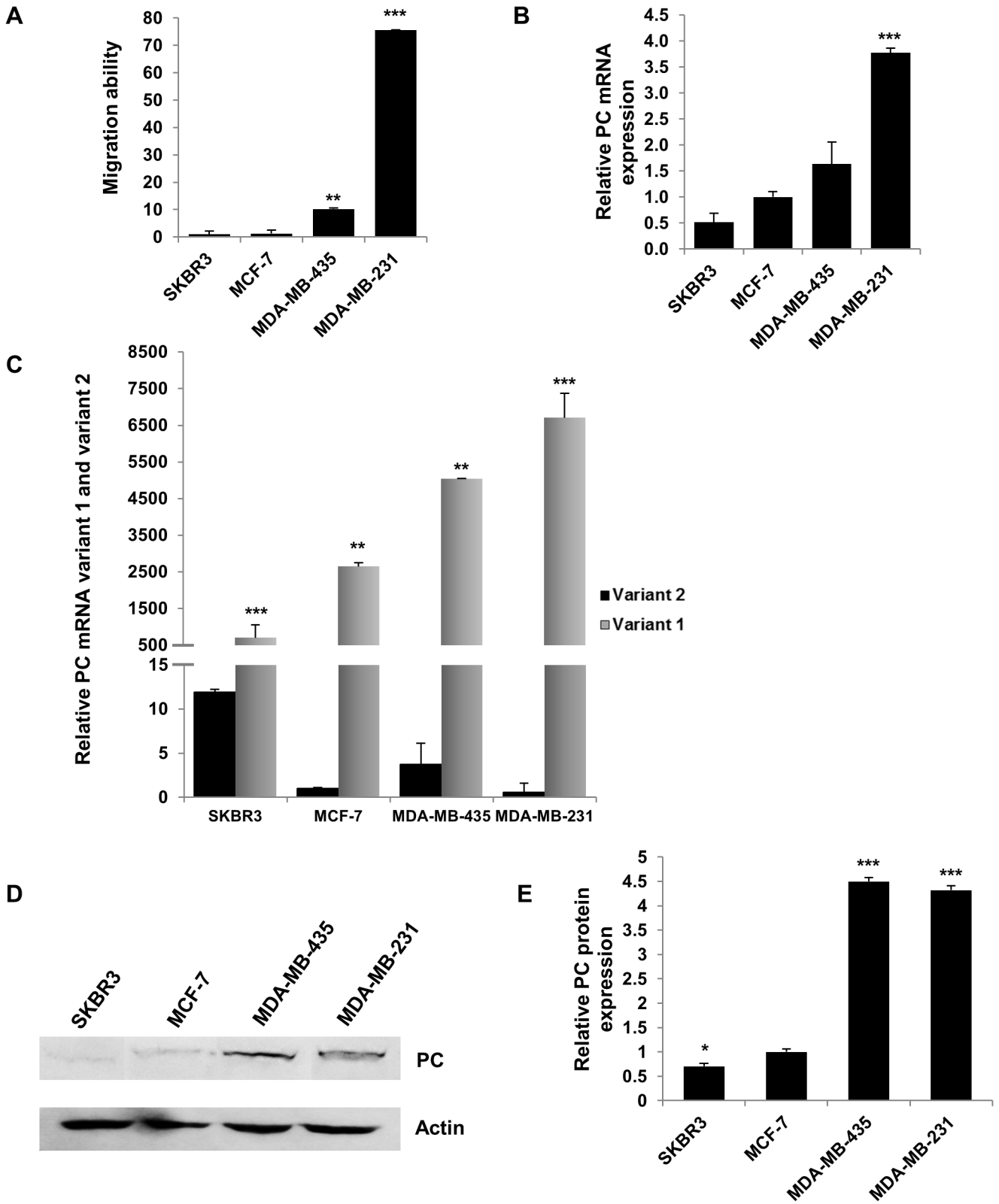

Fig 2. Migration ability of various breast cancer cell lines and the expression levels of PC in these cell lines. A, Migration ability of SKBR3, MCF-7, MDA-MB-435 and MDA-MB-231. **B**, Q-PCR analysis of PC mRNA expression in the above cell lines. The expression of PC was normalized with the expression of 18s rRNA gene and shown as the relative gene expression. The relative PC expression in MCF-7 was arbitrarily set as 1. **C**, Real time PCR

analysis of PC mRNA variant 1 and 2 expression in the above cell lines. The expression of PC was normalized with the expression of 18s rRNA gene and shown as the relative gene expression. The expression of the relative PC mRNA variants in MCF-7 was arbitrarily set as 1. **D**, Western blot analysis of PC protein in the above cell lines. The blot was also probed with anti-actin antibody to serve as loading control. **E**, The immunoreactive band intensity of PC in D was quantitated and normalized with that of the β-actin and shown as the relative PC expression. The statistical analysis was conducted using student's t-test where $*P < 0.05$, $**P < 0.01$, $***P < 0.001$.

doi:10.1371/journal.pone.0129848.g002

promoters, the distal and the proximal promoters, respectively [24]. To examine which of these two PC mRNA isoforms was up-regulated in MDA-MB-231 and MDA-MB-435 cells, quantitative real-time PCR using primers specific for variants 1 and 2 was performed. As shown in Fig 2C, expression of variant 1 was up-regulated in all cell lines however both MDA-MB-231 and MDA-MB-431 possessed expression of variant 1 more than MCF-7 and SKBR3.

Western blot analysis of PC protein of these four cell lines was also consistent with their motility phenotype and PC mRNA expression i.e. the abundance of PC in MDA-MB-231 and MDA-MB-435 are 4.5-fold higher than in MCF-7 and SKBR3 (Fig 2D and 2E).

Suppression of PC expression lowers growth, migration and invasion ability of highly metastasized breast cancer cell lines

We next examined whether overexpression of PC in the MDA-MB-231 cell line was necessary to support its growth and invasion ability. We suppressed expression of PC in this cell line by siRNA and assessed the phenotypes of the knockdown cells. As shown in Fig 3A and 3B, suppression of PC expression in MDA-MB-231 resulted in 90% and 80% decreases in PC mRNA and PC protein levels, respectively. PC knockdown MDA-MB-231 cell line did not affect proliferation in the first day but showed a 50% reduction in growth by day 2 (Fig 4A). Similar degrees of reduction were observed until day 7. Real-time PCR analysis also confirmed that the retarded proliferation rate of this cell line was accompanied by suppression of PC mRNA throughout day 7 (Fig 4B). Because suppression of PC expression did not completely inhibit the cell proliferation rate, the ability of the PC knockdown MDA-MB-231 cells to grow in the complete growth medium may have resulted from the compensation of anaplerosis via glutaminolysis. To examine whether this latter pathway contributes to the survival of the PC knockdown cells, the glutamine-independent PC deficient MDA-MB-231 cell line was generated. In

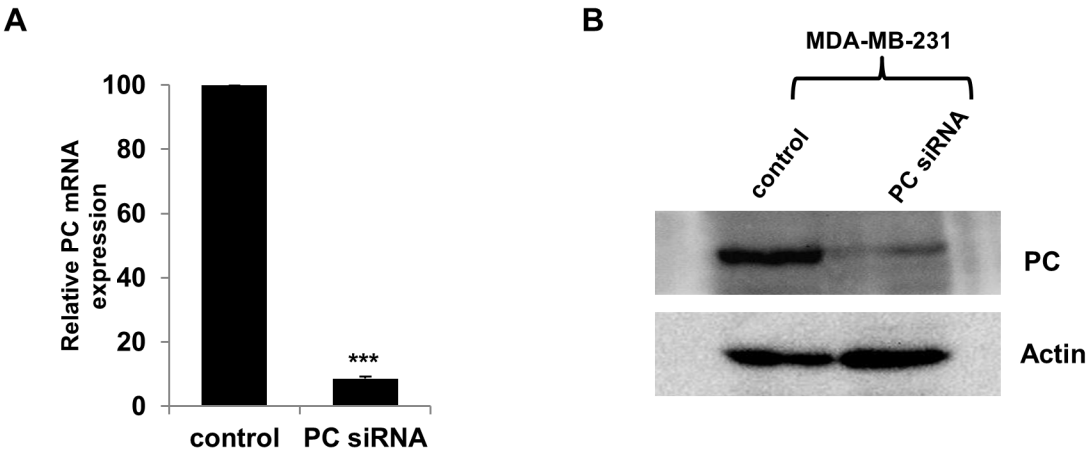

Fig 3. siRNA-mediated suppression of PC expression in MDA-MB-231 cell line. Real time PCR analysis of PC mRNA expression in MDA-MB-231 cells transfected with scrambled control (Control) or PC siRNA. The PC mRNA level was determined by Q-PCR at 48 h post-transfection (A). Western blot analysis of PC protein in the PC knockdown MDA-MB-231 and the scrambled control (B). The statistical analysis was conducted using student's t-test $***P \leq 0.001$.

doi:10.1371/journal.pone.0129848.g003

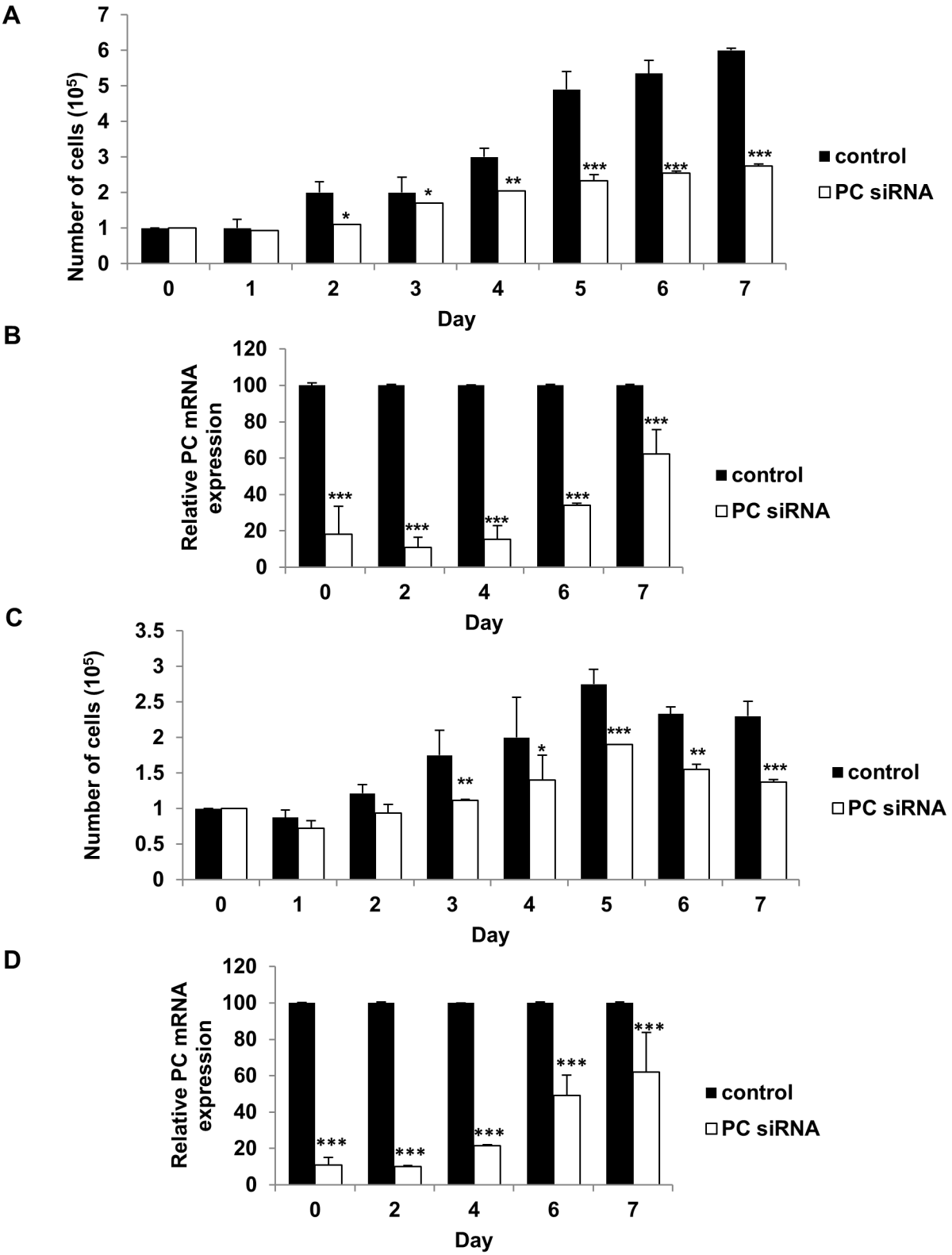

Fig 4. Suppression of PC expression in MDA-MB-231 retarded proliferation both in glutamine-nourished and glutamine-depleted conditions. MDA-MB-231 cells were transiently transfected with PC or scrambled control siRNAs. At 48 h post transfection cells were trypsinized, re-plated and grown in the presence of 0 mM or 4 mM glutamine for 7 days. The proliferation rate of the PC knocked down (PC siRNA) and the control MDA-MB-231 cell lines (Control) grown in the medium containing 4 mM (A) or 0 mM (C) glutamine. The relative expression of PC mRNA in the knocked down MDA-MB-231 cells

grown in the presence of 4 mM (B) or 0 mM (D) glutamine throughout the assay. The results are means obtained from two independent experiments, each in triplicate. The statistical analysis was conducted using ANOVA test where $*P < 0.05$, $**P < 0.01$, $***P < 0.001$.

doi:10.1371/journal.pone.0129848.g004

the absence of glutamine supplementation in the medium, any anaplerotic reaction would rely exclusively on a PC-catalyzed reaction. We generated the glutamine-independent MDA-MB-231 cell line (Gln^-) by gradually depleting glutamine from the culture medium before transfecting this cell line with PCsiRNA so that the phenotype of this cell line became glutamine-independent and PC deficient (Gln^-/PC^--MDA-MB-231). The Gln^-/PC^--MDA-MB-231cells grown in the glutamine-free medium showed a growth rate similar to the control cell line in the first two days but showed approximately 30–40% reduction of cell proliferation from day 3 until day 7 (Fig 4C). Real time PCR analysis also confirmed that the retarded proliferation rate of this cell line was accompanied by suppression of PC mRNA throughout day 7 (Fig 4D). As the levels of PC expression were significantly correlated with the stages of cancer progression, we hypothesized that PC was involved in the aggressive phenotypes of breast cancer cells, particularly migration and invasion. We investigated whether PC was required to support migration and invasion ability of MDA-MB-231 cells. We first examined the ability of the PC knockdown MDA-MB-231 cells to migrate across a wound. As shown in Fig 5A and 5B, the PC knockdown cells exhibited a 40% reduction of migration across the wound compared to the scrambled control. A similar degree of reduction was observed from the glutamine-independent PC knockdown cell line (Fig 5C and 5D).

We next examined the ability of the knockdown cells to invade through an extracellular matrix by performing an *in vitro* invasion assay using transwell coated with Matrigel. As shown in Fig 6A and 6B, the PC knockdown cells showed a 40% reduction of their invasion ability. However, the reduced invasion ability was more pronounced (60%) in the glutamine-independent knockdown MDA-MB-231 cells (Fig 6C and 6D).

We also performed similar experiments in MDA-MB-435 cells which also bear a high level of PC protein although its migration ability is less than MDA-MB-231. Suppression of PC mRNA expression by 80% (Fig 7A) resulted in 70% down-regulation of PC protein (Fig 7B and 7C). The PC knockdown MDA-MD-435 cells showed retarded growth rates at day 4 onwards (Fig 7D). Suppression of PC was also associated with 40% reduction of cell migration (Fig 7E) and 50% reduction of invasion ability (Fig 7F). Similar results were obtained when the knockdown cells were grown in the absence of glutamine (data not shown).

Overexpression of PC in MCF-7 cells increases their proliferation and *in vitro* invasion

To confirm whether overexpression of PC in breast cancer cells with low metastatic ability would increase their proliferation rate and invasion ability, we generated stable MCF-7 cell overexpressing PC. As shown in Fig 8A, the proliferation rate of MCF-7 cells at day 3 onward of MCF-7 with overexpressed PC was 2-fold higher than the MCF-7 cell line transfected with an empty vector. Similar results were observed when the MCF-7 cell line with overexpressed PC was grown in glutamine-depleted medium (Fig 8B). It is noted that the level of endogenous PC was slightly increased in the MCF-7 cell line harboring empty vector when these cells were grown in the absence of glutamine, suggesting a compensatory increase of PC expression in response to the deprivation of glutamine. MCF-7 cells with overexpressed PC also showed 2-fold and 2.5-fold increases in the migration and invasion ability, respectively. Similar results were obtained when the cells were assayed under glutamine-depleted medium (Fig 8C and 8D).

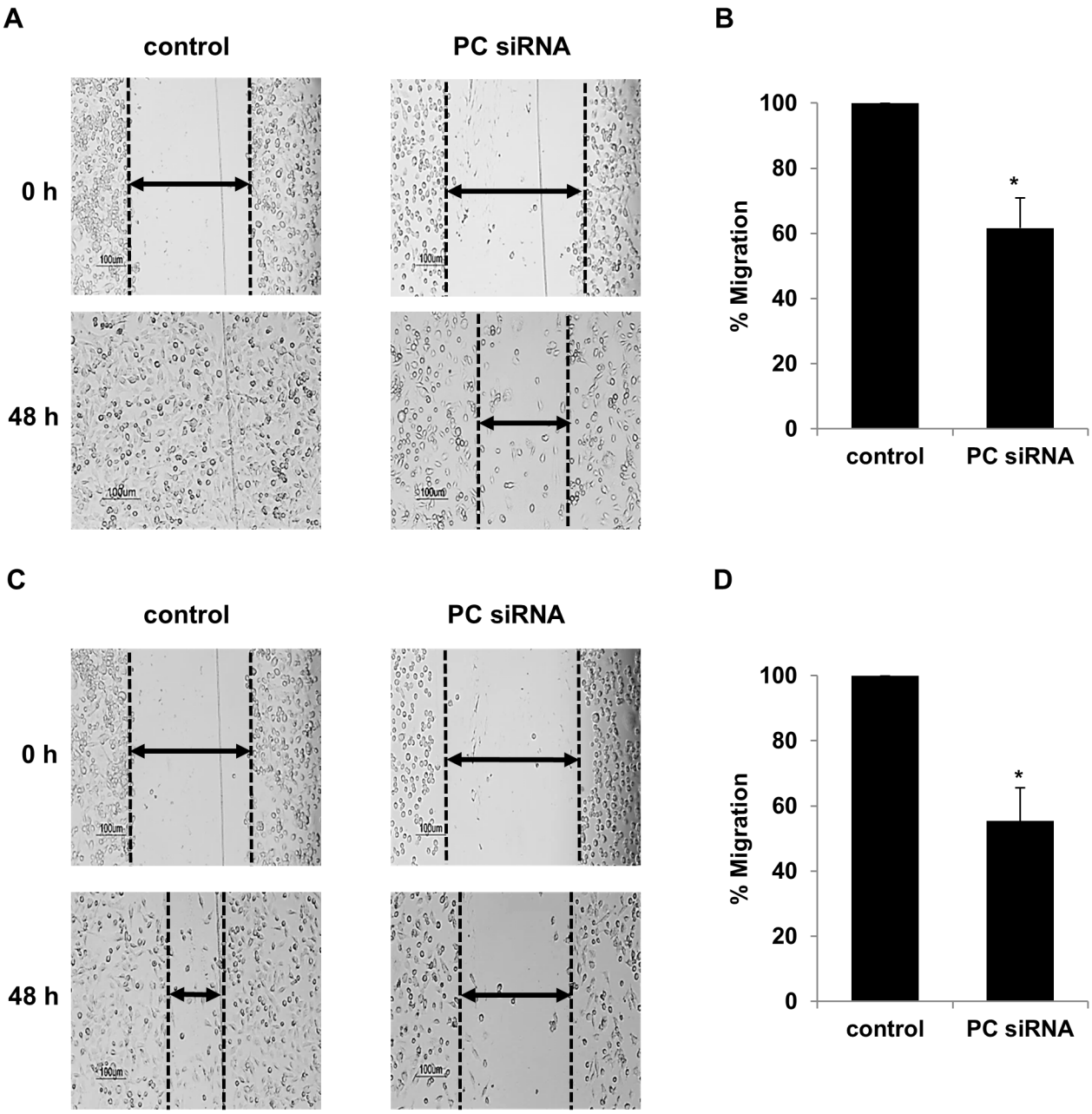

Fig 5. Suppression of PC expression in MDA-MB-231 cells reduced migration. Representative images of wound-healing assays. MDA-MB-231 cells were transiently transfected with PC or scrambled control siRNAs. At 48 h post transfection, wound-healing assays were performed as described in the materials and methods. (A, C) Representative images of the PC knockdown (PC siRNA) or scrambled control cells (Control) migrated across the wound areas in the presence of 4 mM (A) or absence of glutamine (C). The wound's closure (width) of the PC knockdown was measured and shown as the means ± standard deviation of that of the scrambled control which was arbitrarily set as 100% (B, D). The results were obtained from two independent experiments, each in triplicate. The statistical analysis was conducted using student's t-test where $*P < 0.05$.

doi:10.1371/journal.pone.0129848.g005

Discussion

Anaplerotic reactions are important to replenish the levels of TCA cycle intermediates upon their removal for biosynthetic purposes [9,28]. Anaplerosis via glutaminolysis is well known to be important in many tumors as they rely on this reaction to provide precursors needed for the

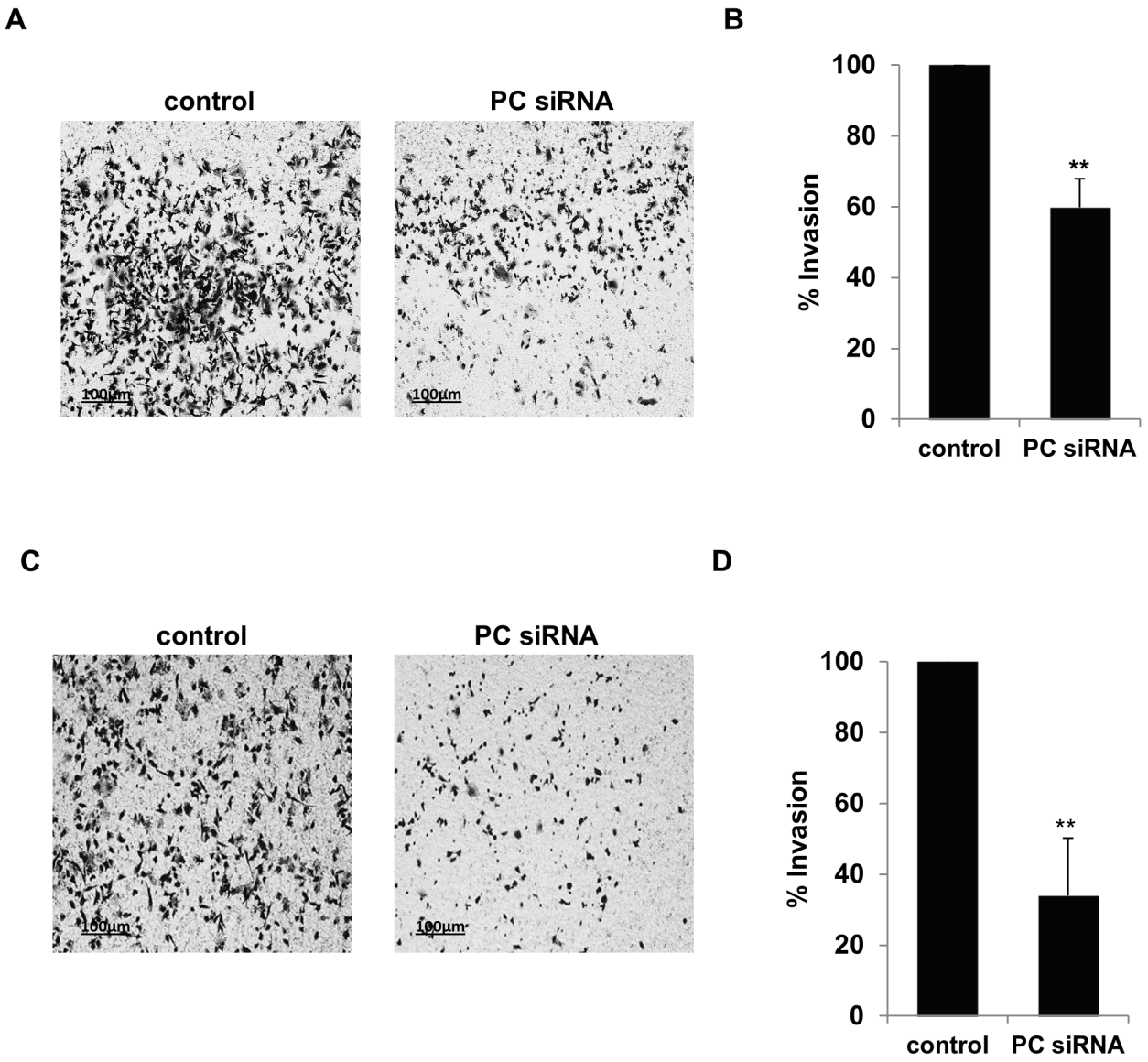

Fig 6. Suppression of PC expression in MDA-MB-231 lowers invasion ability. MDA-MB-231 cells were transiently transfected with PC or scrambled control siRNAs. At 48 h post transfection, an *in vitro* invasion assay was performed for 4 h in the presence of 4 mM (A) or 0 mM (C) glutamine. The number of PC siRNA-transfected cells that invaded the transwell coated with Matrigel was counted in 5 different fields and shown as means ± standard deviation in comparison with that of the scrambled control which was arbitrarily set as 100% (B, D). The results were obtained from three independent experiments, each done in duplicate. The statistical analysis was conducted using student's t-test where ** $P < 0.01$.

doi:10.1371/journal.pone.0129848.g006

syntheses of structural components, i.e. membrane lipids and nucleic acids. Disruption of glutamine supply to many tumors is proposed to be one means of inhibiting their growth [29]. Anaplerosis via PC has received much attention in the past few years. Fan *et al.* [14] have reported a high rate of pyruvate carboxylation flux as a result of overexpression of PC protein in non-small cell lung cancer, suggesting that this cancer is highly anabolic. Overexpression of PC in this type of cancer indicates its need to fulfill the high anabolic demands during the establishment of the primary location [14]. Cheng *et al* [19] have also found that PC is overexpressed in glioblastomas in which PC is required to support tumor growth. Subsequent studies revealed that the presence of PC activity in glioblastomas is consistent with its anaplerotic role

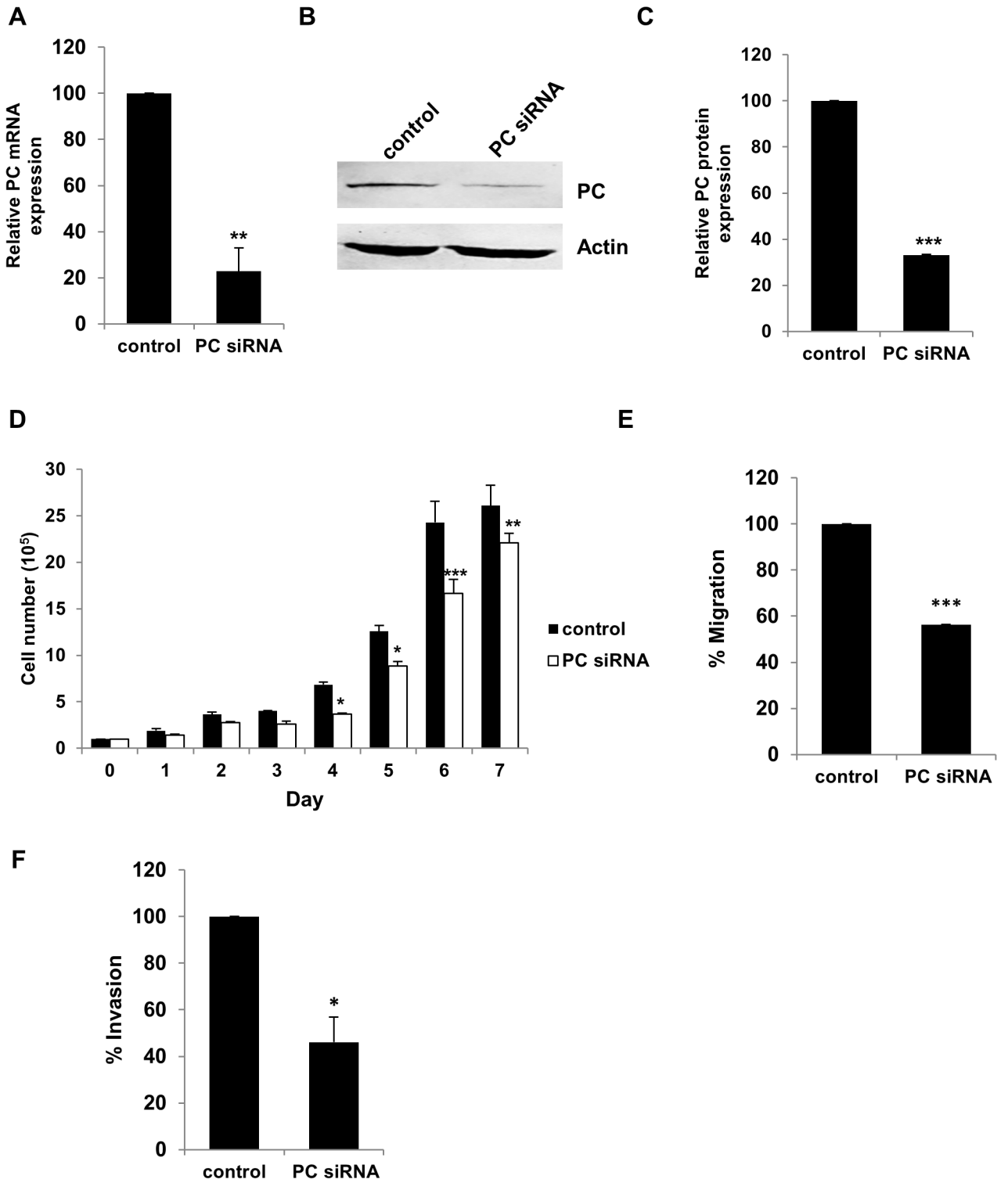

Fig 7. Suppression of PC expression in MDA-MB-435 cells reduces their proliferation, migration and invasion. PC mRNA expression in the knockdown MDA-MB-435 was quantitated by Q-PCR (A). Western blot analysis of MDA-MB-435 cells transfected with PC siRNA (PC siRNA) or scrambled control (Control) (B). The band intensity of PC in B was quantitated and normalized with β-actin band and expressed as relative PC expression (C). Proliferation assay (D), migration assay (E) and invasion assay (F) of the PC knockdown MDA-MB-435 cells. The statistical analyses in B, C, E and F were conducted using student's t-test while in D was conducted using ANOVA test. $*P < 0.05$, $**P < 0.01$, $***P < 0.001$.

doi:10.1371/journal.pone.0129848.g007

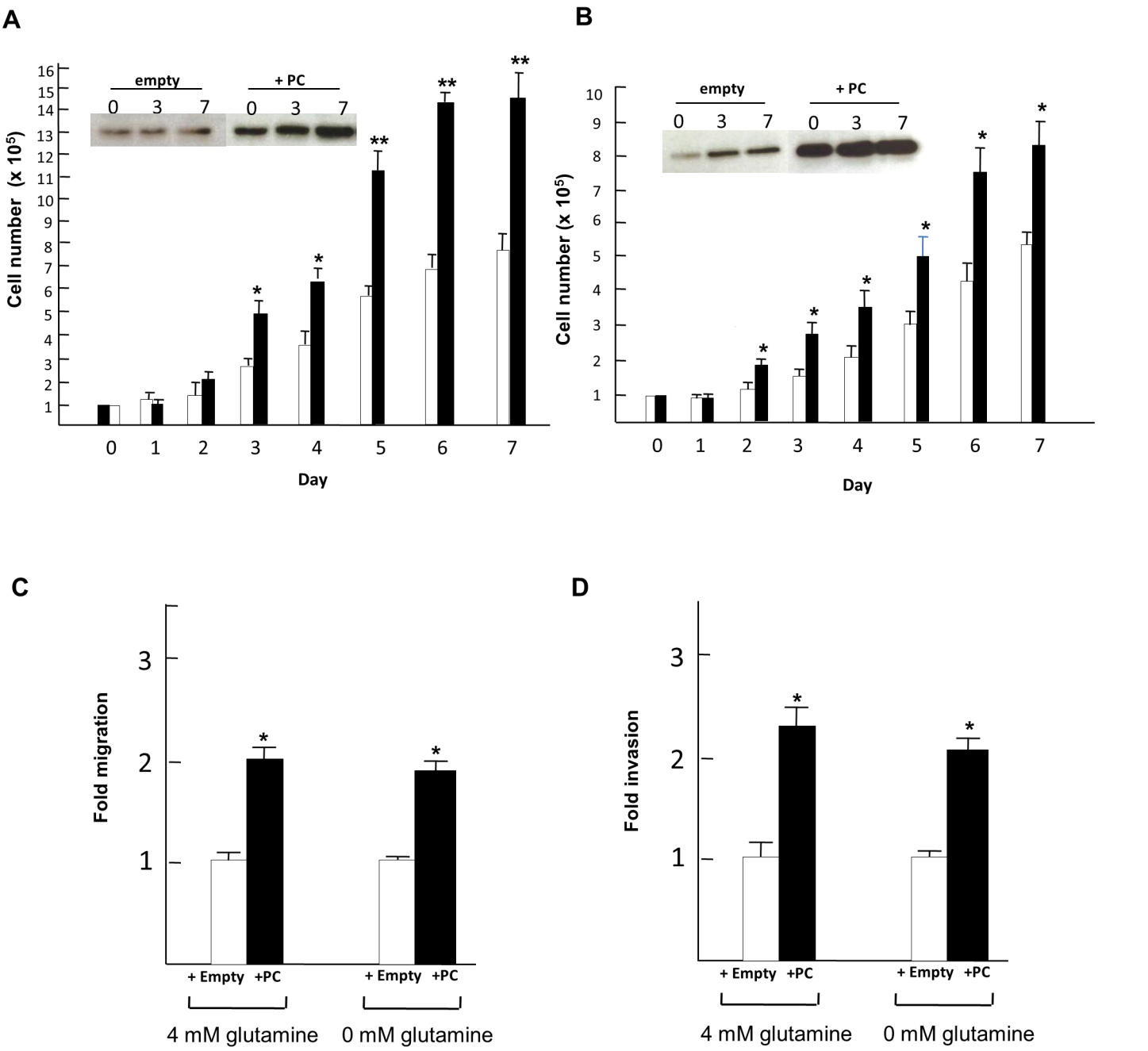

Fig 8. Overexpression of PC in MCF-7 cells increases their proliferation, migration and invasion. Proliferation rate of MCF-7 cells overexpressing PC grown in the medium containing 4 mM (A) or 0 mM glutamine (B). Insets in A and B are the Western blot analysis of MCF-7 cells transfected with empty vector (+empty, white bars) or with overexpressed PC (+PC, black bars) at days 0, 3 and 7. MCF-7 cells overexpressing PC grown in the presence or absence of glutamine were also subjected to migration (C) and invasion (D) assays. The statistical analysis was conducted using student's t-test where * $P < 0.05$, ** $P < 0.01$.

doi:10.1371/journal.pone.0129848.g008

[30]. Furthermore, pyruvate carboxylation is also shown to be an important anaplerotic reaction that contributes to the citrate pool during reductive carboxylation in osteosarcoma and renal carcinoma cell lines [31].

Here we show that PC is also highly expressed in breast cancer tissue but not in the normal breast tissue. The statistical association between the levels of PC expression and the tumor size and stage prompted us to investigate the role of this enzyme in supporting growth and invasion. That expression of PC was highly abundant in two aggressive breast cancer cell lines, i.e. MDA-MB-231 and MDA-MB-435 but low in less aggressive cell lines, i.e. MCF-7 and SKBR3 hints at the involvement of this enzyme in the aggressive phenotype of these two metastatic cell lines. Suppression of PC expression in both MDA-MB-231 and MDA-MB-435 cells retarded cell proliferation rate, suggesting that these cell lines modestly depend on anaplerosis via the PC reaction. The necessity for PC in supporting growth of MDA-MB-231 cells appears to be different from the SF-XL glioblastoma cell line which utilizes glutaminolysis rather than pyruvate carboxylation as the primary anaplerotic reaction [32] because suppression of PC expression does not affect its growth under glutamine-dependent conditions [15]. However, under glutamine-depleted growth conditions, the PC-knockdown SF-XL glioblastoma cell line shows marked reduction (>80%) of proliferation [15], indicating that the glioblastoma cell line uses pyruvate carboxylation as an alternative route to support its growth during glutamine-depleted conditions. However this is not the case for MDA-MB-231 and MDA-MB-435 cells because suppression of PC expression still allows them to grow, albeit at the 50% reduced proliferation rate observed under glutamine-dependent growth conditions. A similar but not identical phenotype of the PC-knockdown MDA-MB-231 and MDA-MB-435 cells was observed under glutamine-independent growth conditions. An involvement of PC in the growth phenotype of MDA-MB-231 cells is also consistent with the association between the levels of PC expression and sizes of breast tumor in clinical samples. Low expression levels of PC in breast tumors with a smaller size of tumor (< 4 cm^3) may limit their growth compared with the larger size of tumors which contain higher levels of PC expression ($P < 0.05$) [Table 1]. The above observations were also confirmed by overexpression of PC in MCF-7, which is a low metastatic cell line. MCF-7 cells overexpressing PC show enhanced growth rate, motility and invasion. The enhanced growth phenotype of MCF-7 with overexpressed PC was consistent with previous reports which show that ectopic expression of PC in many mammalian cell lines enhances cell growth and biomass production [33,34,35].

Although several studies have pointed to the importance of PC in providing oxaloacetate which is the first TCA cycle intermediate, that in turn is converted to other precursor molecules such as citrate required for lipid and nucleic acid synthesis for rapid tumor growth, not much is known as to whether PC is required to support migration and invasion ability of some tumors [14, 15, 19]. Our present study is the first report to show a strong association between the levels of PC expression in breast tissues of patients and stages of cancer progression ($P < 0.05$), which suggests PC is involved in metastasis. This was also studied in MDA-MB-231 and MDA-MB-435 cells. Suppression of expression of PC markedly reduced both migration and invasion ability through an extracellular matrix under both glutamine-nourished and glutamine-depleted conditions, suggesting that PC is required to support these aggressive phenotypes of MDA-MB-231 cells. The negative staining of PC expression by immunohistochemistry in the normal area of breast tissue is consistent with the low level of expression of PC in the MCF-7 cell line. The transcriptional mechanism underlying overexpression of PC in MDA-MB-231 over MCF-7 is due to the selective activation of the distal rather than the proximal promoter of the human PC gene (Fig 2C). The specific transcription of the distal rather than the proximal promoter of the human PC gene may be attributed to the presence of different putative transcription factor binding sites of both promoters [24] during the transition of a low to a high metastatic phenotype. Interestingly, Lee *et al.* (2012) have shown that the MCF-7 cells stimulated with Wnt 1 or Wnt3a ligands, or ectopically expressed with Snail, a target transcription factor of Wnt signaling, show a marked increase in PC expression. Because the Wnt

signaling pathway also induces Snail-dependent epithelial-mesenchymal transition (EMT), which is responsible for invasion and metastasis in many tumors [36,37], the authors suggest that anaplerosis via up-regulation of PC expression is one of several metabolic responses of breast tumor during EMT [38]. Although this study underscores that the Wnt signaling pathway is important for transcriptional induction of the PC gene, the authors cannot detect direct binding of Snail, an effector transcription factor in response to Wnt signaling to the distal promoter of human PC gene [38].

Although the involvement of PC with migration and *in vitro* invasion of MDA-MB-231 cells *per se* is yet to be elucidated, it is apparent that migration of the tumors from the primary location to the distal organs during metastasis requires multiple biological steps such as intravasation into the circulation, followed by migration, extravasation to a second site for adhesion, tumorigenesis and angiogenesis [39], all of which require substantial amounts of ATP to provide a source of energy [40]. This is consistent with the findings that metastasized tumors including breast and osteosarcoma show up-regulation of energy generating pathways including TCA cycle activity and nucleotide metabolism [40,41,42]. As PC provides oxaloacetate, the first intermediate in the TCA cycle, disruption of oxaloacetate supply by suppressing PC expression may disrupt the continual supply of this intermediate required for oxidation of pyruvate hence lowering ATP production required to support cell movement. Although many tumors are highly glycolytic, growing evidence have shown that highly metastasized tumors also utilize mitochondria to oxidize glucose. In ovarian cancer and possibly breast cancer [43,44], the metastasized tumor invades the adjacent adipose tissue to hijack lipids to use as an alternative fuel apart from glucose to support tumor growth and invasion. Since β-oxidation of fatty acids produces large amounts of acetyl-CoA which is subsequently oxidized via the condensation with oxaloacetate in the TCA cycle, a high abundance of PC would ensure that oxaloacetate is not limited during β-oxidation of the hijacked lipids. The presence of PC may be involved in gluconeogenesis. Leithner *et al* [45] have recently shown that lung cancer utilizes gluconeogenesis to recycle lactate back to glucose as an adaptive metabolic response to glucose depletion. This was born out by the observation of overexpression of mitochondrial phosphoenolpyruvate carboxykinase (PEPCK-M), one of four gluconeogenic enzymes concomitant with the increased flux of lactate to phosphoenolpyruvate. However, the level of PC expression varied in the three lung cancers examined in this study and was not up-regulated by low glucose concentrations.

Other possible roles of PC in supporting breast cancer growth and metastasis may be linked to the metabolic coupling factor, NADPH. In pancreatic β-cells, PC is highly abundant to support the high activity of pyruvate cycling which provides a large amount of NADPH, required for glucose-induced insulin secretion [46]. In tumors, it is possible that the similar pyruvate/malate shuttle [47,48,49] may operate in the similar manner as in the pancreatic islet. Several lines of evidence have suggested that NADPH may be a key molecule which links between reactive oxygen species (ROS) formation and the EMT via the overexpression of NADPH oxidase, notably the NOX4 isoform which is overexpressed in many tumors [50,51]. NOX4 is known to mediate the production of ROS which triggers cellular senescence, resistance to apoptosis and tumorigenic transformation [52].

The lack of statistical association between expression of PC and ER as well as PR and HER2 in cancer breast tissues indicates that PC is not regulated by these hormones or growth factor. This is also consistent with the phenotypes of MCF-7 and MDA-MB-231 cells which are ER^+ and ER^-, respectively [53].

In summary we have shown that PC is expressed in breast cancer at a higher level than in the normal breast tissue, and exhibits a statistical association with tumor size and the progression of metastasis. Using the highly metastatic breast cancer cell lines, MDA-MB-231 and

MDA-MB-435 as models, we showed that suppression of PC expression markedly reduces the proliferation, migration and *in vitro* invasion ability of cells, highlighting the possible roles of PC in supporting these processes during oncogenesis and progression of breast cancer.

Author Contributions

Conceived and designed the experiments: PP CT SJ. Performed the experiments: PP. Analyzed the data: PP CT MW SJ. Contributed reagents/materials/analysis tools: CT MW JCW MJM SJ. Wrote the paper: PP CT SJ. N/A.

References

1. Cairns RA, Harris IS, Mak TW (2011) Regulation of cancer cell metabolism. *Nat Rev* Cancer 11: 85–95.
2. Warburg O (1956) On the origin of cancer cells. Science 123: 309–314. PMID: 13298683
3. Vander Heiden MG, Cantley LC, Thompson CB (2009) Understanding the Warburg effect: the metabolic requirements of cell proliferation. Science 324: 1029–1033. doi: 10.1126/science.1160809 PMID: 19460998
4. Ward PS, Thompson CB (2012) Metabolic reprogramming: a cancer hallmark even warburg did not anticipate. Cancer Cell 21: 297–308. doi: 10.1016/j.ccr.2012.02.014 PMID: 22439925
5. Kim JW, Tchernyshyov I, Semenza GL, Dang CV (2006) HIF-1-mediated expression of pyruvate dehydrogenase kinase: a metabolic switch required for cellular adaptation to hypoxia. Cell Metab 3: 177–185. PMID: 16517405
6. Kim JC, Gao P, Liu YC, Semenza GL, Dang CV (2007) Hypoxia-inducible factor 1 and dysregulated c-Myc cooperatively induce vascular endothelial growth factor and metabolic switches hexokinase 2 and pyruvate dehydrogenase kinase 1. Mol Cell Biol 27: 7381–7393. PMID: 17785433
7. Dang CV, Kim JW, Gao P, Yustein J (2008) Hypoxia and metabolism—Opinion—The interplay between MYC and HIF in cancer. Nat Rev Cancer 8: 51–6. PMID: 18046334
8. Levine AJ, Puzio-Kuter AM (2010) The control of the metabolic switch in cancers by oncogenes and tumor suppressor genes. Science 330: 1340–1344. doi: 10.1126/science.1193494 PMID: 21127244
9. Owen OE, Kalhan SC, Hanson TW (2002) The key role of anaplerosis and cataplerosis for citric acid cycle function. J Biol Chem 277: 30409–30412. PMID: 12087111
10. Eagle H (1955) Nutrition needs of mammalian cells in tissue culture. Science 122: 501–4. PMID: 13255879
11. Reitzer LJ, Wice BM, Kennell D (1979) Evidence that glutamine, not sugar, is the major energy source for cultured HeLa cells. J Biol Chem 254: 2669–2676. PMID: 429309
12. Wise DR, DeBerardinis RJ, Mancuso A, Sayed N, Zhang XY, Pfeiffer HK, et al. (2008) Myc regulates a transcriptional program that stimulates mitochondrial glutaminolysis and leads to glutamine addiction. Proc Natl Acad Sci USA 105: 18782–18787. doi: 10.1073/pnas.0810199105 PMID: 19033189
13. Gao P, Tchernyshyov I, Chang TC, Lee YS, Kita K, Ochi T, et al. (2009) c-Myc suppression of miR-23a/b enhances mitochondrial glutaminase expression and glutamine metabolism. Nature 458: 762–765. doi: 10.1038/nature07823 PMID: 19219026
14. Fan TW, Lane AN, Higashi RM, Farag MA, Gao H, Bousamra M, et al. (2009) Altered regulation of metabolic pathways in human lung cancer discerned by (13)C stable isotope-resolved metabolomics (SIRM). Mol Cancer 8:41. doi: 10.1186/1476-4598-8-41 PMID: 19558692
15. Sellers K, Fox MP, Bousamra M, Slone SP, Higashi RM, Miller DM, et al. (2015) Pyruvate carboxylase is critical for non-small-cell lung cancer proliferation. J Clin Invest 125: 687–98. doi: 10.1172/JCI72873 PMID: 25607840
16. Parsons DW, Jones S, Zhang X, Lin JC, Leary RJ, Angenendt P, et al. (2008) An integrated genomic analysis of human glioblastoma multiforme. Science 32: 1807–12.
17. Yang M, Soga T, Pollard PJ (2011) Oncometabolites: linking altered metabolism with cancer. J Clin Invest 12:3652–8.
18. Izquierdo-Garcia JL, Cai LM, Chaumeil MM, Eriksson P, Robinson AE, Pieper RO, et al. (2014) Glioma Cells with the IDH1 Mutation Modulate Metabolic Fractional Flux through Pyruvate Carboxylase. PLoS ONE 9: e108289. doi: 10.1371/journal.pone.0108289 PMID: 25243911

19. Cheng T, Sudderth J, Yang C, Mullen AR, Jin ES, Matés JM, et al. (2011) Pyruvate carboxylase is required for glutamine-independent growth of tumor cells. Proc Natl Acad Sci USA 108: 8674–8679. doi: 10.1073/pnas.1016627108 PMID: 21555572

20. Soule HD, Vazguez J, Long A, Albert S, Brennan M (1973) A human cell line from a pleural effusion derived from a breast carcinoma. J Natl Cancer Inst 51: 1409–1416. PMID: 4357757

21. Cailleau R, Young R, Olive M, Reeves WJ (1974) Breast tumor cell lines from pleural effusions. J Natl Cancer Inst 53: 661–674. PMID: 4412247

22. Jitrapakdee S, Walker ME, Wallace JC (1999) Functional expression, purification, and characterization of recombinant human pyruvate carboxylase. Biochem Biophys Res Communs 266: 512–7. PMID: 10600533

23. Thonpho A, Sereeruk C, Rojvirat P, Jitrapakdee S (2010) Identification of the cyclic AMP responsive element (CRE) that mediates transcriptional regulation of the pyruvate carboxylase gene in HepG2 cells. Biochem Biophys Res Communs 393: 714–9. doi: 10.1016/j.bbrc.2010.02.067 PMID: 20171190

24. Thonpho A, Rojvirat P, Jitrapakdee S, MacDonald MJ (2013) Characterization of the distal promoter of the human pyruvate carboxylase gene in pancreatic beta cells. PloS one 8: e55139. doi: 10.1371/journal.pone.0055139 PMID: 23383084

25. Livak KJ, Schmittgen TD (2001) Analysis of relative gene expression data using real-time quantitative PCR and the 2(-Delta Delta C(T)) Method. Methods 25: 402–408. PMID: 11846609

26. Laemmli UK (1970) Cleavage of structural proteins during the assembly of the head of bacteriophage T4. Nature 227: 680–685. PMID: 5432063

27. Rohde M, Lim F, Wallace JC (1991) Electron-Microscopic Localization of Pyruvate-Carboxylase in Rat-Liver and *Saccharomyces cerevisiae* by Immunogold Procedures. Arch Biochem Biophys 290: 197–201. PMID: 1898090

28. Jitrapakdee S, St Maurice M, Rayment I, Cleland WW, Wallace JC, Attwood PV (2008) Structure, mechanism and regulation of pyruvate carboxylase. Biochem J 413: 369–387. doi: 10.1042/BJ20080709 PMID: 18613815

29. Wise DR, Thompson CB (2010) Glutamine addiction: a new therapeutic target in cancer. Trends Biochem Sci 35: 427–433. doi: 10.1016/j.tibs.2010.05.003 PMID: 20570523

30. Marin-Valencia I, Yang C, Mashimo T, Cho S, Baek H, Yang XL, et al. (2012) Analysis of tumor metabolism reveals mitochondrial glucose oxidation in genetically diverse human glioblastomas in the mouse brain *in vivo*. Cell Metab 15: 827–837. doi: 10.1016/j.cmet.2012.05.001 PMID: 22682223

31. Mullen AR, Hu Z, Shi X, Jiang L, Boroughs LK, Kovacs Z, et al. (2014) Oxidation of alpha-ketoglutarate is required for reductive carboxylation in cancer cells with mitochondrial defects. Cell Rep 7: 1679–1690. doi: 10.1016/j.celrep.2014.04.037 PMID: 24857658

32. DeBerardinis RJ, Mancuso A, Daikhin E, Nissim I, Yudkoff M, Wehrli S, et al. (2007) Beyond aerobic glycolysis: transformed cells can engage in glutamine metabolism that exceeds the requirement for protein and nucleotide synthesis. Proc Nat Acad Sci USA 104: 19345–50. PMID: 18032601

33. Kim SH, Lee GM (2007) Functional expression of human pyruvate carboxylase for reduced lactic acid formation of Chinese hamster ovary cells (DG44). Appl Microbiol Biotechnol 76: 659–665. PMID: 17583807

34. Henry O, Durocher Y (2011) Enhanced glycoprotein production in HEK-293 cells expressing pyruvate carboxylase. Metab Eng 13: 499–507. doi: 10.1016/j.ymben.2011.05.004 PMID: 21624497

35. Vallee C, Durocher Y, Henry O (2014) Exploiting the metabolism of PYC expressing HEK293 cells in fed-batch cultures. J Biotechnol 169: 63–70. doi: 10.1016/j.jbiotec.2013.11.002 PMID: 24246270

36. Thiery JP, Sleeman JP (2006) Complex networks orchestrate epithelial-mesenchymal transitions. Nat Rev Mol Cell Biol 7: 131–42. PMID: 16493418

37. Yook JI, Li XY, Ota I, Hu C, Kim HS, Cha SY, et al. (2006) A Wnt-Axin2-GSK3beta cascade regulates Snail1 activity in breast cancer cells. Nat Cell Biol 8: 1398–1406. PMID: 17072303

38. Lee SY, Jeon HM, Ju MK, Kim CH, Yoon G, Han SI, et al. (2012) Wnt/Snail signaling regulates cytochrome C oxidase and glucose metabolism. Cancer Res 72:3607–3617. doi: 10.1158/0008-5472.CAN-12-0006 PMID: 22637725

39. Mego M, Mani SA, Cristofanilli M (2010) Molecular mechanisms of metastasis in breast cancer-clinical applications. Nat Rev Clin Oncol 7: 693–701. doi: 10.1038/nrclinonc.2010.171 PMID: 20956980

40. Lu X, Bennet B, Mu E, Rabinowitz J, Kang Y (2010) Metabolomic changes accompanying transformation and acquisition of metastatic potential in a syngeneic mouse mammary tumor model. J Biol Chem 285: 9317–9321. doi: 10.1074/jbc.C110.104448 PMID: 20139083

41. Hua Y, Qiu Y, Zhao A, Wang X, Chen T, Zhang Z, et al. (2011) Dynamic metabolic transformation in tumor invasion and metastasis in mice with LM-8 osteosarcoma cell transplantation. J Proteome Res 10: 3513–3521. doi: 10.1021/pr200147g PMID: 21661735

42. Scott DA, Richardson AD, Filipp FV, Knutzen CA, Chiang GG, Ronai ZA et al. (2011) Comparative metabolic flux profiling of melanoma cell lines: beyond the Warburg effect. J Biol Chem 286: 42626–42634. doi: 10.1074/jbc.M111.282046 PMID: 21998308

43. Nieman KM, Kenny HA, Penicka CV, Ladanyi A, Buell-Gutbrod R, Zillhardt MR, et al. (2011) Adipocytes promote ovarian cancer metastasis and provide energy for rapid tumor growth. Nat Med 17: 1498–1503. doi: 10.1038/nm.2492 PMID: 22037646

44. Nieman KM, Romero IL, Van Houten B, Lengyel E (2013) Adipose tissue and adipocytes support tumorigenesis and metastasis. Biochim Biophys Acta 1831: 1533–1541. doi: 10.1016/j.bbalip.2013.02.010 PMID: 23500888

45. Leithner K, Hrzenjak A, Trotzmuller N, Moustafa T, Köfeler HC, Wohlkoenig C, et al. (2014) PCK2 activation mediates an adaptive response to glucose depletion in lung cancer. Oncogene doi: 10.1038/onc.2014.47

46. MacDonald MJ, Fahien LA, Brown LJ, Hasan NM, Buss JD, Kendrick MA (2005) Perspective: emerging evidence for signaling roles of mitochondrial anaplerotic products in insulin secretion. Am J Physiol Endocrinol Metab 288: E1–E15. PMID: 15585595

47. MacDonald MJ (1995) Feasibility of a mitochondrial pyruvate malate shuttle in pancreatic islets. Further implication of cytosolic NADPH in insulin secretion. J Biol Chem 270: 20051–2058. PMID: 7650022

48. Farfari S, Schulz V, Corkey B, Prentki M (2000) Glucose-regulated anaplerosis and cataplerosis in pancreatic beta-cells: possible implication of a pyruvate/citrate shuttle in insulin secretion. Diabetes 49: 718–726. PMID: 10905479

49. Ronnebaum SM, Ilkayeva O, Burgess SC, Joseph JW, Lu D, Stevens RD, et al. (2006) A pyruvate cycling pathway involving cytosolic NADP-dependent isocitrate dehydrogenase regulates glucose-stimulated insulin secretion. J Biol Chem 281: 30593–30602. PMID: 16912049

50. Ushio-Fukai M, Nakamura Y (2008) Reactive oxygen species and angiogenesis: NADPH oxidase as target for cancer therapy. Cancer Lett 266: 37–52. doi: 10.1016/j.canlet.2008.02.044 PMID: 18406051

51. Wu WS (2006) The signaling mechanism of ROS in tumor progression. Cancer Metastasis Rev 25: 695–705. PMID: 17160708

52. Graham KA, Kulawiec M, Owens KM, Li X, Desouki MM, Singh KK (2010) NADPH oxidase 4 is an oncoprotein localized to mitochondria. Cancer Biol Ther 10: 223–231. PMID: 20523116

53. Holliday DL, Speirs V (2011) Choosing the right cell line for breast cancer research. Breast Cancer Res 13:215. doi: 10.1186/bcr2889 PMID: 21884641

Computational and Structural Biotechnology Journal 14 (2016) 223–233

COMPUTATIONAL AND STRUCTURAL BIOTECHNOLOGY JOURNAL

journal homepage: www.elsevier.com/locate/csbj

MicroRNAs and oncogenic transcriptional regulatory networks controlling metabolic reprogramming in cancers

Pannapa Pinweha [a,1], Khanti Rattanapornsompong [a,1], Varodom Charoensawan [a,b], Sarawut Jitrapakdee [a,*]

[a] Department of Biochemistry, Faculty of Science, Mahidol University, Bangkok 10400, Thailand
[b] Integrative Computational BioScience (ICBS) Center, Mahidol University, Nakhon Pathom 73170, Thailand

ARTICLE INFO

Article history:
Received 16 March 2016
Received in revised form 25 May 2016
Accepted 27 May 2016
Available online 4 June 2016

Keywords:
Cancer
Metabolism
MicroRNA
Oncogene
Transcriptional regulation network

ABSTRACT

Altered cellular metabolism is a fundamental adaptation of cancer during rapid proliferation as a result of growth factor overstimulation. We review different pathways involving metabolic alterations in cancers including aerobic glycolysis, pentose phosphate pathway, *de novo* fatty acid synthesis, and serine and glycine metabolism. Although oncoproteins, c-MYC, HIF1α and p53 are the major drivers of this metabolic reprogramming, post-transcriptional regulation by microRNAs (miR) also plays an important role in finely adjusting the requirement of the key metabolic enzymes underlying this metabolic reprogramming. We also combine the literature data on the miRNAs that potentially regulate 40 metabolic enzymes responsible for metabolic reprogramming in cancers, with additional miRs from computational prediction. Our analyses show that: (1) a metabolic enzyme is frequently regulated by multiple miRs, (2) confidence scores from prediction algorithms might be useful to help narrow down functional miR-mRNA interaction, which might be worth further experimental validation. By combining known and predicted interactions of oncogenic transcription factors (TFs) (c-MYC, HIF1α and p53), sterol regulatory element binding protein 1 (SREBP1), 40 metabolic enzymes, and regulatory miRs we have established one of the first reference maps for miRs and oncogenic TFs that regulate metabolic reprogramming in cancers. The combined network shows that glycolytic enzymes are linked to miRs via p53, c-MYC, HIF1α, whereas the genes in serine, glycine and one carbon metabolism are regulated via the c-MYC, as well as other regulatory organization that cannot be observed by investigating individual miRs, TFs, and target genes.

1. Overall metabolic reprograming in cancers

In response to overstimulation of growth factor signaling, cancer cells reprogram their metabolism in order to accommodate a high demand for macromolecules during rapid proliferation [1–4]. The hallmark of the above metabolic reprograming is the shift from oxidative phosphorylation to aerobic glycolysis, known as the "Warburg effect" [5]. This phenomenon provides some advantages to the tumors because aerobic glycolysis allows them to survive under hypoxic conditions, while an acidic environment selects a highly aggressive population of cancers to survive and metastasize to distal tissues or organs [3,6]. Cancers are also highly anabolic because they require lipids, protein and nucleic acids as constituents of the structural components of the newly divided cells [2]. This highly anabolic phenotype is partly attributed to the Warburg effect because inhibition of pyruvate entering into the mitochondria results in the redirection of glycolytic intermediates to the pentose phosphate pathway (PPP), which provides biosynthetic precursors for nucleotides and lipids [4]. Furthermore, mitochondrial metabolism of cancers is also reprogrammed toward cataplerosis where substantial amounts of tricarboxylic acid (TCA) cycle intermediates are used as the biosynthetic precursors of lipids and amino acids [2]. Therefore, it is not surprising to see up-regulate expression of key enzymes that catalyze the above biosynthetic pathways in several types of cancers. Fig. 1 shows the overall metabolic reprogramming pathways in cancers together with the key regulatory enzymes.

Abbreviations: ACC, acetyl-CoA carboxylase; ACL, ATP-citrate lyase; BRCA1, breast cancer type 1 susceptibility protein; c-MYC, V-myc avian myelocytomatosis viral oncogene homolog; FAS, fatty acid synthase; FH, fumarate hydratase; G6PD, glucose-6-phosphate dehydrogenase; GDH, glutamate dehydrogenase; GLS, glutaminase; GLUT, glucose transporter; HK, hexokinase; 2-HG, 2-hydroxyglutarate; HIF1α, hypoxia inducible factor 1α; IDH, isocitrate dehydrogenase; miR/miRNA, LDH, lactate dehydrogenase micro RNA; p53, tumor protein p53; PEP, phosphoenolpyruvate; MCT, monocarboxylic acid transporter; ME, malic enzyme; PEPCK, phosphoenolpyruvate carboxykinase; PFK, phosphofructokinase; PHGDH, phosphoglycerate dehydrogenase; PGK, phosphoglycerate kinase (PGK); PSAT, phosphoserine aminotransferase; PSPH, phosphoserine phosphatase; PKM, muscle-pyruvate kinase; PDH, pyruvate dehydrogenase; PC, pyruvate carboxylase; PDK, pyruvate dehydrogenase kinase; PPP, pentose phosphate pathway; SDH, succinate dehydrogenase; SHMT, serine hydroxymethyl transferase; SREBP1, sterol regulatory element binding protein 1; TCA, tricarboxylic acid; TFs, transcription factors.

* Corresponding author at: Department of Biochemistry, Faculty of Science, Mahidol University, Rama 6 Rd, Rajathewee, Bangkok 10400, Thailand. Tel.: +66 2 201 5458; fax: +66 2 354 7174.
E-mail address: sarawut.jit@mahidol.ac.th (S. Jitrapakdee).

[1] Equal authorship.

http://dx.doi.org/10.1016/j.csbj.2016.05.005

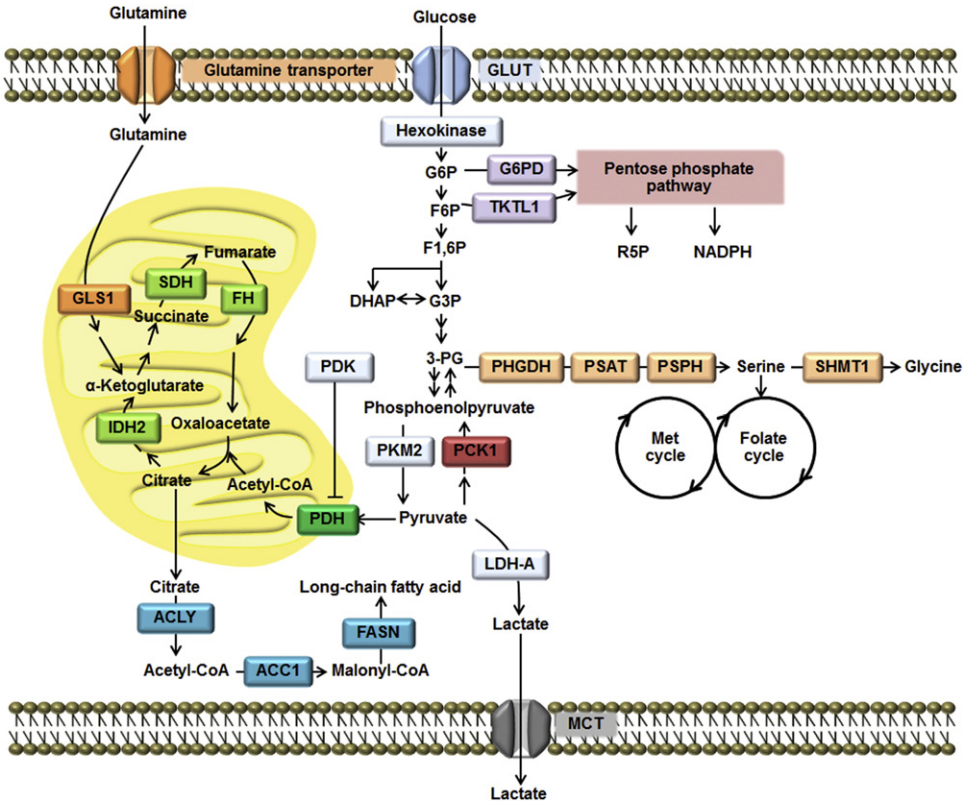

Fig. 1. Metabolic pathways in cancers. Glucose and glutamine are two major carbon sources that are metabolized through these biochemical pathways.

Here we review the altered metabolic pathways and the relevant enzymes in cancers inferred from experimental and computational based data [7–9]. We also review the oncogenic transcription factors (TFs) and miRNAs that regulate those metabolic pathways. In addition, using known and predicted miRNA-target gene interaction, we establish and analyze the network of oncogenic miRNA-metabolic target gene networks that interplay and regulate metabolic reprograming in cancers.

1.1. miRNAs regulate metabolic pathways

Post-transcriptional regulation by microRNAs (miRNAs) has long been known as a mechanism to silence gene expression. miRNAs are short double stranded RNAs, comprising 15–25 nucleotides. They are first transcribed in the nucleus as the primary miRNAs, consisting of multiple stem loop structures, which are then subsequently digested to precursor miRNAs (pre-miRNAs) by Drosha, an RNase III family enzyme [10]. Pre-miRNAs are then transported to the cytoplasm where the hairpin structure is further removed by a dicer enzyme, yielding approximately 21 base pairs miRNA duplex. The miRNA duplex is subsequently incorporated in the Argonaute protein which digests one strand of the duplex miRNA, generating a single stranded miRNA. This single stranded miRNA is further brought to their target mRNAs by an RNA-induced silencing (RISC) complex. Binding of single stranded miRNAs to their targets is mediated by hybridization of 7–8 nucleotides of the miRNAs (known as seed match) to their complementary nucleotides in the 3′-untranslated regions of their targets. Such hybridization results in translational inhibition or degradation of target mRNAs, thus providing a means to inhibit gene expression. Furthermore, one miRNA can bind to more than one species of mRNA targets due to a non-stringent hybridization of the seed match region, allowing simultaneous down-regulation of multiple target mRNAs. In the same way, multiple species of miRNAs can bind to the same mRNA targets and enhance translational inhibition [11]. It is estimated that 45,000 miRNA target sites are found in the human genome, and these miRNAs control expression of up to 60% of human genes [12].

miRNAs are implicated in the regulation of various biological processes. Biochemically, miRNAs also regulate cellular metabolism either directly by targeting key enzymes of metabolic pathways or indirectly by modulating the expression of important transcription factors. Multiple studies have revealed that the altered metabolic pathways in cancers are tightly regulated by miRNAs [13]. In the first half of the review, we describe the metabolic pathways and key enzymes that are altered in various cancers and regulated by miRNAs. This will be followed by the second half on the regulatory networks between metabolic enzymes, regulatory miRNAs and oncogenic transcription factors.

1.2. Glycolytic and pentose phosphate pathways

The Warburg effect is a primary event of metabolic reprogramming during tumorigenesis. This effect includes induced expression of enzymes such as GLUT1, hexokinase 2 (HK2), phosphofructokinase 2 (PFK2) and pyruvate dehydrogenase kinase 1 (PDK1) [3]. Up-regulation of the expression of the first three targets results in a rapid uptake of glucose and increased glycolytic rate, while increased expression of PDK1 inactivates pyruvate dehydrogenase, restricting the conversion of pyruvate to acetyl-CoA in the mitochondria and thus uncoupling glycolysis from subsequent mitochondrial oxidation. Increased expression of lactate dehydrogenase and monocarboxylic acid transporter 4 (MCT4) further sequesters pyruvate toward lactate production, lowering the pH of the extracellular environment [14]. The muscle-specific pyruvate kinase M (PKM) isoform has also been implicated in metabolic reprogramming in certain cancers [15]. PKM exists in two isoforms, PKM1 and PKM2 that have arisen from alternative splicing of exons 9 and 10 [16]. The activities of these two enzymes are determined by their conformers. PKM1 has a tendency to form tetramers that possess high enzymatic activity while PKM2 shows relatively low activity due to its main conformer being dimers. PKM1 is the

most abundant isoform in skeletal muscle while PKM2 is highly expressed during embryonic development. In many cancers, PKM2 is selectively expressed, resulting in the accumulation of phosphoenolpyruvate, and thus redirecting the flow of glycolytic intermediates toward the pentose phosphate pathway (PPP) [15]. This mechanism provides a great benefit for cancers because PPP provides the ribose-5-phosphate and NADPH required for the synthesis of nucleotides and fatty acids. PKM2 also plays a non-metabolic role in which it can act as a co-activator of TFs including HIF1α, STAT3, Oct4 and β-catinin which regulate expression of certain oncogenes [16,17]. Therefore PKM2 switching can reprogram metabolic pathways and alter the program of gene expression in cancers.

In response to PKM2 activation or by other mechanisms, PPP activity has been reported to be elevated in many cancers [18]. Therefore it is not surprising to see up-regulation of key enzymes in this pathway including glucose-6-phosphate dehydrogenase (G6PD), 6-phosphogluconate dehydrogenase (6-PGD) and transketolase-like enzyme [19–21]. NADPH produced by PPP is also crucial for maintaining the proper glutathione-redox loop that cancers use to counter the reactive oxygen species formed especially during epithelial–mesenchymal-transition (EMT) or anoikis resistance [22,23]. Inhibition of PPP via the use of specific enzyme inhibitors or siRNAs targeted to their corresponding enzymes retards growth and biosynthesis of lipid and nucleotides in many types of cancers [21,24,25].

1.3. Mitochondrial metabolism

The tricarboxylic acid cycle (TCA cycle) provides both catabolic and anabolic functions for living cells. In normal cells, the TCA cycle functions as a central oxidation hub where acetyl-CoA derived from oxidations of glucose, amino acids and fatty acids enters for complete oxidation. However in dividing cells or cancers, the TCA cycle is used as an anabolic hub because its intermediates are used as biosynthetic precursors of amino acids, nucleotides and lipids, in a process known as “cataplerosis” [26]. Mutations of certain TCA cycle enzymes such as isocitrate dehydrogenase (IDH), succinate dehydrogenase (SDH) and fumarate hydratase (FH) can contribute to tumorigenesis [27,28]. In certain cancers especially glioma, mutations of the cytosolic (IDH1) or mitochondrial (IDH2) enzymes create a novel function in which they can further convert α-ketoglutarate to 2-hydroxyglutarate (2-HG) [29]. 2-HG is an oncometabolite because it acts as an inhibitor of α-ketoglutarate-dependent dioxygenase involved in DNA and histone demethylation. Inhibition of such a process can lead to tumorigenesis [2,29]. Similarly, mutations of the genes encoding succinate dehydrogenase (SDH) and fumarate hydratase (FH) result in the accumulation of succinate or fumarate, respectively. These two metabolites are inhibitors of prolyl hydroxylase (PHD), which hydroxylates hypoxia-inducible factor 1α (HIF1α), resulting in its degradation by proteolysis. Therefore elevated levels of both metabolites stabilize HIF1α, activating glycolysis in cancers [27].

Cancers also require the replenishment of TCA cycle intermediates after their removal for biosynthetic purposes. In order to prevent a discontinuity in the supply of biosynthetic precursors, there is a biochemical pathway known as “anaplerosis” which is composed of two main reactions, glutaminolysis [30] and pyruvate carboxylation [31]. Glutaminolysis is the conversion of glutamine to glutamate by glutaminase (GLS) before glutamate is further converted to α-ketoglutarate in the TCA cycle by glutamate dehydrogenase. The second anaplerotic reaction is the carboxylation of pyruvate to oxaloacetate by pyruvate carboxylase (PC). Different cancers use these two different anaplerotic reactions to certain extents, to support biosynthesis by up-regulation of either or both enzymes during tumorigenesis [32–35]. Inhibition of these two enzymes results in impaired growth of cancers accompanied with marked reduction in biosynthesis of lipids, nucleotides and amino acids [33–36]. Recent studies show that a gluconeogenic enzyme, phosphoenolpyruvate carboxykinase (PEPCK) also plays an important role in supporting biosynthesis of tumors [37–39]. PEPCK catalyzes a further conversion of oxaloacetate to phosphoenolpyruvate (PEP). This enzyme occurs in two isoforms: the cytosolic (PEPCK1 or PEPCK-C) and the mitochondrial (PEPCK2 or PEPCK-M) isoforms. Colon cancer, for instance, uses PEPCK1 [39] while non-small cell lung cancer uses PEPCK2 [37,38] to supply PEP to support their growth, respectively. However, PEP formed by both enzymes is not only converted to glucose but also used locally as a biosynthetic precursor of serine and glycine. Furthermore, elevated levels of PEP also drive the flow of the upstream glycolytic intermediate glucose-6-phosphate to enter the PPP for the synthesis of ribose sugar required for nucleotide synthesis [37,39]. Interestingly, this function becomes more obvious when the nutrient that supports the growth of a tumor is shifted from glucose to glutamine [37,39]. This adaptive mechanism enables cancers to grow and survive under glucose-limited conditions.

1.4. Amino acid synthesis

Amino acids serve as not only the building blocks of polypeptides, but also the precursors of nucleotides. As cancers require large amounts of proteins and nucleic acids, it is not surprising that up-regulation of key enzymes involved in biosynthesis of certain amino acids were observed in cancer cells. Serine and glycine are essential for synthesis of nucleotides as deprivations of these two amino acids endogenously or exogenously, retard growth of many cancers [40]. *De novo* synthesis of these two amino acids is started from 3-phosphoglycerate (3-PG), an intermediate in the glycolytic pathway. 3-PG is then converted to serine via a three-step reaction, in which 3-PG is first converted to 3-phosphohydroxypyruvate by phosphoglycerate dehydrogenase (PHGDH). 3-phosphohydroxypyruvate is further converted to serine by another two reactions catalyzed by phosphoserine aminotransferase (PSAT) and phosphoserine phosphatase (PSPH) [40]. As only 10% of 3-PG in the glycolytic pool enters serine and glycine biosynthesis, this seems paradoxical with such a high demand for both amino acids during the rapid proliferation of cancers. However, many cancers cope with this limitation via an aberrant activation of the serine biosynthetic pathway by increasing the copy number of the *PHGDH* gene or up-regulating its mRNA expression, resulting in much a higher rate of serine synthesis [41,42]. Serine is further converted to glycine by the serine hydroxymethyl transferase (SHMT), a folate-dependent pathway [40]. SHMT is comprised of two isoforms, SHMT1 which is expressed in the cytoplasm whereas SHMT2 is expressed in mitochondria. It remains unclear about the functional redundancy of these two isoforms as inhibiting activity of either isoform or suppressing their expression retards growth in different cancer models [43–45]. Nevertheless, both SHMT1 and SHMT2 are associated with the folate cycle, which is involved in one-carbon metabolism including synthesis of methionine and nucleotides, and in histone methylation. Thus, disruption of both SHMT isoforms can potentially perturb these metabolic processes [40].

1.5. Lipid biosynthesis

Fatty acids especially in phospholipids are important components of the plasma membrane. In cancers, fatty acids are mainly synthesized through the *de novo* pathway either from glucose or glutamine via glycolysis or glutaminolysis, respectively. However, the latter pathway plays a more significant role in this process [46]. As mentioned earlier, glutamine enters the TCA cycle via glutamate before being converted to α-ketoglutarate by glutamate dehydrogenase. This glutaminolytic flux increases TCA cycle intermediate pools, enabling citrate to leave the mitochondria to enter the cytosol where it is decarboxylated to oxaloacetate and acetyl-CoA by the ATP-citrate lyase (ACL). It has been reported that ACL expression and activity are elevated in many cancers. Thus, inhibition of its activity impairs lipid synthesis and is accompanied by reduced cell growth and survival [47,48]. The cytosolic acetyl-CoA

then serves as a precursor for long chain acyl-CoA synthesis, which is highly regulated by two enzymes, acetyl-CoA carboxylase 1 (ACC1) and fatty acid synthase (FAS). ACC1 catalyzes the carboxylation of acetyl-CoA to form malonyl-CoA, a building block that donates two carbon units for fatty acid synthesis. ACC1 activity can be modulated by a reversible phosphorylation. Among other kinases, the AMP-activated protein kinase (AMP) can phosphorylate ACC1, transforming it into an inactive form while protein phosphatase 1 dephosphorylates ACC1 back to an active form [49]. The phosphorylated ACC1 is subjected to a second mode of regulation through interaction with a DNA repair protein, BRCA1 which is highly expressed in breast tissue [49]. This interaction sequesters phosphorylated ACC1 from being dephosphorylated thereby blocking fatty acid synthesis [50,51]. A high incidence of the oncogene BRCA1 mutations is associated with breast cancer because these mutations not only result in the loss of BRCA1 function as a DNA repair protein but also perturbs its interaction with phosphorylated ACC1, freeing it to be dephosphorylated and subsequently stimulate lipogenesis in breast tissue [51,52]. ACC1 is one of the anti-cancer drug targets because inhibiting its expression or activity induces apoptosis in many cancers [53–55]. FAS has also been reported to be aberrantly activated in many cancers [56–58]. Like ACC1, inhibition of FAS expression or activity markedly reduces cancer growth [52,59,60].

1.6. Metabolic pathway crosstalk contributing to tumorigenesis

Although the crosstalk of signaling pathway is well implicated in tumorigenesis [61], only a few examples of metabolic pathway crosstalk are reported in certain cancers. As mentioned earlier, accumulation of succinate in cancers bearing mutations of succinate dehydrogenase gene not only results in the inactivation of HIF1α, contributing to Warburg effect but this also promotes tumorigenesis by attenuating the production of glutathione, an important redox protein which functions in detoxifying reactive oxygen species (ROS). Several cancers overproduce ROS in order to enhance PI3K, MAPK and NF-κB signaling pathways that support cellular proliferation [1]. Elevated levels of fumarate are found to react with glutathione to form succinated glutathione thereby reducing the NADP/NADPH-couple regeneration system required to eliminate ROS [62]. Similar reduction of glutathione levels was also observed in glioma bearing IDH1 or IDH2 mutation which accumulates 2-HG, suggesting that this oncometabolite may support ROS formation through attenuating the anti-oxidant system [63]. Warburg effect may also enhance tumorigenesis via conversion of fructose-6-phosphate into hexosamine biosynthetic pathway, yielding O-linked N-acetylglucosamine that can enhance mitogenic signaling pathway [64].

1.7. Coordinate regulation of metabolic reprogramming in cancers by oncogenic transcription factors

Having outlined different pathways and mechanisms of metabolic reprogramming in cancers, an important question remains: what controls this metabolic reprogramming in cancers? Three major TFs, namely c-MYC, hypoxia inducible factor 1α (HIF1α) and p53 are responsible for simultaneous up-regulation of the above key metabolic enzymes [65]. Aberrant expression of c-MYC is observed in more than 50% of cancers and it is one of the most amplified oncogenes. The c-MYC regulates various biological processes including proliferation, apoptosis and metabolic reprogramming [66]. Elevated c-MYC levels in turn bind to its target gene promoters, which contain a canonical E-box (CANNTG) element, resulting in increased mRNA transcripts. In normal situations, c-MYC expression is tightly regulated i.e., its expression is high during cell division but rapidly declines during cell cycle arrest [67]. In situations of metabolic alterations, c-MYC targets expression of genes encoding GLUT1, HK2, PDK1 and GLS1 [65,66,68].

The hypoxia-inducible factor (HIF1α), another key oncogenic TF, is functionally coordinated with c-MYC in controlling metabolic reprogramming in cancers [69]. HIF1α exists into two forms: the non-hydroxylated and the hydroxylated forms. In the presence of oxygen, HIF1α undergoes hydroxylation by prolyl hydroxylase, making it prone to proteolysis. However, when oxygen concentration is low, HIF1α escapes hydroxylation, allowing it to enter to the nucleus where it is hetero-dimerized with HIF1β and binds to the hypoxia-responsive element (HRE) in the promoters of genes whose products are involved in angiogenesis and metabolism [3]. HIF1α's metabolic targets appear to overlap with those of c-MYC, including GLUT1, GLUT3, HK1, HK2, aldolase A, phosphoglycerate kinase (PGK), lactate dehydrogenase (LDH), monocarboxylic acid transporter 4 (MCT4), PDK1 and PKM2 [65,70].

Unlike c-MYC and HIF1α, p53 functions as a tumor suppressor protein. Expression of p53 is highly regulated as its expression is essentially low in unstressed cells whereas it becomes highly expressed under stress conditions such as oxidative damage, nutrient limitations and DNA damage [67]. De-regulation of p53 expression caused by mutations is associated with more than half of all cancers [71]. As a transcription factor, p53 binds to the promoter of other tumor suppressor genes such as those involved in cell cycle arrest, DNA repair, apoptosis and metabolism. In addition, p53 can regulate turnover of many proteins independently of transcription [67]. In regard to its regulatory roles on metabolism, p53 inhibits expression of GLUT1, GLUT3, GLUT4, phosphoglycerate mutase 1 (PGM 1), and thus blocking excessive entry of glucose through glycolytic flux [67,72]. p53 inhibits expression of MCT1 and PDK2 while activates expression of PDH1α subunit of PDH complex thereby coupling glycolysis with oxidative phosphorylation [73]. The p53 also down-regulates biosynthesis by decreasing the activity and abundance of glucose-6-phosphate dehydrogenase (G6PD) [74] and decreasing expression of malic enzymes ME1 and ME2 [67,73]. As these three enzymes provide NADPH for biosynthesis, reducing their expression or activities would favor oxidative rather than biosynthetic pathways. In addition to controlling pathways that provide NADPH, p53 can also regulate *de novo* fatty acid synthesis via down-regulating the expression of the sterol regulatory protein 1c (SREBP1c), which is a key transcriptional factor controlling expression of ACL and FAS genes [73]. Therefore, loss-of-function mutations of p53 in cancers literally shift their metabolic phenotype from an oxidative fate to aerobic glycolysis and anabolism. The p53 protein also targets degradation of PEPCK and G6Pase in non-small cell lung cancer [75,76].

1.8. Expanding the repertoire of miRNA target of the alterative expressed metabolic genes in cancer using computational prediction

It has now become clear that many cellular genes including those encoding metabolic enzymes are regulated by miRNAs [13]. Several studies have identified regulatory miRNAs of the key enzymes responsible for metabolic reprogramming while some miRNAs regulate the expression of oncogenic TFs (e.g. c-MYC, HIF1α and p53), which in turn regulate expression of those metabolic enzymes. Despite an increasing number of studies on regulation of metabolic genes through miRNAs in cancers, it is clear that the list of studies on miRNA-regulated metabolic enzymes in cancers is nowhere close to the completion. Furthermore, it is still not known whether some key metabolic enzymes e.g. HK1, Aldolase, MCT4, SHMT2, ACC1, can be regulated by certain miRNAs. Thus, here we sought to explore the repertoire of miRNAs that target expression of key enzymes involved in metabolic reprogramming in cancers by combining known interactions from literature (Table 1) and computational prediction (Supplementary Tables S1 and S2). One of the most important challenges of computational prediction of miRNA is the specificity of the prediction algorithms, which are known to give a large number of false positives. To this end, we examined whether the prediction miRNAs are consistent with the functional validation shown in Table 1, and the predicted miRNA-mRNA interactions that would potentially be worth following up experimentally.

The most frequently used algorithms and webtools currently available for miRNA prediction include miRanda–mirSVR [77,78], DIANA-

Table 1
A list of 40 metabolic enzymes that are involved in metabolic reprogramming in cancers.

Enzyme	Full name	Gene	miRNA	References
Aerobic glycolysis, Warburg effect				
GLUT1	Glucose transporter 1	NM_006516	miR-1291 [123]	[124–126]
GLUT2	Glucose transporter 2	NM_000340	N/A	[124]
GLUT3	Glucose transporter 3	NM_006931	miR-195-5p [127], miR-106-5p [90,128]	[124,129,125,126]
GLUT4	Glucose transporter 4	NM_001042	N/A	[124,130,125]
HK1	Hexokinase1	NM_000188	N/A	[3]
HK2	Hexokinase2	NM_000189	miR-143 [131], [132]	[133,3]
Aldolase A	Aldolase A	NM_000034	N/A	[134]
PGAM1	Phosphoglycerate mutase 1	NM_002629	N/A	[135]
PKM2	Pyruvate kinase 2	NM_002654	miR-122, miR-133a, miR-133b,miR-326 [136–138]	[139,140]
LDHA	Lactate dehydrogenase A	NM_005566	miR-21 [141]	[142,143]
MCT1	Monocarboxylate transporter 1	NM_003051	miR-124 [144]	[145]
MCT4	Monocarboxylate transporter 4	NM_004696	N/A	[145,146]
Pentose phosphate pathway				
G6PD	Glucose-6-phosphate dehydrogenase	NM_000402	miR-206, miR-1 [120]	[20]
TKTL1	Transketolase-like1	NM_012253	miR-206, miR-1 [120]	[19]
Gluconeogenesis				
PCK1	Phosphoenolpyruvate carboxykinase 1	NM_002591	N/A	[39]
PCK2	Phosphoenolpyruvate carboxykinase 2	NM_004563	N/A	[38,37]
Tricarboxylic acid (TCA) cycle				
PDK1	Pyruvate dehydrogenase kinase 1	NM_002610	N/A	[147]
PDH	Pyruvate dehydrogenase	NM_003477	miR-26a [148]	[149]
IDH1	Isocitrate dehydrogenase 1	NM_005896	N/A	[28]
IDH2	Isocitrate dehydrogenase 2	NM_002168	miR-183 [150]	[28]
SDH-B	Succinate dehydrogenase complex iron sulfur subunit B	NM_003000	N/A	[27]
SDH-C	Succinate dehydrogenase complex subunit C	NM_003001	N/A	[27]
SDH-D	Succinate dehydrogenase complex subunit D	NM_003002	miR-210 [151]	[27]
FH	Fumarate hydratase	NM_000143	N/A	[27]
ME1	Malic enzyme 1	NM_002395	N/A	[152]
Glutaminolysis				
GLS1	Glutaminase 1	NM_014905	miR-23a, miR-23b [118]	[32]
GLS2	Glutaminase 2	NM_013267	miR-23a, miR-23b [118]	[153,154]
Serine, Glycine and one carbon metabolism				
SHMT2	Serine hydroxymethyltransferase 2	NM_005412	miR-193b [90,155]	[156]
SHMT1	Serine hydroxymethyltransferase 1	NM_004169	miR-198 [157]	[156]
MTHFD2	Methylenetetrahydrofolate dehydrogenase	NM_006636	miR-9 [158]	[156]
MTHFD1L	Methylenetetrahydrofolate dehydrogenase 1-like	NM_015440	miR-9 [158]	[156]
PHGDH	Phosphoglycerate dehydeogenase	NM_006623	N/A	[41]
PSAT1	Phosphoserine aminotransferase 1	NM_021154	miR-340 [159]	[160,161]
PSPH	Phosphoserine phosphatase	NM_004577	N/A	[161]
GNMT	Glycine-N-methyltransferase	NM_018960	N/A	[162]
de novo fatty acid synthesis				
CIC	Citrate carrier	NM_005984	N/A	[163]
ACLY	ATP citrate lyase Y	NM_001096	N/A	[152,164]
ACC1	Acetyl-CoA carboxylase 1	NM_198836	N/A	[152,165]
FASN	Fatty acid synthase	NM_004104	miR-320 [166]	[58,56,57]
SCD	Stearoyl-CoA desaturase	NM_005063	N/A	[152]

Abbreviation: not available (N/A).

microT-CDS [79], TargetScan [80,81], Pictar [82], miRDB [83], and RNA22 [84], which use common features such as seed match and sequence conservation across the species [85]. In brief, the seed match is a perfect pairing between miRNA and the 3′-UTR of mRNA targets, which usually starts at the 5′ end of miRNA at the positions 2 to 8. There are four main classes of canonical seed matches including (1) 6-mer (6 perfect nucleotide matches between miRNA at positions 2 to 7 and mRNA target), (2) 7mer-A1 (perfect match of miRNA at positions 2 to 7 with an A opposite position 1 of mRNA target), (3) 8-mer (perfect seed paring of miRNA at positions 2 to 8 with an A opposite position 1 of mRNA target) [86] and (4) 7mer-8mer (perfect match of miRNA at positions 2 to 8 and mRNA target) [87,88]. However, these different seed matches do not reflect the degrees of gene expression suppression by miRNAs [89].

With an aim to explore other potential miRNAs that may regulate key metabolic enzymes listed in Table 1, we choose two widely-used miRNA prediction tools that utilize different features to predict miRNA of the target mRNAs of interest, TargetScan7.0 and miRanda–mirSVR. The former predicts the miRNAs targeting a given gene based on the seed match and sequence conservation across the species, whilst the latter uses free energy binding between miRNA and mRNA targets, and the site accessibility for miRNA target prophecy [85]. The context++ scores and mirSVR scores were used as the parameters to indicate the confidence of predictions from the TargetScan7.0 and miRanda–mirSVR, respectively. The context++ score is the sum of contribution from 14 features [81], such as site-type, 3′ pairing, the local AU content [89], target site abundance, seed-pairing stability [80]. The mirSVR scores, on the other hand, can also rank the empirical probability of down-regulation using supervised machine learning of mRNA expression changes as a result of specific microRNA transfection [78]. In short, the more negative context++ scores and mirSVR scores from

the predictions reflect the higher "likelihood" that the mRNA is targeted by miRNA, and thus down-regulated gene expression.

As shown in Fig. 2A, TargetScan7.0 predicted that 40 metabolic enzymes shown in Table 1 are regulated by 299 miRNAs (blue circle). Sixteen out of 40 metabolic enzymes were predicted to be regulated by 113 miRNAs. However, only 8 out of these 113 miRNAs have been reported to functionally regulate expression of these enzymes, leaving the other 105 miRNAs (yellow) whose functional verification is yet to be elucidated. We also noted that there are 14 miRNAs (red) that have been experimentally verified to regulate this set of metabolic genes but elude prediction by TargetScan7.0, suggesting a considerable degree of false negatives. TargetScan7.0 also predicted 186 additional miRNAs that are likely to regulate another 24 metabolic enzymes, whose regulatory miRNAs have not been studied. The list of miRNAs that are predicted to regulate theses 40 metabolic enzymes can be found in Supplementary Table S1.

In a similar trend but not identical, miRanda–mirSVR predicted that there are 395 miRNAs that can potentially regulate these metabolic enzymes (Fig. 2B). One hundred and seventy three miRNAs were predicted to regulate 16 metabolic enzymes while the other 222 miRNAs (gray) were predicted to target another 24 metabolic enzymes which are currently unknown to be regulated by any miRNAs. Within those 16 metabolic enzymes regulated by 173 miRNAs, only 14 miRNAs were independently reported to regulate expression of these metabolic enzymes while the functional verifications of the other 159 miRNAs (pink) are yet to be elucidated. Similar to the TargetScan7.0 prediction but with fewer number of false negatives, eight additional miRNAs have been reported to functionally regulate expression of these 16 metabolic enzymes but were not detected by the miRanda–mirSVR prediction.

Due to the issues of sensitivity and specificity of miRNA prediction algorithms mentioned earlier, we generated boxplots of the context++ scores (Fig. 2C) and mirSRV scores (Fig. 2D), in three miRNA groups: (1) experimentally verified miRNAs with prediction, (2) miRNAs predicted for target genes with other verified miRNAs, but their own functions are yet to be validated, and (3) the predicted miRNAs of metabolic enzymes whose functions have not be validated for any miRNA before (as outlined in the Venn diagrams). We did indeed observe a modest trend that the validated miRNAs have lower context++ scores, than predicted miRNAs without validation; however, the number of miRNAs in each group is likely to be too small to give a statistical significant result. Similarly, the same can be said about the scores assigned to mirSVR prediction, indicating that confidence scores from the prediction might be useful as an extra indicator to extract the predicted miRNA that are likely to be "real" functional miRNAs, and would be worth further experimental validation.

1.9. MicroRNAs and oncogenic transcriptional regulatory networks

To observe the overall interplay of oncogenic TFs, metabolic enzymes, and regulatory miRNAs, we combined the experimentally validated (Table 1), the experimentally validated miRNA-target data from miRTarBase [90] and predicted interactions (from the two algorithms as shown in Fig. 2) into a regulatory network of TFs-metabolic enzymes and miRNA-TFs using Cytoscape [91], as shown in Figs. 3 and 4. Fig. 3 focuses on the known miRNAs that regulate expression of metabolic enzymes via controlling the expression of oncogenic TFs, whereas we expand the network to cover both validated and predicted miRNA-mRNA interactions in Fig. 4. The predicted interactions shown here are the overlaps of the two algorithms used: TargetScan7.0 and miRanda–mirSVR, shown as gray dashed edges, whereas the functional verified miRNA-gene targets from the Table 1 and miRTarBase database [90] are shown in black solid lines. The edges' colors (blue, red, green and purple) represent the miRNAs that regulate expression of metabolic enzymes through the expression of oncogenic TFs (HIF1α, c-MYC, p53, SREBP1, respectively), as in Fig. 3. The colors of node genes in Fig. 4 are classified by metabolic pathways: pale blue color for anaerobic glycolytic genes; white for enzymes involved in serine, glycine and one carbon metabolism; orange for GLS; blue-green nodes for enzymes in the TCA cycle; pink nodes for enzymes in the *de novo* fatty acid synthesis; gray nodes for gluconeogenic enzyme, and purple nodes for enzymes in the pentose phosphate pathway.

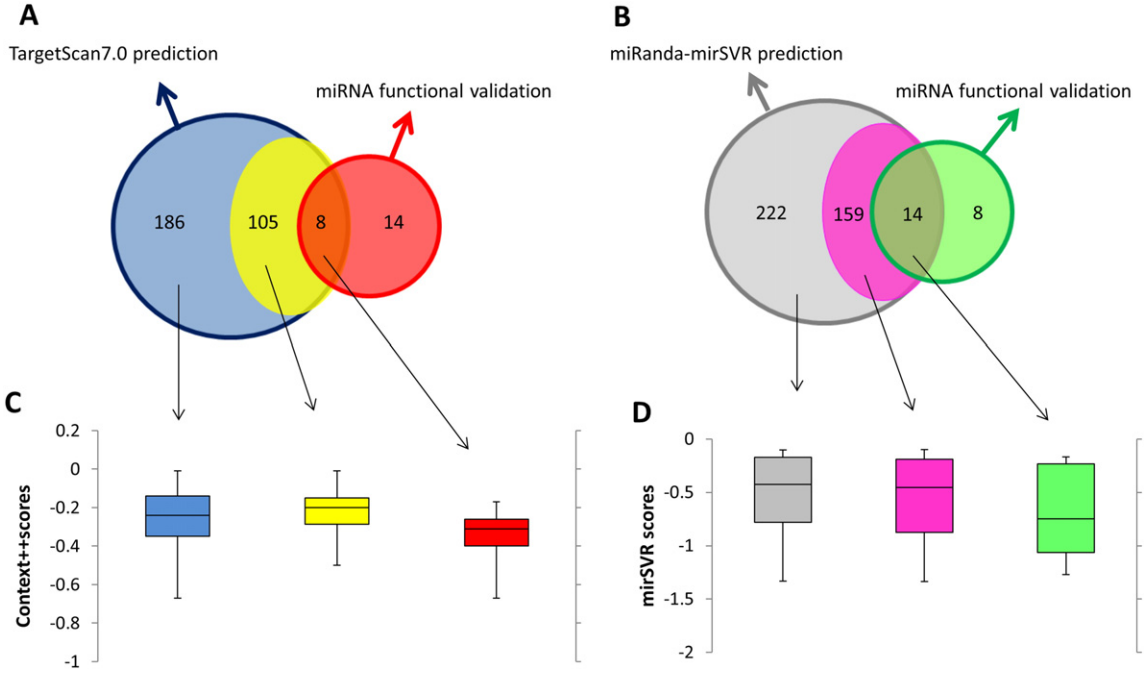

Fig. 2. Venn diagrams and boxplots representing the association between miRNA prediction scores and their functional validation. The Venn diagrams of TargetScan7.0 (Fig. 2A) and miRanda–mirSVR (Fig. 2B) show the numbers of validated and predicted miRNAs that regulate metabolic enzymes in cancers. Boxplots illustrate the association of between context++ scores (Fig. 2C) or miRanda–mirSVR scores (Fig 2D), and three miRNA groups: (1) experimentally validated miRNAs with prediction (2) miRNAs predicted to target metabolic enzymes with other verified miRNAs (3) the predicted miRNAs of altered metabolic enzymes whose functions have not been validated for any miRNA before.

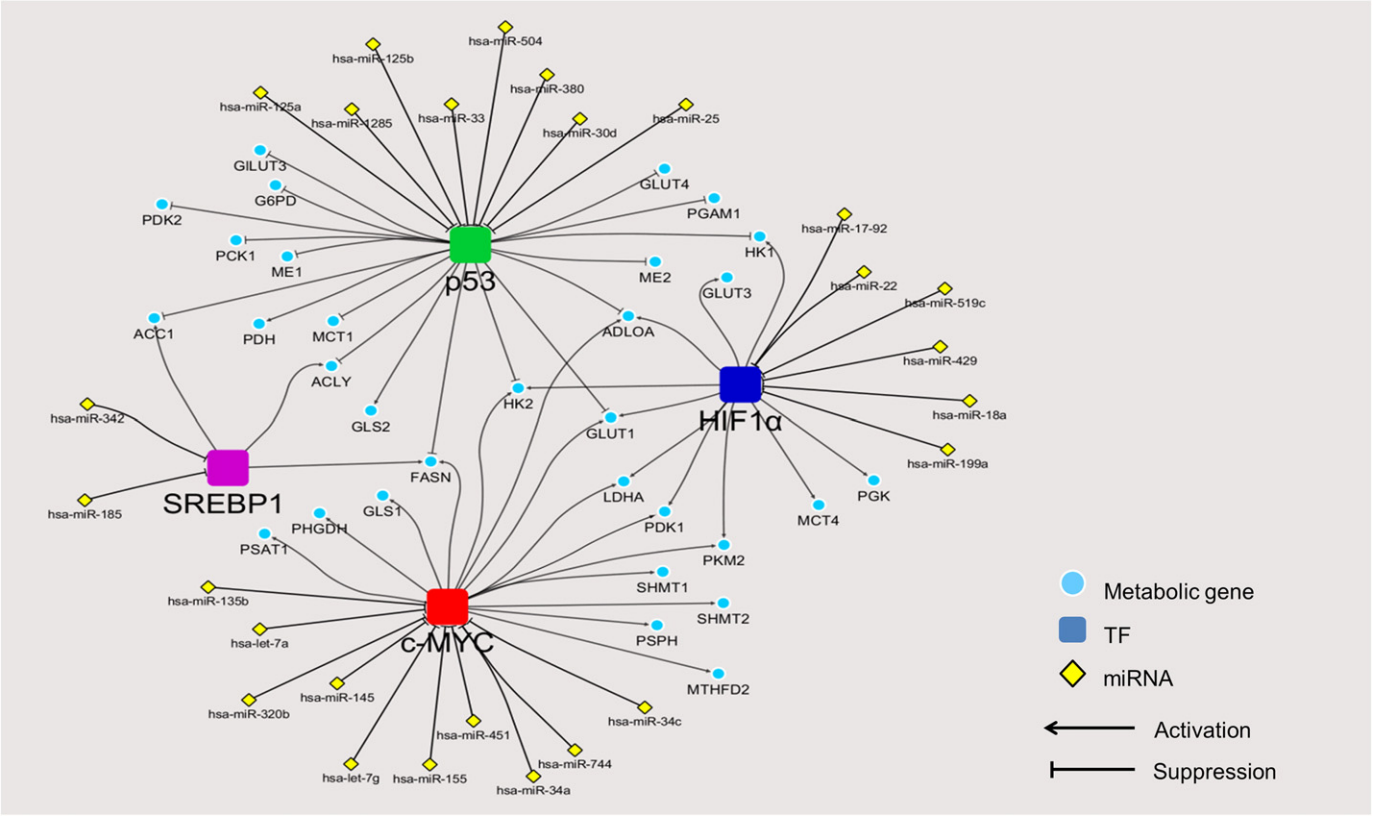

Fig. 3. Regulatory network of experimentally verified miRNAs and oncogenic transcription factors controlling metabolic reprogramming in cancers. The figure shows the integration of experimentally validated regulatory network of TFs-cancer metabolic genes and miRNAs-TFs.

Overall, our miRNAs and oncogenic transcriptional regulatory network depicts individual "modules" of post-transcriptional regulation by miRNA via major drivers of metabolic reprogramming in cancers, acting as hubs that link multiple incoming miRNAs (yellow nodes, Fig. 3) that can bind and suppress transcription of these oncogenes, to their downstream metabolic gene targets (blue nodes). For instance, the expression of c-MYC (red node in Fig. 3, and interaction between miRNA and targeting metabolic genes via c-MYC are in red lines in Fig. 4) is regulated by let-7a in Burkitt Lymphoma [92], miR-145 in non-small cell lung cancer [93], let-7g and miR-744 in hepatocellular carcinoma cells [94,95], miR-34 in prostate cancer cells [96], miR-135b in osteosarcoma cells [97], miR-155 in gastric carcinoma cells [98], miR-320b in colorectal cancer [99] and miR-451 in head and neck squamous cell carcinoma [100]. Suppression of these miRNAs contributes to overexpression of key metabolic enzymes in these tumors. Similarly, HIF1α (dark blue node) expression is regulated by several miRNAs including miR-17-92 in lung cancer cells [101], miR-519c and miR-18a in breast and lung cancer cells [102,103], miR-22 in colon cancer cells [104], miR-199a in non-small cell lung cancers [105] and miR-429 in human endothelial cells [106]. Ectopic expression of these miRNAs reduces the expression of vascular endothelial growth factor (VEGF), a crucial transcriptional target of HIF1α, thereby decreasing angiogenesis, a process of blood vessel formation required for tumor growth and metastasis [107]. Likewise, p53 (green node), a tumor suppressor is also post-transcriptionally regulated by several miRNAs such as miR-25 and miR-30d in myeloma cells [108], miR-125a in breast and hepatoblastoma cells [109], miR-125b in neuroblastoma and lung fibroblalst cells [110], miR-504 in breast and colon cancer cells [111], miR-1285 in neuroblastoma, hepatoblastoma and breast cancer cells [112], miR-33 in hematopoietic stem cells [113] and miR-380 in neuroblastoma cells [114]. Tight regulation of these miRNAs results in substantial expression of p53 which then leads to cell cycle arrest, thus maintaining cells in the non-proliferative state [115]. In contrast, an aberrant overexpression of these p53-target miRNAs results in the down-regulation of p53, causing malignancy. Because this group of miRNAs exerts its effect on the oncogenic transformation, they are generally now classified as the "oncomiR" miRNAs [116].

In addition to these three oncogenes, the sterol regulatory element binding protein (SREBP1, purple node) is also involved in metabolic reprogramming. SREBP1 is a TF that regulates expression of liver type-pyruvate kinase (PKL) and lipogenic enzymes, ACL, ACC and FAS, thus allowing *de novo* fatty acid synthesis from glucose in liver. Cancers also use SREBP1 to up-regulate expression of these lipogenic enzymes to support fatty acid synthesis. Similar to c-MYC, HIF1α and p53, expression of SREBP1 by itself is also regulated by miRNAs. miR-185 and miR-342 play important role in regulation of SREBP1 expression by direct binding to the 3′UTR of its mRNA [117]. Of particular interest, most lipogenic enzymes are co-regulated by more than one TF. For example ACL and ACC1 are regulated by both SREBP1 and p53, while FASN is regulated by SREBP1, p53 and c-MYC. Expression of HK1 is co-regulated by HIF1a and p53 while that of LDHA and PKM2 are co-regulated by HIF1α and c-MYC. GLU1, HK2 and ALDOA are the only three enzymes that are regulated by p53, HIF1α and c-MYC. Interestingly, the expression of certain miRNAs that regulate these metabolic enzymes can also be regulated by an oncogenic TFs. Gao et al. [118] showed that c-MYC indirectly regulates GLS expression in B lymphoma and prostate cancer by suppressing the expression of miR-23a/b that directly regulates the expression of GLS. Kim and coworkers also demonstrated that p53 blocks the expression of HK1, HK2, glucose-6-phosphate isomerase (GPI) and PDK1 by inducing miR-34a expression which in turn, down-regulates the expression of the above four enzymes [119].

Looking at the expanded miRNA–mRNA interaction networks (Fig. 4), we observe a global overview of how metabolic genes involving cancer progression are regulated by miRNA through their direct interaction (black lines for validated interactions and gray lines for those predicted

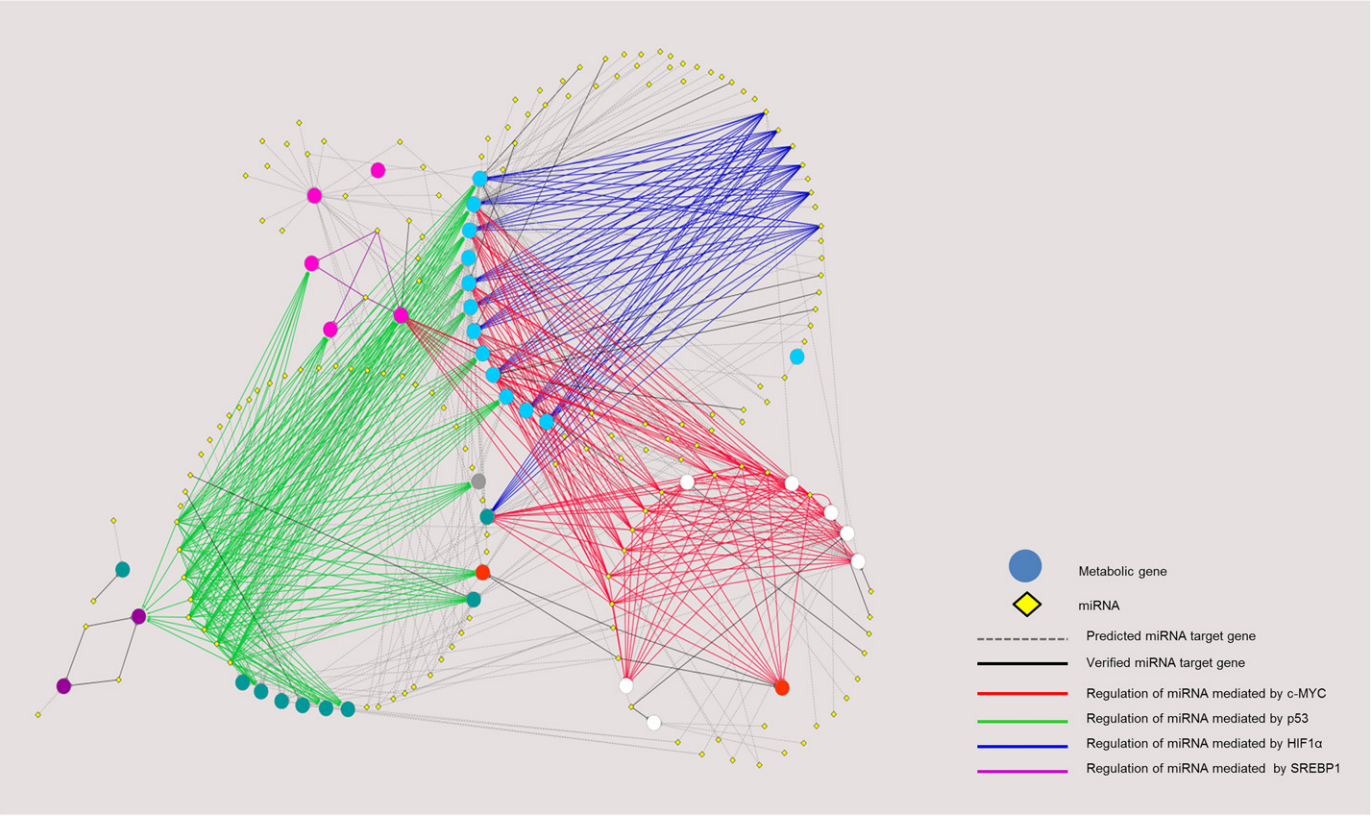

Fig. 4. Regulatory network of miRNAs and oncogenic transcription factors controlling metabolic reprogramming in cancers. The figure shows direct and indirect miRNAs-metabolic genes interaction. The miRNAs that have already verified their regulatory function show in solid edges whereas the dash edges represent the overlap miRNAs from predictions only. In addition, direct interaction of experimentally verified miRNAs and gene targets are showed in black edges whilst the color edges (blue, green, red and purple) illustrate the interaction of miRNAs and cancer metabolic genes via oncogenic transcription factors. Blue edges represent the regulation of miRNA mediated HIF1α, green edges represent the regulation of miRNA mediated p53, red edges represent the regulation of miRNA mediated c-MYC and the purple edges represent the regulation of miRNA mediated SREBP1. The pale blue circle nodes show the anaerobic glycolytic genes, white circle nodes show genes in serine, glycine and one carbon metabolism, orange circle nodes show genes in glutaminolysis, pink circle nodes show genes in *de novo* fatty acid synthesis, purple circle nodes show genes in PPP pathways, gray circle node is PCK1 and the blue-green nodes show genes in TCA cycle. High resolution of the figure with complete labels can be found in Fig. S1.

by TargetScan7.0 and miRanda–mirSVR), or through oncogenic TFs (colored edges). We have seen notable miRNAs such as miR-23a/b that directly control glutaminolysis, whereas the miR-1 and miR-206 are responsible for regulation of the PPP pathway genes, G6PD and TKTL1 [118,120]. The overall network also highlights the "hub" miRNA. miR-429, a tumor suppressor that down-regulates almost all genes in anaerobic glycolytic pathway (e.g. GLUTs) via the oncogenic TF HIF1α. The anaerobic glycolytic genes themselves are also targeted by several other miRNAs such as miR-22, miR-199a, miR-17-92 via HIF1α (blue edges), miR-30d, miR-25, miR-125a/b, miR-1285 via p53 (green edges), and miR-451, miR-155, let-7a, let-7g via c-MYC (red edges). The network also demonstrates other relationships between metabolic pathways and miRNA regulation via TFs. For instance, three out of five genes in *de novo* fatty acid synthesis pathway (ACC1, ACLY, and FASN) share regulation by miRNAs via p53 and SREBP1. The genes in the serine, glycine and one carbon metabolism pathways (white nodes) heavily rely on the regulation of miRNAs via c-MYC. Post-transcriptional regulatory networks have demonstrated intricate regulation of metabolic genes by different miRNAs [13,121,122]. Here, we aim to provide a detailed regulatory network of metabolic genes under direct control of miRNAs, or oncogenic TFs regulated by miRNAs. The high resolution network with complete labels can be found in Supplementary material (Fig. S1 and Table S3). Such overall organization of metabolic gene expression regulation cannot be observed by studying miRNAs, TFs, and target genes individually. Saying that, we note that the current version of network relies on the accuracy of the two prediction algorithms used in this study. The known interactions taken from literature might also be biased toward well-characterized oncogenes such as p53 or c-MYC.

In conclusion, our review not only provides the current status of understanding metabolic reprogramming in cancers but also establishes the regulatory network of miRNA-oncogenic TF-cancer metabolic genes that would provide benefits for research guidance in this emerging field the future.

Supplementary data to this article can be found online at http://dx.doi.org/10.1016/j.csbj.2016.05.005.

Acknowledgements

The authors thank Professor John Wallace, University of Adelaide for helpful comments on the manuscript. PP and KR are supported by the Science Achievement Scholarship of Thailand (SAST), Office of Higher Education Commission. Research in SJ laboratory is supported by grant BRG5780007 from the Thailand Research Fund (TRF) and Mahidol University. VC acknowledges the TRF Grant for New Researcher: TRG5880067, Faculty of Science, Mahidol University, and the Crown Property Bureau Foundation. The authors have no conflict of interest.

References

[1] Cairns RA, Harris IS, Mak TW. Regulation of cancer cell metabolism. Nat Rev Cancer 2011;11:85–95.

[2] Schulze A, Harris AL. How cancer metabolism is tuned for proliferation and vulnerable to disruption. Nature 2012;491:364–73.
[3] Kroemer G, Pouyssegur J. Tumor cell metabolism: cancer's Achilles' heel. Cancer Cell 2008;13:472–82.
[4] Ward PS, Thompson CB. Metabolic reprogramming: a cancer hallmark even Warburg did not anticipate. Cancer Cell 2012;21:297–308.
[5] Warburg O. On the origin of cancer cells. Science 1956;123:309–14.
[6] Vander Heiden MG, Cantley LC, Thompson CB. Understanding the Warburg effect: the metabolic requirements of cell proliferation. Science 2009;324:1029–33.
[7] Li C, Han J, Yao Q, Zou C, Xu Y, et al. Subpathway-GM: identification of metabolic subpathways via joint power of interesting genes and metabolites and their topologies within pathways. Nucleic Acids Res 2013;41, e101.
[8] Xia J, Wishart DS. MSEA: a web-based tool to identify biologically meaningful patterns in quantitative metabolomic data. Nucleic Acids Res 2010;38:W71–7.
[9] Li F, Xu Y, Shang D, Yang H, Liu W, et al. MPINet: metabolite pathway identification via coupling of global metabolite network structure and metabolomic profile. Biomed Res Int 2014;2014:325697.
[10] Ha M, Kim VN. Regulation of microRNA biogenesis. Nat Rev Mol Cell Biol 2014;15:509–24.
[11] Ameres SL, Zamore PD. Diversifying microRNA sequence and function. Nat Rev Mol Cell Biol 2013;14:475–88.
[12] Friedman RC, Farh KK, Burge CB, Bartel DP. Most mammalian mRNAs are conserved targets of microRNAs. Genome Res 2009;19:92–105.
[13] Rottiers V, Naar AM. MicroRNAs in metabolism and metabolic disorders. Nat Rev Mol Cell Biol 2012;13:239–50.
[14] Parks SK, Chiche J, Pouyssegur J. Disrupting proton dynamics and energy metabolism for cancer therapy. Nat Rev Cancer 2013;13:611–23.
[15] Christofk HR, Vander Heiden MG, Harris MH, Ramanathan A, Gerszten RE, et al. The M2 splice isoform of pyruvate kinase is important for cancer metabolism and tumour growth. Nature 2008;452:230–3.
[16] Tamada M, Suematsu M, Saya H. Pyruvate kinase M2: multiple faces for conferring benefits on cancer cells. Clin Cancer Res 2012;18:5554–61.
[17] Luo W, Semenza GL. Emerging roles of PKM2 in cell metabolism and cancer progression. Trends Endocrinol Metab 2012;23:560–6.
[18] Langbein S, Frederiks WM, zur Hausen A, Popa J, Lehmann J, et al. Metastasis is promoted by a bioenergetic switch: new targets for progressive renal cell cancer. Int J Cancer 2008;122:2422–8.
[19] Zhang S, Yue JX, Yang JH, Cai PC, Kong WJ. Overexpression of transketolase protein TKTL1 is associated with occurrence and progression in nasopharyngeal carcinoma: a potential therapeutic target in nasopharyngeal carcinoma. Cancer Biol Ther 2008;7:517–22.
[20] Wang J, Yuan W, Chen Z, Wu S, Chen J, et al. Overexpression of G6PD is associated with poor clinical outcome in gastric cancer. Tumour Biol 2012;33:95–101.
[21] Lin R, Elf S, Shan C, Kang HB, Ji Q, et al. 6-Phosphogluconate dehydrogenase links oxidative PPP, lipogenesis and tumour growth by inhibiting LKB1-AMPK signalling. Nat Cell Biol 2015;17:1484–96.
[22] Radisky DC, Levy DD, Littlepage LE, Liu H, Nelson CM, et al. Rac1b and reactive oxygen species mediate MMP-3-induced EMT and genomic instability. Nature 2005;436:123–7.
[23] Zhou G, Dada LA, Wu M, Kelly A, Trejo H, et al. Hypoxia-induced alveolar epithelial–mesenchymal transition requires mitochondrial ROS and hypoxia-inducible factor 1. Am J Physiol Lung Cell Mol Physiol 2009;297:L1120–30.
[24] Sukhatme VP, Chan B. Glycolytic cancer cells lacking 6-phosphogluconate dehydrogenase metabolize glucose to induce senescence. FEBS Lett 2012;586:2389–95.
[25] Xu IM, Lai RK, Lin SH, Tse AP, Chiu DK, et al. Transketolase counteracts oxidative stress to drive cancer development. Proc Natl Acad Sci U S A 2016;113:E725–34.
[26] Owen OE, Kalhan SC, Hanson RW. The key role of anaplerosis and cataplerosis for citric acid cycle function. J Biol Chem 2002;277:30409–12.
[27] King A, Selak MA, Gottlieb E. Succinate dehydrogenase and fumarate hydratase: linking mitochondrial dysfunction and cancer. Oncogene 2006;25:4675–82.
[28] Yan H, Parsons DW, Jin G, McLendon R, Rasheed BA, et al. IDH1 and IDH2 mutations in gliomas. N Engl J Med 2009;360:765–73.
[29] Dang L, White DW, Gross S, Bennett BD, Bittinger MA, et al. Cancer-associated IDH1 mutations produce 2-hydroxyglutarate. Nature 2009;462:739–44.
[30] Wise DR, Thompson CB. Glutamine addiction: a new therapeutic target in cancer. Trends Biochem Sci 2010;35:427–33.
[31] Jitrapakdee S, Vidal-Puig A, Wallace JC. Anaplerotic roles of pyruvate carboxylase in mammalian tissues. Cell Mol Life Sci 2006;63:843–54.
[32] Huang F, Zhang Q, Ma H, Lv Q, Zhang T. Expression of glutaminase is upregulated in colorectal cancer and of clinical significance. Int J Clin Exp Pathol 2014;7:1093–100.
[33] Sellers K, Fox MP, Bousamra 2nd M, Slone SP, Higashi RM, et al. Pyruvate carboxylase is critical for non-small-cell lung cancer proliferation. J Clin Invest 2015;125:687–98.
[34] Phannasil P, Thuwajit C, Warnnissorn M, Wallace JC, MacDonald MJ, et al. Pyruvate carboxylase is up-regulated in breast cancer and essential to support growth and invasion of MDA-MB-231 cells. PLoS One 2015;10, e0129848.
[35] Cheng T, Sudderth J, Yang C, Mullen AR, Jin ES, et al. Pyruvate carboxylase is required for glutamine-independent growth of tumor cells. Proc Natl Acad Sci U S A 2011;108:8674–9.
[36] Wise DR, DeBerardinis RJ, Mancuso A, Sayed N, Zhang XY, et al. Myc regulates a transcriptional program that stimulates mitochondrial glutaminolysis and leads to glutamine addiction. Proc Natl Acad Sci U S A 2008;105:18782–7.
[37] Vincent EE, Sergushichev A, Griss T, Gingras MC, Samborska B, et al. Mitochondrial phosphoenolpyruvate carboxykinase regulates metabolic adaptation and enables glucose-independent tumor growth. Mol Cell 2015;60:195–207.
[38] Leithner K, Hrzenjak A, Trotzmuller M, Moustafa T, Kofeler HC, et al. PCK2 activation mediates an adaptive response to glucose depletion in lung cancer. Oncogene 2015;34:1044–50.
[39] Montal ED, Dewi R, Bhalla K, Ou L, Hwang BJ, et al. PEPCK coordinates the regulation of central carbon metabolism to promote cancer cell growth. Mol Cell 2015;60:571–83.
[40] Locasale JW. Serine, glycine and one-carbon units: cancer metabolism in full circle. Nat Rev Cancer 2013;13:572–83.
[41] Possemato R, Marks KM, Shaul YD, Pacold ME, Kim D, et al. Functional genomics reveal that the serine synthesis pathway is essential in breast cancer. Nature 2011;476:346–50.
[42] Locasale JW, Grassian AR, Melman T, Lyssiotis CA, Mattaini KR, et al. Phosphoglycerate dehydrogenase diverts glycolytic flux and contributes to oncogenesis. Nat Genet 2011;43:869–74.
[43] Paone A, Marani M, Fiascarelli A, Rinaldo S, Giardina G, et al. SHMT1 knockdown induces apoptosis in lung cancer cells by causing uracil misincorporation. Cell Death Dis 2014;5, e1525.
[44] Kim D, Fiske BP, Birsoy K, Freinkman E, Kami K, et al. SHMT2 drives glioma cell survival in ischaemia but imposes a dependence on glycine clearance. Nature 2015;520:363–7.
[45] Marani M, Paone A, Fiascarelli A, Macone A, Gargano M, et al. A pyrazolopyran derivative preferentially inhibits the activity of human cytosolic serine hydroxymethyltransferase and induces cell death in lung cancer cells. Oncotarget 2015.
[46] Currie E, Schulze A, Zechner R, Walther TC, Farese Jr RV. Cellular fatty acid metabolism and cancer. Cell Metab 2013;18:153–61.
[47] Bauer DE, Hatzivassiliou G, Zhao F, Andreadis C, Thompson CB. ATP citrate lyase is an important component of cell growth and transformation. Oncogene 2005;24:6314–22.
[48] Hatzivassiliou G, Zhao F, Bauer DE, Andreadis C, Shaw AN, et al. ATP citrate lyase inhibition can suppress tumor cell growth. Cancer Cell 2005;8:311–21.
[49] Tong L. Acetyl-coenzyme A carboxylase: crucial metabolic enzyme and attractive target for drug discovery. Cell Mol Life Sci 2005;62:1784–803.
[50] Magnard C, Bachelier R, Vincent A, Jaquinod M, Kieffer S, et al. BRCA1 interacts with acetyl-CoA carboxylase through its tandem of BRCT domains. Oncogene 2002;21:6729–39.
[51] Moreau K, Dizin E, Ray H, Luquain C, Lefai E, et al. BRCA1 affects lipid synthesis through its interaction with acetyl-CoA carboxylase. J Biol Chem 2006;281:3172–81.
[52] Chajes V, Cambot M, Moreau K, Lenoir GM, Joulin V. Acetyl-CoA carboxylase alpha is essential to breast cancer cell survival. Cancer Res 2006;66:5287–94.
[53] Brusselmans K, De Schrijver E, Verhoeven G, Swinnen JV. RNA interference-mediated silencing of the acetyl-CoA-carboxylase-alpha gene induces growth inhibition and apoptosis of prostate cancer cells. Cancer Res 2005;65:6719–25.
[54] Beckers A, Organe S, Timmermans L, Scheys K, Peeters A, et al. Chemical inhibition of acetyl-CoA carboxylase induces growth arrest and cytotoxicity selectively in cancer cells. Cancer Res 2007;67:8180–7.
[55] Zhan Y, Ginanni N, Tota MR, Wu M, Bays NW, et al. Control of cell growth and survival by enzymes of the fatty acid synthesis pathway in HCT-116 colon cancer cells. Clin Cancer Res 2008;14:5735–42.
[56] Rashid A, Pizer ES, Moga M, Milgraum LZ, Zahurak M, et al. Elevated expression of fatty acid synthase and fatty acid synthetic activity in colorectal neoplasia. Am J Pathol 1997;150:201–8.
[57] Pizer ES, Lax SF, Kuhajda FP, Pasternack GR, Kurman RJ. Fatty acid synthase expression in endometrial carcinoma: correlation with cell proliferation and hormone receptors. Cancer 1998;83:528–37.
[58] Kuhajda FP. Fatty acid synthase and cancer: new application of an old pathway. Cancer Res 2006;66:5977–80.
[59] Thupari JN, Pinn ML, Kuhajda FP. Fatty acid synthase inhibition in human breast cancer cells leads to malonyl-CoA-induced inhibition of fatty acid oxidation and cytotoxicity. Biochem Biophys Res Commun 2001;285:217–23.
[60] Knowles LM, Axelrod F, Browne CD, Smith JW. A fatty acid synthase blockade induces tumor cell-cycle arrest by down-regulating Skp2. J Biol Chem 2004;279:30540–5.
[61] Kolch W, Halasz M, Granovskaya M, Kholodenko BN. The dynamic control of signal transduction networks in cancer cells. Nat Rev Cancer 2015;15:515–27.
[62] Sullivan LB, Martinez-Garcia E, Nguyen H, Mullen AR, Dufour E, et al. The proto-oncometabolite fumarate binds glutathione to amplify ROS-dependent signaling. Mol Cell 2013;51:236–48.
[63] Reitman ZJ, Jin G, Karoly ED, Spasojevic I, Yang J, et al. Profiling the effects of isocitrate dehydrogenase 1 and 2 mutations on the cellular metabolome. Proc Natl Acad Sci U S A 2011;108:3270–5.
[64] Onodera Y, Nam JM, Bissell MJ. Increased sugar uptake promotes oncogenesis via EPAC/RAP1 and O-GlcNAc pathways. J Clin Invest 2014;124:367–84.
[65] Li Z, Zhang H. Reprogramming of glucose, fatty acid and amino acid metabolism for cancer progression. Cell Mol Life Sci 2015;73:377–92.
[66] Dang CV. MYC, metabolism, cell growth, and tumorigenesis. Cold Spring Harb Perspect Med 2013;3.
[67] Kruiswijk F, Labuschagne CF, Vousden KH. p53 in survival, death and metabolic health: a lifeguard with a licence to kill. Nat Rev Mol Cell Biol 2015;16:393–405.
[68] Zeller KI, Jegga AG, Aronow BJ, O'Donnell KA, Dang CV. An integrated database of genes responsive to the Myc oncogenic transcription factor: identification of direct genomic targets. Genome Biol 2003;4:R69.
[69] Dang CV, Kim JW, Gao P, Yustein J. The interplay between MYC and HIF in cancer. Nat Rev Cancer 2008;8:51–6.

[70] Semenza GL. HIF-1: upstream and downstream of cancer metabolism. Curr Opin Genet Dev 2010;20:51–6.
[71] Liu J, Zhang C, Hu W, Feng Z. Tumor suppressor p53 and its mutants in cancer metabolism. Cancer Lett 2015;356:197–203.
[72] Schwartzenberg-Bar-Yoseph F, Armoni M, Karnieli E. The tumor suppressor p53 down-regulates glucose transporters GLUT1 and GLUT4 gene expression. Cancer Res 2004;64:2627–33.
[73] Berkers CR, Maddocks OD, Cheung EC, Mor I, Vousden KH. Metabolic regulation by p53 family members. Cell Metab 2013;18:617–33.
[74] Jiang P, Du W, Wang X, Mancuso A, Gao X, et al. p53 regulates biosynthesis through direct inactivation of glucose-6-phosphate dehydrogenase. Nat Cell Biol 2011;13:310–6.
[75] Zhang P, Tu B, Wang H, Cao Z, Tang M, et al. Tumor suppressor p53 cooperates with SIRT6 to regulate gluconeogenesis by promoting FoxO1 nuclear exclusion. Proc Natl Acad Sci U S A 2014;111:10684–9.
[76] Goldstein I, Yizhak K, Madar S, Goldfinger N, Ruppin E, et al. p53 promotes the expression of gluconeogenesis-related genes and enhances hepatic glucose production. Cancer Metab 2013;1:9.
[77] Betel D, Wilson M, Gabow A, Marks DS, Sander C. The microRNA.org resource: targets and expression. Nucleic Acids Res 2008;36:D149–53.
[78] Betel D, Koppal A, Agius P, Sander C, Leslie C. Comprehensive modeling of microRNA targets predicts functional non-conserved and non-canonical sites. Genome Biol 2010;11:R90.
[79] Paraskevopoulou MD, Georgakilas G, Kostoulas N, Vlachos IS, Vergoulis T, et al. DIANA-microT web server v5.0: service integration into miRNA functional analysis workflows. Nucleic Acids Res 2013;41:W169–73.
[80] Garcia DM, Baek D, Shin C, Bell GW, Grimson A, et al. Weak seed-pairing stability and high target-site abundance decrease the proficiency of lsy-6 and other microRNAs. Nat Struct Mol Biol 2011;18:1139–46.
[81] Agarwal V, Bell GW, Nam JW, Bartel DP. Predicting effective microRNA target sites in mammalian mRNAs. Elife 2015;4.
[82] Krek A, Grun D, Poy MN, Wolf R, Rosenberg L, et al. Combinatorial microRNA target predictions. Nat Genet 2005;37:495–500.
[83] Wong N, Wang X. miRDB: an online resource for microRNA target prediction and functional annotations. Nucleic Acids Res 2015;43:D146–52.
[84] Miranda KC, Huynh T, Tay Y, Ang YS, Tam WL, et al. A pattern-based method for the identification of MicroRNA binding sites and their corresponding heteroduplexes. Cell 2006;126:1203–17.
[85] Peterson SM, Thompson JA, Ufkin ML, Sathyanarayana P, Liaw L, et al. Common features of microRNA target prediction tools. Front Genet 2014;5:23.
[86] Lewis BP, Burge CB, Bartel DP. Conserved seed pairing, often flanked by adenosines, indicates that thousands of human genes are microRNA targets. Cell 2005;120:15–20.
[87] Brennecke J, Stark A, Russell RB, Cohen SM. Principles of microRNA-target recognition. PLoS Biol 2005;3, e85.
[88] Lewis BP, Shih IH, Jones-Rhoades MW, Bartel DP, Burge CB. Prediction of mammalian microRNA targets. Cell 2003;115:787–98.
[89] Grimson A, Farh KK, Johnston WK, Garrett-Engele P, Lim LP, et al. MicroRNA targeting specificity in mammals: determinants beyond seed pairing. Mol Cell 2007;27:91–105.
[90] Chou CH, Chang NW, Shrestha S, Hsu SD, Lin YL, et al. miRTarBase 2016: updates to the experimentally validated miRNA-target interactions database. Nucleic Acids Res 2016;44:D239–47.
[91] Shannon P, Markiel A, Ozier O, Baliga NS, Wang JT, et al. Cytoscape: a software environment for integrated models of biomolecular interaction networks. Genome Res 2003;13:2498–504.
[92] Sampson VB, Rong NH, Han J, Yang Q, Aris V, et al. MicroRNA let-7a down-regulates MYC and reverts MYC-induced growth in Burkitt lymphoma cells. Cancer Res 2007;67:9762–70.
[93] Chen Z, Zeng H, Guo Y, Liu P, Pan H, et al. miRNA-145 inhibits non-small cell lung cancer cell proliferation by targeting c-Myc. J Exp Clin Cancer Res 2010;29:151.
[94] Lan FF, Wang H, Chen YC, Chan CY, Ng SS, et al. Hsa-let-7g inhibits proliferation of hepatocellular carcinoma cells by downregulation of c-Myc and upregulation of p16(INK4A). Int J Cancer 2011;128:319–31.
[95] Lin F, Ding R, Zheng S, Xing D, Hong W, et al. Decrease expression of microRNA-744 promotes cell proliferation by targeting c-Myc in human hepatocellular carcinoma. Cancer Cell Int 2014;14:58.
[96] Yamamura S, Saini S, Majid S, Hirata H, Ueno K, et al. MicroRNA-34a modulates c-Myc transcriptional complexes to suppress malignancy in human prostate cancer cells. PLoS One 2012;7, e29722.
[97] Liu Z, Zhang G, Li J, Liu J, Lv P. The tumor-suppressive microRNA-135b targets c-Myc in osteoscarcoma. PLoS One 2014;9, e102621.
[98] Sun S, Sun P, Wang C, Sun T. Downregulation of microRNA-155 accelerates cell growth and invasion by targeting c-Myc in human gastric carcinoma cells. Oncol Rep 2014;32:951–6.
[99] Wang H, Cao F, Li X, Miao H, E J, et al. miR-320b suppresses cell proliferation by targeting c-Myc in human colorectal cancer cells. BMC Cancer 2015;15:748.
[100] Wang H, Zhang G, Wu Z, Lu B, Yuan D, et al. MicoRNA-451 is a novel tumor suppressor via targeting c-Myc in head and neck squamous cell carcinomas. J Cancer Res Ther 2015;11(Suppl. 2):C216–21.
[101] Taguchi A, Yanagisawa K, Tanaka M, Cao K, Matsuyama Y, et al. Identification of hypoxia-inducible factor-1 alpha as a novel target for miR-17-92 microRNA cluster. Cancer Res 2008;68:5540–5.
[102] Cha ST, Chen PS, Johansson G, Chu CY, Wang MY, et al. MicroRNA-519c suppresses hypoxia-inducible factor-1alpha expression and tumor angiogenesis. Cancer Res 2010;70:2675–85.
[103] Krutilina R, Sun W, Sethuraman A, Brown M, Seagroves TN, et al. MicroRNA-18a inhibits hypoxia-inducible factor 1alpha activity and lung metastasis in basal breast cancers. Breast Cancer Res 2014;16:R78.
[104] Yamakuchi M, Yagi S, Ito T, Lowenstein CJ. MicroRNA-22 regulates hypoxia signaling in colon cancer cells. PLoS One 2011;6, e20291.
[105] Ding G, Huang G, Liu HD, Liang HX, Ni YF, et al. MiR-199a suppresses the hypoxia-induced proliferation of non-small cell lung cancer cells through targeting HIF1alpha. Mol Cell Biochem 2013;384:173–80.
[106] Bartoszewska S, Kochan K, Piotrowski A, Kamysz W, Ochocka RJ, et al. The hypoxia-inducible miR-429 regulates hypoxia-inducible factor-1alpha expression in human endothelial cells through a negative feedback loop. FASEB J 2015;29:1467–79.
[107] Deng G, Sui G. Noncoding RNA in oncogenesis: a new era of identifying key players. Int J Mol Sci 2013;14:18319–49.
[108] Kumar M, Lu Z, Takwi AA, Chen W, Callander NS, et al. Negative regulation of the tumor suppressor p53 gene by microRNAs. Oncogene 2011;30:843–53.
[109] Zhang Y, Gao JS, Tang X, Tucker LD, Quesenberry P, et al. MicroRNA 125a and its regulation of the p53 tumor suppressor gene. FEBS Lett 2009;583:3725–30.
[110] Le MT, Teh C, Shyh-Chang N, Xie H, Zhou B, et al. MicroRNA-125b is a novel negative regulator of p53. Genes Dev 2009;23:862–76.
[111] Hu W, Chan CS, Wu R, Zhang C, Sun Y, et al. Negative regulation of tumor suppressor p53 by microRNA miR-504. Mol Cell 2010;38:689–99.
[112] Tian S, Huang S, Wu S, Guo W, Li J, et al. MicroRNA-1285 inhibits the expression of p53 by directly targeting its 3′ untranslated region. Biochem Biophys Res Commun 2010;396:435–9.
[113] Herrera-Merchan A, Cerrato C, Luengo G, Dominguez O, Piris MA, et al. miR-33-mediated downregulation of p53 controls hematopoietic stem cell self-renewal. Cell Cycle 2010;9:3277–85.
[114] Swarbrick A, Woods SL, Shaw A, Balakrishnan A, Phua Y, et al. miR-380-5p represses p53 to control cellular survival and is associated with poor outcome in MYCN-amplified neuroblastoma. Nat Med 2010;16:1134–40.
[115] Hermeking H. MicroRNAs in the p53 network: micromanagement of tumour suppression. Nat Rev Cancer 2012;12:613–26.
[116] Esquela-Kerscher A, Slack FJ. Oncomirs — microRNAs with a role in cancer. Nat Rev Cancer 2006;6:259–69.
[117] Li X, Chen YT, Josson S, Mukhopadhyay NK, Kim J, et al. MicroRNA-185 and 342 inhibit tumorigenicity and induce apoptosis through blockade of the SREBP metabolic pathway in prostate cancer cells. PLoS One 2013;8, e70987.
[118] Gao P, Tchernyshyov I, Chang TC, Lee YS, Kita K, et al. c-Myc suppression of miR-23a/b enhances mitochondrial glutaminase expression and glutamine metabolism. Nature 2009;458:762–5.
[119] Kim HR, Roe JS, Lee JE, Cho EJ, Youn HD. p53 regulates glucose metabolism by miR-34a. Biochem Biophys Res Commun 2013;437:225–31.
[120] Singh A, Happel C, Manna SK, Acquaah-Mensah G, Carrerero J, et al. Transcription factor NRF2 regulates miR-1 and miR-206 to drive tumorigenesis. J Clin Invest 2013;123:2921–34.
[121] Feng L, Xu Y, Zhang Y, Sun Z, Han J, et al. Subpathway-GMir: identifying miRNA-mediated metabolic subpathways by integrating condition-specific genes, microRNAs, and pathway topologies. Oncotarget 2015;6:39151–64.
[122] Vienberg S, Geiger J, Madsen S, Dalgaard LT. MicroRNAs in metabolism. Acta Physiol (Oxf) 2016.
[123] Yamasaki T, Seki N, Yoshino H, Itesako T, Yamada Y, et al. Tumor-suppressive microRNA-1291 directly regulates glucose transporter 1 in renal cell carcinoma. Cancer Sci 2013;104:1411–9.
[124] Noguchi Y, Marat D, Saito A, Yoshikawa T, Doi C, et al. Expression of facilitative glucose transporters in gastric tumors. Hepatogastroenterology 1999;46:2683–9.
[125] Ito T, Noguchi Y, Satoh S, Hayashi H, Inayama Y, et al. Expression of facilitative glucose transporter isoforms in lung carcinomas: its relation to histologic type, differentiation grade, and tumor stage. Mod Pathol 1998;11:437–43.
[126] Kurata T, Oguri T, Isobe T, Ishioka S, Yamakido M. Differential expression of facilitative glucose transporter (GLUT) genes in primary lung cancers and their liver metastases. Jpn J Cancer Res 1999;90:1238–43.
[127] Fei X, Qi M, Wu B, Song Y, Wang Y, et al. MicroRNA-195-5p suppresses glucose uptake and proliferation of human bladder cancer T24 cells by regulating GLUT3 expression. FEBS Lett 2012;586:392–7.
[128] Dai DW, Lu Q, Wang LX, Zhao WY, Cao YQ, et al. Decreased miR-106a inhibits glioma cell glucose uptake and proliferation by targeting SLC2A3 in GBM. BMC Cancer 2013;13:478.
[129] Boado RJ, Black KL, Pardridge WM. Gene expression of GLUT3 and GLUT1 glucose transporters in human brain tumors. Brain Res Mol Brain Res 1994;27:51–7.
[130] Binder C, Binder L, Marx D, Schauer A, Hiddemann W. Deregulated simultaneous expression of multiple glucose transporter isoforms in malignant cells and tissues. Anticancer Res 1997;17:4299–304.
[131] Gregersen LH, Jacobsen A, Frankel LB, Wen J, Krogh A, et al. MicroRNA-143 down-regulates Hexokinase 2 in colon cancer cells. BMC Cancer 2012;12:232.
[132] Jiang S, Zhang LF, Zhang HW, Hu S, Lu MH, et al. A novel miR-155/miR-143 cascade controls glycolysis by regulating hexokinase 2 in breast cancer cells. EMBO J 2012;31:1985–98.
[133] Mathupala SP, Ko YH, Pedersen PL. Hexokinase II: cancer's double-edged sword acting as both facilitator and gatekeeper of malignancy when bound to mitochondria. Oncogene 2006;25:4777–86.
[134] Du S, Guan Z, Hao L, Song Y, Wang L, et al. Fructose-bisphosphate aldolase a is a potential metastasis-associated marker of lung squamous cell carcinoma and promotes lung cell tumorigenesis and migration. PLoS One 2014;9, e85804.

[135] Li C, Shu F, Lei B, Lv D, Zhang S, et al. Expression of PGAM1 in renal clear cell carcinoma and its clinical significance. Int J Clin Exp Pathol 2015;8:9410–5.
[136] Liu AM, Xu Z, Shek FH, Wong KF, Lee NP, et al. miR-122 targets pyruvate kinase M2 and affects metabolism of hepatocellular carcinoma. PLoS One 2014;9, e86872.
[137] Kefas B, Comeau L, Erdle N, Montgomery E, Amos S, et al. Pyruvate kinase M2 is a target of the tumor-suppressive microRNA-326 and regulates the survival of glioma cells. Neuro Oncol 2010;12:1102–12.
[138] Wong TS, Liu XB, Chung-Wai Ho A, Po-Wing Yuen A, Wai-Man Ng R, et al. Identification of pyruvate kinase type M2 as potential oncoprotein in squamous cell carcinoma of tongue through microRNA profiling. Int J Cancer 2008;123:251–7.
[139] Feng C, Gao Y, Wang C, Yu X, Zhang W, et al. Aberrant overexpression of pyruvate kinase M2 is associated with aggressive tumor features and the BRAF mutation in papillary thyroid cancer. J Clin Endocrinol Metab 2013;98:E1524–33.
[140] Zhou CF, Li XB, Sun H, Zhang B, Han YS, et al. Pyruvate kinase type M2 is upregulated in colorectal cancer and promotes proliferation and migration of colon cancer cells. IUBMB Life 2012;64:775–82.
[141] Yang X, Cheng Y, Li P, Tao J, Deng X, et al. A lentiviral sponge for miRNA-21 diminishes aerobic glycolysis in bladder cancer T24 cells via the PTEN/PI3K/AKT/mTOR axis. Tumour Biol 2015;36:383–91.
[142] Xian ZY, Liu JM, Chen QK, Chen HZ, Ye CJ, et al. Inhibition of LDHA suppresses tumor progression in prostate cancer. Tumour Biol 2015;36:8093–100.
[143] Shi M, Cui J, Du J, Wei D, Jia Z, et al. A novel KLF4/LDHA signaling pathway regulates aerobic glycolysis in and progression of pancreatic cancer. Clin Cancer Res 2014;20:4370–80.
[144] Li KK, Pang JC, Ching AK, Wong CK, Kong X, et al. miR-124 is frequently downregulated in medulloblastoma and is a negative regulator of SLC16A1. Hum Pathol 2009;40:1234–43.
[145] Pinheiro C, Longatto-Filho A, Ferreira L, Pereira SM, Etlinger D, et al. Increasing expression of monocarboxylate transporters 1 and 4 along progression to invasive cervical carcinoma. Int J Gynecol Pathol 2008;27:568–74.
[146] Koukourakis MI, Giatromanolaki A, Bougioukas G, Sivridis E. Lung cancer: a comparative study of metabolism related protein expression in cancer cells and tumor associated stroma. Cancer Biol Ther 2007;6:1476–9.
[147] Zabkiewicz J, Pearn L, Hills RK, Morgan RG, Tonks A, et al. The PDK1 master kinase is over-expressed in acute myeloid leukemia and promotes PKC-mediated survival of leukemic blasts. Haematologica 2014;99:858–64.
[148] Chen B, Liu Y, Jin X, Lu W, Liu J, et al. MicroRNA-26a regulates glucose metabolism by direct targeting PDHX in colorectal cancer cells. BMC Cancer 2014;14:443.
[149] Koukourakis MI, Giatromanolaki A, Sivridis E, Gatter KC, Harris AL, et al. Pyruvate dehydrogenase and pyruvate dehydrogenase kinase expression in non-small cell lung cancer and tumor-associated stroma. Neoplasia 2005;7:1–6.
[150] Tanaka H, Sasayama T, Tanaka K, Nakamizo S, Nishihara M, et al. MicroRNA-183 upregulates HIF-1alpha by targeting isocitrate dehydrogenase 2 (IDH2) in glioma cells. J Neurooncol 2013;111:273–83.
[151] Puissegur MP, Mazure NM, Bertero T, Pradelli L, Grosso S, et al. miR-210 is overexpressed in late stages of lung cancer and mediates mitochondrial alterations associated with modulation of HIF-1 activity. Cell Death Differ 2011;18:465–78.
[152] Yahagi N, Shimano H, Hasegawa K, Ohashi K, Matsuzaka T, et al. Co-ordinate activation of lipogenic enzymes in hepatocellular carcinoma. Eur J Cancer 2005;41:1316–22.
[153] Hu W, Zhang C, Wu R, Sun Y, Levine A, et al. Glutaminase 2, a novel p53 target gene regulating energy metabolism and antioxidant function. Proc Natl Acad Sci U S A 2010;107:7455–60.
[154] Suzuki S, Tanaka T, Poyurovsky MV, Nagano H, Mayama T, et al. Phosphate-activated glutaminase (GLS2), a p53-inducible regulator of glutamine metabolism and reactive oxygen species. Proc Natl Acad Sci U S A 2010;107:7461–6.
[155] Leivonen SK, Rokka A, Ostling P, Kohonen P, Corthals GL, et al. Identification of miR-193b targets in breast cancer cells and systems biological analysis of their functional impact. Mol Cell Proteomics 2011;10(M110):005322.
[156] Jain M, Nilsson R, Sharma S, Madhusudhan N, Kitami T, et al. Metabolite profiling identifies a key role for glycine in rapid cancer cell proliferation. Science 2012;336:1040–4.
[157] Wu S, Zhang G, Li P, Chen S, Zhang F, et al. miR-198 targets SHMT1 to inhibit cell proliferation and enhance cell apoptosis in lung adenocarcinoma. Tumour Biol 2015;37:5193–202.
[158] Selcuklu SD, Donoghue MT, Rehmet K, de Souza GM, Fort A, et al. MicroRNA-9 inhibition of cell proliferation and identification of novel miR-9 targets by transcriptome profiling in breast cancer cells. J Biol Chem 2012;287:29516–28.
[159] Yan S, Jiang H, Fang S, Yin F, Wang Z, et al. MicroRNA-340 inhibits esophageal cancer cell growth and invasion by targeting phosphoserine aminotransferase 1. Cell Physiol Biochem 2015;37:375–86.
[160] Vie N, Copois V, Bascoul-Mollevi C, Denis V, Bec N, et al. Overexpression of phosphoserine aminotransferase PSAT1 stimulates cell growth and increases chemoresistance of colon cancer cells. Mol Cancer 2008;7:14.
[161] Kim SK, Jung WH, Koo JS. Differential expression of enzymes associated with serine/glycine metabolism in different breast cancer subtypes. PLoS One 2014;9, e101004.
[162] Song YH, Shiota M, Kuroiwa K, Naito S, Oda Y. The important role of glycine N-methyltransferase in the carcinogenesis and progression of prostate cancer. Mod Pathol 2011;24:1272–80.
[163] Catalina-Rodriguez O, Kolukula VK, Tomita Y, Preet A, Palmieri F, et al. The mitochondrial citrate transporter, CIC, is essential for mitochondrial homeostasis. Oncotarget 2012;3:1220–35.
[164] Qian X, Hu J, Zhao J, Chen H. ATP citrate lyase expression is associated with advanced stage and prognosis in gastric adenocarcinoma. Int J Clin Exp Med 2015;8:7855–60.
[165] Wang C, Rajput S, Watabe K, Liao DF, Cao D. Acetyl-CoA carboxylase-a as a novel target for cancer therapy. Front Biosci (Schol Ed) 2010;2:515–26.
[166] Cheng C, Chen ZQ, Shi XT. MicroRNA-320 inhibits osteosarcoma cells proliferation by directly targeting fatty acid synthase. Tumour Biol 2014;35:4177–83.

FEBS Letters 589 (2015) 2073–2079

FEBS Letters

journal homepage: www.FEBSLetters.org

Residues in the acetyl CoA binding site of pyruvate carboxylase involved in allosteric regulation

Kamonman Choosangtong [a], Chaiyos Sirithanakorn [a], Abdul Adina-Zada [b], John C. Wallace [c], Sarawut Jitrapakdee [a,*], Paul V. Attwood [b,*]

[a] Department of Biochemistry, Faculty of Science, Mahidol University, Bangkok 10400, Thailand
[b] School of Chemistry and Biochemistry, The University of Western Australia, 35 Stirling Highway, Crawley, WA 6009, Australia
[c] School of Molecular and Biomedical Sciences, University of Adelaide, Adelaide, SA 5005, Australia

ARTICLE INFO

Article history:
Received 24 April 2015
Revised 24 June 2015
Accepted 24 June 2015
Available online 3 July 2015

Edited by Peter Brzezinski

Keywords:
Pyruvate carboxylase
Rhizobium etli
Acetyl coenzyme A
Allosteric regulation

ABSTRACT

We have examined the roles of Asp1018, Glu1027, Arg469 and Asp471 in the allosteric domain of *Rhizobium etli* pyruvate carboxylase. Arg469 and Asp471 interact directly with the allosteric activator acetyl coenzyme A (acetyl CoA) and the R469S and R469K mutants showed increased enzymic activity in the presence and absence of acetyl CoA, whilst the D471A mutant exhibited no acetyl CoA-activation. E1027A, E1027R and D1018A mutants had increased activity in the absence of acetyl CoA, but not in its presence. These results suggest that most of these residues impose restrictions on the structure and/or dynamics of the enzyme to affect activity.

1. Introduction

Pyruvate carboxylase [EC 6.4.1.1] is a biotin-dependent enzyme that supplies oxaloacetate for replenishment of tricarboxylic acid cycle intermediates and in some specialised mammalian tissues, for gluconeogenesis, glucose-induced insulin release and neurotransmitter synthesis [1,2]. The enzyme from most organisms is highly regulated by the allosteric activator, acetyl CoA although there is some variation of the dependence of the enzyme on acetyl CoA, in terms of its activity in the absence of acetyl CoA and the K_a for activation [3,4]. In addition, the cooperativity of the activation of PC by acetyl CoA varies between species [3], with the Hill coefficient for the activation of the *Rhizobium etli* enzyme (RePC) being about 2.8 [5]. In recent years, the structures of the α_4 tetrameric pyruvate carboxylase holoenzyme from *R. etli*, *Staphylococcus aureus* (SaPC) and *Listeria monocytogenes* (LmPC) have been solved [6–10] and the catalytic mechanism of the RePC has been well characterised [11–15]. However, many aspects of the mechanism of action of acetyl CoA in its role as an allosteric activator of RePC remain to be established.

Fig. 1 shows the structure of the RePC monomer and the reactions occurring in the biotin carboxylase (BC) and carboxyltransferase (CT) domains, with the biotin being covalently attached to the mobile biotin carboxyl carrier protein (BCCP) domain. The allosteric domain, where acetyl CoA binds, occupies a central position between the three other domains [7]. The RePC tetramer is very asymmetrical and only two of the four subunits had ethyl CoA (an analogue of acetyl CoA) bound to them. Only this pair of

Abbreviations: acetyl CoA, acetyl coenzyme A; PC, pyruvate carboxylase; RePC, *Rhizobium etli* pyruvate carboxylase; SaPC, *Staphylococcus aureus* pyruvate carboxylase; LmPC, *Listeria monocytogenes* pyruvate carboxylase; BC, biotin carboxylase; CT, carboxyl transferase; BCCP, biotin carboxyl carrier protein; PCR, polymerase chain reaction; DTE, dithioerythritol

Author contributions: Kamonman Choosangtong: prepared and expressed the mutants, performed the major part of the kinetic assays and contributed to the writing of the manuscript. Chaiyos Sirithanakorn: performed some of the kinetic assays and contributed to the writing of the manuscript. Abdul Adina-Zada: supervised much of the kinetic work performed at UWA and contributed to the writing of the manuscript. John C. Wallace: helped plan the mutations and contributed to the writing of the manuscript. Sarawut Jitrapakdee: helped planned the mutations, supervised their production in Bangkok and had a major contribution to the writing of the manuscript. Paul V. Attwood: helped plan the mutations, planned and helped supervise the kinetic work and was a major author of the manuscript.

* Corresponding authors. Fax: +61 8 354 7174 (S. Jitrapakdee), +61 8 6488 1148 (P. Attwood).

E-mail addresses: kamonman.c@hotmail.com (K. Choosangtong), yozinomycetes@hotmail.com (C. Sirithanakorn), adinazada@bigpond.com (A. Adina-Zada), john.wallace@adelaide.edu.au (J.C. Wallace), sarawut.jit@mahidol.ac.th (S. Jitrapakdee), paul.attwood@uwa.edu.au (P.V. Attwood).

http://dx.doi.org/10.1016/j.febslet.2015.06.034
0014-5793/

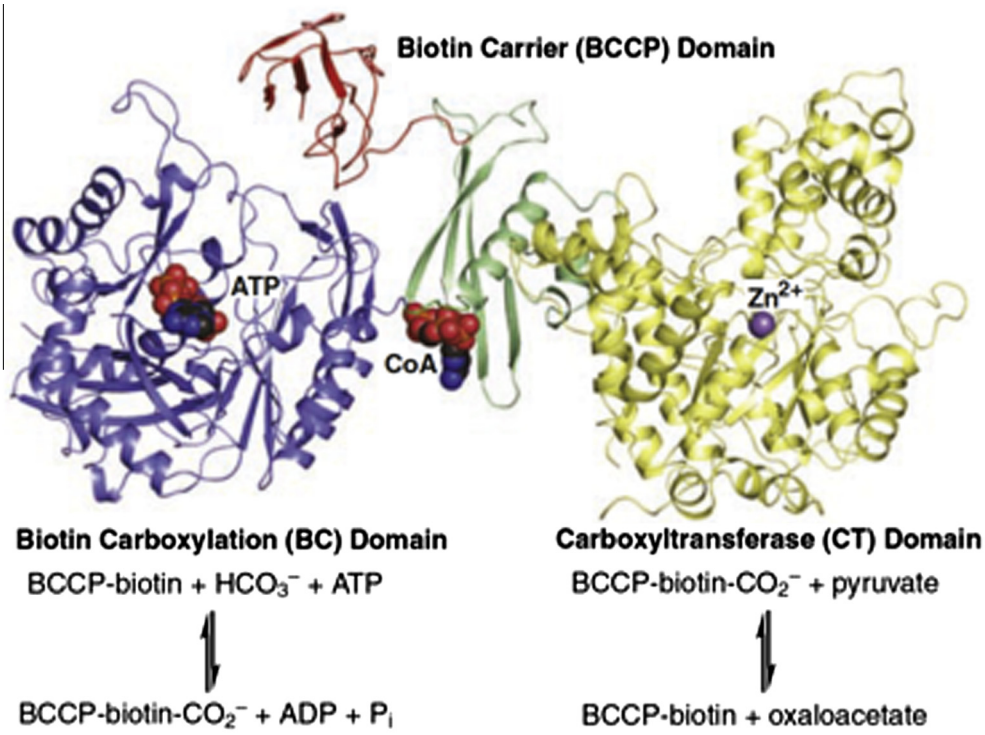

Fig. 1. The domain structure of the RePC subunit and the reactions catalysed by the BC and CT domains. Different colours in the primary structure of the enzyme represent various portions of the polypeptide attributed to the biotin carboxylase (BC), carboxyltransferase (CT), biotin carboxyl carrier protein (BCCP) and allosteric domains [6]. Reproduced with permission from [7].

subunits, on one face of the tetramer, appeared to be correctly configured to carry out the inter-subunit catalysis demonstrated to occur whereby the biotin bound to one subunit is carboxylated in its own BC domain but transfers its carboxyl group to pyruvate in its partner's CT domain [7]. The main locus of action of acetyl CoA is in the BC domain [3]. Fig. 2 shows part of the allosteric domain, with residues that directly interact with acetyl CoA and those that interact with these residues. Arg427 and Arg472 were the target of earlier mutagenesis studies that showed their crucial role in acetyl CoA binding and activation of RePC [5]. The current work extends these studies to examine the roles in the allosteric action of acetyl CoA of Arg469 and Asp471 residues, which interact directly with bound acetyl CoA, and Glu1027 which interacts with Arg472, when acetyl CoA is bound. In addition, the role of Asp1018 was examined, since this residue was shown to interact with Arg427 in the absence of acetyl CoA, but not in its presence [7].

2. Materials and methods

2.1. Construction of mutants

Mutations of Arg469 and Asp471 residues were performed on a 1.4 kb *Sac*II–*Xho*I DNA fragment of *R. etli* PC gene, encompassing the BC domain while those of Asp1018 and Glu1027 residues were performed on a 1.0 kb *Bam*HI–*Not*I fragment of *R. etli* PC gene, encompassing the BCCP domain. Mutagenesis was performed using a site-directed mutagenesis kit (Agilent) as described previously [7,11] (see Table 1 for the mutagenic primers used). The putative mutagenic clones were verified by automated DNA sequencing (Macrogen). Appropriate fragments of the correctly mutagenized clones were excised with *Sac*II–*Xho*I or *Bam*HI–*Not*I and used to replace the equivalent wild-type fragments in the full length RePC gene in pET17b vector [6].

2.2. Preparation of WT and mutant RePC

pET17b plasmid containing wild-type RePC or mutants was co-transformed with pCY216 plasmid encoding *Escherichia coli* biotin protein ligase (BirA) into *E. coli* BL21 (DE3). RePC was expressed and purified as described previously [11].

2.3. Pyruvate carboxylase assay

Pyruvate carboxylating activities in the absence and presence of acetyl-CoA were determined spectrophotometrically using a coupled reaction with malate dehydrogenase to detect oxaloacetate formation, as described previously [11]. Briefly, the assays were performed at 30 °C in 1 ml mixture containing 0.1 M Tris–HCl, pH 7.8, 20 mM $NaHCO_3$, 6 mM $MgCl_2$, 1 mM MgATP, 0.22 mM NADH, 10 mM sodium pyruvate and 5 units of MDH. The concentrations of acetyl-CoA were varied from 0 to 150 μM. The data were analysed by non-linear regression fits to Eq. (1) [5]:

$$^{app}k_{cat} = k_{0cat} + k_{cat}/(1 + (K_a/[\text{acetyl CoA}])^n) \quad (1)$$

where $^{app}k_{cat}$ is the measured k_{cat} at each concentration of acetyl CoA, k_{cat} is the catalytic rate constant at saturating acetyl CoA, K_a is the activation constant for acetyl CoA and n is the Hill coefficient of the activation by acetyl CoA. The catalytic rate constant in the absence of acetyl CoA is k_{0cat} and in the case of the wild-type enzyme the value shown in Table 2 was determined experimentally as a mean and standard deviation of three measurements, since although the value estimated from the fit was similar to the experimental value it had a relatively large error. In the cases of the mutants, the values of k_{0cat} reported are the values estimated from non-linear regression fits of the $^{app}k_{cat}$ vs [acetyl CoA] data to Eq. (1), although the data analysed included an experimental value of k_{0cat}.

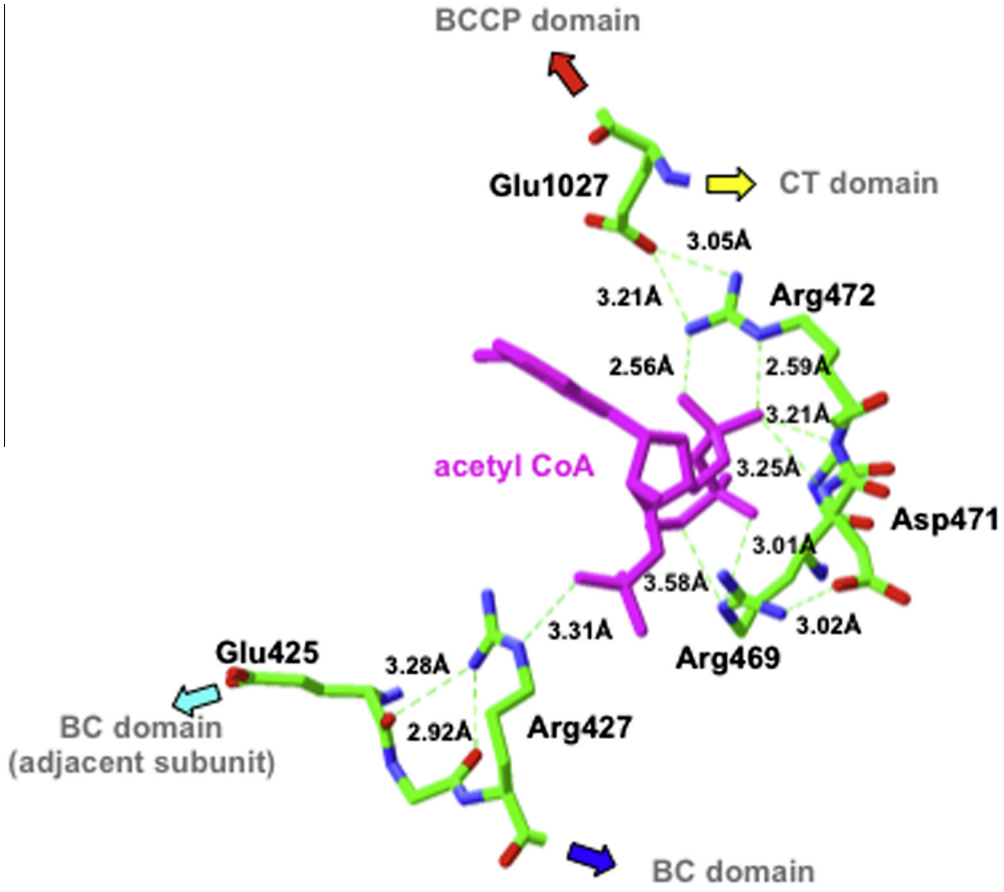

Fig. 2. Residues in the allosteric domain of RePC that directly interact with acetyl CoA and those that interact with these residues. Residues are taken from the structure of RePC determined by Lietzan et al. (2011) (PDB: 3TW6). Dashed lines indicate potential hydrogen bonds and the coloured arrows indicate connexions from the allosteric domain to other parts of the enzyme structure.

Table 1
Mutagenic oligonucleotide primers used to generate RePC mutants.

Mutant construct	Forward primer	Reverse primer
R469S	5′-gca-ggt-caa-gag-cca-gga-ccg-3′	5′-cgg-tcc-tgg-ctc-ttg-acc-tgc-3′
R469K	5′-cag-cag-gtc-aag-aaa-cag-gac-cgc-gcg-3′	5′-cgc-gcg-gtc-ctg-ttt-ctt-gac-ctg-ctg-3′
D471A	5′-aag-cgc-cag-gcg-cgc-gcg-acg-3′	5′-ctg-cgc-gcg-cgc-ctg-gcg-ctt-3′
D1018A	5′-acg-ggt-tgg-cgg-ccg-gcg-agg-agc-t-3′	5′-agc-tcc-tcg-ccg-gcc-gcc-aac-ccg-t-3′
E1027A	5′-tcg-ccg-aca-tcg-cga-agg-gca-aga-c-3′	5′-gtc-ttg-ccc-ttc-gcg-atg-tcg-gcg-a-3′
E1027R	5-tgt-tcg-ccg-aca-tca-gga-agg-gca-aga-cgc	5′-gcg-tct-tgc-cct-tcc-tga-tgt-cgg-cga-aca-3′

Table 2
Effects of mutations on acetyl CoA-activation of pyruvate carboxylation.

Wild-type (WT)/mutant form of RePC	k_{0cat} (−acetyl CoA) (s^{-1})	k_{cat} (+acetyl CoA) (s^{-1})	Hill coefficient	K_a (μM)
WT	0.18 ± 0.01	17.6 ± 0.1	2.7 ± 0.2	7.7 ± 0.6
R469S	1.61 ± 0.15	11.3 ± 0.3	2.3 ± 0.2	25.4 ± 0.8
R469K	0.68 ± 0.16	6.05 ± 0.44	0.9 ± 0.1	39.9 ± 6.0
D471A	0.11 ± 0.01	0.105 ± 0.002	N.D.	N.D.
E1027A	3.94 ± 0.28	14.9 ± 0.4	3.0 ± 0.3	12.9 ± 0.5
E1027R	1.18 ± 0.07	2.71 ± 0.18	2.3 ± 0.4	74.8 ± 6.4
D1018A	2.17 ± 0.25	12.3 ± 0.3	2.1 ± 0.2	10.9 ± 0.5

2.4. Bicarbonate-dependent MgATP cleavage assay

Bicarbonate-dependent MgATP cleavage activities in the presence and absence of acetyl-CoA at saturating MgATP were determined by coupled assay with pyruvate kinase and lactate dehydrogenase as described previously [11]. Briefly, the reactions were performed at 30 °C in 1 ml mixture containing 0.1 M Tris–HCl, pH 7.8, 20 mM $NaHCO_3$, 5 mM $MgCl_2$, 1 mM ATP, 0.22 mM NADH, 10 mM phosphoenolpyruvate, 5 units of pyruvate kinase and 4 units of lactate dehydrogenase. When acetyl CoA was present in the assay, a concentration of 0.25 mM was used.

3. Results

3.1. Arg469 mutations

To examine whether the guanidinium group of the side chain of Arg469 participates binding acetyl-CoA as shown in Fig. 2, this residue was mutated to serine (R469S) such that the interaction would be disrupted. To see if the length of the side chain of Arg469 affects participation in such an interaction, R469K mutant was also generated and characterised. Fig. 3 shows the activation by acetyl CoA of the pyruvate carboxylation reaction in the wild-type enzyme and R469S mutant. As shown in Table 2, the R469S mutant showed a 9-fold increase in the acetyl CoA-independent activity (k_{0cat}) and a 3.3-fold increase in K_a compared to the wild-type enzyme. There was only a small effect on the Hill coefficient and k_{cat} was reduced to about 70% of the value

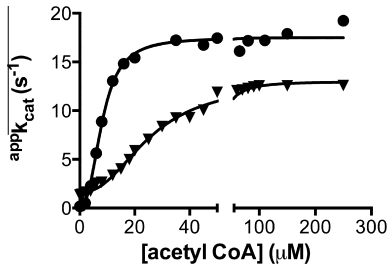

Fig. 3. Activation of pyruvate carboxylation by acetyl CoA in (●) wild-type RePC and (▼) R469S. Lines are non-linear regression fits of the data to Eq. (1).

for the wild-type enzyme. In contrast, the R469K mutation resulted in a 3.8-fold increase in k_{0cat} and a 5.2-fold increase in K_a compared to the wild type enzyme. The value of k_{cat} of R469K was 37% of that in wild-type RePC, but the largest difference between R469S and R469K mutants was that the cooperativity of acetyl CoA activation of R469K was abolished, with the value of the Hill coefficient being close to 1. The net result of the mutations was to reduce the effectiveness of activation of RePC-catalysed pyruvate carboxylation by acetyl CoA ($(k_{cat}/K_a)/k_{0cat}$) to 0.28 (R469S) and 0.22 (R469K) compared to 12.70 in wild-type RePC.

As shown in Table 3, the effect of the R469S mutation on bicarbonate-dependent MgATP cleavage was to increase both k_{0cat} (34-fold) and k_{cat} (7.1-fold) relative to the values for wild-type RePC. Similar, but slightly smaller effects were seen in the R469K mutant, with k_{0cat} being 23-fold greater than the wild-type value and k_{cat} being 5.3-fold greater.

3.2. Asp471 mutation

The mutation of Asp471 to alanine resulted in a relatively small reduction in k_{0cat} of about 40%, but completely abolished the activation of the pyruvate carboxylation reaction by acetyl CoA (see Table 2).

3.3. Glu1027 mutations

As shown in Table 2, E1027A showed a 22-fold increase in k_{0cat} and a 1.7-fold increase in K_a compared to those of the wild-type enzyme. The E1027A mutant showed only a marginal effect on the Hill coefficient, and the k_{cat} was reduced slightly to about 85% of the value for the wild-type enzyme. Thus, the effect of the E1027A substitution was to reduce the effectiveness of activation by acetyl CoA to approximately 0.29 compared to 12.7 in the wild-type RePC. The E1027R mutant showed a lesser increase in k_{0cat} (6.6-fold) but a larger increase in K_a (10-fold) compared to wild-type RePC. There was again little effect on the Hill coefficient, but k_{cat} was reduced to only 16% of the value for the wild-type enzyme. Again, the net result in E1027R was to greatly decrease the effectiveness of activation of the enzyme-catalysed pyruvate carboxylation by acetyl CoA to 0.03.

Table 3
Effects of mutations on bicarbonate-dependent MgATP cleavage in the absence of pyruvate.

WT/mutant form of RePC	k_{0cat} (−acetyl CoA) (s^{-1})	k_{cat} (+acetyl CoA) (s^{-1})
WT	0.058 ± 0.002	0.53 ± 0.01
R469S	1.98 ± 0.15	3.75 ± 0.15
R469K	1.33 ± 0.16	2.82 ± 0.03
E1027A	3.25 ± 0.13	4.10 ± 0.03
E1027R	0.39 ± 0.04	1.49 ± 0.03
D1018A	2.050 ± 0.002	4.38 ± 0.09

As shown in Table 3, the effect of the E1027A mutation on bicarbonate-dependent MgATP cleavage was to dramatically increase both k_{0cat} (56-fold) and k_{cat} (7.7-fold) relative to those values for wild-type RePC. Similar, but considerably smaller effects were seen in the E1027R mutant, with k_{0cat} being 6.7-fold greater than the wild-type value and k_{cat} being 2.8-fold greater.

3.4. Asp1018 mutation

As shown in Table 2 the mutation D1018A resulted in a 12-fold increase in k_{0cat} and a 1.4-fold increase in K_a compared to the wild-type enzyme. The Hill coefficient and k_{cat} were reduced to 78% and 70% respectively of those values for the wild-type enzyme. The effectiveness of activation by acetyl CoA was 0.52.

As shown in Table 3, the effect of the D1018A mutation on bicarbonate-dependent MgATP cleavage was to dramatically increase both k_{0cat} (35-fold) and k_{cat} (8.3-fold) relative to the values for wild-type RePC.

4. Discussion

In summary there are mainly two types of result that are produced by mutation of the residues. Firstly, there are the mutations that affect acetyl CoA action by producing relatively large reductions in k_{cat} and/or increases in K_a in the pyruvate carboxylation reaction relative to wild-type enzyme (R469S/K, D471A, E1027R). These can be explained in terms of disruption of acetyl CoA binding and/or action, either by disruption of a direct interaction between the mutated residue and acetyl CoA or disruption of acetyl CoA interaction with other residues. The other type of result is where the mutations have resulted in increased pyruvate carboxylating activity in the absence of acetyl CoA and increased bicarbonate-dependent MgATP cleavage activity both in the presence and absence of acetyl CoA (R469S/K, E1027A/R, D1018A). As can be seen, some mutations produced both types of result.

To deal with mutations producing the first type of result, as can be seen in Figs. 2 and 4, the side chain guanidinium group of Arg469 and the α-amide of Asp471 interact directly with acetyl CoA. In addition, in the presence of acetyl CoA, both Glu1027 and Asp471 interact with the acetyl CoA-binding residues Arg472 and Arg469 respectively. It is easy to understand how the mutation R469S could result in a reduction of binding of acetyl CoA and hence produce the increase in K_a. However, the more conservative mutation R469K actually produced a greater increase in K_a than R469S, abolished the cooperativity of action acetyl CoA and reduced k_{cat} more than R469S. These effects of mutation of Arg469 do however, mirror the effects of mutation of the other major acetyl CoA-binding residues, Arg427 and Arg472 [5]. Mutation of Arg427 to serine or lysine produced increases in K_a for acetyl CoA of 15- and 76-fold relative to wild-type respectively and the R427K mutant also resulted in a loss of cooperativity of the action of acetyl CoA. Mutation of Arg472 to serine or lysine resulted in increases in K_a of 203- and 252-fold, respectively. Adina-Zada et al. [5] rationalised these observations by suggesting that the mutation of the arginine residues (Arg427 and Arg472) to serine removed any interaction between these residues and acetyl CoA, leaving acetyl CoA to be positioned in the binding pocket by the remaining interacting residues. Mutation of the arginine to lysine however suggested that whilst lysine could interact with acetyl CoA, lysine could not form the interactions with other residues in the allosteric binding site that arginine can, thus resulting in incorrect positioning of acetyl CoA in the binding site. This rationale may also apply to Arg469, which also interacts with Asp471 (see Fig. 4).

To some degree the very pronounced effect of the D471A mutation on acetyl CoA-activation of the RePC may be explained by the

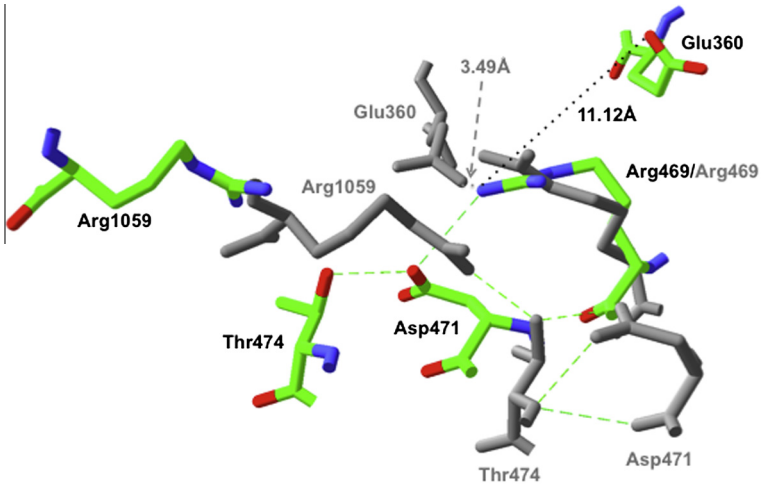

Fig. 4. Relative positions of Glu360, Arg469, Asp471, Thr474 and Arg1059 residues in the RePC subunit with acetyl CoA bound (coloured residues/black labels) and without acetyl CoA bound (grey residues/grey labels) obtained by aligning Arg469 from both subunits in the structure of RePC obtained by Leitzan et al. (PDB: 3TW6) where the positions of all the residues are well defined (which is not the case in 2QF7). Dashed lines indicate potential hydrogen bonds and the distances indicated are between the guanidinium of Arg471 and the carboxyl of Glu360 in the presence and absence of acetyl CoA.

loss of interaction with Arg469. As can be seen in Fig. 4, Asp471 (including its α-amide) is capable of a large degree of displacement in the absence of acetyl CoA to a position where its carboxyl group no longer interacts with Arg469. The abolition of the interaction with Arg469 in D471A, may result in the displacement of D471A and loss of binding of its α-amide with acetyl CoA. The dramatic effects of mutation of Asp471 on acetyl CoA activation of RePC indicate that any reductions in acetyl CoA binding affinity are probably accompanied by loss in the ability of acetyl CoA to activate the enzyme, even at saturating acetyl CoA concentrations. This points to a very important role for Asp471 in the mechanism of activation by acetyl CoA, in addition, the reduction in k_{0cat} resulting from mutation of Asp471 suggests it also plays some role in basal catalysis, however Asp471 has not been reported to play a direct catalytic role in RePC. Thus the roles of Asp471 in catalysis and acetyl CoA-activation of RePC warrant further investigation.

As can be seen in Fig. 2, Glu1027 interacts with Arg472 in the subunit of RePC with acetyl CoA bound. The location of Glu1027 relative to Arg472 in subunits of RePC where acetyl CoA is not bound is unclear due to imprecise positioning (due to disorder) of Glu1027 and/or Arg472 in the structures of these subunits (in PDB files 2QF7, 3TW6 and 3TW7) [6,7]. The imprecise positioning of some residues in one structure but not another explains why Figs. 2 and 4 use PDB file 3TW6 and Fig. 5 uses 2QF7. Again, one result of mutation of Glu1027 to arginine may be due to mis-positioning of Arg472 in the binding of acetyl CoA, owing to charge-repulsion between the positive charge of arginine in the E1027R mutant and this residue (which would not occur with E1027A). This would then produce a reduction in the affinity of acetyl CoA binding and loss of activation of the enzyme as previously argued for lysine mutations of Arg427 and Arg472 [5].

Increased values of k_{0cat} produced by some mutations are not, by definition, caused by effects on acetyl CoA binding and thus, it is likely that these mutations have affected the interactions of these residues with others that occur in the absence of acetyl CoA. The obvious approach would seem to be to examine what interactions these residues make with others in the subunits of RePC without acetyl CoA bound compared to subunits with bound acetyl CoA. As seen in Fig. 4, Arg469 interacts with Glu360 in the absence of bound acetyl CoA and similarly Asp1018 interacts with Arg427 (Fig.5) (differential interactions between Glu1027 and

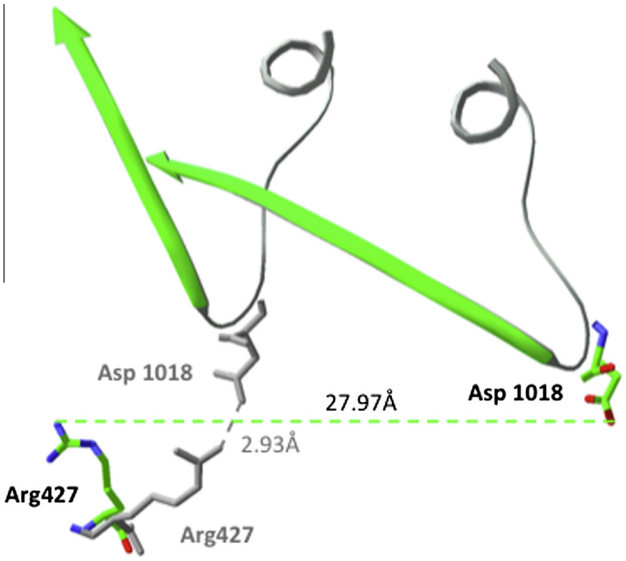

Fig. 5. Positioning of Arg427 and Glu1018 in the RePC subunit with acetyl CoA bound (coloured residues/black labels) and without acetyl CoA bound (grey residues/grey labels. Figure obtained by aligning the ATPγS bound in the subunit containing the acetyl CoA analogue, ethyl CoA, with that in the subunit with no ethyl CoA bound (from PDB file 2QF7; [7]).

Arg472 in RePC subunits with and without acetyl CoA bound cannot be determined because of the imprecise positioning of these residues described above). The implication being that acetyl CoA binding results in the loss of such interactions and releases any constraints that these interactions have on conformational changes required for catalysis in the absence of the activator. However the crystal structure of the RePC tetramer is very asymmetrical, even in the absence of acetyl CoA [6,7], giving rise to the possibility that it is this asymmetry that results in the differential positioning of the residues discussed above, not acetyl CoA binding. Comparison of the positions of these residues in the RePC tetramer structure determined with acetyl CoA bound with those in the structure of RePC tetramer without acetyl CoA bound is not possible because of the low resolution of the latter structure [6,7].

The crystal structures of other pyruvate carboxylase tetramers that have been determined have not exhibited this very marked asymmetry [8–10,16]. The crystal structure of SaPC has been determined in the absence of acetyl CoA (PDB: 3BG5) and also in its presence (PDB: 3H08), where the activator is bound to all four subunits. The residues in SaPC that correspond to Glu360, Arg427, Arg469, Arg472, Asp1018, Glu1027 and Arg1059 in RePC from sequence alignments are Leu353, Arg420, Ser462, Arg465, Asn1012, Asp1021 and Arg1053, respectively. The positions of pairs residues in SaPC subunits that correspond to those that interact in RePC subunits with no acetyl CoA bound were examined. None of the residues within these pairs are close enough to interact with each other in either of the SaPC structures and their positions relative to each other are not markedly different between the two structures. This is suggestive that in RePC it is not primarily acetyl CoA binding that changes the positions of these residues, rather it is the asymmetry of the tetramer. Unlike Arg1059 in RePC, Arg1053 in SaPC interacts directly with acetyl CoA and in the structure without acetyl CoA, it interacts directly with Asp465 that is equivalent to Asp471 in RePC.

So what is the relevance of these interactions between residues that occur in the asymmetrical tetramer of RePC? Although the crystal structure of the SaPC tetramer is more symmetrical than that of RePC, it still exhibits asymmetry [16]. In addition, Tong and co-workers have recently presented cryo-electron microscopy evidence that the SaPC tetramer undergoes transitions between symmetrical and asymmetrical conformations, depending on the stage of the enzyme-catalysed reaction, and that the half-of-the-sites activity alternates between pairs of subunits on opposite faces of the tetramer [17]. Thus, the difference between the crystal structure of the RePC tetramer and those of the SaPC and LmPC tetramers is likely due to enhanced stabilization of the asymmetrical conformer in RePC. Tong and coworkers [17] have speculated that differences in inter-tetramer contacts between SaPC and RePC in the crystal may result in stabilization of the different tetrameric conformers. It is possible that the interactions between residues in the allosteric domain of RePC that do not occur in SaPC may also contribute to this enhanced stabilization of the asymmetrical conformation of the RePC tetramer (Arg469–Glu360; Arg427–Asp1018).

In addition, these interactions between residues that are evident in the asymmetrical conformer may constrain the conversion to the symmetrical conformer. Thus mutation of these residues so as to remove such interactions would relieve these constraints, allowing freer inter-conversion between the two conformers. This inter-conversion may be much more rate-limiting in the absence of acetyl CoA than in its presence and so the effects of the mutations would be much more pronounced on the acetyl CoA-independent activity. It is interesting to note that the acetyl CoA-independent activity of SaPC is very much higher than that of RePC both in terms of the percentage of the activity in the presence of acetyl CoA (about 25%) and in absolute terms, 5 s^{-1} (at room temperature) [10].

The MgATP cleavage reactions were performed in the absence of pyruvate and the decarboxylation of the carboxybiotin, formed in the BC domains, in the CT domains to complete the catalytic cycle becomes rate-limiting [18,19], even in the presence of acetyl CoA. In SaPC this reaction has been shown to be associated with a conversion from the asymmetrical conformer to the symmetrical conformer [17]. Thus the mutation of some of the residues in the current work may again remove interactions that stabilize the asymmetrical conformer and so enhance the rate of conversion to the symmetrical form and hence the overall rate of catalysis. The smaller effects of the mutations on the rate constants of the pyruvate carboxylation reactions compared to those on bicarbonate-dependent MgATP cleavage, even in the presence of acetyl CoA, suggest that binding of pyruvate may enhance the inter-conversion of the asymmetrical conformer to symmetrical conformer, making it less rate-limiting.

If the analysis of the effects of the mutation of residues that enhance enzymic activity is correct, this would suggest that one mode of activation of PC by acetyl CoA is that the binding of acetyl CoA to all four subunits in the PC tetramer, in conjunction with pyruvate, enhances the ease of inter-conversion of the two conformers of the tetramer. What is the purpose of stabilizing the structure in the asymmetrical conformation? This would serve to place the enzyme in the resting state in a conformation ready for biotin carboxylation, but also by increasing the stabilization of this conformer, this would make the enzyme more highly regulated by acetyl CoA, so that there is a tighter coupling between PC activity, fatty acid oxidation and anaplerosis.

Acknowledgements

This work was supported by the National Institutes of Health Grant GM070455 to JCW and PVA and the Thailand Research Fund (BRG5780007) to SJ. KC and CS were supported by DPST and RGJ-PhD (PHD/0308/2551) scholarships respectively, from the Institute for the Promotion of Teaching Science and Technology and Thailand Research Fund, Thailand, respectively.

References

[1] Jitrapakdee, S., St Maurice, M., Rayment, I., Cleland, W.W., Wallace, J.C. and Attwood, P.V. (2008) Structure, mechanism and regulation of pyruvate carboxylase. Biochem. J. 413, 369–387.
[2] Jitrapakdee, S. and Wallace, J.C. (1999) Structure, function and regulation of pyruvate carboxylase. Biochem. J. 340 (Pt 1), 1–16.
[3] Adina-Zada, A., Zeczycki, T.N. and Attwood, P.V. (2012) Regulation of the structure and activity of pyruvate carboxylase by acetyl CoA. Arch. Biochem. Biophys. 519, 118–130.
[4] Adina-Zada, A., Zeczycki, T.N., St Maurice, M., Jitrapakdee, S., Cleland, W.W. and Attwood, P.V. (2012) Allosteric regulation of the biotin-dependent enzyme pyruvate carboxylase by acetyl-CoA. Biochem. Soc. Trans. 40, 567–572.
[5] Adina-Zada, A., Sereeruk, C., Jitrapakdee, S., Zeczycki, T.N., St Maurice, M., Cleland, W.W., Wallace, J.C. and Attwood, P.V. (2012) Roles of Arg427 and Arg472 in the binding and allosteric effects of acetyl CoA in pyruvate carboxylase. Biochemistry 51, 8208–8217.
[6] Lietzan, A.D., Menefee, A.L., Zeczycki, T.N., Kumar, S., Attwood, P.V., Wallace, J.C., Cleland, W.W. and St Maurice, M. (2011) Interaction between the biotin carboxyl carrier domain and the biotin carboxylase domain in pyruvate carboxylase from *Rhizobium etli*. Biochemistry 50, 9708–9723.
[7] St Maurice, M., Reinhardt, L., Surinya, K.H., Attwood, P.V., Wallace, J.C., Cleland, W.W. and Rayment, I. (2007) Domain architecture of pyruvate carboxylase, a biotin-dependent multifunctional enzyme. Science 317, 1076–1079.
[8] Sureka, K., Choi, P.H., Precit, M., Delince, M., Pensinger, D.A., Huynh, T.N., Jurado, A.R., Goo, Y.A., Sadilek, M., Iavarone, A.T., Sauer, J.D., Tong, L. and Woodward, J.J. (2014) The cyclic dinucleotide c-di-AMP is an allosteric regulator of metabolic enzyme function. Cell 158, 1389–1401.
[9] Xiang, S. and Tong, L. (2008) Crystal structures of human and *Staphylococcus aureus* pyruvate carboxylase and molecular insights into the carboxyltransfer reaction. Nat. Struct. Mol. Biol. 15, 295–302.
[10] Yu, L.P., Xiang, S., Lasso, G., Gil, D., Valle, M. and Tong, L. (2009) A symmetrical tetramer for *S. aureus* pyruvate carboxylase in complex with coenzyme A. Structure 17, 823–832.
[11] Adina-Zada, A., Jitrapakdee, S., Wallace, J.C. and Attwood, P.V. (2014) Coordinating role of His216 in MgATP binding and cleavage in pyruvate carboxylase. Biochemistry 53, 1051–1058.
[12] Duangpan, S., Jitrapakdee, S., Adina-Zada, A., Byrne, L., Zeczycki, T.N., St Maurice, M., Cleland, W.W., Wallace, J.C. and Attwood, P.V. (2010) Probing the catalytic roles of Arg548 and Gln552 in the carboxyl transferase domain of the *Rhizobium etli* pyruvate carboxylase by site-directed mutagenesis. Biochemistry 49, 3296–3304.
[13] Zeczycki, T.N., Menefee, A.L., Adina-Zada, A., Jitrapakdee, S., Surinya, K.H., Wallace, J.C., Attwood, P.V., St Maurice, M. and Cleland, W.W. (2011) Novel insights into the biotin carboxylase domain reactions of pyruvate carboxylase from *Rhizobium etli*. Biochemistry 50, 9724–9737.

[14] Zeczycki, T.N., Menefee, A.L., Jitrapakdee, S., Wallace, J.C., Attwood, P.V., St Maurice, M. and Cleland, W.W. (2011) Activation and inhibition of pyruvate carboxylase from *Rhizobium etli*. Biochemistry 50, 9694–9707.
[15] Zeczycki, T.N., St Maurice, M., Jitrapakdee, S., Wallace, J.C., Attwood, P.V. and Cleland, W.W. (2009) Insight into the carboxyl transferase domain mechanism of pyruvate carboxylase from *Rhizobium etli*. Biochemistry 48, 4305–4313.
[16] Lasso, G., Yu, L.P., Gil, D., Xiang, S., Tong, L. and Valle, M. (2010) Cryo-EM analysis reveals new insights into the mechanism of action of pyruvate carboxylase. Structure 18, 1300–1310.
[17] Lasso, G., Yu, L.P., Gil, D., Lazaro, M., Tong, L. and Valle, M. (2014) Functional conformations for pyruvate carboxylase during catalysis explored by cryoelectron microscopy. Structure 22, 911–922.
[18] Attwood, P.V. and Wallace, J.C. (1986) The carboxybiotin complex of chicken liver pyruvate carboxylase. A kinetic analysis of the effects of acetyl-CoA, Mg^{2+} ions and temperature on its stability and on its reaction with 2-oxobutyrate. Biochem. J. 235, 359–364.
[19] Attwood, P.V., Wallace, J.C. and Keech, D.B. (1984) The carboxybiotin complex of pyruvate carboxylase. A kinetic analysis of the effects of Mg^{2+} ions on its stability and on its reaction with pyruvate. Biochem. J. 219, 243–251.

Biochimica et Biophysica Acta 1863 (2017) 537–551

Contents lists available at ScienceDirect

Biochimica et Biophysica Acta

journal homepage: www.elsevier.com/locate/bbadis

Mass spectrometry analysis shows the biosynthetic pathways supported by pyruvate carboxylase in highly invasive breast cancer cells

Phatchariya Phannasil [a], Israr-ul H. Ansari [b], Mahmoud El Azzouny [c], Melissa J. Longacre [b], Khanti Rattanapornsompong [a], Charles F. Burant [c], Michael J. MacDonald [b], Sarawut Jitrapakdee [a,*]

[a] Department of Biochemistry, Faculty of Science, Mahidol University, Bangkok, Thailand
[b] Childrens Diabetes Center, University of Wisconsin School of Medicine and Public Health, Madison, WI, USA
[c] Department of Internal Medicine, University of Michigan, Ann Arbor, MI, USA

ARTICLE INFO

Article history:
Received 26 July 2016
Received in revised form 28 October 2016
Accepted 22 November 2016
Available online 24 November 2016

Keywords:
Gene knockout
Pyruvate carboxylase (PC)
Breast cancer
Cell proliferation rate
Mitochondrial biosynthesis
Cancer biology
Anaplerosis
Mitochondrial metabolism

ABSTRACT

We recently showed that the anaplerotic enzyme pyruvate carboxylase (PC) is up-regulated in human breast cancer tissue and its expression is correlated with the late stages of breast cancer and tumor size [Phannasil et al., PloS One 10, e0129848, 2015]. In the current study we showed that PC enzyme activity is much higher in the highly invasive breast cancer cell line MDA-MB-231 than in less invasive breast cancer cell lines. We generated multiple stable PC knockdown cell lines from the MDA-MB-231 cell line and used mass spectrometry with $^{13}C_6$-glucose and $^{13}C_5$-glutamine to discern the pathways that use PC in support of cell growth. Cells with severe PC knockdown showed a marked reduction in viability and proliferation rates suggesting the perturbation of pathways that are involved in cancer invasiveness. Strong PC suppression lowered glucose incorporation into downstream metabolites of oxaloacetate, the product of the PC reaction, including malate, citrate and aspartate. Levels of pyruvate, lactate, the redox partner of pyruvate, and acetyl-CoA were also lower suggesting the impairment of mitochondrial pyruvate cycles. Serine, glycine and 5-carbon sugar levels and flux of glucose into fatty acids were decreased. ATP, ADP and NAD(H) levels were unchanged indicating that PC suppression did not significantly affect mitochondrial energy production. The data indicate that the major metabolic roles of PC in invasive breast cancer are primarily anaplerosis, pyruvate cycling and mitochondrial biosynthesis of precursors of cellular components required for breast cancer cell growth and replication.

1. Introduction

Breast cancer is one of the most common malignancies in women, with an estimated one million cases diagnosed every year, and remains one of the cancer types that cause an extremely high mortality rate worldwide [1]. Similar to other cancers, regardless of tissue oxygen levels, breast cancer oxidizes glucose excessively via glycolysis known as the Warburg effect. Mitochondrial energy production by oxidative phosphorylation is essentially normal or occasionally slightly repressed in cancer cells [2]. This and other recent indirect evidence suggests that mitochondrial metabolism could be important in other ways, such as for supplying the substrates for biosynthesis of fatty acids, amino acids and nucleic acids as the structural and functional components of the rapidly dividing cells [2,3]. In this regard, "anaplerosis", which is the net mitochondrial biosynthesis of certain citric acid cycle intermediates [4], could be extremely important for cancer cell proliferation and invasiveness. However, there is a paucity of data on the role of individual metabolic pathways that support cancer cell growth and survival, especially in breast cancer. Pyruvate carboxylation and glutaminolysis are the two major anaplerotic reactions that replenish citric acid cycle intermediates when they are depleted by their export from the mitochondria for biosynthetic reactions that take place mostly in the extramitochondrial compartment of the cell. A major anaplerotic reaction involves the carboxylation of pyruvate to oxaloacetate catalyzed by pyruvate carboxylase (PC) followed by oxaloacetate's conversion to malate, citrate and aspartate and their export from mitochondria to the cytosol where they become precursors for the synthesis of carbohydrates, lipids and amino acids [5]. Glutaminolysis involves the conversion of glutamine to glutamate by glutaminase followed by oxidative deamination of glutamate to α-ketoglutarate catalyzed by glutamate dehydrogenase. α-Ketoglutarate is then converted to other citric acid cycle intermediates that can be exported from the mitochondria to the cytosol [6]. Different cancers use these anaplerotic reactions to various degrees [7–9].

We recently showed that PC is up-regulated in human breast cancer tissue and its expression levels correlated with the late stages of breast cancer and tumor size but not with the expression of estrogen receptor

Abbreviations: PC, pyruvate carboxylase; MS, mass spectrometry.

* Corresponding author at: Mahidol University, 272 Rama 6 Rd, Rajathewee, Bangkok 10400, Thailand.
E-mail address: sarawut.jit@mahidol.ac.th (S. Jitrapakdee).

http://dx.doi.org/10.1016/j.bbadis.2016.11.021
0925-4439/

Table 1
Oligonucleotides used to generate shRNA constructs for suppressing human pyruvate carboxylase (PC) expression.

Sequence name	Sequence (5′ 3′)	Length (bp)
PC 179 (forward)	GATCCTCGGAGTATAAGCCCATCAAGAATGTGCTTTTCTTGATGGGCTTATACTCCTTTTTGGAAA	66
PC 179 (reverse)	AGCTTTTCCAAAAAGGAGTATAAGCCCATCAAGAAAAGCACATTCTTGATGGGCTTATACTCCGAG	66
PC 847 (forward)	GATCCTCGGAACATCCTGCACCTGTATGTGCTTTACAGGTGCAGGATGTTCCTTTTTGGAAA	62
PC 847 (reverse)	AGCTTTTCCAAAAAGGAACATCCTGCACCTGTATGTGCTTTACAGGTGCAGGATGTTCCGAG	62
PC 2054 (forward)	GATCCTCCGTGGTCTTCAAGTTCTGTTGTGCTTACAGAACTTGAAGACCACGTTTTTGGAAA	62
PC 2054 (reverse)	AGCTTTTCCAAAAACGTGGTCTTCAAGTTCTGTTGTGCTTACAGAACTTGAAGACCACGGAG	62
PC 2096 (forward)	GATCCTCGGATGTCTTCCGTGTGTTTGATGTGCTTTCAAACACACGGAAGACATCCTTTTTGGAAA	66
PC 2096 (reverse)	AGCTTTTCCAAAAAGGATGTCTTCCGTGTGTTTGATGTGCTTTCAAACACACGGAAGACATCCGAG	66
PC 2653 (forward)	GATCCTCGCAACTCGGACGTGTATGATGTGCTTTCATACACGTCCGAGTTGCTTTTTGGAAA	62
PC 2653 (reverse)	AGCTTTTCCAAAAAGCAACTCGGACGTGTATGAAAGCACATCATACACGTCCGAGTTGCGAG	62
PC 3436 (forward)	GATCCTCGGAAGGTGATAGACATCAAAGTGTGCTTCTTTGATGTCTATCACCTTCCTTTTTGGAAA	66
PC 3436 (reverse)	AGCTTTTCCAAAAAGGAAGGTGATAGACATCAAAGTGTGCTTCTTTGATGTCTATCACCTTCCGAG	66

(ER), progesterone receptor (PR) and epidermal growth factor receptor 2 (HER2) in patients' breast tissues [10]. In supporting these clinical data, we also found that the levels of PC and its mRNA were not correlated with expression of these three receptors in four independent breast cancer cell lines, namely MDA-MB-231 ($ER^-/PR^-/HER2^-$), MDA-MB-435 ($ER^-/PR^-/HER2^+$), MCF-7 ($ER^+/PR^+/HER2^-$) and SKRB3 ($ER^-/PR^-/HER2^+$) [11] but highly correlated with their invasive phenotype i.e., highly expressed in highly metastasized cell lines (MDA-MB-231 > MDA-MB-435) but poorly expressed in low or non-metastasizing cell lines (SKRB3 and MCF-7) [10]. Ectopic expression of PC in MCF-7 cells increases their proliferation, motility and invasion abilities, suggesting a further link between PC and aggressive phenotype of breast cancer. Transient suppression of PC expression in MDA-MB-231 and MDA-MB-435 cell lines reduced their proliferation, migration and invasion *in vitro* indicating the essential role of PC in supporting breast cancer growth and invasiveness [10].

It remains unclear which biochemical pathways and metabolites are altered by PC knockdown and contribute to the slow proliferation and decreased motility phenotypes in breast cancer. In the current study we generated multiple stable PC knockdown cell lines from the MDA-MB-231 breast cancer cell line, a highly invasive cell line with a high PC enzyme activity. The cell lines with severe PC knockdown showed marked decreases in cell viability and proliferation rates. PC knockdown caused decreases in malate, citrate and pyruvate levels and glucose incorporation into these metabolites suggesting the inhibition of mitochondrial pyruvate cycling, decreases in aspartate and other amino acids, some nucleotides and their derivatives needed for cell structure, as well as decreased incorporation of glucose carbon into palmitate. ATP, ADP and pyridine nucleotide levels were not significantly affected demonstrating that PC knockdown does not inhibit mitochondrial energy production. The results demonstrate the important role of PC in anaplerosis and pyruvate cycling via mitochondrial biosynthesis for growth and survival of the MDA-MB-231 cells.

2. Materials and methods

2.1. Materials

Human breast cancer cell lines, MCF-7 and MDA-MB-231 were generous gifts from Dr. Wei Xu, University of Wisconsin-Madison. Cells were grown in Dulbecco's modified Eagle's medium (DMEM) (Corning) supplemented with 10% (v/v) fetal bovine serum (FBS), 100 units/ml penicillin and 100 μg/ml streptomycin, and maintained at 37 °C with 5% CO_2.

2.2. Designation of Pcx shRNA constructs and generation of Pcx-knockdown MDA-MB-231 cell lines

Six different shRNAs targeted to human pyruvate carboxylase (hPcx) coding sequence (ACCESSION BC011617.2) were designed using "siRNA Wizard v 3.1" (http://www.invivogen.com/sirnawizard/design.php). The oligonucleotides corresponding to the shRNA sequences with *Bam*HI or *Hind*III restriction sites overhang at their 5′-ends were synthesized by Eurofins (Fisher Scientific, USA), and their sequences are shown in Table 1. Double stranded oligonucleotide cassettes with *Bam*HI and *Hind*III sites at 5′- and 3′-ends were generated upon annealing each pair of oligonucleotides, and subsequently ligated at the *Bam*HI and *Hind*III sites of the modified pSilencer 2.1-U6 puro TOL2 vector (Ambion, USA) [16]. The constructs carrying six different Pcx shRNA cassettes in the pSilencer 2.1-U6 puromycin vector were sequenced to confirm the correct oligo nucleotide sequence. Similarly, a scrambled shRNA control from Ambion (Life Technologies) (5′-ACTACCGTTGTTATAGGTG-3′) was cloned into the same vector to serve as a control.

2.3. Generation of MDA-MB-231 PC knockdown cell lines

Approximately 1×10^6 MDA-MB-231 cells were plated in a 35-mm culture dish (6-well plate) containing DMEM supplemented with 100 units/ml penicillin and 100 μg/ml streptomycin, and grown at 37 °C with 5% CO_2 overnight. The cells were then transfected with 2.0 μg of shRNA expression constructs along with 1.0 μg of pCMV-Tol2 vector using Lipofectamine2000 (Life Technologies, USA). After 24 h, the cells were selected in the complete medium containing 0.5 μg/ml puromycin (Invitrogen, USA) that was maintained throughout the selection. The MDA-MB-231 cell line stably transfected with a scrambled shRNA construct was similarly generated. Multiple puromycin resistant colonies were formed after 15 days of selection. Thus each "cell line" is actually a population of PC knockdown cells rather than a single clone. The selected cells were expanded and maintained in selection media at all times before subsequent biochemical analyses.

2.4. Quantitative real time reverse transcriptase polymerase chain reaction (QRT-PCR)

Total RNA was extracted from cells using RNeasy mini kit (Qiagen) following the manufacturer's instructions. The 10 μl RT reaction contained 2 μg of total RNA and oligo(dT) primers (Ambion) at 85 °C for 3 min and chilled at 4 °C. Reverse transcription was initiated by adding 10 μl of mixture containing 2 μl 10x RT buffer, 0.5 mM dNTP mix, 2 units of RNase inhibitor and reverse transcriptase (Ambion), to the primed-RNA mixture and the reaction was incubated at 43 °C for 60 min, 92 °C for 10 min and held at 4 °C, respectively. The cDNA was stored at −20 °C until used. Quantitative real time PCR was performed using SYBR Premium Ex Taq (Takara) using MyiQ™ single-color real time PCR detection system (BioRad). The standard curve of PC cDNA was obtained from amplification plots of PC prepared from various dilutions of MDA-MB-231 cDNAs. The expression of PC mRNA was normalized to the glutamate dehydrogenase (GLUD) mRNA level and is shown as the relative gene expression. Fold change was calculated using the ΔQ method. The thermal profiles consisted of initial denaturation at

95 °C for 3 min followed by 40 cycles of denaturation at 95 °C for 10 s and annealing at 60 °C for 20 s and extension at 72 °C for 30 s.

2.5. Cell viability assay

The numbers of viable cells were determined with the CellTiter 96® AQueous One Solution Cell Proliferation Assay (MTS) kit (Promega). Four thousand cells of various stable PC knockdown MDA-MB-231 cell lines were plated into 96 well plates and grown in DMEM supplement with 10% (v/v) FBS, 100 units/ml penicillin and 100 μg/ml streptomycin, at 37 °C in a CO_2 incubator overnight. Twenty microliters of CellTiter one solution reagent was added to the cells and incubated at 37 °C in CO_2 incubator for 1 h. The amount of soluble formazan was measured immediately using a 96-well plate reader (Molecular Devices) at 490 nm. The absorbance is directly proportional to the number of viable cells in culture.

2.6. Cell proliferation

2×10^4 cells of the PC-knockdown MDA-MB-231 or the scrambled shRNA control cell line were plated into 35 mm^2 dishes and cultured in complete DMEM supplemented with 1.0 μg/ml puromycin at 37 °C with 5% CO_2. Cells were trypsinized and counted by staining with 0.4% (w/v) trypan blue (Gibco) at days 4, 5, 6 and 7.

2.7. PC enzyme activity

The cells were trypsinized off tissue culture plates with 0.05% trypsin and 0.5 mM EDTA. The cell pellet was washed twice with PBS and suspended in KMSH solution containing a protease inhibitor mixture (Pierce). PC enzyme activity was measured as previously described [12]. Ten microliters of the homogenate was incubated in a final volume of 50 μl of enzyme reaction mixture of 100 mM KCl, 10 mM $MgCl_2$, 2 mM Na-ATP, 0.1% Triton X-100, 1 mM DTT, 1.6 mM acetyl CoA, 20 mM $NaHCO_3$, 0.2 μCi [^{14}C]$NaHCO_3$, and 100 mM Tris-Cl buffer, pH 7.85 with or without 8 mM pyruvate at 37 °C for 30 min. The reaction was stopped by adding 50 μl 10% (v/v) trichloroacetic acid and after 10 min, 80 μl of the mixture was removed and added to a 20 ml scintillation vial that was left open for 2 h to allow evaporation of the unincorporated CO_2. Then, 0.5 ml of water and 5 ml of Scintisafe scintillation mixture (catalog number SX21-5, Fisher Scientific) were added to the vial and the carbon fixed was measured by liquid scintillation spectrometry. Background radioactivity present in the absence of pyruvate was subtracted from the radioactivity in the presence of pyruvate to give the enzyme rate attributable to PC enzyme activity.

2.8. Measurement of pyruvate, malate and citrate from PC knockdown cells by alkali enhanced fluorescence

The cells were maintained in DMEM cell culture medium (contains 25 mM glucose and 4 mM glutamine) 10% (v/v) FBS 100 units/ml penicillin and 100 μg/ml streptomycin with 0.5 μg/ml puromycin on 150 mm. culture plates. The media was changed to RPMI 1640 cell culture medium (contains 2 mM glutamine) modified to contain 5 mM glucose the day before the experiment. On the day of the experiment the cells were washed twice with PBS and once with Krebs Ringer solution. Five milliliters of Krebs Ringer bicarbonate solution, pH 7.3, containing no glucose was added to the plates of cells, and the cells were incubated at 37 °C. After 10 min Krebs Ringer bicarbonate solution containing 10 mM glucose was added and the cells were incubated at 37 °C. After 35 min all liquid was quickly removed from the cells and the plates were put on ice. Then 0.75 ml of 6% PCA was added and the cells were scraped off the plates and transferred into the microtube. The mixture was homogenized and centrifuged to precipitate the protein and the supernatant fraction was neutralized with 30% KOH. The resulting precipitated potassium perchlorate was removed by centrifugation and the metabolite concentrations in the neutralized extract were measured by alkali enhanced fluorescence, as previously described [12].

2.9. Metabolites analysis by LC-MS and GC-MS

The cells were maintained in DMEM supplemented with 10% (v/v) FBS, 100 units/ml penicillin, 100 μg/ml streptomycin, and 0.5 μg/ml puromycin. Cells were plated at a density of 14×10^3 cells/cm^2 in 6 cm culture dishes at 37 °C and 5% CO_2 in a humidified atmosphere to 70% confluence over 5 days prior to experimentation. On the day of an experiment metabolism was stopped in four plates of each cell line and cells were harvested and saved for LC-MS analysis (time zero control). The medium was changed to DMEM without FBS modified to contain 10 mM $^{13}C_6$-glucose plus 2 mM glutamine or 2 mM $^{13}C_5$-glutamine plus 10 mM glucose. Four plates of each cell line were used for each condition. After incubation for 1 h, metabolism of cells was stopped and cells were harvested and analyzed with LC-MS as previously described [13,14].

2.10. Enzyme activities

Homogenates were prepared and activities of all enzymes except citrate synthase were measured as previously described [15]. The activity of citrate synthase was measured as described in reference [16].

2.11. Statistical analysis

Values of relative PC mRNA, PC enzyme activity, MTS cell proliferation and metabolite levels were expressed as mean ± standard error. The statistical analysis was confirmed with Student's t-test.

3. Results

3.1. Characterization of the PC knockdown MDA-MB-231 cell lines

The PC enzyme activity of the MDA-MB-231 cell line, which is a highly invasive breast cancer cell line, was 10-fold higher than the PC enzyme activity of the less invasive breast cancer cell line MCF-7 (Table 2). Six shRNA constructs (PC179, PC847, PC2054, PC2096, PC2653 and PC3436) targeted to human PC mRNA were transfected to MDA-MB-231 cells. The stable cell lines were named according to the first nucleotide of the PC mRNA sequence targeted. Fig. 1A and B show that the degree of knockdown of PC mRNA correlated fairly well with the degree of knockdown of PC enzyme activity and PC protein in the various PC targeted cell lines. As we have previously observed, knockdown of PC enzyme activity and PC protein, although correlated well with the degree of mRNA knockdown was in general slightly less than the knockdown of PC mRNA [12]. Cell line PC 2096 4B possessed a PC mRNA level of approximately 10% compared to the scrambled shRNA control cell line, while cell lines PC 179 1A, PC 847 2C, PC 2054 3D, PC 3436 6A and PC 3436 6C contained PC mRNA levels of 20–40% that of the scrambled shRNA control cell line. Only modest reductions (50–70%) of PC mRNA level were observed in cell lines PC 179 1B, PC 2054 3A and PC 2096 4C, while the level of PC mRNA was not decreased in cell lines PC 2653 5A and PC 2653 5B. PC enzyme activity of these cell lines was proportional to the levels of PC mRNA, with PC enzyme activity being lowest (5%) in the PC 2096 4B cell line (Fig. 1B). Cell lines PC

Table 2
Pyruvate carboxylase (PC) enzyme activity is much higher in the invasive breast cancer cell line MDA-MB-231 than in the less invasive breast cancer cell line MCF-7. Results are means ± SE nmol CO_2 fixed/min/mg cell protein of 4 replicate measurements.

Cell line	PC enzyme activity (nmol CO_2 fixed/min)
MDA-MB-231	13.2 ± 0.6
MCF-7	1.2 ± 0.2

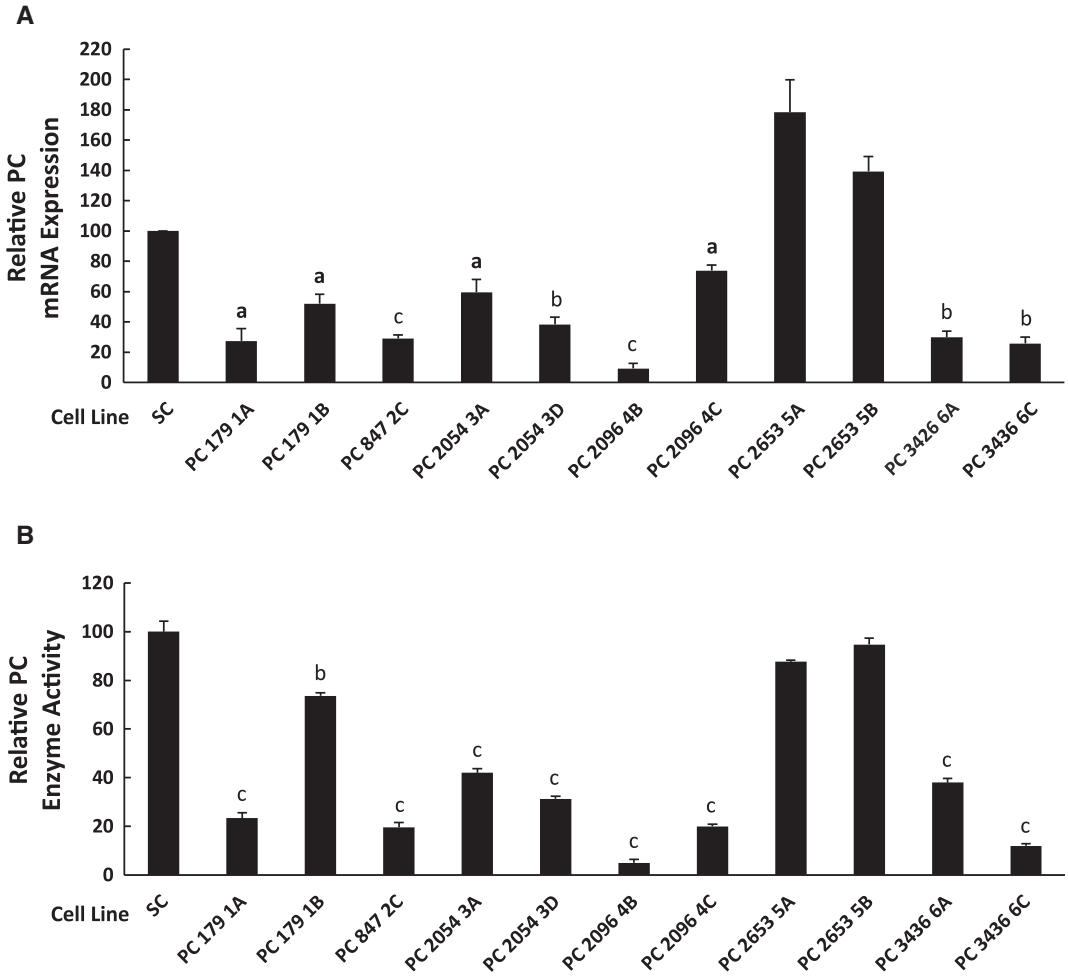

Fig. 1. Decreased pyruvate carboxylase mRNA levels induced by gene silencing correlate with decreased PC enzyme activity in multiple cell lines derived from the breast cancer cell line MDA-MB 231. *A*, Relative pyruvate carboxylase (PC) mRNA expression in various PC knockdown cell lines (179 1A, 179 1B, 847 2C, 2054 3A, 2054 3D, 2096 4B, 2096 4C, 2653 5A, 2653 5B, 3426 6A, 3436 6C and scramble control (SC)). *B*, PC enzyme activity of PC knockdown cell lines relative to that of the scramble control which was arbitrarily set as 100%. $^{a}p < 0.05$; $^{b}p < 0.01$; $^{c}p < 0.001$ vs scramble control.

2096 4B, PC 179 1A, PC 847 2C, PC 2054 3D, PC 3436 6C and PC 2653 5B showed the highest, modest and lowest PC knockdown levels, respectively.

3.2. Decreased cell proliferation rates in PC knockdown cell lines

Cell lines with lower PC mRNA and enzyme activity showed lower cell viability (Fig. 2A and B). We selected two cell lines, PC 847 2C and PC 2096 4B, for further analysis of cell growth. Both knockdown cell lines showed decreased cell numbers at day 4, that became more obvious at days 5–7, with the PC 847 2C cell line showing a 35% lower cell count vs. the scrambled shRNA control cell line at day 7 and the PC 2096 B cell line showing a 65% lower cell count vs. the control cell line at day 7 (Fig. 2C).

3.3. Metabolite analysis

Because most cancers use glucose and glutamine as the two main carbon sources for both energy production and biosynthesis [3], we used uniformly labeled $^{13}C_6$-glucose or $^{13}C_5$-glutamine and LC-MS or GC-MS to track the fluxes of these two substrates into the synthesis of various metabolites. This allowed us to distinguish which of the fluxes of the carbon sources might be more impaired in the PC knockdown cell lines PC 847 2C and PC 2096 4B compared to the shRNA scramble control MDA-MB-231 cell line. Prior to the experiment these three cell lines were maintained in DMEM cell culture medium for four or more days. DMEM is the standard cell culture medium used for maintaining the MDA-MB-231 cell line and it contains 25 mM glucose and 4 mM glutamine. For the LC-MS/MS analysis experiment, the cell lines were maintained for 1 h in DMEM medium modified to contain either 10 mM U-$^{13}C_6$ glucose plus 2 mM unlabeled glutamine or 2 mM U-$^{13}C_5$ glutamine plus 10 mM unlabeled glucose. For the experiment to look for a crossover point in the levels of the metabolites around the PC reaction, the cells were incubated in the presence of 5 mM glucose in RPMI 1640 cell culture medium because the high concentration of glucose in the DMEM medium would produce high levels of metabolites possibly obscuring a crossover point in the levels of the metabolites.

3.4. No decrease in glycolytic intermediates with PC knockdown

As expected, because PC is a mitochondrial enzyme its suppression did not affect the levels of glycolytic intermediates as glucose-6-phosphate, fructose-6-phosphate and fructose bisphosphate were not

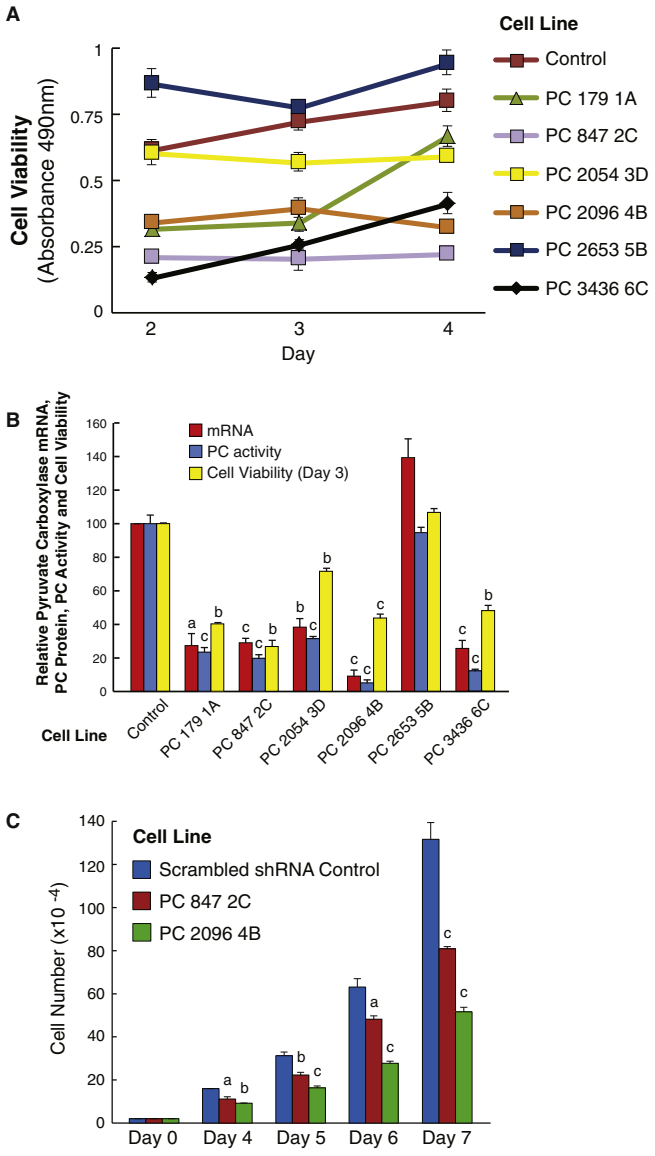

Fig. 2. Knockdown of pyruvate carboxylase (PC) mRNA and PC enzyme activity correlate with decreased breast cancer cell viability and growth. *A*, Viability of cells was measured with the MTS assay at days 2, 3 and 4. $p > 0.001$ vs the RNA scramble control of the four cell lines with the lowest viability. $p < 0.05$ for PC 2054 3D vs the control. *B*, PC mRNA, PC enzyme activity and viability of various knockdown cells at day 3. $^{a}p < 0.05$; $^{b}p < 0.01$, $^{c}p > 0.001$ vs RNA scramble control. C. Decreased cell counts in the PC 2096 4B and PC 847 2C cell lines with knockdown of PC. $^{a}p < 0.05$; $^{b}p < 0.01$, $^{c}p > 0.001$ vs RNA scramble control.

altered in each of these PC knockdown cell lines (Fig. 3A and B). Also as expected, glucose-6-phosphate and fructose-6-phosphate were labeled from U-$^{13}C_6$ glucose but not from U-$^{13}C_5$ glutamine (Fig. 3C and D).

3.5. Suppression of PC lowers malate and citrate

The immediate product of the PC reaction is oxaloacetate which is then directly converted to malate and citrate (Fig. 4). Oxaloacetate is very unstable and its concentration in most tissues is so low (about 5 μM) that it is impractical to accurately measure its concentration. Therefore, the levels of ^{13}C incorporation into the immediate metabolites of oxaloacetate, which are citrate and malate, were measured. In the mass spectrometry experiments using either LC-MS/MS or GCMS, metabolite levels were measured in the cell lines immediately before (zero time control) and then 60 min after 10 mM [U-^{13}C]glucose or 2 mM [U-^{13}C]glutamine were added to the cells. Strong suppression of PC expression (cell line PC 2096 4B) markedly decreased the levels of both citrate and malate and decreased the incorporation of carbon from glucose and glutamine into citrate and malate (Fig. 5). Citrate was mainly +2 labeled with $^{13}C_6$-glucose, suggesting that pyruvate dehydrogenase supplied acetyl-CoA that was incorporated into citrate in the citrate synthase reaction. In contrast, malate was about equally +2 labeled and +3 labeled from $^{13}C_6$-glucose. This indicates that the +3 labeled malate came from oxaloacetate formed in the PC reaction and the +2 labeled malate came from the citric acid cycle after the pyruvate dehydrogenase reaction produced +2 labeled acetyl-CoA that was incorporated into citrate that then became +2 labeled malate after flux through the citrate-pyruvate cycle or through the citric acid cycle. $^{13}C_5$ labeled glutamine produced mostly +4 labeled citrate and malate that entered mitochondrial metabolism through α-ketoglutarate derived from glutamate in the glutamate dehydrogenase reaction. The decreased ^{13}C incorporation into malate and citrate from glucose and glutamine in the PC 2096 4B cell line can be explained by PC knockdown inhibiting pyruvate flux through the citrate-pyruvate and the malate-pyruvate cycles.

To confirm the mass spectrometry measurements the levels of malate and citrate were measured by alkali-enhanced fluorescence in cell lines maintained in RPMI 1640 tissue culture medium (usually contains 11.1 mM glucose and 2 mM glutamine) modified to contain a physiologically normal concentration of glucose (5 mM) (and still 2 mM glutamine) for one day followed by a brief starvation period in the presence of no fuel and then a 35 min incubation period in Krebs Ringer bicarbonate buffer solution containing 10 mM glucose. Similarly to the mass spectrometry measurements of malate and citrate in the cell lines maintained in DMEM cell culture medium the cell lines with knocked down PC maintained in the modified RPMI 1640 medium followed by the Krebs Ringer solution, the PC knockdown cell lines PC 847 2C, PC 2096 4B and PC 179 1A, showed decreased levels of malate and citrate compared to the control cell line containing a scrambled shRNA (Fig. 6).

3.6. Effects of suppression of PC on levels of pyruvate, lactate and acetyl-CoA

The mass spectrometry measurements showed that pyruvate was mostly labeled from glucose rather than from glutamine (Fig. 7A). Suppression of PC caused a marked reduction in the level of glucose-derived pyruvate in the mass spectrometry experiments in which the cells were cultured in DMEM for four or more days prior to the experiment (see Fig. 7A). Since pyruvate is the substrate for the PC reaction, it might be expected that suppression of PC expression would result in the accumulation of pyruvate, which is the substrate of PC, as we previously observed in pancreatic beta cells with knocked down PC [12]. The lower levels of pyruvate seen in the PC knockdown cell lines were likely due to decreased malate and citrate cycling to pyruvate because the levels of these two metabolites were markedly decreased by PC knockdown (Fig. 5). As shown in Fig. 4, malate can exit mitochondria and be converted back to pyruvate by malic enzyme in the cytosol. Pyruvate can then re-enter mitochondria and be reconverted to oxaloacetate by PC (the pyruvate-malate shuttle) [17,18]. Alternatively in the pyruvate-citrate shuttle, citrate can exit mitochondria and be converted to oxaloacetate and acetyl-CoA by ATP-citrate lyase [18,19]. Oxaloacetate can then be converted to malate by cytosolic malate dehydrogenase. Malic enzyme can then convert malate to pyruvate the same as in the pyruvate-malate cycle. The malate-pyruvate and citrate-pyruvate cycles are very active in pancreatic beta cells where PC protein and enzyme activity are high and support these cycles [17,18]. The low pyruvate also explains the low level of lactate (Fig. 7B), which is the redox partner of pyruvate, in these cells. Because glycolysis was not inhibited (Fig. 3), the decreased $^{13}C_6$-glucose incorporation into pyruvate and lactate in the two PC knockdown cell lines (Fig. 7A and B) can only be explained by a decreased activity of pyruvate cycling due to decreased PC enzyme activity.

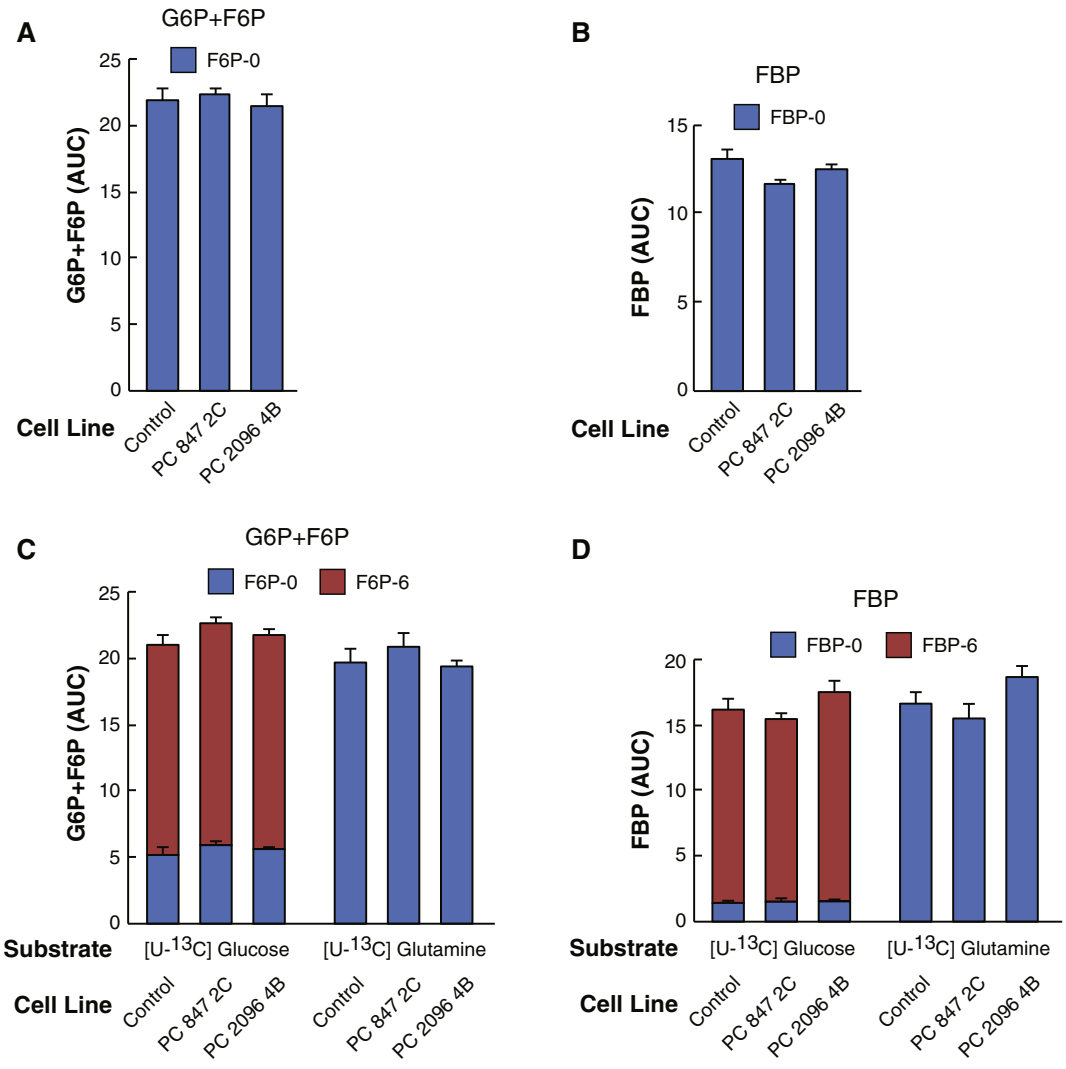

Fig. 3. Knockdown of pyruvate carboxylase (PC) expression does not alter the levels of glycolytic intermediates glucose-6-phosphate plus fructose-6-phosphate or fructose-biphosphate from U-$^{13}C_6$-glucose or U-$^{13}C_5$-glutamine in MDA-MB-231-derived cell lines. PC 847 2C and PC 2096 4B or a scramble shRNA control cell line were maintained in DMEM cell culture medium (contains 25 mM glucose and 4 mM glutamine) and 10% FBS for four or more days. Cells were then maintained in DMEM medium containing either 10 mM [U-$^{13}C_6$] glucose or 2 mM [U-$^{13}C_5$]glutamine for 1 h before metabolism was stopped and cells were analyzed by LC-MS/MS as described under Experimental Procedures. *A*, The levels of glucose-6-phosphate (G6P) plus fructose-6-phosphate (F6P) before the uniformly labeled glucose or glutamine was added (zero time point). *B*, The level of fructose-1,6-bisphosphate (FBP) before the uniformly labeled glucose or glutamine was added (zero time point). *C* and *D*, Upon adding the labeled glucose or glutamine to the culture media, the metabolites were extracted and analyzed by LC-MS/MS spectroscopy. Fractions of different isotopomers of U-^{13}C glucose-6-phosphate plus U-^{13}C fructose-6-phosphate or fructose-biphosphate are shown within the bars. AUC indicates "area under the curve".

The concentration of glucose in the cell culture medium can have a strong influence on the concentration of pyruvate in the cells. As mentioned above, for LC-MS or GC-MS analysis the cells were maintained for four or more days in DMEM cell culture medium right up to the time of the experiment when the cells were maintained in DMEM medium modified to contain 10 mM glucose and 2 mM glutamine for 60 min. DMEM contains a high concentration of glucose (25 mM glucose) and glutamine (4 mM) which are much higher concentrations of these fuels than in the RPMI 1640 cell culture medium that was modified to contain 5 mM glucose (and contains 2 mM glutamine) that the cells were maintained in for 24 h before the cells were incubated in Krebs Ringer bicarbonate solution for the experiments in which malate, citrate and pyruvate were measured by alkali enhanced fluorescence. Because the concentration of glucose was so high in the DMEM medium, it was expected that this could cause a higher level of pyruvate in both the control and PC knockdown cell lines making it difficult to see a crossover point with an expected even higher level of pyruvate in the PC knockdown cell lines. Therefore the incubation conditions of the experiment shown in Fig. 6 were made identical to those of a previous experiment with pancreatic beta cells in which the cell lines were incubated in the presence of the physiological concentration of glucose and glucose-starved for a short time period enabling us to observe an increase in pyruvate after glucose (10 mM) was added to the cells for 30 min [12]. Similarly to experiments in which pure beta cells with knocked down PC were maintained at a physiological concentration of glucose prior to a 35 min incubation with 10 mM glucose, an increase in pyruvate was observed along with the decreases in malate and citrate in all three PC knockdown cell lines shown in Fig. 6. This crossover point with high pyruvate and low malate and low citrate [12] is consistent with a block at the PC reaction [17,18]. The levels of malate and citrate were much lower in cell line PC 179 1A than in the other two PC knockdown cell lines shown in Fig. 6, and the level of pyruvate was increased less than in the other two cell lines in this cell line (only 24% higher than in the control cell line, as compared to 350% higher in the other two PC

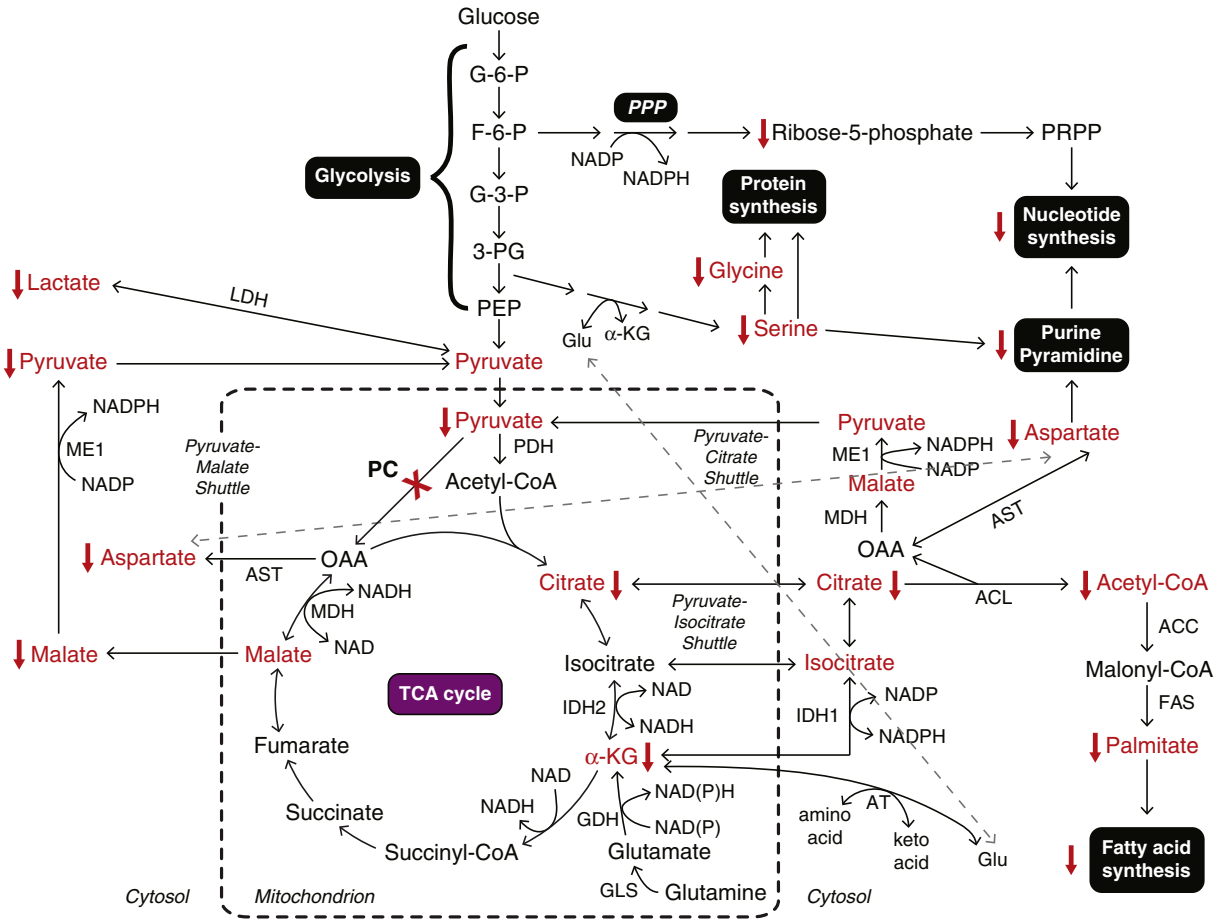

Fig. 4. Schematic summary of metabolic pathways disturbance caused by suppression of pyruvate carboxylase in MDA-MB-231-derived cell lines. The abbreviations used are: ACC, acetyl-CoA carboxylase; α-KG, α-ketoglutarate; AT, aminotransferase; ACL, ATP-citrate lyase; AST, aspartate aminotransferase; F-6-P, fructose-6-phosphate; FAS, fatty acid synthase; G-3-P, glyceraldehyde-3-phosphate; G-6-P, glucose-6-phosphate; GDH, glutamate dehydrogenase; GLS, glutaminase; Glu, glutamate; IDH1, isocitrate dehydrogenase 1; IDH2, isocitrate dehydrogenase 2; LDH, lactate dehydrogenase; MDH, malate dehydrogenase; ME, cytosolic malic enzyme; 3-PG, 3-bisphosphoglycerate; PC, pyruvate carboxylase; PDH, pyruvate dehydrogenase; PEP, phosphoenolpyruvate; PPP, pentose phosphate pathway; PRPP, phosphoribosylpyrophosphate. Metabolites that are altered in the knockdown cell lines are shown in red.

knockdown cell lines (Fig. 6)). Cell line PC 179 1A also showed a 50% lower level of malic enzyme (as later shown in Fig. 12) that, in addition to the extremely low levels of the substrates malate and citrate could contribute to decreased pyruvate cycling.

The decreased levels of acetyl-CoA (Fig. 7C) and the decreased labeling of acetyl-CoA from glucose (Fig. 7D) in the PC 2096 4B cell line are also likely due to the decreased citrate levels. Most of the +2 labeled acetyl-CoA would be expected to come from the pyruvate dehydrogenase reaction. However, there was slightly decreased +2 labeling of acetyl-CoA from glucose and from glutamine in the PC 2096 4B cell line (Fig. 7D) and this can only be explained by the decreased PC enzyme activity inhibiting flux of citrate through the citrate-pyruvate cycle. The lower concentrations of total cellular acetyl-CoA (Fig. 7C) and lower ^{13}C incorporation into acetyl-CoA (Fig. 7D) in the PC knockdown cells are consistent with a lower cytosolic level of acetyl-CoA resulting from decreased formation of mitochondrial citrate and its export to the cytosol via the pathway that uses ATP citrate lyase shown in Fig. 4.

3.7. Suppression of PC lowers aspartate, glycine and serine

Aspartate was labeled from both glucose and glutamine, albeit slightly more from glutamine, indicating that both nutrients contribute to aspartate synthesis (Fig. 8). Aspartate is produced directly from oxaloacetate catalyzed by aspartate aminotransferase. Suppression of PC expression should lower oxaloacetate, resulting in a lowered level of aspartate. As expected, the decrease of +2 and +3 aspartate from glucose and +4 labeled aspartate from glutamine in the PC 2096 4B cell line are consistent with a depleted oxaloacetate level caused by PC suppression in the case of labeling from glucose and decreased activity of the citrate-pyruvate cycle in the case of labeling from glutamine (Fig. 8). Both PC 847 2C and PC 2096 4B knockdown cell lines showed decreased levels of serine and glycine (Fig. 8). The negligible or absent incorporation of ^{13}C from glucose and glutamine into both amino acids is due to the short incubation time of the cells in the presence of the labeled glucose or glutamine and indicates that the levels of these two amino acids was low before two cells were incubated in the presence of the labeled fuels.

3.8. Decreased ^{13}C-glucose incorporation into palmitate in PC knockdown cell lines

Fatty acids act as a sink for carbon flowing from mitochondrial citrate and then through cytosolic acetyl-CoA and malonyl-CoA (Fig. 4). Thus, the ^{13}C incorporation from glucose into palmitate is an indication of the rate of flux of glucose through biosynthetic pathways. Cell lines were incubated in the presence of the ^{13}C-labeled glucose for 18 h. Fig. 9 shows that suppression of PC decreased the incorporation of

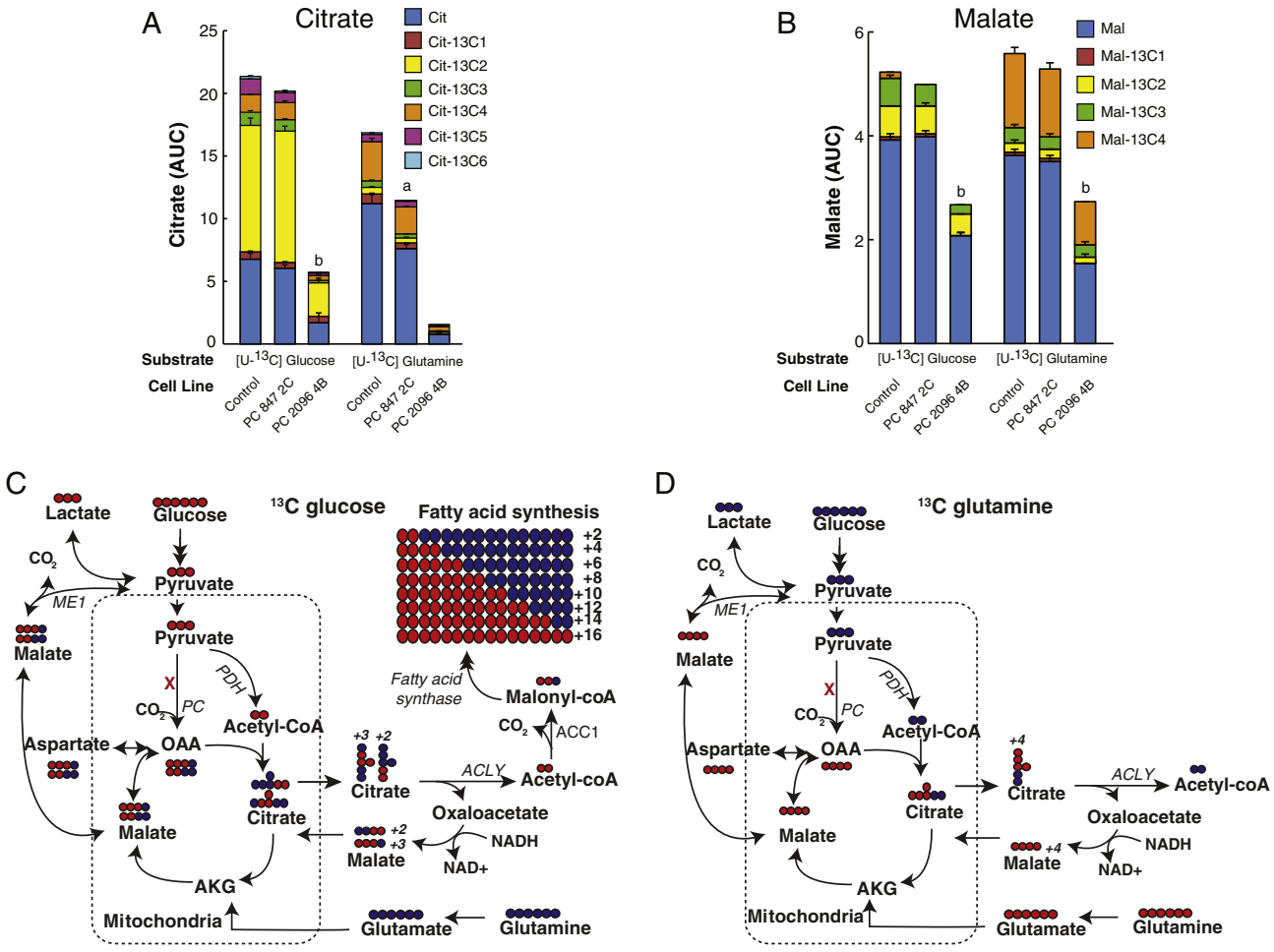

Fig. 5. Decreased labeled citrate and malate from U-$^{13}C_6$-glucose or U-$^{13}C_5$-glutamine in pyruvate carboxylase (PC) knockdown cell lines derived from the MDA-MB-231 breast cancer cell line. PC 847 2C and PC 2096 4B cell lines or the scramble control cell line were maintained in the presence of U-$^{13}C_6$ glucose or U-$^{13}C_5$ glutamine for 1 h in the same experiment described in Fig. 3. Fractions of different isotopomers of ^{13}C citrate (A) and ^{13}C malate (B) in the PC knockdown cell lines and scramble control cell line are shown within the same bars. $^{a}p < 0.01$, $^{b}p < 0.001$ vs scramble control. Metabolic pathways showing incorporation and distribution of labeled carbon from $^{13}C_6$-glucose (C) or $^{13}C_5$-glutamine (D) to various downstream metabolites. Labeled glucose and glutamine are indicated in red while unlabeled glucose and glutamine are indicated in blue. Abbreviations: ACC1, acetyl-CoA carboxylase1; α-KG, α-ketoglutarate; ACLY, ATP-citrate lyase; PC, pyruvate carboxylase; PDH, pyruvate dehydrogenase.

glucose carbon into palmitate. This is consistent with PC suppression inhibiting the mitochondrial synthesis of citrate and consequently the export of citrate to the cytosol thus lowering the supply of cytosolic acetyl-CoA and malonyl-CoA needed for fatty acid synthesis as depicted in Fig. 4.

3.9. PC knockdown lowers various metabolites including nucleotides

Table 3 and the heat map in Fig. 10 show several selected metabolites that were altered in the strong knockdown cell line PC 2096 4B or both PC knockdown cell lines. In addition to the metabolites discussed above moderate or strong suppression of PC resulted in the decreased levels of α-ketoglutarate, ADP-glucose, GDP-fucose and GDP-mannose while decreases in the levels of ribose-5-phosphate, CTP, hypoxanthine, UDP and GDP were observed only in the strong PC suppression cell line PC 2096 4B (Fig. 10 and Table 3).

Suppression of PC caused no or a very slight and insignificant reduction of unlabeled and labeled ATP and ADP from glucose (Fig. 11, left panel) such that the ATP/ADP ratio was unaltered by PC knockdown. This indicates that the energy charge of the cell was not impaired by PC knockdown. The slightly decreased levels of ADP and ATP in the PC 2096 4B cell line may be linked to the lowered levels of ribose-5-phosphate (see Table 3 and Fig. 10), which supplies the ribose moiety of these nucleotides and/or decreased aspartate (Fig. 8) which contributes to nitrogen-donation in purine ring synthesis. The levels of NADH and NAD^+ including NADH/NAD^+ ratios were not different between the knockdown cells and the scramble control (Fig. 11) also indicating that the energy charge of the cell was not affected by PC not down.

3.10. Enzyme levels in PC knockdown cell lines

We measured the activities of several mitochondrial and cytosolic enzymes that catalyze reactions of anaplerosis/cataplerosis including pyruvate cycling or might influence the levels of the metabolites measured in our study. As shown in Fig. 4, these included cytosolic malic enzyme, NADP-isocitrate dehydrogenase, ATP-citrate lyase, glutamate dehydrogenase, aspartate aminotransferase and citrate synthase. The activity of only one enzyme in the PC knockdown cells was significantly different from that of the scrambled shRNA control cell line. This was malic enzyme and in two of the three cell lines with very low PC malic enzyme activity was about 50% lower than that of the control cell line (Fig. 12). Malic enzyme activity was not lower in the PC cell line with moderate knockdown of PC, PC 847 2C (Fig. 12). The shRNA nucleotide sequences used to target the PC mRNA were not similar to any of the nucleotide sequence of cytosolic malic enzyme mRNA. Therefore, the lower malic enzyme activities were probably a response to the effects

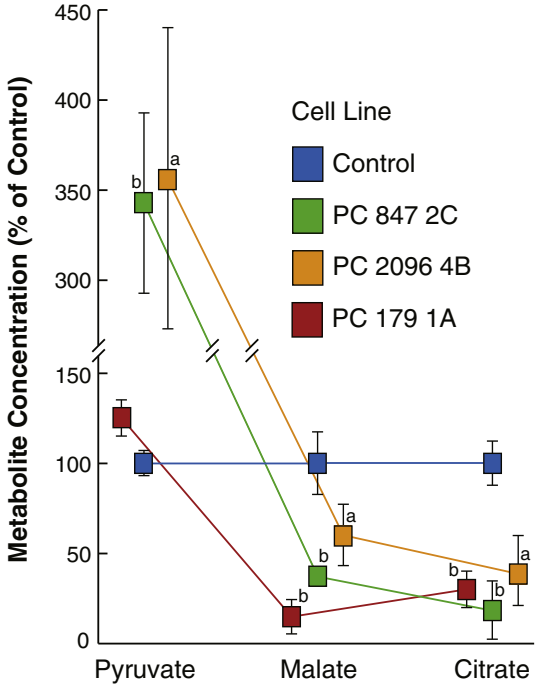

Fig. 6. An increase in pyruvate and decreases in malate and citrate in pyruvate carboxylase (PC) knockdown MDA-MB-231 cells show a cross over point at the PC consistent with inhibition of the PC reaction. PC 847 2C, PC 2096 4B and PC179 1A cell lines and the scramble shRNA control cell line were maintained in RPMI 1640 medium containing 5 mM glucose for 22 h and then in Krebs Ringer bicarbonate solution containing 10 mM glucose for 35 min before the concentrations of metabolites were measured as described under Experimental Procedures. The concentrations of each metabolite in the three PC knockdown cell lines are shown relative to those of the scramble shRNA control cell line were measured by alkali enhanced fluorescence. $^{a}p < 0.05$, $^{b}p < 0.01$ vs scramble control.

of lower PC enzyme activity. The 50% lower activity of malic enzyme in the cell lines with severe knockdown of PC might contribute to the lower pyruvate levels seen in these cell lines (Fig. 5) due to lower pyruvate cycling from malate and citrate. The enzyme activities were measured in the cell lines after they had been frozen for several months and then re-plated. Unfortunately the cell line PC 2096 4B with one of the lowest levels of PC and that was used for mass spectrometry studies would not grow after having been stored frozen so that the enzyme activities could not be measured in this cell line.

4. Discussion

4.1. The role of PC in cancer cell proliferation

Pyruvate carboxylation is an important anaplerotic reaction that replenishes citric acid cycle intermediates when they intermediates are removed from mitochondria by their export to the cytosol (cataplerosis). Anaplerosis and cataplerosis are necessary for gluconeogenesis in liver and kidney, lipogenesis in liver and adipose tissue, glutamate synthesis in astrocytes and glucose-induced insulin secretion in pancreatic beta cells [5,18–21]. We and others have shown that PC mRNA and PC protein are up-regulated in many cancers [7–10].

In the current study we generated multiple stable PC knockdown MDA-MB-231-derived cell lines by shRNA with various levels of PC knockdown and investigated the biochemical changes associated with the defects in growth and motility phenotypic defects of the PC knockdown cells. The various degrees of decreases in PC mRNA and PC enzyme activity were correlated with the decreased cell proliferation rates among the cell lines (Fig. 2). This is a confirmation of the relationship between PC enzyme levels and proliferation rates in breast cancer cells. This retarded proliferation phenotype of the PC knockdown MDA-MB-231 cell lines was also similar to that of the transient knockdown of PC in the MDA-MB-231 cell line that we reported previously [10]. A dose-dependent suppression effect on metabolism and inhibition of insulin secretion were also observed in the rat insulinoma cell line INS-1 832/13 with different degrees of PC suppression [12]. A similar disturbance of common metabolites was observed in both moderate and strong PC suppression MDA-MB-231-derived cells as shown in Table 3 and Figs. 5 and 6.

4.2. Knockdown of PC inhibits anaplerosis

The central metabolic pathway affected by the suppression of PC appears to lie within the anaplerosis. The product of the PC reaction is oxaloacetate, which immediately condenses with acetyl-CoA to produce citrate or is converted to malate in the mitochondrial malate dehydrogenase reaction. Suppression of PC resulted in the depletions of malate and citrate levels as expected (Figs. 5 and 6). Suppression of PC decreased the levels of total citrate and malate and ^{13}C incorporation into their isotopomers from $^{13}C_6$-labeled glucose and $^{13}C_5$-labeled glutamine (Fig. 5). This indicates that PC knockdown inhibits anaplerosis from both pyruvate carboxylation and glutaminolysis.

4.3. PC knockdown lowers pyruvate cycling

In contrast to suppression of PC expression in pancreatic beta cells, in which the knockdown cells showed a metabolic crossover point with increased levels of pyruvate and low levels of malate and citrate [12], suppression of PC in MDA-MB-231 cell lines showed lowered levels of pyruvate and lactate when cells were maintained in the presence of a high concentration of glucose (25 mM) (in DMEM cell culture medium) prior to the experiment (Fig. 7). Similar to experiments with pancreatic beta cells [12], when the PC knockdown cells were maintained in a cell culture medium containing a lower and physiologic concentration of glucose (5 mM) before glucose was added as in the experiments with beta cells, pyruvate was increased and malate and citrate were decreased indicating a crossover point and a block at the PC reaction (Fig. 6). The changes in the levels of pyruvate, lactate, malate and citrate raise the possibility of certain pathway(s) in which these three metabolites are connected. In pancreatic beta cells, there is a cycling of pyruvate into mitochondria known as the pyruvate-malate shuttle [17,18], as well as in the pyruvate-citrate cycle [18,19]. In the pyruvate-malate shuttle PC converts pyruvate to oxaloacetate followed by the conversion of oxaloacetate to malate by mitochondrial malate dehydrogenase, enabling malate to exit mitochondria. In the cytosol malate is in turn converted back to pyruvate by cytosolic malic enzyme, allowing pyruvate to re-enter mitochondria for carboxylation again by PC (Fig. 4). In the citrate-pyruvate shuttle citrate is exported from the mitochondria and cleaved to oxaloacetate in the ATP citrate lyase reaction. The oxaloacetate is then reduced to malate catalyzed by cytosolic malate dehydrogenase. The resulting malate then participates in the pyruvate-malate shuttle as shown in Fig. 4. These cycles provide cytosolic NADPH, a coupling factor, required for glucose-induced insulin secretion in pancreatic beta cells [17,21] and lipid synthesis in many different tissues. In addition, the acetyl-CoA derived from the ATP citrate lyase reaction can be converted to malonyl-CoA and utilized for lipid synthesis in the cytosol. The higher levels of PC mRNA and PC protein [10] and PC enzyme activity (Table 2) in the highly metastatic MDA-MB-231 cell line than in the low metastatic MCF-7 cell line suggest that similar to pyruvate cycling operative in pancreatic beta cells, pyruvate cycling is important for cell invasiveness or metastasis in breast cancer. In the PC knockdown MDA-MB-231 cells, the depleted levels of malate and citrate caused by the chronic suppression of PC may slow down the overall pyruvate cycling rate, resulting in the low level of pyruvate (Fig. 7).

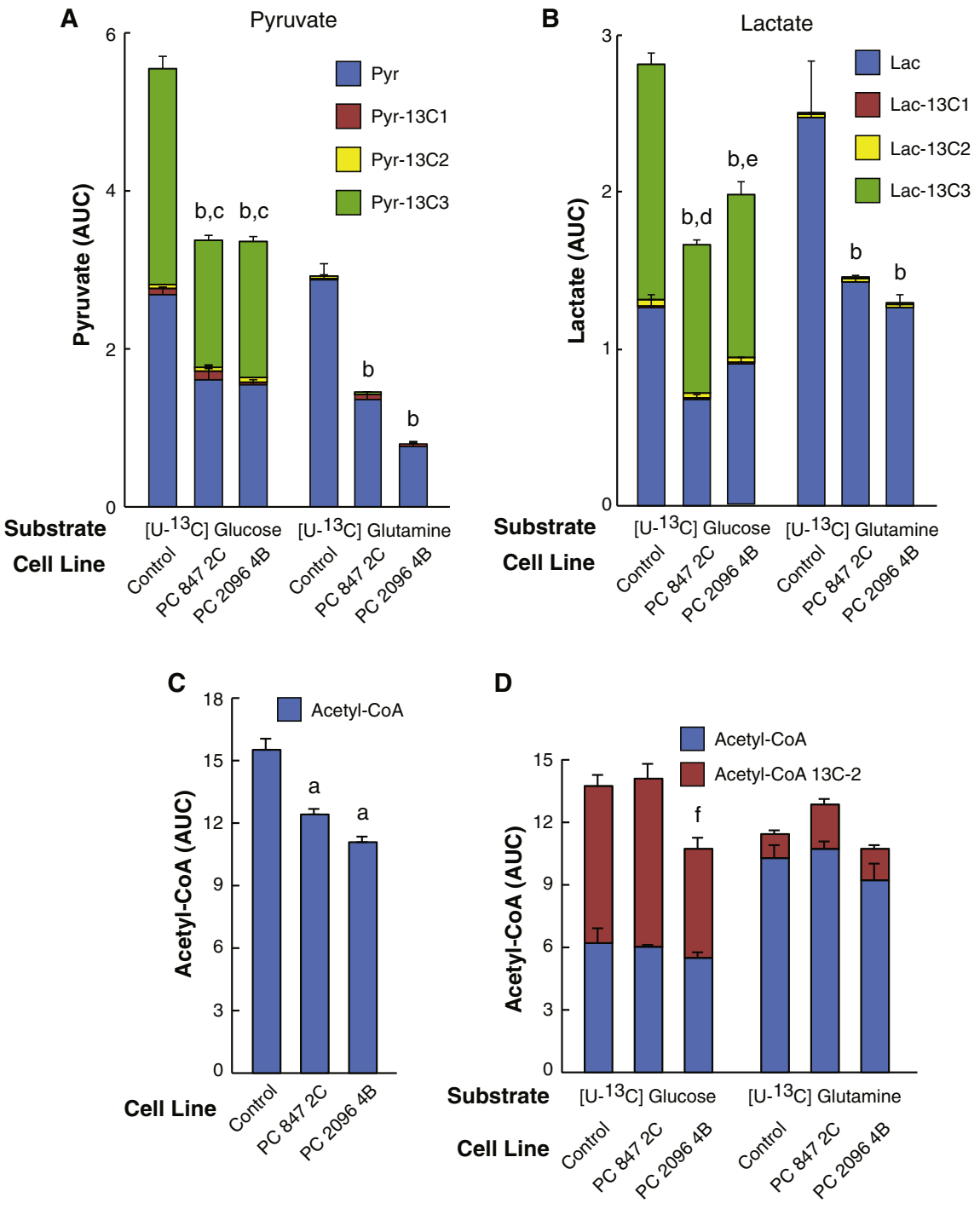

Fig. 7. Decreased labeled pyruvate, lactate and acetyl-CoA from U-$^{13}C_6$-glucose or U-$^{13}C_5$-glutamine in pyruvate carboxylase (PC) knockdown cell lines derived from the MDA-MB 231 breast cancer cell line. PC 847 2C and PC 2096 4B cell lines or scramble control cell line were maintained in the presence of U-$^{13}C_6$ glucose or U-$^{13}C_5$ glutamine for 1 h in the same experiment described in Fig. 3. Fractions of different isotopomers of ^{13}C-pyruvate *(A)*, ^{13}C–lactate *(B)* or ^{13}C-acetyl-CoA *(D)* in the PC knockdown cell lines and the scramble control cell line are shown within the same bars. *C*, The levels of acetyl-CoA in cells before labeled glucose or glutamine was added to the culture media. [a]$p < 0.01$; [b]$p < 0.001$ total metabolite vs scramble control same substrate; [c]$p < 0.01$ Pyr-^{13}C3 vs scramble control; [d]$p < 0.001$ or [e]$p < 0.01$ Lac-^{13}C3 vs scramble control; [f]$p < 0.05$ acetyl-CoA-^{13}C2 vs scramble control.

Interestingly, the level of cytosolic malic enzyme was 50% lower in two of the three cell lines with severe knockdown of PC studied. The shRNA nucleotide sequence used to target the PC mRNA was not similar to any of the nucleotide sequence of the malic enzyme mRNA indicating the lower level of the malic enzyme was not due to an off target effect of PC targeting. Therefore, the lower malic enzyme level was probably a down-regulatory response of the cell to a lower level of the substrate malate for reasons that are not exactly clear. In any case, the 50% lower level of malic enzyme is probably enough lower to contribute to decreased conversion of malate to pyruvate and thus a decrease in pyruvate cycling.

4.4. Generalized effects of PC knockdown on metabolite precursors needed for cell structure and energy production

Since citrate and malate are the two major citric acid cycle intermediates that are capable of exiting mitochondria for the biosynthesis of lipids, nucleic acids and certain amino acids, the reduction in the cellular

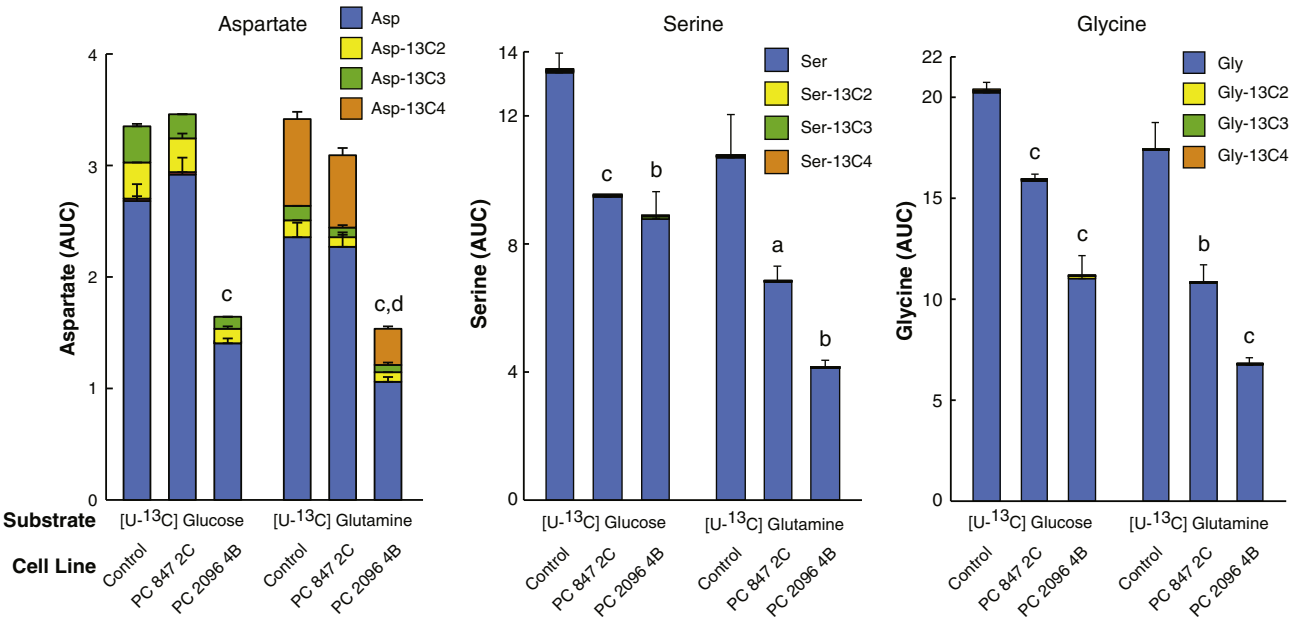

Fig. 8. Decreased labeled aspartate, glycine and serine from U-$^{13}C_6$-glucose or U-$^{13}C_5$-glutamine in pyruvate carboxylase (PC) knockdown cell lines derived from MDA-MB 231 breast cancer cell line. PC 847 2C and PC 2096 4B cell lines or the shRNA scramble control cell line were maintained in the presence of U-$^{13}C_6$-glucose or U-$^{13}C_5$-glutamine for 1 h in the same experiment described in Fig. 3. Fractions of different isotopomers of ^{13}C aspartate, ^{13}C-glycine and ^{13}C-serine between the PC knockdown cell lines and scramble control cell lines are shown within the same bars. $^{a}p < 0.05$, $^{b}p < 0.01$ and $^{c}p < 0.001$ total metabolite level vs scramble control. $^{d}p < 0.001$ vs Asp-$^{13}C4$.

levels of nucleotides (Table 3 and Fig. 11), aspartate, glycine, serine (Fig. 8) and lower glucose carbon incorporation into palmitate (Fig. 9) are consistent with the anaplerotic/cataplerotic role of PC in growth of breast cancer cells.

Transamination of oxaloacetate with glutamate catalyzed by aspartate aminotransferase would produce aspartate. Therefore, it is likely that the lowered level of oxaloacetate caused by suppression of PC may be responsible for the low level of aspartate (Fig. 8). A lowered level of aspartate was also reported in the PC knockdown non-small cell lung cancer (NSCLC), which showed a marked decrease in the cellular aspartate level [9]. In renal adenocarcinoma and paraganglioma cancers harboring loss of function mutations of succinate dehydrogenase, PC was found essential to support cancer proliferation [22,23].

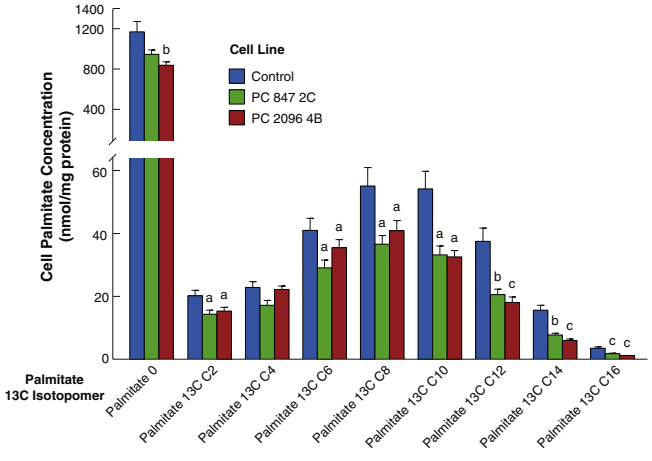

Fig. 9. Decreased U-$^{13}C_6$-glucose incorporation into palmitate in pyruvate carboxylase (PC) knockdown cell lines derived from the MDA-MB-231 breast cancer cell line. PC 847 2C and PC 2096 4B cell lines or the shRNA scramble control cell line were maintained in DMEM for 24 h or longer without labeled glucose of glutamine (the same as the zero time control shown in Fig. 3A and B). Cells were then maintained for 18 h in DMEM modified to contain 10 mM [U-$^{13}C_6$]glucose and ^{13}C incorporation into palmitate was measured by LC-MS/MS. $^{a}p < 0.05$, $^{b}p < 0.01$ and $^{c}p < 0.001$ vs scramble control.

Suppression of PC slows down proliferation of these cancers, concomitant with reduced cellular levels of aspartate. Supplementation of the knockdown cancer cells with aspartate rescued this slow growth phenotype. As aspartate is the structural component of several biomolecules including the backbone of purine and pyrimidine rings in nucleic acids, the decreased levels of nucleotides (Fig. 10 and Table 3) and aspartate observed in the PC knockdown MDA-MB-231 cells can potentially slow the synthesis of these nucleotides, contributing to the low rates of cell proliferation. As the ribose-5-phosphate is also the backbone of nucleotides, the lowered level of total ribose-5-phosphate in the knockdown cells as shown in Table 3 and may also contribute to the decreased levels of some nucleotides and their derivatives i.e. hypoxanthine, ADP-glucose, UDP, GDP, GDP-mannose and GDP-fucose. Similar to our study, the PC knockdown non-small cell lung cancer (NSCLC) also showed reduction of glucose- and glutamine- derived CTP and UTP levels [9].

The marked reduction of serine and glycine levels in the PC knockdown cells may underlie the retarded growth phenotype of the knockdown cells because serine contributes to various biosynthetic pathways including protein synthesis, phospholipids and nucleotides which are in high demand during tumorigenesis [24].

The perturbation of serine biosynthesis may occur during the conversion of 3-phosphoglycerate to serine. The conversion of 3-

Table 3
Selected metabolites that are altered in pyruvate carboxylase (PC) knockdown MDA-MB-231 cell lines.

Metabolite	KD cell line PC 847 2C		KD cell line PC 2096 4B	
	Fold change	P-value	Fold change	P-value
Ribose-5-phosphate	0.98	NS	0.84	$P < 0.05$
α-ketoglutarate	0.70	$P < 0.05$	0.72	$P < 0.05$
ADP-glucose	0.85	$P < 0.05$	0.80	$P < 0.01$
CTP	0.9	NS	0.70	$P < 0.01$
Hypoxanthine	1.01	NS	0.84	$P < 0.05$
UDP	0.78	NS	0.70	$P < 0.05$
GDP	0.85	NS	0.76	$P < 0.05$
GDP-fucose	0.84	$P < 0.05$	0.76	$P < 0.005$
GDP-mannose	0.84	$P < 0.05$	0.45	$P < 0.005$

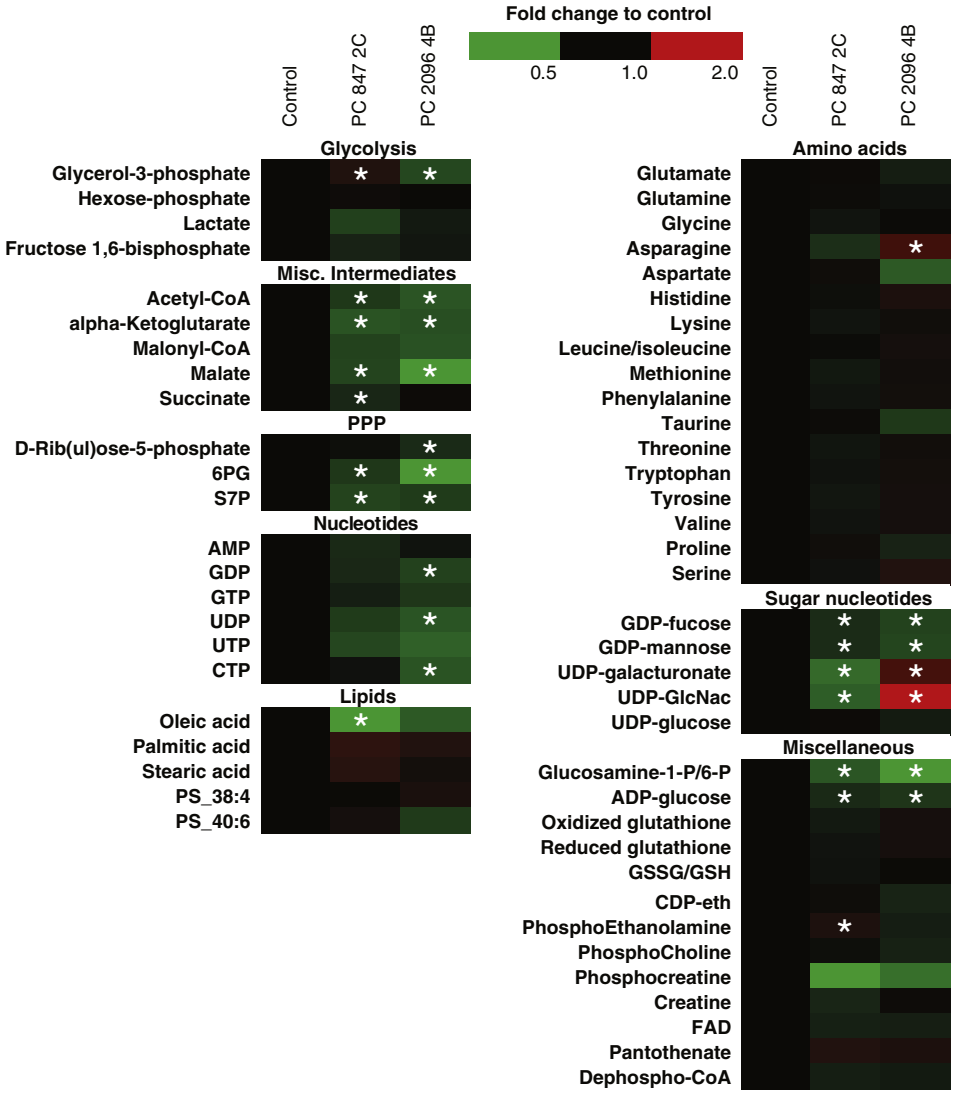

Fig. 10. Heat map showing global lowering of metabolites in pyruvate carboxylase (PC) knockdown MDA-MB 231 breast cancer cell lines. Metabolites were measured by LC-MS in the same experiments shown in Fig. 3 at the zero time point, i.e. before a ^{13}C labeled substrate was added. Metabolite levels are coded by *m/z*. The asterisk indicates different from the scramble control cell line with $p < 0.05$.

phosphoglycerate to serine is mediated through three sequential reactions (see Fig. 4). The first reaction is the conversion of 3-phosphoglycerate to 3-phosphohydroxypyruvate by phosphoglycerate dehydrogenase followed by further conversion to 3-phosphoserine by phosphoserine aminotransferase before the final conversion to serine by protein serine phosphatase. Then phosphoserine aminotransferase catalyzes the transfer of the amino group from glutamate to 3-phosphohydroxypyruvate. Because glutamate is produced from α-ketoglutarate via a transamination reaction, the lowered level of α-ketoglutarate in the PC-knockdown MDA-MB-231 cells (Fig. 10) may in turn lower the rate of glutamate formation which consequently affects the transamination reaction catalyzed by phosphoserine aminotransferase. Interestingly, up-regulation of serine and glycine biosynthesis caused by amplification of phosphoglycerate dehydrogenase gene copy number was also reported to contribute to oncogenesis in melanoma and breast cancer [24,25]. Suppression of phosphoglycerate dehydrogenase expression in several breast cancer cell lines including MDA-MB-231 cells, lowered serine biosynthesis concomitant with a decreased cell proliferation rate, indicating the crucial role of serine in supporting breast cancer growth. Suppression of phosphoglycerate dehydrogenase expression in invasive breast cancer cells also reduces the level of α-ketoglutarate which is produced from the transamination of glutamate [26]. These findings mirror the PC knockdown MDA-MB-231 cells that showed lowered levels of α-ketoglutarate and serine in the current study.

Lowered levels of total cellular acetyl-CoA in the PC knockdown cell lines can most likely be attributed to decreased export of citrate from mitochondria causing decreased citrate available for conversation to oxaloacetate and acetyl-CoA catalyzed by ATP citrate lyase in the cytosol. The latter route for acetyl-CoA regeneration also forms part of alternate route of pyruvate cycling: the well-known pyruvate/citrate cycle [4,18,19] (Fig. 4).

In addition to the lowered levels of certain mitochondrial metabolites, pyruvate cycling and nucleotide synthesis, we also found that suppression of PC causes a reduction of glucose incorporation into palmitate (Fig. 9), suggesting that inhibition of anaplerosis caused by PC knockdown results in lower fatty acid synthesis which restricts membrane biogenesis of the newly dividing cells.

Suppression of PC only slightly and insignificantly lowered the concentrations of ATP and ADP without affecting the ATP/ADP ratio and NAD(P)(H) concentrations (Fig. 11) indicating suppression of PC did not seriously affect the cell energy charge. The decreases in other nucleotides and nucleotide derivatives (Table 3 and Fig. 11) can be attributed

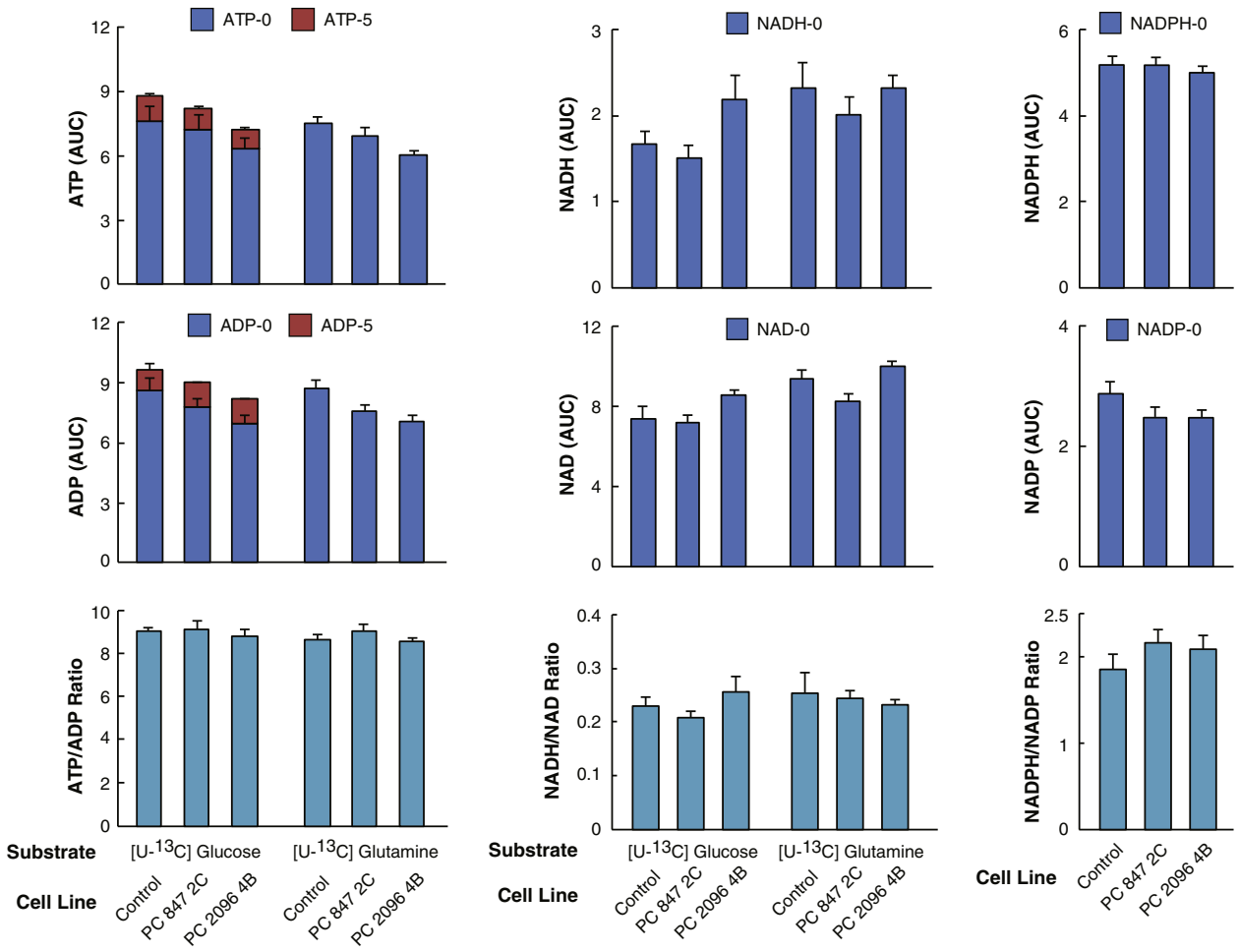

Fig 11. Normal ATP and ADP concentrations, ATP/ADP ratio, NAD(P)H and NAD(P) concentrations and NAD(P)H/NAD(P) ratios in pyruvate carboxylase (PC) knockdown cell lines derived from the MDA-MB-231 breast cancer cell line supplied with U-$^{13}C_6$-glucose or U-$^{13}C_5$-glutamine. PC 847 2C and PC 2096 4B cell lines or the shRNA scramble control cell line were maintained in the presence of U-$^{13}C_6$ glucose or U-$^{13}C_5$ glutamine for 1 h in the same experiment described in Fig. 3. Fractions of different isotopomers of ^{13}C-ATP and ^{13}C-ADP and levels of the pyridine nucleotides NAD(P), NAD(P)H (which showed no incorporation of ^{13}C) between the PC knockdown cell lines and scramble control group are shown within the same bars. $^{a}p < 0.01$ vs total metabolite same substrate control.

to decreased nucleotide biosynthesis via the reduced level of ribose-5-phosphate which is a backbone nucleotide derivatives and decreased aspartate which is a precursor for purine and pyrimidine synthesis.

Since we studied the MDA-MB-231 cell line which is triple negative for estrogen receptor (ER), progesterone receptor (PR) and epidermal growth factor receptor 2 (HER2) in our study, one might argue whether

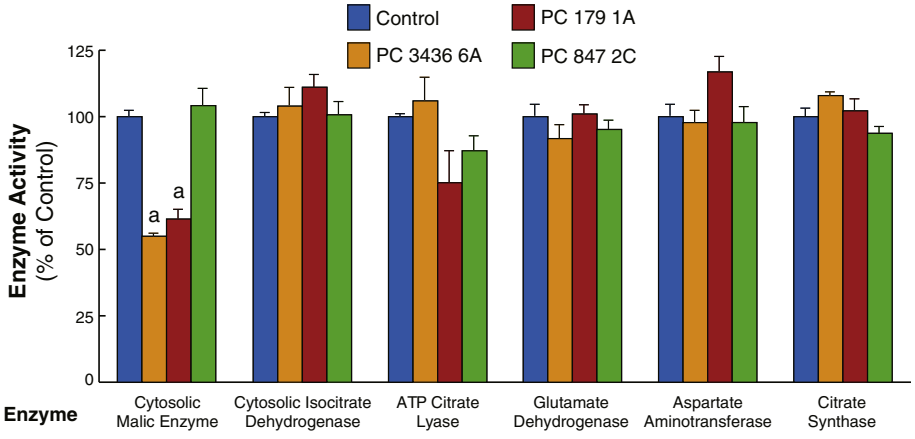

Fig. 12. Malic enzyme is the only enzyme out of several anaplerotic/cataplerotic pyruvate cycling enzymes that is decreased in breast cancer cell lines with severely knocked down pyruvate carboxylase (PC). Cell lines PC 3436 6A and PC 179 1A possess severely lower levels of pyruvate carboxylase enzyme activity and cell line and PC 847 2C possesses moderately decreased PC activity compared to the scrambled shRNA control cell line. These cell lines show low cell proliferation rates compared to the control cell line (Figs. 1 and 2). The lower level malic enzyme in two cell lines with severely knocked down PC is consistent with lower pyruvate cycling and lower malate, citrate and pyruvate levels (Figs. 5-8) in these cell lines (means ± SE, $^{a}p < 0.01$ vs scramble control). Only malic enzyme showed decreased activity vs the control cell line.

overexpression of PC is a specific characteristic of breast cancer cell lines. Using various other breast cancer cell lines expressing these three receptors differently, we found no correlation between the expression of these receptors and PC expression. For example, the two most invasive breast cancer cell lines, MDA-MB-231 and MDA-MB-435, which are $ER^-/PR^-/HER2^-$ and $ER^-/PR2^-/HER2^+$, respectively, express PC much higher than MCF-7 and SKBR3 cell lines, which are $ER^+/PR^+/HER2^-$ and $ER^-/PR^-/HER2^+$, respectively (10). Furthermore, unlike MDA-MB-231, MCF-10A, a non-invasive cell line that is also negative for those three receptors was found to possess an extremely low level of PC enzyme activity (data not shown). Most importantly, our clinicopathological investigation of breast cancer patients has also shown that the level of PC expression was not correlated with the status of these receptors in breast cancer tissues of patients but rather shows a positive correlation with tumor size and stages (10). Thus the level of expression of PC appears to be independent of the status of ER, PR and HER2 receptor expression.

5. Conclusion

Fig. 4 summarizes the disturbance of various metabolic pathways resulting in the growth retarded phenotype of PC knockdown MDA-MB-231 cells. In conclusion, suppression of PC expression in MDA-MB-231 breast cancer cells results in the lowered levels of citrate, malate and α-ketoglutarate. The depleted levels of these metabolites perturb mitochondrial cataplerosis for the synthesis of serine, glycine, aspartate and fatty acids which are used as the building blocks for synthesis of proteins, lipids and nucleotides. The lowered levels of citrate and malate also impair pyruvate cycling between mitochondria and cytosol. This global perturbation of biosynthesis contributes to the retarded growth phenotype of the PC knockdown MDA-MB-231 cells. The findings that suppression of PC inhibits cell proliferation in glioblastoma [7], NSCLC [9], renal carcinoma, paraganglioma [22,23] and, in our study, breast cancer (Fig. 2), highlights the crucial role of PC in cancer cell growth and suggests PC may be an attractive drug target of cancer treatment.

Author contribution

Phatchariya Phannasil, Israr Ansari, Mahmoud El Azzouny, Khanti Rattanapornsompong, Sarawut Jitrapakdee and Michael MacDonald designed the experiments and interpreted data. Phatchariya Phannasil, Israr Ansari, Mahmoud El Azzouny, Melissa Longacre (Melissa Longacre designed parts of experiments) and Khanti Rattanapornsompong performed the experiments. Phatchariya Phannasil, Sarawut Jitrapakdee and Michael MacDonald wrote the manuscript. Israr Ansari and Mahmoud El Azzouny contributed to the writing of the manuscript. Sarawut Jitrapakdee, Michael MacDonald and Charles Burant contributed reagents, materials and analysis tools. All authors analyzed the results and approved the final version of the manuscript. Michael MacDonald and Sarawut Jitrapakdee contributed equally to this work.

Funding

This work was supported by grant BRG5780007 from the Thailand Research Fund and Mahidol University to S.J. and a gift to M.J.M. from the Nowlin Family Trust of the InFaith Community Foundation. P.P. was supported by the RGJ-PhD scholarship (PHD/0412/2552) from the Thailand Research Fund. K.R. was supported by the Science Achievement Scholarship of Thailand. C.F.B. was supported by the Michigan Regional Comprehensive Metabolomics Resource Core Graft U24 (NIH Grant Number DK097153).

Conflict of interest

The authors declare that they have no conflicts of interest with the contents of this article.

Transparency document

The Transparency document associated with this article can be found, in online version.

Acknowledgments

The excellent technical support of Mindy A. Kendrick and Scott W. Stoker is greatly appreciated.

References

[1] H.G. Welch, D.H. Gorski, P.C. Albertsen, Trends in metastatic breast and prostate cancer - lessons in cancer dynamics, N. Engl. J. Med. 373 (2015) 1685–1687.
[2] S.Y. Lee, H.M. Jeon, M.K. Ju, C.H. Kim, G. Yoon, S.I. Han, H.G. Park, H.S. Kang, Wnt/Snail signaling regulates cytochrome C oxidase and glucose metabolism, Cancer Res. 72 (2012) 3607–3617.
[3] M.G. Vander Heiden, L.C. Cantley, C.B. Thompson, Understanding the Warburg effect: the metabolic requirements of cell proliferation, Science 324 (2009) 1029–1033.
[4] O.E. Owen, S.C. Kalhan, R.W. Hanson, The key role of anaplerosis and cataplerosis for citric acid cycle function, J. Biol. Chem. 277 (2002) 30409–30412.
[5] S. Jitrapakdee, M. St. Maurice, I. Rayment, W.W. Cleland, J.C. Wallace, P.V. Attwood, Structure, mechanism and regulation of pyruvate carboxylase, Biochem. J. 413 (2008) 369–387.
[6] R.A. Moreadith, A.L. Lehninger, The pathways of glutamate and glutamine oxidation by tumor cell mitochondria. Role of mitochondrial NAD(P)$^+$-dependent malic enzyme, J. Biol. Chem. 259 (1984) 6215–6221.
[7] T. Cheng, J. Sudderth, C. Yang, A.R. Mullen, E.S. Jin, J.M. Matés, R.J. DeBerardinis, Pyruvate carboxylase is required for glutamine-independent growth of tumor cells, Proc. Natl. Acad. Sci. U. S. A. 108 (2011) 8674–8679.
[8] T.W. Fan, A.N. Lane, R.M. Higashi, M.A. Farag, H. Gao, M. Bousamra II, D.M. Miller, Altered regulation of metabolic pathways in human lung cancer discerned by (13) C stable isotope-resolved metabolomics (SIRM), Mol. Cancer 8 (2009) 41.
[9] K. Sellers, M.P. Fox, M. Bousamra II, S.P. Slone, R.M. Higashi, D.M. Miller, A.N. Lane, Pyruvate carboxylase is critical for non-small-cell lung cancer proliferation, J. Clin. Invest. 125 (2015) 687–698.
[10] P. Phannasil, C. Thuwajit, M. Warnnissorn, J.C. Wallace, M.J. MacDonald, S. Jitrapakdee, Pyruvate carboxylase is up-regulated in breast cancer and essential to support growth and invasion of MDA-MB-231 cells, PLoS One 10 (2015), e0129848.
[11] K. Subik, J.-F. Lee, L. Baxter, T. Strzepek, D. Costello, P. Crowley, L. Xing, M.-C. Hung, T. Bonfiglio, D.G. Hicks, P. Tang, The expression patterns of ER, PR, HER2, CK5/6, EGFR, Ki-67 and AR by immunohistochemical analysis in breast cancer cell lines, Breast Cancer (Auckl.) 4 (2010) 35–41.
[12] N.M. Hasan, M.J. Longacre, S.W. Stoker, T. Boonsaen, S. Jitrapakdee, M.A. Kendrick, M.J. MacDonald, Impaired anaplerosis and insulin secretion in insulinoma cells caused by small interfering RNA-mediated suppression of pyruvate carboxylase, J. Biol. Chem. 283 (2008) 28048–28059.
[13] M.A. Lorenz, C.F. Burant, R.T. Kennedy, Reducing time and increasing sensitivity in sample preparation for adherent mammalian cell metabolomics, Anal. Chem. 83 (2011) 3406–3414.
[14] M.A. Lorenz, M.A. El Azzouny, R.T. Kennedy, C.F. Burant, Metabolome response to glucose in the β-cell line INS-1 832/13, J. Biol. Chem. 288 (2013) 10923–10935.
[15] M.J. MacDonald, M.J. Longacre, S.W. Stoker, M.A. Kendrick, A. Thonpho, L.J. Brown, N.M. Hasan, S. Jitrapakdee, T. Fukao, M.S. Hanson, L.A. Fernandez, J. Odorico, Differences between human and rodent pancreatic islets: low pyruvate carboxylase, ATP citrate lyase and pyruvate carboxylation; high glucose-stimulated acetoacetate in human pancreatic islets, J. Biol. Chem. 286 (2011) 18383–18396.
[16] P.A. Srere, in: J.M. Lowenstein (Ed.), Citrate Synthase in Methods in Enzymology, Citric Acid Cycle, vol. XIII, Academic Press, Inc., New York, NY, 1969.
[17] M.J. MacDonald, Feasibility of a mitochondrial pyruvate malate shuttle in pancreatic islets. Further implications of cytosolic NADPH in insulin secretion, J. Biol. Chem. 270 (1995) 20051–20058.
[18] M.J. MacDonald, L.A. Fahien, L.J. Brown, N.M. Hasan, J.D. Buss, M.A. Kendrick, Perspective: emerging evidence for signaling roles of mitochondrial anaplerotic products in insulin secretion, Am. J. Physiol. Endocrinol. Metab. 288 (2005) E1–E15.
[19] S. Farfari, V. Schulz, B. Corkey, M. Prentki, Glucose-regulated anaplerosis and cataplerosis in pancreatic beta-cells: possible implication of a pyruvate/citrate shuttle in insulin secretion, Diabetes 49 (2000) 718–726.
[20] S. Jitrapakdee, M. Slawik, G. Medina-Gomez, M. Campbell, J.C. Wallace, J.K. Sethi, S. O'Rahilly, A.J. Vidal-Puig, The peroxisome proliferator-activated receptor-γ regulates murine pyruvate carboxylase gene expression *in vivo* and *in vitro*, J. Biol. Chem. 280 (2005) 27466–27476.
[21] S. Jitrapakdee, A. Wutthisathapornchai, J.C. Wallace, M.J. MacDonald, Regulation of insulin secretion: role of mitochondrial signaling, Diabetologia 53 (2010) 1019–1032.
[22] S. Cardaci, L. Zheng, G. MacKay, N.J. Van Den Broek, E.D. MacKenzie, C. Nixon, D. Stevenson, S. Tumanov, V. Bulusu, J.J. Kamphorst, A. Vazquez, S. Fleming, F. Schiavi, G. Kalna, K. Blyth, D. Strathdee, E. Gottlieb, Pyruvate carboxylation enables growth of SDH-deficient cells by supporting aspartate biosynthesis, Nat. Cell Biol. 17 (2015) 1317–1326.
[23] C. Lussey-Lepoutre, K.E. Hollinshead, C. Ludwig, M. Menara, A. Morin, L.J. Castro-Vega, S.J. Parker, M. Janin, C. Martinelli, C. Ottolenghi, C. Metallo, A.P. Gimenez-

Roqueplo, J. Favier, D.A. Tennant, Loss of succinate dehydrogenase activity results in dependency on pyruvate carboxylation for cellular anabolism, Nat. Commun. 6 (2015) 8784.

[24] R. Possemato, K.M. Marks, Y.D. Shaul, M.E. Pacold, D. Kim, K. Birsoy, S. Sethumadhavan, H.K. Woo, H.G. Jang, A.K. Jha, W.W. Chen, F.G. Barrett, N. Stransky, Z.Y. Tsun, G.S. Cowley, J. Barretina, N.Y. Kalaany, P.P. Hsu, K. Ottina, A.M. Chan, B. Yuan, L.A. Garraway, D.E. Root, M. Mino-Kenudson, E.F. Brachtel, E.M. Driggers, D.M. Sabatini, Functional genomics reveal that the serine synthesis pathway is essential in breast cancer, Nature 476 (2011) 346–350.

[25] J.W. Locasale, Serine, glycine and one-carbon units: cancer metabolism in full circle, Nat. Rev. Cancer 13 (2013) 572–583.

[26] J.W. Locasale, A.R. Grassian, T. Melman, C.A. Lyssiotis, K.R. Mattaini, A.J. Bass, G. Heffron, C.M. Metallo, T. Muranen, H. Sharfi, A.T. Sasaki, D. Anastasiou, E. Mullarky, N.I. Vokes, M. Sasaki, R. Beroukhim, G. Stephanopoulos, A.H. Ligon, M. Meyerson, A.L. Richardson, L. Chin, G. Wagner, J.M. Asara, J.S. Brugge, L.C. Cantley, M.G. Vander Heiden, Phosphoglycerate dehydrogenase diverts glycolytic flux and contributes to oncogenesis, Nat. Genet. 43 (2011) 869–874.